# STATIC AND DYNAMIC PROPERTIES OF PROTEINS ADSORBED AT LIQUID INTERFACES

Promotor:      dr J. Lyklema,
               emeritus hoogleraar in de fysische chemie,
               met bijzondere aandacht voor de grensvlak- en kolloïdchemie


Co-promotor:  dr E.H. Lucassen-Reynders
               gepensioneerd wetenschappelijk medewerker van Unilever Research
               Vlaardingen

# STATIC AND DYNAMIC PROPERTIES
# OF PROTEINS
# ADSORBED AT LIQUID INTERFACES

## J. Benjamins

Stellingen

1. De inductieperiode voor de oppervlaktedruk, zoals waargenomen bij eiwitadsorptie vanuit verdunde oplossingen aan vloeibare grensvlakken, mag niet geïnterpreteerd worden als een inductieperiode voor de adsorptie.

Dit proefschrift, Hoofdstuk 2

2. De term "ontvouwing" voor conformatie aanpassingen van eiwitmoleculen bij adsorptie suggereert een te grote verandering van de vorm van het molecuul, vooral in het geval van globulaire eiwitten.

Dit proefschrift, Hoofdstukken 2 en 6

3. Conclusies over het adsorptieproces van eiwitten enkel gebaseerd op indirecte metingen, zoals b.v. oppervlaktedruk, zijn verdacht.

Dit proefschrift, Hoofdstuk 2

4. De dilatatiemodulus metingen aan geadsorbeerde eiwitlagen, zoals beschreven door Graham en Phillips, zijn dubieus. Ten onrechte is door de auteurs demping van de oppervlaktespanningsoscillatie, door een hoge afschuifmodulus en hechting aan de wand, toegeschreven aan demping van een longitudinale golf door wrijving met de onderliggende vloeistof.

D.E. Graham, M.C. Phillips. Proteins at Liquid Interfaces; IV. Dilational Properties. Journal of Colloid and Interface Science. 76 (1980) 227

5. De viscoelastische eigenschappen van olie/water grensvlakken met geadsorbeerde eiwitlagen hangen sterk af van het type olie. Het is dus niet geoorloofd gegevens gemeten aan minerale olie/water grensvlakken zonder meer toe te passen op triglyceride olie/water grensvlakken.

Dit proefschrift, Hoofdstuk 4

6. De populariteit van oppervlakte shearviscositeits metingen aan geadsorbeerde eiwitlagen bij grote deformaties kan niet gebaseerd zijn op de relevantie van de verkregen structuur informatie, omdat zulke metingen de te onderzoeken structuur grotendeels vernietigen.

Dit proefschrift, Hoofdstuk 5

7. Het onderzoeken van de structuurvorming in geadsorbeerde eiwitlagen, zonder directe metingen van de geadsorbeerde hoeveelheid, kan leiden tot een overschatting van de tijdsafhankelijkheid.

Dit proefschrift, Hoofdstuk 5

8. Druppel "break-up" experimenten en ook coalescentie experimenten zonder emulgatoren geven weinig inzicht in wat er gebeurt bij het maken en stabiliseren van echte emulsies.

A.Williams, J.J.M. Janssen, A. Prins. Behaviour of Droplets in Simple Shear Flow in the presence of a Protein Emulsifier. Colloids and Surfaces A. 125 (1997) 189
J.J.M. Janssen, A.Boon, W.G.M. Agterof. Influence of Dynamic Interfacial Properties on Droplet Break- in Simple Shear Flow. AIChE Journal. 40 (1994) 1929

9. In het kader van het verminderen van het gebruik van fossiele brandstoffen zouden sportscholen en fitnesscentra verplicht moeten worden hun instrumentarium om te bouwen in energieopwekkende, tredmolenachtige varianten.

10. De ramp met de russische onderzeeboot de Koersk toont weer eens aan dat alles relatief is. Voor slachtoffers en nabestaanden bleek 100 meter wel heel erg ver.

11. Gelukkig zingen vogeltjes niet zoals ze geboekt zijn.

Stellingen behorende bij het proefschrift:
Static and dynamic properties of proteins adsorbed at liquid interfaces
J. Benjamins Wageningen, 8 november 2000.

# VOORWOORD

Dit boekje is op een wat ongebruikelijke manier tot stand gekomen. Het onderzoek en het schrijven vond niet plaats binnen een tijdsbestek van 4 à 5 jaar, maar over een veel langere periode.

In feite is dit "project " meer dan 25 jaar geleden gestart. Toen werd in de toenmalige groep Fysische Chemie, onder leiding van Dr. M. van den Tempel, begonnen met een onderzoek naar het dynamische gedrag van geadsorbeerde eiwitlagen. Mijn bijdrage aan dit onderzoek begon met het ontwikkelen (samen met Rik Veer) van een ellipsometer die geschikt moest zijn voor adsorptiemetingen aan vloeistof/vloeistof grensvlakken. Met Jan de Feijter werd dit onderzoek voortgezet en uitgebreid met het bestuderen van het rheologisch gedrag van geadsorbeerde eiwitlagen. Ongeveer 10 jaar geleden kreeg dit onderzoek een nieuwe inpuls door de samenwerking met Emmie Lucassen-Reynders. Het zwaartepunt kwam toen te liggen op het rheologisch gedrag van eiwitlagen geadsorbeerd aan het olie/water grensvlak.

Het is ook Emmie geweest, die, in 1994, mij er toe aangezet heeft het onderzoek te bundelen tot een proefschrift. Het is voor mij duidelijk, Emmie, dat zonder jouw altijd stimulerende medewerking dit boekje nooit was verschenen. Ik ben ook blij dat deze medewerking niet ophield na je pensionering in 1997. Bedankt daarvoor en ik hoop dat we deze wetenschappelijke samenwerking ook in de toekomst kunnen voortzetten.

Ook wil ik mijn promotor Prof. Dr. J. Lyklema bedanken. Hans, bedankt voor het vertrouwen dat je vanaf het begin in deze wat vreemde manier van promoveren hebt gehad. Het was voor mij een grote stimulans toen je positief reageerde op mijn verzoek of je mijn promotor zou willen zijn. Temeer omdat mijn officiële opleiding niet helemaal voldeed om toegelaten te worden tot de promotie. Deze rimpel heb jij ook moeiteloos voor mij glad gestreken. Ook bedankt voor het altijd nuttige commentaar en zinvolle suggesties waarvan je mijn manuscripten steeds weer voorzien hebt.

Mijn dank gaat ook uit naar Robert de Bruijn en Solke Bruin, respectievelijk mijn sectieleider en groepsleider, voor hun medewerking tijdens de start van de echte promotie periode en naar Wim Agterof (unitleider Product Principles) en Arjen Sein (skillbase leader Emulsions) voor hun medewerking bij het vervolg. Arjen, bedankt voor de ruimte die je me gaf om het boekje op tijd af te ronden.

I am also grateful to Alain Cagna and Bernard Delorme from IT Concept (France) for the pleasant and effective collaboration that we had during the development of the Dynamic Drop Tensiometer.

Ook wil ik niet nalaten mijn chefs uit de Fysische Chemie-periode te bedanken. Jan de Feijter en Frits van Voorst Vader ben ik veel dank verschuldigd voor hun "cursus" Oppervlakte- en Kolloidchemie die ze mij, bijna terloops, gedurende vele jaren gegeven hebben.

Karel Kuijpers wil ik bedanken voor zijn bereidheid mij altijd weer te helpen een computer/software probleem op te lossen. Dit geldt ook voor mijn zoon Jan-Willem, die sinds kort ook werkzaam is in de ellipsometrie.

Tenslotte wil ik mijn gezin bedanken voor hun ondersteuning en begrip. Ik weet zeker dat ik ze de afgelopen 6 jaar en vooral de laatste 2 jaar niet de aandacht heb gegeven die ze nodig hadden en verdienden. Joke, Jan-Willem en Ingrid: bedankt!

# Contents

Chapter 5: SURFACE SHEAR PROPERTIES OF ADSORBED PROTEIN LAYERS

Chapter 6: MODELS FOR THE SURFACE EQUATION OF STATE OF ADSORBED PROTEIN LAYERS AND THE RELATION WITH SURFACE DILATIONAL MODULUS.

Chapter 7: RELATIONSHIP BETWEEN INTERFACIAL PROPERTIES OF ADSORBED
PROTEIN LAYERS AND EMULSION AND FOAM FORMATION AND STABILITY

Chapter 8. SUMMARY

SAMENVATTING

# 1 INTRODUCTION

## 1.1 General introduction.

Proteins play a very important role in foods and food production. In the first place, of course, because of their nutritional value: they are needed as amino acid source for protein production. A second function of proteins is that they act as stabilizers in food emulsions and foams. In this second function, proteins can change both the rheology of the aqueous phase (e.g. by thickening and gelation), and the interfacial properties contributing to colloid-chemical stability. Much has been published about the effectiveness of proteins in the production of stable emulsions and foams (reviews 1,2), but predictive theories on this subject are still sparse. The aim of the investigation described in this thesis is to increase the level of understanding of the role that proteins play in preparing foams and emulsions and the subsequent stabilization of these systems. This was achieved by a systematic experimental and theoretical study of the changes in the static and dynamic interfacial properties induced by proteins.

## 1.2 Proteins

Proteins are biopolymers consisting of long chains of amino acids linked together by peptide bonds. The molecular weight ranges from 10,000 to over 100,000. Proteins have a strong tendency to adsorb at interfaces, which makes them suitable to act as emulsifier or foamer.

Compared to low molecular weight surfactants, the structure of protein molecules is complex. In this complex protein molecule four levels of structure can be distinguished; the primary, secondary, tertiary and, for some proteins, also a quaternary structure. The primary structure is the sequence of the amino acids in the polypeptide chain. The secondary structure is determined by ordering in the polypeptide chain (3), resulting in α-helices and β-sheets. The way in which twists or bends of the whole polypeptide are folded together in space is called the tertiary structure. Protein molecules that consist of more than one polypeptide chain have a quaternary structure which is related to interchain interactions. Secondary, tertiary and quaternary structures together determine the conformation of the protein. Interactions that are important for the formation of these conformations are: electrostatic interactions, hydrogen bonds, hydrophobic interactions and covalent bonds (e.g. disulphide bridges). With respect to their structural stability, proteins can be divided in flexible random-coil type molecules, e.g. β-casein, and globular molecules with a more rigid structure, e.g. ovalbumin and lysozyme.

The conformations of many proteins in aqueous solution have been elucidated to a large extent, and for some three-dimensional structures can also be obtained using molecular modelling.

Upon adsorption the conformation of a protein molecule will generally change. The extent of these changes depends on protein type, the surface on which adsorption takes place and environmental parameters such as pH and ionic strength. At solid surfaces, conformational changes have been investigated quite extensively (4). At liquid interfaces, conformational changes that occur upon adsorption have been studied less thoroughly, because this system is less accessible to some experimental techniques, e.g. circular dichroism. In emulsions and foams adsorption de facto occurs at a hydrophobic surface, implying that the change in conformation, if any, can at least partly result from the movement of hydrophobic groups to that surface. In the native protein molecule these hydrophobic groups are mostly buried in the interior of the molecule. Under certain conditions, e.g. at high surface pressures or in destabilised foams, these conformational changes can be very drastic, leading to irreversible denaturation (5).

Conformational changes at liquid interfaces are important for the stability of food emulsions, but our present understanding of them is largely qualitative. The occurrence of some processes involved, including unfolding and decrease of $\alpha$-helix content, is established, but there are only rough estimates of the consequences of these conformational changes for the overall size, shape and rigidity of the molecule, and the time scales of these changes . As direct means to quantify these parameters are not yet available, a detailed analysis under static and dynamic conditions of the adsorbed layers of proteins with different structural stability, as performed in this thesis, may shed some light on the relation between protein molecular structure and its role in emulsification and foaming.

1.3. From adsorption to emulsion and foam stabilization

Proteins are effective in emulsion and foam formation and subsequent stabilization. In this respect proteins are similar to low molecular weight surfactants.

Emulsification (the description for foaming is similar) can be defined as the break-up of large drops of one liquid in another, immiscible liquid. The resulting average drop size is in the 0.2 to 50 µm range. Due to this break-up the interfacial area in an emulsion is strongly increased. The excess Gibbs energy associated with this large interfacial area renders the emulsion thermodynamically unstable against phase separation. However, with the help of emulsifiers kinetic stability can be achieved over quite long time spans. The basic functions of emulsifiers to achieve this kinetic stability can be described simply as, first, to help make drops small and, second, to keep them small by retarding coalescence.

Emulsifiers facilitate break-up because they adsorb at the droplet interface. A consequence of this adsorption is that the interfacial tension is lowered and this lower interfacial tension is required to get break-up into smaller droplets at a given shear force (6,7). Insight into the adsorption behaviour of proteins and the resulting interfacial tension is conducive to the understanding of the emulsifying action of proteins.

An even more essential role of emulsifiers is the stabilising function, which retards the coalescence of the droplets, once they are formed. One of the mechanisms is that due to the presence of emulsifiers in the interface, gradients in interfacial tension can arise, which enable the interface to resist tangential stresses from the adjoining flowing liquids. The result will be that the liquid flow in the film between two approaching droplets will be retarded significantly (8,9). Thus, the stabilizing effect of emulsifiers is determined by the visco-elastic properties of the adsorbed interfacial layer. The relevance of dynamic interfacial properties in emulsification was extensively reviewed recently (10).

For low molecular weight surfactants, a model is available that describes dynamic interfacial behaviour under simple conditions in terms of material constants of the surfactant (11). The relevance of the interfacial viscoelasticity to drop break-up has been confirmed in experiments on single droplets under model conditions (12). For proteins, there is no complete model that can predict the interfacial behaviour under break-up conditions i.e. fast expansion. In the present investigation we report on a systematic study of all relevant aspects of this dynamic behaviour, in order to collect the building blocks for such a model.

1.4 Protein adsorption and dynamic interfacial behaviour.

1.4.1 Static properties

Proteins adsorb strongly at solid as well as liquid interfaces. Much attention has been paid to the adsorption at solid interfaces, which has led to a rather complete picture of the adsorption process at these interfaces (4,13,14). Effects of hydrophobic and hydrophilic interfaces and the consequences of both surface and protein charge have been established. These studies also show that upon adsorption most proteins undergo at least a limited change in conformation. Studies of the adsorption at liquid interfaces are more scarce, and less fundamental in character (15,16,17). For the interpretation of results concerning liquid interfaces we can make use of knowledge obtained from the adsorption at solid surfaces. However, we have to take into account that liquid interfaces offer more possibilities for conformational change because the interface is homogeneous and fluid. This implies that changes in area are possible and it may also allow parts of the molecule to protrude to a small extent into the hydrophobic phase.

It has been customary (18,19,20) to interpret the kinetics of protein adsorption in terms of the rate of various sub-processes taking place in or near the interfacial layer: (a) diffusion from the bulk solution to the sub-surface region in direct contact with the interface; (b) penetration of the protein molecule into the surface layer (the actual adsorption step); and (c) conformational changes of the adsorbed molecule. These conformational changes may include the partial unfolding of the molecule to bring at least some of its more hydrophobic segments from the interior of the molecule to the

interface. Various attempts have been made to assess the relative importance of the different physical processes taking place when proteins adsorb at liquid interfaces. In many cases the interpretation is solely based on interfacial tension measurements. This requires assumptions to be made about the relation between adsorbed amount and interfacial tension. The validity of these assumptions is not always self-evident and consequently the often detailed conclusions from these studies must be considered with reservation. Direct information about the adsorption process at liquid interfaces can only be obtained from direct measurement of the amount adsorbed. Such direct techniques are ellipsometry, neutron reflectometry and the radio-tracer method. Graham and Phillips (18) studied the adsorption of various proteins at the air/water and oil/water interface using the radio-tracer method. Adsorption results to be described in this thesis were obtained using the ellipsometric method. Neutron reflectometry (21) provides more detailed information about the adsorbed layer, for instance on the thickness and volume fraction profile normal to the surface. However, the measuring rate is too low for adsorption rate studies. Another direct method is based on spread protein layers. However, the spreading method is a very delicate one, because it is not always possible to ascertain that all spread protein is actually present in the interface (chapter 2 of this thesis and 22,23). Nevertheless, the use of this method has contributed considerably to the understanding of the behaviour of proteins at liquid interfaces (17,23). By slow compression of a spread layer (conformation in equilibrium), a surface equation of state ($\Pi$-A/$\Gamma$ curve) can be determined. Such a curve is also applicable to adsorbed protein layers, because differences between adsorbed and spread layers are likely to be small (16).

Many of the results indicate that adsorption is not always fully irreversible (23) and that, under strong/fast compression, conformational changes can lead to surface coagulation, i.e. to irreversible denaturation (5,24).

Insight into conformational changes of protein molecules in the interface, can also be obtained using the film transfer technique. Spread films can be transferred to a solid support and investigated by infrared spectrometry, optical rotatory dispersion and circular dichroism. The results lead to the overall conclusion that only the tertiary structure is significantly altered on adsorption and not the secondary structure. However, results are often ambiguous and there is little agreement between different workers (16).

It is questionable whether application of dynamic interfacial properties of spread protein layers to adsorbed layers is allowed. The reasons for this reservation are that, first, with spread layers any interplay between bulk solution and interface (as will occur during adsorption to a clean or expanding interface) cannot be taken into account, and second, during deformations of a spread layer at high frequencies or high rates there is also a considerable risk of protein loss to the solution or to a coagulate. This leads to the conclusion that dynamic behaviour of proteins is better studied with protein layers formed by adsorption than by spreading, and that dynamic results should preferably be

combined with directly measured adsorbed amounts. This combination of techniques will be used in the investigation described in this thesis.

1.4.2 Dynamic interfacial properties

Emulsification and foaming involve interfacial deformations that are both large and fast, and the response of the adsorbed layer to such deformations is crucial for understanding the role of proteins in food systems. The relevant time-scale of the break-up process in a homogeniser was estimated to be $10^{-3}$ seconds or even faster (25). The time scale of recoalescence during emulsification can be of the same order of magnitude. It is questionable whether proteins can adopt their equilibrium conformational at these short time-scales.

In the absence of an overall model that links the various sub-processes involved, the dynamic behaviour of proteins at interfaces must be determined by direct measurements. Methods that are available for this purpose are:

(i) surface shear measurements, which measure the response of the surface to changes in shape at constant area;

(ii) surface compression/dilation measurements, which measure the response to changes in area at constant shape.

Both measurements can be performed at small periodical deformations as well as under continuous expansion or shear (10,26,27). If the relaxation mechanisms are understood quantitatively the relation between periodical and continuous deformations can be formulated (10).

Recently, significant progress has been made in the field of dynamic interfacial processes at short time scales e.g. high expansion rate of drops (28,29) and high frequencies of compression/expansion (30,31)

For low molecular weight surfactants the dynamic behaviour is more or less fully understood and can often be explained in terms of properties of the surfactant, e.g. diffusion coefficients and surface-equation-of-state parameters. For proteins it has not been possible yet to build a comprehensive model in spite of many experimental data (18,20,27). Bottlenecks for building such a model from literature data are: (i) the data are obtained under different experimental conditions, e.g. pH, ionic strength, (ii) the same proteins from different sources will sometimes give different results, especially if the molecules have been modified, e.g., in radio tracer probing, and (iii) the experimental techniques that have been used are not always complementary.

1.5 Outline of this thesis.

This thesis will consider many aspects that determine the role of a number of representative adsorbed protein layers in foams and emulsions. The emphasis will be on the study of the behaviour of these layers under dynamic conditions, because of its

relevance for foaming and emulsification. The first step in the study of proteins at interfaces is its adsorption. This can only be investigated by using a direct method for the determination of the amount of protein that is present in the interface. To this end we constructed a sensitive ellipsometer.

In Chapter 2 the existing knowledge and models about the adsorption behaviour of proteins will be discussed. Main emphasis in this chapter will be on the adsorption behaviour of several proteins, as determined by ellipsometry. This involves the rate of the adsorption, the adsorption isotherms and the relation between surface pressure and surface concentration. The results will be related to structural parameters of the protein molecule.

In Chapter 3 the development of a method to measure the visco-elasticity modulus of adsorbed protein layers under compression and dilation will be described. The results will be explained on the basis of the static behaviour ($\Pi(\Gamma)$ curve) and the structure of the protein molecule. It is shown that relaxation is not caused by diffusion to and from the interface, but more probably by intermolecular and/or intra molecular structural rearrangements.

In Chapter 4 the dynamic behaviour of proteins adsorbed at three different interfaces (triacylglycerol-water, tetreadecane/water and air/water) will be compared. To this end a new experimental technique, the Dynamic Drop Tensiomenter, especially suitable to measure this behaviour at the oil/water interface, was developed. The results will be explained in terms of the structure of the protein and the degree of non-ideality of the adsorbed layer.

Using the conventional (Trough-Barrier-Plate) method it became obvious from preliminary dilational experiments that adsorbed protein layers showed a considerable resistance against shear deformation. In Chapter 5 a Double Ring Surface Rheometer will be described, which was developed to investigate the relative importance of this phenomenon. The shear modulus will be compared with the dilational modulus. The origin of the strong increase of the shear modulus with time and surface concentration will be discussed.

In chapter 6 it will be demonstrated to what extent models describing the surface equation of state of macromolecules are suited to describe the experimental $\Pi(\Gamma)$ curves of adsorbed protein layers. A comparison will be made between the applicability of (i) statistical theories, (ii) the Soft Particle Concept, a modification of Helfand theory, treating protein molecules as deformable soft particles and (iii) a 2-D solution model, a Frumkin-type expression, in which both entropy and enthalpy are being accounted for. The possibility to apply these models to the dynamic behaviour will be illustrated.

In chapter 7 the results obtained in the previous chapters will be applied to emulsions and foams. The consequences of the specific features of the static and dynamic interfacial behaviour of proteins for foaming, emulsification and stabilization are discussed. Conclusions about the relative importance of proteins and low molecular weight surfactants during emulsification and stabilization are drawn.

In chapter 8 the results are summarized.

1.6 References

1.      J.E. Kinsella. Functional Properties of Proteins in Foods: a survey. CRC Critical
        Reviews in Food Science and Nutrition 7 219 (1976)
2.      P.J. Halling. Protein-Stabilized Foams and Emulsions. CRC Critical Reviews in
        Food Science and Nutrition 15 155 (1981)
3.      T.E. Creighton. Proteins. Structures and Molecular Properties. W.H. Freeman
        and Co., New York, 515 (1983)
4.      W. Norde. Adsorption of Proteins from Solution at the Solid-Liquid Interface.
        Advances in Colloid and Interface Science 25 267 (1986)
5.      A.F. Henson, J.R. Mitchell, P.R. Musselwhite. The Surface Coagulation of
        Proteins during Shaking. Journal of Colloid and Interface Science. 32 162
        (1970)
6.      H.P. Grace. Dispersion Phenomena in high Viscosity Immiscible Fluid systems
        and application of Static Mixers as Dispersion Devices in such systems.
        Chemical Engineering Communication. 14 2257 (1982)
7.      R.A. de Bruijn. Deformation  and Break-up of Drops in Simple Shear flows.
        Chem. Eng. Sci. 48 277 (1993); PhD Thesis Technical University Eindhoven
        (1989)
8.      C. Marangoni. On the Theory of Surface Viscosity of Mr J Plateau. Nuovo
        Cimento, Ser, 5/6 239 (1872)
9.      J.W. Gibbs. On the Equilibrium of Heterogeneous Substances. Trans.
        Connecticut Acad., III: 108 343 (1878). Reprinted in: The scientific papers of
        J.Willard Gibbs, Volume 1, Dover Publications Inc., New York. p.55.
10.     E.H. Lucassen-Reynders. Dynamic Interfacial Properties and Emulsification.
        The Encyclopedia of Emulsion Technology, Volume 4, P. Becher, ed., Marcel
        Dekker, Inc. New York (1996)
11.     J. Lucassen, M. van den Tempel. Longitudinal Waves on Viscoelastic Surfaces.
        Journal of Colloid and Interface Science. 41 491 (1972)
12.     J.J.M. Janssen, A.Boon, W.G.M. Agterof. Influence of Dynamic Interfacial
        Properties on Droplet Break- in Simple Shear Flow. AIChE Journal. 40 (1994)
        1929.
13.     M. Bos. TIRF and its Application to Protein Adsorption. PhD Thesis
        Agricultural University of Wageningen (1994)
14.     J. Lyklema. Proteins at Solid-Liquid Interfaces, a Colloid-Chemical Review.
        Colloids and Surfaces, 10 33 (1984)
15.     P. Walstra, A.L. de Roos. Proteins at Air-Water and Oil-Water Interfaces: Static
        and Dynamic Aspects. Food Reviews International, 9(4) 503 (1993)

16. I.R. Miller, D. Bach. Biopolymers at Interfaces. Surface and Colloid Science, 6 185 (1973)

17. F. MacRitchie, Spread Monolayers of Proteins. Advances in Colloid and Interface Science, 25 341 (1986)

18. D.E. Graham, M.C. Phillips. Proteins at Liquid Interfaces. Journal of Colloid and Interface Science 70 403 (1979)

19. F. MacRitchie, A.E. Alexander. Kinetics of Adsorption of Proteins at Interfaces. Journal of Colloid Science 18 453 (1963)

20. G. Serrien, G. Geeraerts, L. Ghosh, P. Joos. Dynamic Properties of Adsorbed Protein Solutions. Colloids and Surfaces. 68 219 (1992)

21. E. Dickinson, D.S. Horne, J.S. Phipps, R.M. Richardson. A Neutron Reflectivity Study of the Adsorption of β-Casein at Fluid Interfaces. Langmuir 9 (1993) 242

22. H.J. Trurnit. A Theory and Method for Spreading of Protein Monolayers. Journal of Colloid Science. 15 1 (1960)

23. F. MacRitchie. Protein Adsorption/Desorption at Fluid Interfaces. Colloids and Surfaces. 41 25 (1989)

24. Prins, A.M.P. Jochems, H.K.A.I. van Kalsbeek, M.E. Wijnen, A. Williams. Skin Formation on Liquid Surfaces under Non-equilibrium Conditions. Progress in Colloid Polymer Science. 100 (1996) 321

25. P. Walstra, I. Smulders. Making Emulsions and Foams: An Overview. in "Food Colloids; Proteins, Lipids and Polysaccharides". E. Dickinson and B. Bergenstahl Editors (1997) 367

26. R. Miller, P. Joos, V.B. Fainerman. Dynamic Surface and Interfacial Tensions of Surfactant and Polymer Solutions. Advances in Colloid and Interface Science. 49 249 (1994)

27. E. Dickinson, B.S. Murray, G. Stainsby. Coalescence Stability of Emulsion-sized Droplets at a Planar Oil-Water Interface and the Relationship to Protein Film Surface Rheology. Journal of the Chemical Society Faraday Transactions.1, 84 871 (1988)

28. C.A. MacLeod, C.J. Radke. A Growing Drop Technique for Measuring Dynamic Interfacial tension. Journal of Colloid and Interface Science. 160 435 (1993)

29. V.B. Fainerman, R. Miller, P. Joos. The Measurement of Dynamic Surface Tension by the Maximum Bubble Pressure Method. Colloid & Polymer Science. 272 731 (1994)

30. K.D. Wantke, K. Lunkenheimer, C. Hempt. Calculation of Elasticity of Fluid Boundary Phases with the Oscillating Bubble Method. Journal of Colloid and Interface Science. 159 28 (1993)

31. D. Langevin (Ed.), Light Scattering by Liquid Surfaces. Surfactant Science Series. Marcel Dekker, New York, Chapters 11 and 16 (1991)

## 2 ADSORPTION AT LIQUID/LIQUID INTERFACES AND SURFACE PRESSURES OF PROTEIN SOLUTIONS.

### 2.1 Introduction.

The vital role of proteins in biology and technology cannot be understood without insight into the adsorption process and behaviour of proteins in adsorbed layers. A variety of biological systems of crucial importance are controlled by adsorbed proteins. Examples are membrane systems, the alveolar fluid in the lungs and dispersions of fat in milk and blood. Man has applied the stabilizing ability of proteins, adsorbed at air/water and oil/water interfaces in a variety of foods, including dairy products, dressings, ice cream, bakery products and foam on beer. Because of this widespread importance, there has been a long history of studies of proteinaceous interfacial films.

As early as 1840, it was pointed out by Ascherson (1), that proteins adsorb rapidly and spontaneously onto the surfaces of oil droplets in water to form "visible elastic skins". A variety of investigations on interfacial layers of proteins have followed this observation (for reviews see 2-11). Many of these describe protein adsorption at solid/liquid interfaces. In the case of liquid/liquid interfaces the investigations were mainly performed by studying protein layers obtained by spreading. Around 1970 methods for quantitative measurements of amounts adsorbed at liquid interfaces became available. This led to some detailed investigations on the adsorption rate and the adsorbed amount itself (12,13). Until then, information about adsorption was gained indirectly by measuring the surface pressure ($\Pi \equiv \gamma_0 - \gamma$, where $\gamma_0$ is the surface tension of the pure water and $\gamma$ that of the protein solution). To convert surface pressure data into adsorbed amounts, the $\Pi$-$\Gamma$ relation, obtained from spreading was used. This procedure ignores any possible difference between a protein layer obtained by spreading and by adsorption from solution. Since these differences are not always appreciable this method is still in use (14).

This chapter will first survey existing knowledge in the open literature. Interfacial studies on proteins have generated a fair amount of controversy. Some ambiguity results from the irreversible nature of the adsorption process, rendering the obtained results time and/or history dependent. Quality of the protein sample is another cause.

The present adsorption study is a comprehensive investigation into the adsorption behaviour of a set of proteins covering a broad range of molecular properties, such as molecular weight (M.W.), molecular structure and iso-electric point (I.E.P.). This study was performed using

ellipsometry, which is a direct method. The ellipsometric measurements were combined with surface tension measurements at one and the same interface. The results are used to investigate the applicability of existing models describing the adsorption rate, the adsorption isotherm and the surface equation of state.

2.2. Literature survey.

2.2.1 The adsorption process

Protein adsorption occurs at almost any surface be it solid or liquid, hydrophobic or hydrophilic, charged or uncharged. The implication is that at almost any interface the overall Gibbs energy decreases on adsorption of protein. Mainly from adsorption studies on solid surfaces the many contributions to this Gibbs energy could be identified (6,15). The main contributions are; (i) hydrophobic dehydration causing a positive entropy change upon adsorption, (ii) structural alterations inside the protein molecules, (iii) electrostatic interactions, (iv) van der Waals interaction and (v) specific binding. At liquid-liquid interfaces the overall picture will be similar, except that the roles of electrostatic interactions and specific binding will be less important. Adsorption at liquid/liquid interfaces also enables the more hydrophobic parts, such as hydrophobic amino acids (16) and the hydrocarbon side chains of the various amino acid residues, to protrude into the oil or air. Hence, more extensive unfolding is expected. Depending on conditions, extension of the interfacial area may also take place.

As to the kinetics of the process of protein adsorption and desorption most authors agree to a great extent (13,17,18). It has been customary to interpret the kinetics in terms of the sum of various sub-processes taking place in or near the interfacial layer (see fig 1):
1.   Transport of the protein molecule to the surface layer by diffusion and convection.
2.   The actual adsorption step (binding of the molecule to the interface).
3. Conformational change of molecules after adsorption (unfolding, denaturation). These conformational changes may include the partial unfolding of the molecule to bring at least some of its more hydrophobic segments from the interior of the molecule to the interface. The extent of these changes will depend on the stability or rigidity of the overall molecular structure, and the properties of the interface.
4. Detachment of the adsorbed molecule from the interface.
5. Transport from the surface layer into the solution.
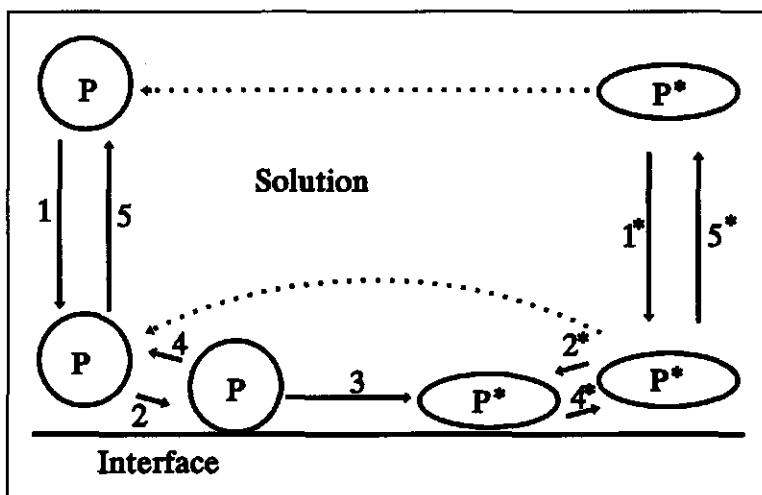
Figure 1

Schematic drawing of protein (P) adsorption and desorption. The asterisks indicate that the conformation of the protein has changed. Dotted arrows represent reactions that are considered less likely.

This division in distinct steps is an oversimplification of the real process. It is very likely that the conformational change is a more gradual process involving more sub-steps. Nevertheless a scheme like in Fig.1 may help to analyse our data.

Steps (1) and (2) are considered to be reversible, while step (3) is usually regarded as irreversible. Before step (3) has taken place, the molecules are in dynamic equilibrium with the bulk solution, which means that it is possible for them to diffuse back into the solution. Step (3) can be considered as a reaction, changing the protein molecule from one state into another. In the system there are now at least two different types of the same protein molecules (18). The general assumption is that, whereas the native protein molecule is still able to desorb by dilution, this has become less probable after a significant change in the conformation. However, under certain conditions (e.g., by compression of a spread layer to a high surface pressure) desorption can occur to a small extent (19). Desorption under these conditions is a very slow process. As pointed out by Dijt (20), very slow desorption is inherent to systems with high-affinity adsorption, where high adsorption values ($\Gamma$) are in equilibrium with very low bulk concentrations. An "energy barrier" against desorption can be expected when considerable conformational changes after adsorption hinder transport back into the solution (21). At hydrophilic interfaces, conformational rearrangements tend to be less extensive (6), and therefore protein molecules are less tightly bound to these interfaces, which makes desorption from these interfaces faster.

The presence of surface-denatured molecules in the solution has been observed by Norde et al. (21,23,24), implying that the conformational change from the surface-denatured to the

11

native state of the molecule in the bulk solution (upper-dotted arrow in Fig.1) is not very likely. So, essentially the adsorbent acts as a heterogeneous catalyst.

From the description given above it is clear that, compared to the adsorption of low molecular weight surfactants, the adsorption process of proteins is more complex. An important extra element in protein adsorption is the possibility of conformational changes affecting the surface pressure.

## 2.2.2 Conformational changes upon adsorption

When proteins adsorb on hydrophobic surfaces, conformational changes are likely to occur because in solution most of the hydrophobic groups will be buried into the interior of the molecule, whereas the hydrophilic groups tend to be directed towards the surface. So, upon adsorption at least part of these hydrophobic groups will be transferred from the interior to the outer region of the molecule. Fluid interfaces, i.e. air-water and oil-water interfaces, offer more possibilities for conformational change than solid interfaces, because they allow part of the molecule to protrude into the hydrophobic phase (16,22). Consequently, adsorbed proteins may assume a variety of conformations, ranging from an almost fully unfolded to an almost completely retained native conformation.

If the compact globular structure in solution is stabilized by hydrophobic interaction, while the sum effect of other structure determining factors favours a more expanded structure, structural rearrangement upon adsorption is probable, because adsorption will promote the formation of external hydrophobic interactions, at the expense of the internal ones. The structural rearrangements may include changes in the $\alpha$-helix and $\beta$-sheet content (stabilized by hydrogen bonds) of the protein molecule (21,23,24).

The idea that irreversibility of adsorption is related to the extent of the conformational changes upon adsorption is in line with the findings of Jönsson et al. (25). They found that lysozyme, a rigid globular protein, with little change in conformation upon adsorption, readily desorbed after dilution. Desorption experiments were performed after adsorption at hydrophilic silica, a type of surface which only gives rise to limited further conformational changes (26).

## 2.2.3 Kinetic models

In the absence of convection, the first step of the adsorption process can be viewed as one-dimensional diffusion involving a single mobile solute and an infinitely large flat surface. An expression relating the rate of adsorption to the diffusion properties of the solute was obtained by Ward and Tordai (27). In the absence of an adsorption barrier and assuming the diffusion

coefficient D to be independent of the concentration, the rate is given by

$$\frac{d\Gamma}{dt} = \left(\frac{D}{\pi}\right)^{1/2} \left\{ c_0 t^{-1/2} - \frac{1}{2} \int_0^t \left[ c_s \frac{\tau}{(t-\tau)^{3/2}} \right] d\tau \right\} \tag{1}$$

and the time-dependent surface concentration by

$$\Gamma(t) = 2\left(\frac{D}{\pi}\right)^{1/2} \left\{ c_0 t^{1/2} - \int_0^t {}^{1/2} c_s(\tau) d(t-\tau)^{1/2} \right\} \tag{2}$$

where $c_s$ is the concentration in the sub-surface (= region in direct contact with the surface), $c_0$ is the initial concentration and $\tau$ is a dummy variable. In equations (1) and (2), the first term in the curly brackets accounts for solute diffusion from bulk solution to the uncovered interface, and the second term (the integral) accounts for the retardation of adsorption due to the fact that the surface layer becomes occupied. The second term can be neglected if $c_s \ll c_0$, which is always the case in the initial stages of adsorption at a clean surface ($\Gamma=0$ at $t=0$). Hence, the rate of adsorption and the adsorption itself are then given by

$$\frac{d\Gamma}{dt} = c_0 \left(\frac{D}{\pi t}\right)^{1/2} \tag{3}$$

$$\Gamma(t) = 2c_0 \left(\frac{Dt}{\pi}\right)^{1/2} \tag{4}$$

Equations (1)-(4) describe the time dependence of $\Gamma$ in terms of only solution parameters ($c_0$, $c_s$ and D). This means that during the initial stage of adsorption, Eq. 3 and Eq. 4, the surface properties do not affect the adsorption kinetics. Whether or not conformational changes occur after adsorption does not matter. However, after longer adsorption times the properties of the already adsorbed proteins do affect the adsorption kinetics through the integral terms in Eq. 1 and Eq. 2, and the extent to which this occurs depends on the extent of the conformational change.

For solid surfaces several models have been postulated to describe the further steps of protein adsorption .
a) The Lundström model (30).

13

In this model it is assumed that protein adsorbs in their native state (combined effect of steps 1 and 2, Fig. 1). Upon adsorption, some of the adsorbed proteins in their native state may conformationally change and become denatured (step 3, Fig. 1). According to this model desorption does not occur. Using the number of molecules per unit area and the areas of the fractions occupied in both states, Lundström derived a set of equations, starting with the adsorption rate of the native molecules and the rate of formation of the denatured molecules. The model produces adsorption isotherms that are similar to those experimentally observed.

b) The Beissinger and Leonard model (29).

This model accounts for desorption of both native and denatured adsorbed species (step 4 and 4* respectively in Fig. 1). They derived a set of equations for the rate of change of fractions of the surface area that are occupied by native and denatured protein molecules.

Using their model they were able to fit their experimental data concerning albumin adsorption on quartz. From the fitted rate constants it appeared that the desorption rate of protein molecules with a conformation change is two orders of magnitude lower compared to that of the native molecules.

c) The Walton-Soderquist model (28).

In this model it is assumed that protein adsorption is reversible for short adsorption times. The adsorbed protein molecules change their conformation towards optimal interaction with the interface. In this model three steps can be distinguished; (i) an adsorption step, the rate of which is proportional to the area available for adsorption (combined step 1 and 2, Fig. 1), (ii) a desorption step, the rate of which is proportional to the adsorbed amount (combined step 4 and 5, Fig. 1) and (iii) the conformational change (step 3 Fig. 1) of the adsorbed molecules, which causes a decrease of the desorption rate with time. A disadvantage of this model is that even after long adsorption times the adsorbed layer must contain desorbable molecules. This is very unlikely because this would mean that there are protein molecules bound to the interface without any conformational change.

d) Another interesting approach to the modelling of protein adsorption is the concept of Random Sequential Adsorption (RSA) as described by Schaaf et al. (31). RSA is essential surface-filling governed by geometry and does not allow for desorption or diffusion of the protein over the surface. It may be considered as the opposite of fully reversible equilibrium adsorption. An important result of this theory is that a so-called jamming limit of surface coverage is reached, beyond which no additional molecules can be accommodated in the surface. For circular disks the jamming limit of surface coverage is 0.547. The fact that coverage of protein adsorption is known to reach much higher values (close to 1) proves that some desorption and/or surface diffusion must occur. Otherwise stated, for proteins, the constraints are too restrictive, and this model is certainly not applicable for liquid-liquid interfaces.

14

Although these models tend to fit experimental data reasonably well, their value is limited. The reason is that the set of equations used contains too many adjustable parameters as rate constants and fractions of native and denatured molecules and it impossible to determine these parameters in an independent way.

For fluid interfaces, Serrien et al. (18) evaluated a model to describe the surface pressure as a function of the adsorption time. The starting point of this model is the adsorption of native molecules by diffusion. Once at the surface some of the native molecules unfold (surface denaturation). So far this model is similar to the Walton Soderquist model. However, in the Serrien model it is assumed that in the surface an equilibrium is established between both modifications: native and unfolded. It is supposed that only native structures are directly exchangeable with the subsurface. Initially this model was developed for low molecular weight surfactants that show a kind of conformation change in the interface. Their model was tested using a variety of experimental techniques: static drop experiments ($\Pi$-t), experiments at constant rate of surface expansion, dilational modulus and stress relaxation experiments. They concluded that their results with proteins are well described by their equations. The model is consistent with an initial diffusion process and the occurrence of at least two reaction steps in the surface could be deduced from the results.

Guzman et al. (32) and Hunter et al. (33,34) described protein adsorption to gas-liquid interfaces using a modified Langmuir model, incorporating coverage-dependent rate constants. In this model both tight adsorption of a first layer and loose packing of a second layer were included. The model further assumes that the first and second layer are both in equilibrium with the protein solution just below the surface. These models adequately fit measured adsorption isotherms of $\beta$-casein and lysozyme. The results indicate that formation of a second layer starts above a certain concentration.

Douillard and Lefebvre (35) described a kinetic and statistical mechanical model based on the Guzman (32) approach. The model assumes that protein adsorption occurs in two layers. The first layer, in which a protein can adopt two conformations, allows for saturation; in the second one, proteins are adsorbed less specifically and without saturation. At equilibrium the first layer is in equilibrium with the second layer, which itself is in equilibrium with the solution. For caseins the model indicates one conformation in the first layer, while for globular proteins best fits are obtained with two conformations in that layer. As in the former model, formation of a second layer starts above a certain bulk concentration.

Most of the above models assume conformational changes upon adsorption. Due to these conformational changes the adsorbed molecule is supposed to be at least partly denatured (here denaturation is defined as an irreversible conformational change). Dickinson et al. proposed that this partly denatured state is close to what is called the "Molten Globule" State (10). This is the partially denatured state of a globular protein which retains the ordered

secondary structure but not the tertiary structure of the native molecule. For some proteins (lactoglobulins) one such stable intermediate state between native and denatured has been identified. For a reduced form of BSA a similar intermediate state is known, but, in contrast with the "Molten Globule" assumption, with a changed secondary structure. This is in line with the finding of Norde et al. (23,24) that adsorbed protein molecules have a reduced helix content. It is likely that future research will show additional well defined intermediate states. Horbett (36) has pointed to the possibility that different processes may lead to protein structural rearrangements or conformational changes on adsorption at a surface. This author suggested the possibility of a continuous range of conformational states of the protein adsorbed on the surface. This view is in line with models for protein adsorption (37) and (38) (see section 2.7.4 and chapter 6) in which a continuous change of molar area of the protein molecules in the surface layer is assumed.

In many protein adsorption studies the existence of an adsorption barrier, also operational during the initial stage of the adsorption is proposed. However, most of the results can be explained by barrier free diffusion controlled adsorption. For the region of relatively high adsorption, MacRitchie and Alexander (39) proposed a model for the existence of a specific adsorption barrier. According to this model, information about this barrier could be obtained from the time-dependence of the surface pressure by plotting $\ln(d\Gamma/dt)$ [or even $\ln(d\Pi/dt)$] versus $\Pi$. Linearity of such a plot indicates the presence of an adsorption barrier, and the slope provides the area occupied by an adsorbed protein molecule. This idea is based on the Ward and Tordai (27) model originally introduced for low-molecular-weight surface active agents. The assumption is that, at high surface coverage, adsorption requires clearance of part of the surface with an area equal to the mean molecular area $A_m$, through compression of the molecules already adsorbed. The activation energy of the process is then equal to $\Pi A_m$. If, in addition, protein adsorption is assumed to be irreversible, the rate of adsorption is given by

$$d\Gamma/dt = k_1 a_b \exp(\Pi A_m/kT) \tag{5}$$

where $k_1$ is a rate constant, and $a_b$ is the protein activity in bulk solution. When $A_m$ is taken to be constant, equation (5) predicts a linear relationship between $\ln(d\Gamma/dt)$ and $\Pi$, the slope being proportional to $A_m$.

MacRitchie and Alexander (39) have applied equation (5) to various protein solutions and have found that for $4 < \Pi(mN/m) < 10$ the required linear relationship holds. Linearity was also found when $\ln(d\Pi/dt)$ was plotted against $\Pi$, which supported their finding that, in the same range of surface pressure, $d\Gamma/d\Pi$ obtained from the $\Pi$-A curves of the spread proteins is

constant. In formula,

$$\ln(d\Pi/dt) = K - (\Pi A_m/kT) \qquad \textbf{(6)}$$

where K is a constant. However, the area $A_m$ obtained from the slope of the experimental plots was much smaller than expected from the dimensions of the protein in solution, and led the authors to suggest(39) that only a small part of a protein molecule needs to penetrate the surface layer for it to remain attached and to unfold.

The same procedure was adopted by other workers (13,40) who often used equation (6) directly without checking whether the condition of constant $d\Gamma/d\Pi$ is actually satisfied in the surface pressure range considered. In agreement with MacRitchie and Alexander it is usually found that $A_m$ is much smaller than the molecular size in solution. We think that such conclusions are premature for three reasons. In the first place, in Eq. 5 $a_b$ should be replaced by $a_s$ (= protein activity in subsurface), otherwise the barrier process is mixed up with the diffusion process. Secondly, it is uncertain whether the assumption of irreversible adsorption is actually satisfied for proteins, as shown by MacRitchie(41), who observed desorption at high surface pressures. And thirdly, it seems physically unrealistic to assume that globular proteins would be able to contact the surface through a relatively small hole in the adsorbed layer (of area <20% of the protein cross-section(39)). This would require major changes in macromolecular shape, which seems unlikely for such rigid proteins (see section 2.7.4 "surface equation of state" and Chapter 6 ).

Hansen and Myrvold (14) used a slight modification of equation (5), with an activation energy that can be interpreted as either the work against the surface pressure ($\Pi A_m$) or electrostatic energy, $q\Psi$, where q is the charge of the molecule and $\Psi$ is the surface potential. Their experiments were better described by assuming an activation energy, E, proportional to the surface concentration in stead of proportional to the surface pressure. This may indicate that the activation energy is of an electrostatic nature. However, this seems to disagree with the finding that the effect of pH on E is small.

Kinetic models can be useful to describe the adsorption process, provided the rate constants of the sub-processes are properly separated. It is also essential to have reliable experimental results from which the rate constants and other adjustable parameters can be deduced. However, a real experimental verification will be difficult. For instance, the ratio native/denatured is difficult to determine by an independent measurement. Up to now these detailed models have not established a clear relation between conformational changes and desorbability. A more fundamental problem is that all kinetic models require knowledge of

17

the surface equation of state, otherwise it is impossible to establish whether deviations are due to the kinetic model or due to the equation of state model.

2.2.4 Equilibrium models

Equilibrium surface properties (adsorption isotherms and surface equations of state) for low molecular weight surfactants can be determined from the change of surface pressure with the substrate concentration by using the Gibbs (42) adsorption equation:

$$d\Pi = RT(\Gamma dlnc_p) \qquad (7)$$

However, for synthetic polymers or biopolymers application of Gibbs adsorption equation is generally found to give unrealistically low values of the surface area per molecule (3,43) and an isotherm of the wrong shape with too low values for the surface pressure (12).

The apparent inapplicability of the Gibbs adsorption equation to protein adsorption cannot easily be pinned down to one single factor. For synthetic polymers the problems that arise when applying this equation are due to the fact that these polymers consist of a mixture of components which differ considerably in surface affinity due to differences in molecular weight and composition (44,45). This cannot be the reason for the inapplicability of the Gibbs equation in the case of pure proteins where all molecules have the same M.W. and composition.

As the Gibbs law is universally applicable, the inapplicability must be only apparent. Possible reasons may be: (i) irreversibility of adsorption, which causes that equilibrium between surface and solution is not attained, even after very long adsorption times. (ii) non ideality of protein solutions, caused by association in solution. (iii) the contribution to the surface activity is different for the different segments and the number of adsorbed segments may decrease with increasing adsorption. (iv) the formation of a multi-component system due to conformational changes.

Several authors (46,47,48) have attempted to analyze their protein adsorption data in terms of the Langmuir (or modified Langmuir, such as Frumkin-Fowler-Guggenheim) theory of adsorption. However, any agreement of an experimental isotherm with one of these corresponding equations is fortuitous since, in the case of protein adsorption, virtually none of the Langmuir premises is satisfied. Apart from the problem of reversibility, it is not justified to ignore (i) the fact that there is no equality of molecular size of protein and solvent (49), (ii) the conformational change of proteins and (iii) lateral interactions between the molecules should not be ignored. Consequently, values for the Gibbs energy of adsorption

18

derived from a Langmuir or analogous analysis are without any physical meaning.

In the past several, often closely related, statistical polymer adsorption theories (50,51,52,53) have been used to describe the adsorption behaviour of synthetic random coil polymers. Especially the more recently developed Advanced SF Lattice theory (45) has proven to be valuable to describe the adsorption of such polymers. However, for application of these theories to proteins, major adaptations have to be made. As polymers, protein molecules adsorb with many segments at an interface, but most protein molecules are very different from random coils. In general, proteins have a more compact, rigid structure, which is mainly determined by specific interactions between the different amino-acid residues (54). As in synthetic polymers, there are internal degrees of freedom in a protein molecule, but their role is less important. In addition, proteins always have a net electrical charge depending on pH and salt concentration. To extend the statistical polymer adsorption theories to protein adsorption the internal structural elements and structural changes upon adsorption have to be taken into account. Consequently a quantitative elaboration will be very complicated and is not expected to be possible in the near future.

Models (see also section 2.7.4 and Chapter 6) that require no detailed molecular structure parameters are:

(i) A two dimensional solution model, put forward recently, in which both entropy and enthalpy are considered (55). The entropy term accounts for the size difference between solvent and polymer by introducing a size parameter S and the enthalpy term H accounts for the non ideal heat of mixing. Using realistic values for S and H, $\Pi(\Gamma)$ curves up to almost full monolayer adsorption can be described. A key element in this model is the prediction of phase separation at very low surface pressures and surface concentrations, for sufficiently high values of H. This describes the almost constant low surface pressure up to surface concentrations $> 0.5$ mg/m$^2$ and the subsequent steep rise of $\Pi$ often found for compact proteins.

(ii) A two dimensional fluid model, the Soft-Particle Model (38), in which adsorbed proteins molecules are modelled as deformable (visco-elastic) particles. The size and shape of these particles are determined by the interplay between external and internal forces. This qualitative model fairly well describes the characteristic features of the surface equation of state of adsorbed protein layers.

19

2.3 Ellipsometry as a tool to study adsorption of proteins and synthetic polymers at the air-water interface.

2.3.1 Methods for adsorption studies.

In ref. 45 an extended survey is given of the numerous techniques that are in use to study the adsorption of proteins and synthetic polymers. All techniques have their advantages and limitations. For instance, reflectometry (20) is a powerful tool to study the adsorption rate, but it does not provide details such as thickness or volume fraction of the adsorbed layer. In addition, the technique is not suitable for adsorption studies at most liquid interfaces, because the refractive index changes due to adsorption are too small. Neutron reflectometry (56,57), on the other hand, provides more detailed information about the adsorbed layer, for instance on the thickness and volume fraction profile normal to the surface. Generally, however, the measuring rate is too low for adsorption rate studies. This technique has proven suitable for measurements at liquid/liquid interfaces. Ellipsometry (see below) is a technique which has almost exclusively been applied to adsorption at solid surfaces. It combines to a certain extent the advantages of both methods. The method is sufficiently fast to study parts of the adsorption process and sufficiently sensitive, even at the water-air interface, to determine thickness and volume fraction of the adsorbed layer. The radiotracer method has proven to be a reliable method to determine adsorbed amount and adsorption rate, not only at the air-water (13,34,58-60) but also at the oil-water interface (58,61). The main disadvantage of this technique is that radioactive labelling modifies the native protein molecule to a certain extent (62,63). The surface force technique is not only suitable to determine interaction between adsorbed protein layers, but also provides information about the thickness and structure of the adsorbed layer (7). The application, however, is restricted to adsorption onto solid surfaces.

Recently some new techniques have become available that provide information about certain aspects of the structure of the adsorbed layer. For example with total internal reflection fluorescence (TIRF), the translational and rotational diffusion of adsorbed proteins may be observed in detail (64). Fluorescence recovery after photo-bleaching (FRAP) gives information about the diffusion rate within the adsorbed layer (65). Reduced mobility within the surface points to interaction between adsorbed molecules. Volume fraction profiles of proteins adsorbed on particulate dispersions can be obtained with small angle neutron scattering (66). With FTIR-ATR (67) surface-induced changes in the secondary structure can be analyzed. With NMR the numbers of segments present in trains and loops can be measured, because the nuclear relaxation times of bound and free segments are different.

2.3.2 Ellipsometry

Ellipsometry is a sensitive optical technique which can be used for measuring the thickness and refractive index of thin films at interfaces. It is based on the fact that, in general, a thin film affects the change in the polarization state of an elliptically polarized light beam reflected by the interface. For a comprehensive review, theoretical aspects and developments over the past 40 years, see Refs. 68-72.

Ellipsometry has almost exclusively been applied to protein and polymer adsorption at solid surfaces (73-75). To apply ellipsometry to the air-water interface a more sensitive set-up is required, because in general the changes in the polarization state are much smaller because of the smaller refractive index difference between adsorbed layer and substrate. The ellipsometer used in this investigation has been described in detail elsewhere (76).

To obtain the required sensitivity, polarizer and analyzer were mounted in rotatable devices, provided with scales which can be read to 10 sec. of arc and the extinction settings were accurately determined from the readings of equal light intensity at either side of the extinction. The ellipsometric parameters $\Psi$ and $\Delta$ (tan $\Psi$ = the change of the amplitude ratio due to reflection and $\Delta$ = the change in phase difference) were determined in two of the four possible zones (77). Basically, the thickness and refractive index (n) of the adsorbate can be obtained from the changes $\delta\Psi$ and $\delta\Delta$ caused by the presence of the adsorbed layer. As the refractive index is related to the concentration of the adsorbate, $\Gamma$ can also be found. The method is not unambiguous because a distribution n(z), with z normal to the surface, has to be assumed. However, for the computation of $\Gamma$, which essentially follows from an integration of the excess density as a function of z, the choice of n(z) is not sensitive. In fact, the resulting $\Gamma$ does not at all depend on it if dn/dc is linear in bulk and adsorbate (76). For proteins this was found to be the case up to the highest concentration that could be obtained (0.4 g/ml). The refractive index and thickness of the film as calculated from $\delta\Psi$ and $\delta\Delta$ represent optical averages. Each measurement (determination of extinction settings in the two zones) took 5-10 min. and the error in $\delta\Psi$ and $\delta\Delta$ is then 0.003° and 0.02°, respectively. To check the reliability of the ellipsometric results, we compared $\Gamma$ as determined by ellipsometry with the results of two independent techniques: (1) a spreading technique (Trurnit method, ref.78) by which a known amount of protein is spread on the surface of a buffer solution (pH=6.7, I=0.01 eq/l) with a known surface area. (2) a radiotracer method, using radioactively labelled protein. The spreading experiment was performed with β-lactoglobulin and for the radiotracer experiment radioactively labelled β-casein was used. The results of this reliability check are given in Table 1.

The comparison with spreading at higher $\Gamma$ values is less reliable because of the risk of protein loss by dissolution in the bulk phase. The agreement between the results is

21

satisfactory.

Table 1
Comparison between adsorbed amounts obtained by ellipsometry, spreading and the radiotracer method.

| surface concentration mg/m$^2$ | | |
|---|---|---|
| ellipsometry | spreading (β-lactoglobulin) | radiotracer (β-casein) |
| 1.00 1.05 | 0.98 1.09 | |
| 2.5 | | 2.7 |

The combination of the ellipsometric parameters $\delta\Psi$ and $\delta\Delta$ is interpreted as giving the thickness and refractive index of an homogeneous adsorbed layer. In ref.76 it was shown that, due to the experimental error in these two parameters, especially at low $\Gamma$ values ($\leq 1$ mg/m$^2$) the uncertainties of the thickness and refractive index are too large to obtain meaningful values. However, as indicated above, the uncertainty in $\Gamma$ is much smaller because the errors in thickness and refractive index tend to compensate each other. At higher $\Gamma$ values, thickness and refractive index become better reproducible. A comparison of these data with e.g. molecular dimensions and results obtained by other techniques, e.g. neutron reflectivity, will be given in sections 2.6 and 2.7.3 of this chapter.

2.4 Molecular properties and existing knowledge about the adsorption behaviour of the proteins under investigation.

The choice of the set of proteins to be investigated is based on the conditions that (i) pure samples of the proteins must be available, (ii) the proteins must be relevant for food systems, (iii) the set of proteins must cover the whole range of molecular properties (MW, structure) being relevant for interfacial behaviour and (iv) there must be a fair amount of existing knowledge about their adsorption. Based on these considerations the following set of proteins was chosen: Caseins (β-casein, κ-casein and Sodium-caseinate), Bovine Serum Albumin (BSA), Ovalbumin and Lysozyme.
Most of the published adsorption studies at the air/water interface were based on surface tension measurements. However, conclusions solely based on surface tension measurements are open to considerable doubt. The method is reliable only if the relation between surface tension and surface concentration is known. In general this information was not available (see

22

below).

## 2.4.1 Molecular properties of the proteins.

A survey of the molecular properties that are thought to be relevant for adsorption is given in Table 2. Ovalbumin is a glycoprotein from egg white. Its overall aminoacid composition is known and part of the sequence has been elucidated (79). From viscosity measurements (80) it is concluded that the native ovalbumin molecule is compact and globular. This compact structure is caused by the relatively high amount of $\alpha$-helix and $\beta$-sheets and the internal disulphide bond.

Lysozyme also is an egg white protein. Its amino acid composition is known and the sequence has been elucidated (81). The molecule is globular and rigid (26) resulting from the four disulphide bonds. The conformational stability is high (11). Its IEP is 10.7. This is much higher than that of the caseins, ovalbumin and BSA, which are between 4.5 and 5.0.

Table 2 Molecular properties of the proteins investigated.
References are in brackets.

| | Ovalbumin | Lysozyme | $\alpha_s$-casein | $\beta$-casein | $\kappa$-casein | BSA |
|---|---|---|---|---|---|---|
| Molecular weight (Dalton) | 45.000 | 14.500 | 23.500 | 24.000 | 19.000 | 69.000 |
| $\alpha$-helix (%) $\beta$-sheet (%) | 30 27 (87) | 42 (26) | 10 20 (88) | 1-10 13-16 ( 88) | 14 31 (88) | 55 16 (88) |
| cystein/mol S-S bridges/mol | 4 (79) 1 (79) | 8 (81) 4 (81) | | | 2 (88) 1 (82) | 35 (88) 17 (88) |
| structure of molecule | compact globular (80) | rigid globular (26) | random coil (82) | random coil (82) | | less * rigid (11) |
| dimensions (nm) shape | 2.9 spherical (80) | 4.5*3*3 ellipsoidal (81) | prolate ellipsoidal (88) | 15*1.5 prolate ellipsoidal (88) | 9.7 sphere (88) | 14*3.8 ellipsoidal (85) |
| diffusion coefficient $(m^2s^{-1})$ | $0.7*10^{-10}$ (89) | $1,2*10^{-10}$ (91) | $0.7*10^{-10}$ (90) | $0.7*10^{-10}$ (90) | $0.6*10^{-10}$ (90) | $0.6*10^{-10}$ (92) |
| I.E.P. | 4.7 | 10.7 | 5.1 (93) | 5.3 (93) | 4 (93) | 4.9 (88) |

\* compared to ovalbumin and lysozyme

Casein from milk consists of a mixture of $\beta$-casein (37%), $\kappa$-casein (15%) and $\alpha_s$-casein

(45%). $\alpha_s$-and $\beta$-casein both have a more or less random coil structure when dissolved in water. $\kappa$-casein is a protein with a considerable internal structure caused by the intra-molecular disulphide bridge (82).

Bovine serum albumin (BSA) is a globular lipo-protein. Its overall aminoacid composition is known (83). BSA contains 1 SH-group and 17 disulphide bridges per molecule (84). The classical perception of the structure of BSA is cigar-shaped with dimensions of the molecule of 14*3.8*3.8 nm (85). However, low resolution dark-field electron micrographs indicated a U-shaped molecule with dimensions of about 8 nm (86).


2.4.2 Adsorption at the air-water interface of the proteins investigated; brief survey of existing knowledge.


The adsorption of ovalbumin at the air-water interface was studied by many investigators (39,94,95,96). In general indirect methods were used. Blank et al. (95) studied the adsorption kinetics of ovalbumin using surface tension measurements. They concluded that the adsorption rate has a maximum at the isoelectric point (IEP=4.7). The rate also increases with increasing ovalbumin concentration. In addition, Bull (96) determined the adsorption isotherm and the desorption rate from compressed surface layers. Ishii and Muramatsu (94) observed an optimum spreadability of ovalbumin at the air-water interface near the IEP.

The adsorption of lysozyme at the air-water interface has been extensively studied by many authors (13,40,58,59,97-100). In refs. 40, 97 and 98, indirect methods were used. Yamashita and Bull (97) studied the adsorption of lysozyme by using the $\Pi$-$\Gamma$ relationship obtained from a pressure vs. area curve of a spread film. They concluded that the adsorbed film of lysozyme was much more condensed than the spread film. Evans et al. (98) and Tornberg (40) studied the adsorption kinetics using surface tension measurements. Graham et al. (13,58,99)and Xu et al. (59) studied the adsorption of lysozyme with a radio-tracer method. This method has the disadvantage that the protein had to be modified by acetylation or methylation, which is known (62) to increase the surface activity. In ref. 100 a modified surface tension measurement is used to determine the adsorption rate. During the adsorption experiment, the surface is compressed at certain time intervals to a surface pressure at which the adsorption was known from the literature (101), followed by expansion to the starting area.

The adsorption of $\beta$-casein has also been studied by several investigators (13,40,98,58,99,34, 60). In some of these investigations adsorption was studied using surface pressure measurements, in others (13,58,99,34,60) a radio-tracer method was used. The radio-tracer procedure provides reliable information about the adsorption of the labelled protein, but it is very likely that these results deviate from those for a native, unlabelled protein, as in the case of lysozyme.

From literature little or no information is available about the adsorption of $\alpha_s$-casein and $\kappa$-casein.

Finally, BSA has also been studied intensively by many authors (13,14,40,58,98,99,102-104 ). In some of these investigations adsorption was studied using surface pressure measurements, in others (13,58,60,99) a radio-tracer method was used.

By using neutron reflectivity, detailed information about the adsorbed layer at equilibrium has been obtained for $\beta$-casein(56,105) and BSA (57).

## 2.5. Experimental

### 2.5.1 Materials

$\beta$-casein and $\kappa$-casein were prepared from acid casein according to the procedure described in ref. (12).

Na-caseinate (whole casein) was obtained from DMV and used without further purification. Ovalbumin (grade V), BSA (grade V) and lysozyme (grade I) were obtained from Sigma Chemicals. They were used as received.

PVA 205 (M.W.=42.000) was obtained from Kurashiki, Japan.

In all experiments buffered solutions (see section 2.6), made up with twice-distilled water, were used. The chemicals used for preparing the buffers were all of analytical grade. One hour before each experiment a fresh protein solution was prepared at room temperature, and at the pH of the measurement.

### 2.5.2 Techniques

The surface tension and the surface concentration were determined as a function of time at the same interface. Surface tensions were measured with a reproducibility of 0.2 mN/m using the static Wilhelmy plate method with a roughened glass plate attached to a force transducer. Between the different experiments the plate and the trough were cleaned by first rinsing with water and storing it for at least one hour in a mixture containing 80% ethanol, 10% KOH and 10% water. After this treatment the plate was rinsed thoroughly with twice-distilled water. Contact was made between plate and surface immediately after filling the teflon trough (10*7*2 cm), and the force measured with the plate remaining in the same fixed position until the end of the experiment (in most cases for at least one day). The straight, horizontal shape of the contact line between plate and solution meniscus indicated that the plate was well wetted during the entire experiment. Surface tension was monitored continuously as a function of time. Solutions were poured into the trough with the help of a separating funnel, the tip

25

of the funnel remaining above the surface of the solution, in order to prevent aged surface of the original solution from entering into the trough.

Surface concentrations (adsorption) were determined with the ellipsometrical technique described in ref. 76. The trough was covered with a lid to reduce evaporation. There was a hole in the lid for the suspending wire of the Wilhelmy plate, and small slits for the incident and the reflected light beam. The refractive index and average optical thickness of the adsorbed layer were obtained from the change of state of polarization of the light beam upon reflection at the surface. To calculate the average concentration in the adsorbed layer from the refractive index, using a specific refractive index increment of 0.18 ml/g for proteins as experimentally determined for concentrated protein solutions(5-40%) (76) and 0,155 ml/g for PVA (106). This value combined with the thickness of the layer, gives the surface concentration $\Gamma$. At high protein concentrations ($>10^{-2}$ %), a correction is made for the fact that the refractive index of the buffer solution is increased by the protein. Each ellipsometric measurement takes 5-10 minutes. The experiments were performed in a temperature-controlled room at 22±1 °C.

## 2.6. Results

Figs. 2A-7A give the adsorption or surface concentration ($\Gamma$) as a function of the square root of the adsorption time ($t^{1/2}$) for $\beta$-casein, whole casein, $\kappa$-casein, ovalbumin, lysozyme, and BSA respectively. For whole casein and $\kappa$-casein the experiments were performed in a phosphate buffer at pH=6.7 and I=0.01. With $\beta$-casein the buffer composition was slightly different; pH=7.0 and I=0.1. In the case of ovalbumin (pH=6.4, 4.6 and 3.6) and lysozyme (pH=6.7) a phosphate-citrate buffer (I=0.02M) was used. For BSA a phosphate buffer (I=0.03M) at pH=6.7 was used. For comparison purposes the adsorption rate of a synthetic polymer PVA (type 205, MW= 42000), with a molecular structure even more flexible than that of $\beta$-casein, is given in Fig. 8.

The thicknesses of the adsorbed layer of the different proteins at various $\Gamma$'s are given in Table 3. Only thickness values at $\Gamma \geq 1$ mg/m$^2$ are given, for reasons given above. In this Table thicknesses determined by neutron reflectivity (56,57,105,107-109), surface force measurements (7) and ellipsometry at solid/water interfaces (74,110) have also been included. The general trend is that the thickness increases with $\Gamma$. This increase continues up to the highest value of $\Gamma$ for caseins, ovalbumin and lysozyme. For BSA and PVA a plateau value was found. Generally the agreement between the thicknesses determined with the various methods is good. For ellipsometry and neutron reflection this is not surprising as both methods are based on refractive index contrast. It must be noted that, for ellipsometry, h represents the mean thickness of the adsorbed layer, assuming the adsorbed layer to be

26

homogeneous (76). The protein concentration in the adsorbed layer was found to range from 0.3 to 0.7 g/ml, which is in fair agreement with neutron reflectivity measurements (56,105,57).

Table 3. The thickness (nm) of the adsorbed protein layer for different values of the surface concentration. (* ovalbumin concentrations $\geq 1$ g/l)

| Ellipsometric thickness of the adsorbed protein layer (nm) | | | | | | | | |
|---|---|---|---|---|---|---|---|---|
| Adsorption mg/m² | β-casein | Whole casein | κ-casein | Ovalbumin | | Lysozyme | BSA | PVA |
| pH ⇒ | 7.0 | 6.7 | 6.7 | 4.6 | 6.4 | 6.7 | 6.7 | |
| 1 | | 2 | 2.5 | 1.5 | 1.5 | 2.5 | 2 | 5-8 |
| 1.5 | 2.5 | | | 2 | 2 | 3 | 3 | 6 |
| 2 | 6 | 5 | 5 | 2.5 | | 3.5 | 2.5 | 6-7 |
| 2.5 | | | | 3* | | | | 9 |
| 3 | 8 | 6 | | | | 7.5 | | 7-10 |
| 3.5 | | | | | | | | 8 |
| 4 | | | 4 | | | 6 | | |
| 6 | | | 13 | 7.5* | | | | |
| Thicknesses measured by other methods | | | | | | | | |
| neutron reflection; A/W | 7 (3mg/m²) (56,105) | | | | | 3 (0.1g/l) 4.7 (1g/l) (107) | 3.1 (2mg/m²) (57) | |
| pH ⇒ | 7.0 | | | | | 6.0 | 6.0 | |
| neutron reflection; S/L | | | | | | 3 (0.03g/l) 6 (1g/l) (108) | 3.5 (109) | |
| pH ⇒ | | | | | | 4.0-7.0 | 7.0 | |
| surface force (7) | 8 | | | | | 3 5 | 5 | |
| pH ⇒ | 7.0 | | | | | 5.6 | 5.6 | |
| Ellipsometric thicknesses at solid/liquid interface | | | | | | | | |
| ellipsometry | 6.6 (110) | | | | | 7-11 (74) | 4 (HSA) (74) | |
| pH ⇒ | 7.0 | | | | | 7.4 | 7.4 | |

Figure 2,3 and 4
Adsorption and surface pressure as a function of time.
Dashed lined: calulated using Eq. 4 with D's from literature.
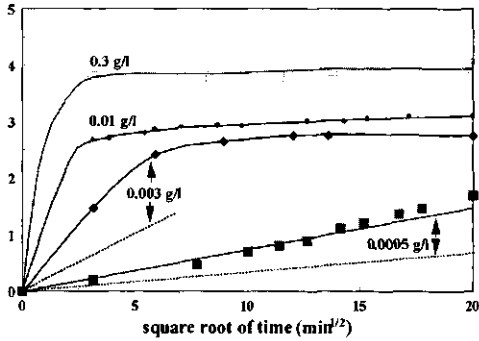


Figure 2a β-casein
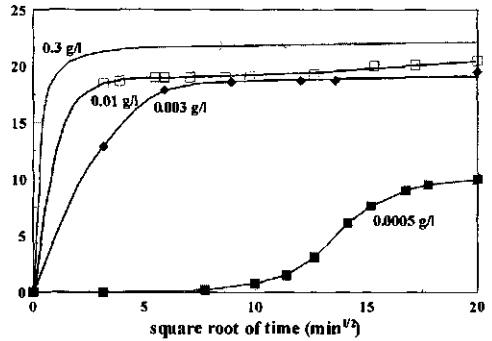
Figure 2b β-casein
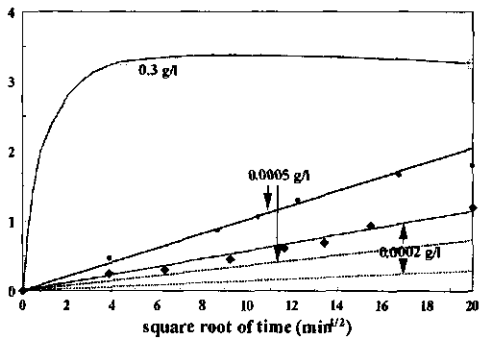


Figure 3a Sodium Caseinate
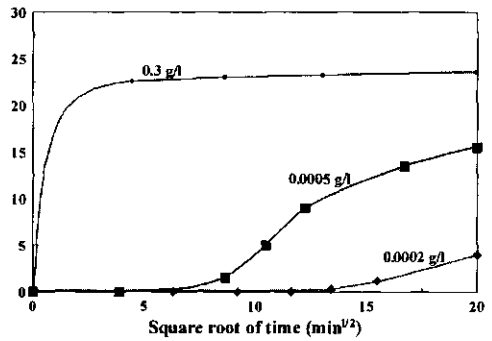
Figure 3b Sodium Caseinate



Figure 4a κ-casein

Figure 4b κ-casein

28
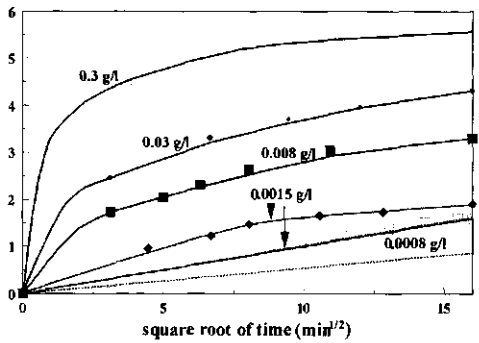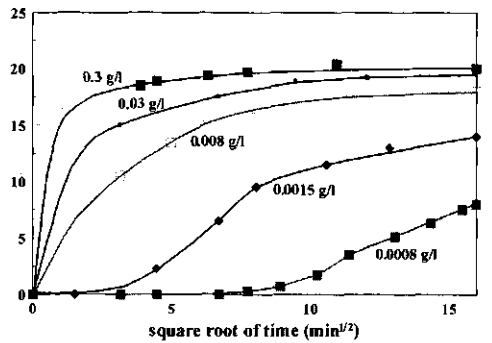
Figure 5,6 and 7
Adsorption and surface pressure as a function of time.
Dashed lined: calulated using Eq. 4 with D's from literature
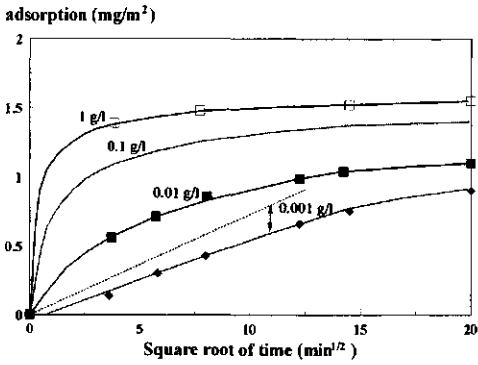


Figure 5a Ovalbumin
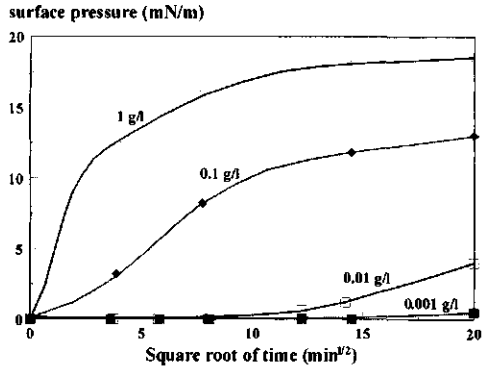


Figure 5b Ovalbumin
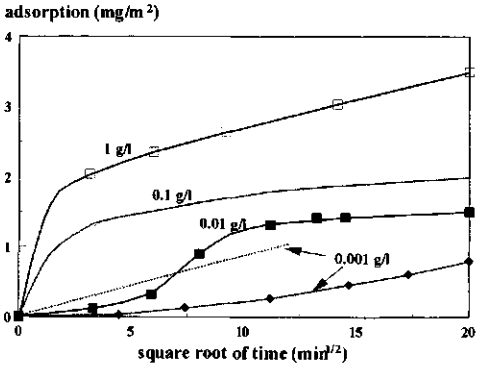


Figure 6a Lysozyme
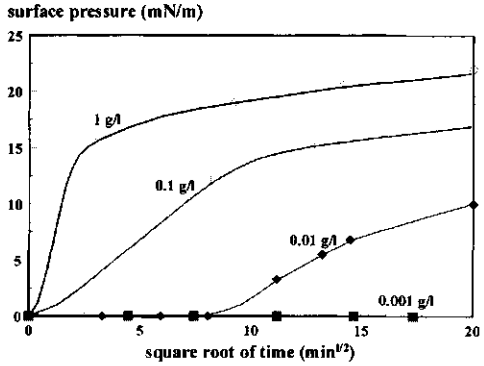


Figure 6b Lysozyme
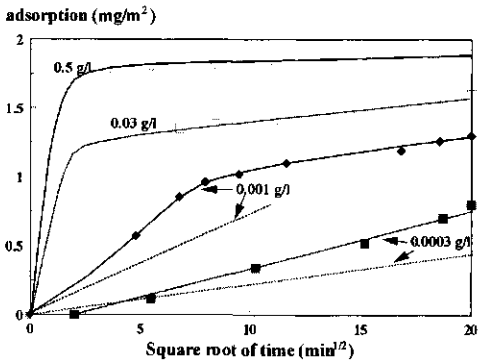


Figure 7a BSA



Figure 7b BSA

29
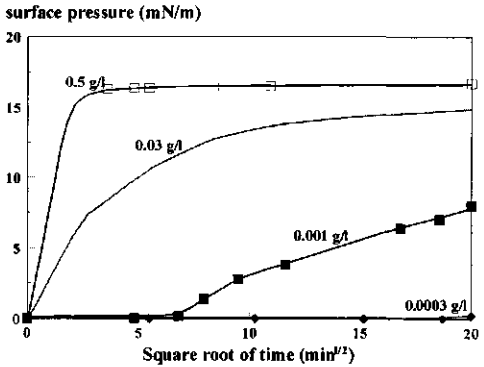
Figure 8 PVA
Adsorption and surface pressure as a function of time.
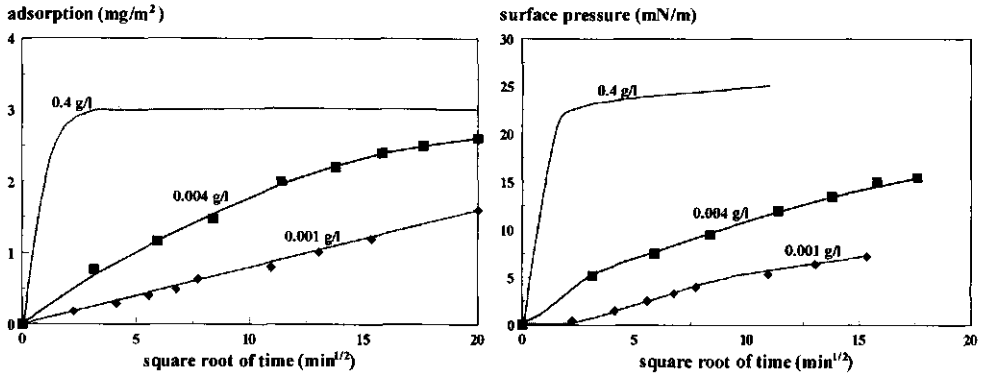


Figure 9. Adsorption isotherms of proteins and PVA
adsorption time = 24 hours
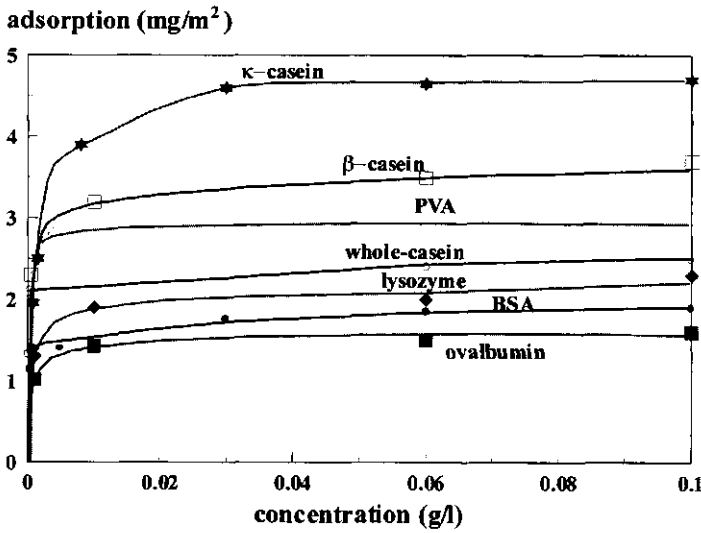
Figure 10
Surface pressure versus surface concentration
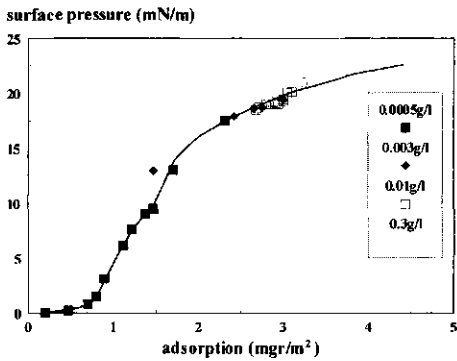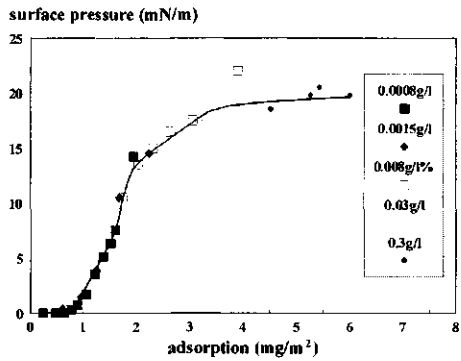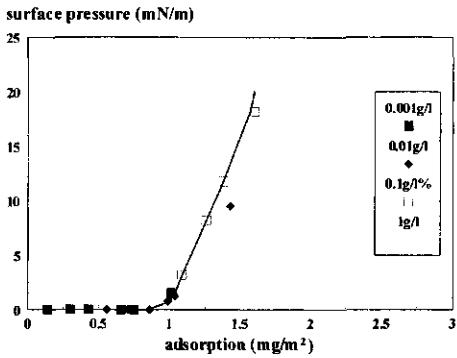
surface pressure (mN/m)



Figure 10a β-casein

surface pressure (mN/m)



Figure 10 b κ-casein

surface pressure (mN/m)



Figure 10c Ovalbumin

surface pressure (mN/m)



Figure 10d Lysozyme

surface pressure (mN/m)



Figure 10e BSA

surface pressure (mN/m)



Figure 10f PVA205

31
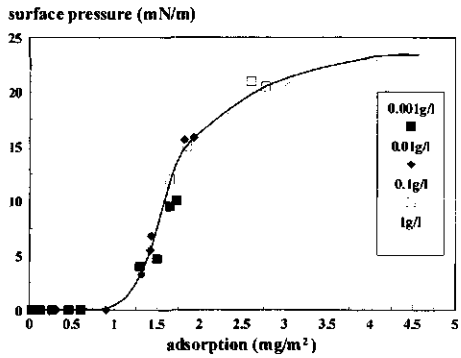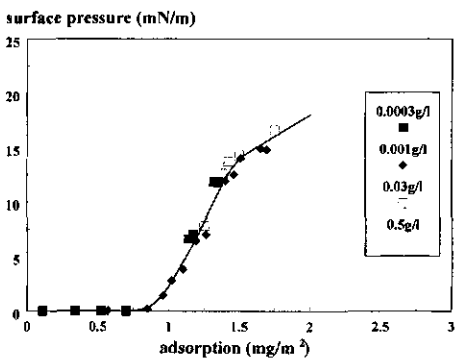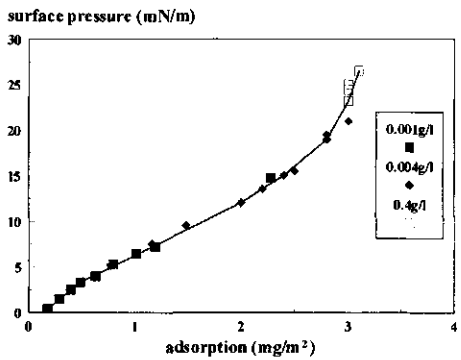
Simultaneously with the adsorption $\Gamma$ the surface pressure $\Pi$ was measured. The results for $\beta$-casein, whole casein, $\kappa$-casein, ovalbumin, lysozyme and BSA are shown in Figs. 2b -7b respectively. In these figures $\Pi$ is plotted as a function of $t^{1/2}$ for different protein concentrations. The figures show that for the lower protein concentrations it takes some time before a measurable surface pressure is detected, in contrast with the $\Gamma$-$t^{1/2}$ plots where the steepest increase is generally found at t=0 (Figs.2a -7a). Lysozyme is the only exception to this rule (Fig 6a.): for this protein at a concentration of 0.01g/l there is a small period where the adsorption rate increases with time. The linear $\Gamma$-$t^{1/2}$ relationship is only found for the lower concentrations up to surface concentrations of about 1 mg/m$^2$.

Values of $\Gamma$ obtained after an adsorption time of 24 hours are plotted in Fig. 9 against the initial bulk concentration $c_0$. Due to adsorption, the actual bulk concentration will be lower, however, for $c_0 > 0.001$g/l this correction is less than 10%. The curves represent apparent adsorption isotherms - not true equilibrium ones - since $\Gamma$ was still tending to increase with time even after such a long time of adsorption. For comparison, the isotherm of a PVA with comparable molecular weight is included.

The surface pressure as a function of the surface concentration is shown in Figs. 10a-10f for the various proteins and PVA. Curves were assembled by combining the corresponding $\Pi$ and $\Gamma$ pairs as given in Figs. 2-7a and 2-7b. The different symbols refer to different initial bulk concentrations. We see, taking into account the experimental error, that the experimental points for each protein collapse into a single curve, independent of $c_0$ and insensitive to the fact that the adsorption time t at which a given $\Pi$ or $\Gamma$ is reached strongly depends on $c_0$. Most of the data were obtained during the adsorption process before $\Pi$ and $\Gamma$ had reached steady state values; hence they refer to a situation in which the layer was not in complete equilibrium with the bulk solution. The inference is that $\Pi$ and $\Gamma$ are at equilibrium even if $\Gamma$ and c are not.

Apart from protein, the solutions studied contain a mixture of electrolytes (buffer salts), which are hardly surface active as such, but which interact with the proteins. This interaction depends on the electrical charge of the protein molecules as determined by the pH of the solution, i.e. negative for caseins, BSA and ovalbumin at pH>5 and positive for lysozyme at pH<11. As we assume that the effect of pH and ionic strength on adsorption behaviour will be qualitatively similar for all proteins examined, these effects were investigated only for the ovalbumin. In Fig. 11 the effect of pH on the initial adsorption rate is given. The highest rate is found at the IEP, i.e., at pH=4.6. In Fig. 12 the effect of pH on the equilibrium adsorption (after 24 hours) is given at low and high ionic strength. Both conditions exhibit maximum adsorption near the I.E.P. The effects of pH and salt effects on the $\Pi$-$\Gamma$ curve for ovalbumin are indicated in Figs. 13 and 14 respectively.

Figure 11 The effect of pH on the initial adsorption rate of ovalbumin

**adsorption (mg/m$^2$)**



**square root of time (min$^{1/2}$)**
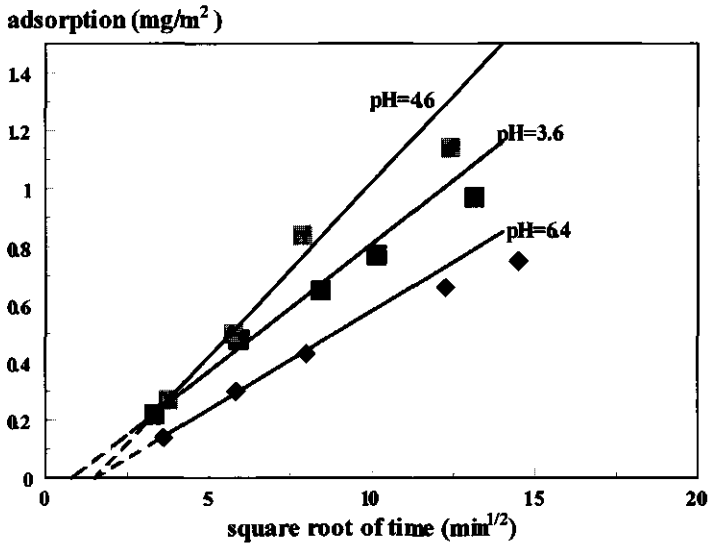
Figure 12 The effect of pH and ionic strength onthe "equilibrium adsorption of ovalbumin. Concentration = $10^{-1}$ g/l. Ionic strenth of buffer = 0.02 M

**adsorption (mg/m$^2$)**



**pH**
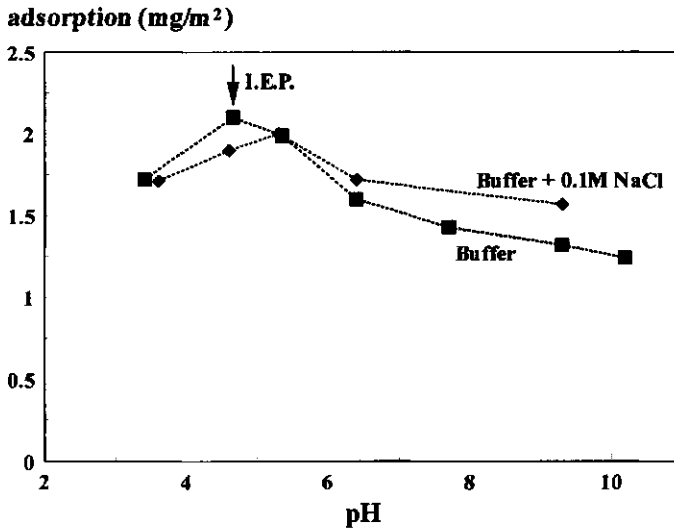
Figure 13 The effect of pH on the Π – Γ curve of ovalbumin.
Ionic strenth of buffer = 0.02 M

**surface pressure (mN/m)**
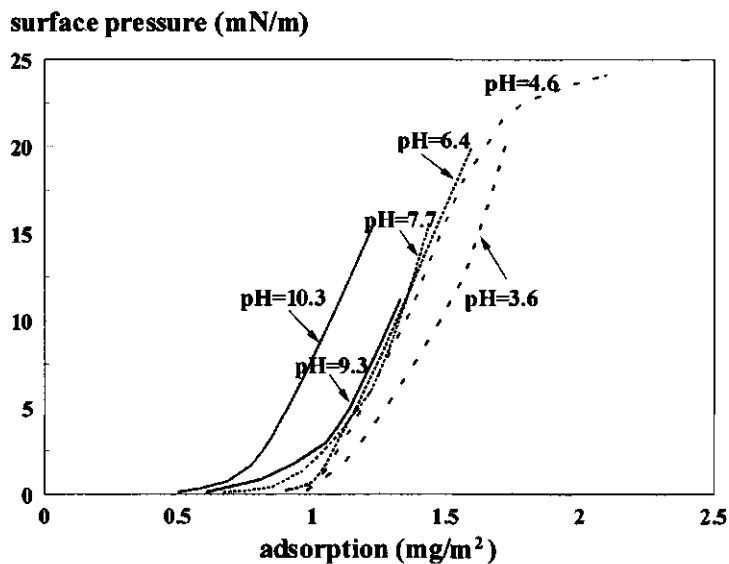


adsorption (mg/m²)

Figure 14 The effect of ionic strength on the Π – Γ curve of ovalbumin.

**surface pressure (mN/m)**
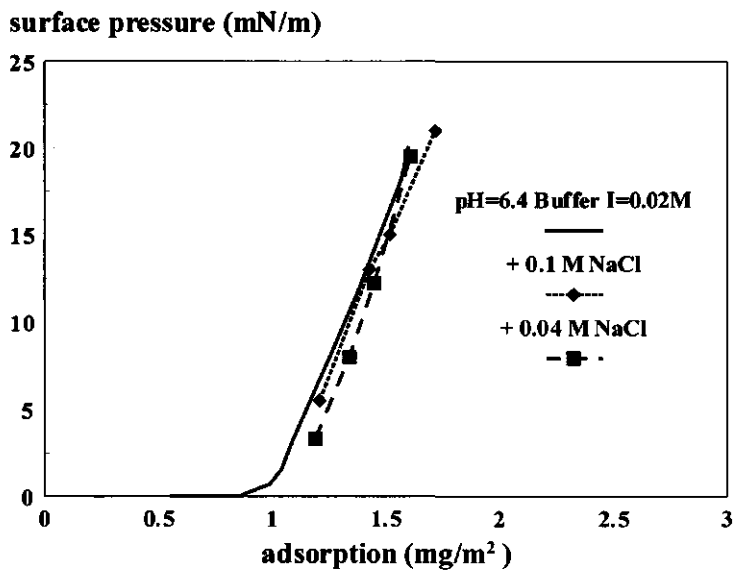


adsorption (mg/m²)

2.7. Discussion.

2.7.1 Adsorption kinetics.

Adsorption requires transport of material from bulk solution to the surface, and this may happen by diffusion, convection, or a combination of the two.

According to equations (2) and (4), the initial parts of curves of the $\Gamma$ versus $t^{1/2}$ should be straight lines through the origin if diffusion is rate determining. For the experimental curves in Figures 2a-7a this condition is fairly well met for the caseins (2a-4a), but with ovalbumin, BSA and especially lysozyme (5a-7a) it is not completely satisfied. We think that this is caused by the fact that t=0 is not well defined experimentally: filling the through and letting the solution come to rest takes about 1 minute, which implies an uncertainty of ca. 1 min$^{1/2}$ in $t^{1/2}$. According to equation (4) the initial part of the $\Gamma$-$t^{1/2}$ should be straight. This is indeed found to be the case for the lowest concentrations ($c_0 \leq 10^{-3}$g/l) up to $\Gamma$ =0.5-1.0 mg.m$^{-2}$. If we assume that diffusion is the only transport process, the initial part of the $\Gamma$ versus $t^{1/2}$ can be calculated according to equation (4) with the use of diffusion coefficients, D, for the different proteins (Table 4). These calculated adsorption curves are also indicated in Figures 2a-7a. A comparison between measured and calculated curves indicates that for whole casein and $\beta$-casein the measured adsorption rate is considerably faster. For $\kappa$-casein, BSA and ovalbumin we also observe that the measured rate is faster than the calculated rate, but compared to the caseins, the difference is smaller. However, with lysozyme the experimental curve indicates a much slower adsorption than expected for a diffusion controlled transport. Adsorption faster than calculated according to equation (4) can be ascribed to a contribution of convective mass transport. Convection will certainly occur under conditions as present before and during the ellipsometric adsorption and surface tension measurements. The protein solution is present in a trough with a relatively large surface area, which will be susceptible to disturbances. These results are in line with findings of Paulsson and Dejmek (103), who, for adsorption experiments under similar conditions, derived that for a protein concentration of $10^{-3}$ g/l the contributions of convection and diffusion are of the same order of magnitude. For lower concentrations convective transport dominates. Hansen and Myrvold (14), who studied protein adsorption in a different experimental set-up (surface pressure by drop shape analyses), also concluded that the convective contribution was considerable.

If we compare measured and calculated adsorption rates as given in Figures 2a-7a, there is indeed a tendency for larger deviations at the lower concentrations.

The results point to a larger convective contribution for whole casein and $\beta$-casein as compared to the other proteins. One can argue that the development of free convection cells is hampered by the higher surface elasticity in the case of $\kappa$-casein, BSA and ovalbumin as

35

will be reported in Chapter 3. However, during the initial stage of the adsorption process the elasticities should be negligibly small for all proteins because the surface pressures are negligible.

Table 4    Protein diffusion coefficients D derived from the initial parts of the $\Gamma$-$t^{1/2}$ plots as compared with literature values (89,90).

| Protein | | Concentration (%) | D ($10^{-10}$ m$^2$s$^{-1}$) | |
|---|---|---|---|---|
| | | | apparent (this work) | literature |
| κ-casein | | $8*10^{-5}$ $1.5*10^{-4}$ | 2 0.9 | |
| Whole casein | | $2*10^{-5}$ $5*10^{-5}$ | 11 6 | 0.7 (90) |
| β-casein | | $5*10^{-5}$ $3*10^{-4}$ | 5 2.5 | 0.6 (90) |
| BSA | | $3*10^{-5}$ $10^{-4}$ | 2 2 | 0.6 (92) |
| ovalbumin; | pH=6.4 pH=4.6 pH=3.6 | $10^{-4}$ $10^{-4}$ $10^{-4}$ | 0.5 1.5 0.7 | 0.7 (89) |
| lysozyme (pH=6.7) | | $10^{-4}$ | 0.2 | 1.2 (91) |

In the case of lysozyme a similar convective contribution as found for BSA or ovalbumin is to be expected, but in fact the experimental adsorption rate is much slower than calculated assuming only diffusion. If we neglect convection, the initial part of the experimental adsorption curve can be explained if we substitute a diffusion coefficient that is too low by a factor of five (Table 4). Similar low values of the apparent diffusion coefficient were deduced from adsorption experiments by Xu et al. (59) and Murray (100).

An extra effect could be the fact that lysozyme in solution at pH>4.5 tends to aggregate (111). This will decrease the effective diffusion coefficient because of the larger diffusing units and the lower monomer concentration.

Xu et al. (59) and Murray (100) raised the possibility of an electrostatic barrier to retard adsorption in the case of lysozyme. However, electrostatic repulsion between adsorbed layer and adsorbing molecule will become operative only after adsorption has reached a certain level. At the early stages of adsorption this effect cannot be important because the surface charge density is too low. Sengupta and Damodoran (61), who found this too slow adsorption of lysozyme only at the air/water but not at the oil/water interface, suggested this effect to be caused by a barrier related to the van der Waals forces near the surface in the case of

36

air/water.

If we compare the $D_{app}$ with $D_{lit}$ (Table 4) it is obvious that the ratio $D_{app}/D_{lit}$ decreases in the sequence casein-BSA-ovalbumin-lysozyme. In the same sequence the rigidity of the molecular structure increases. At this stage we do not have a good explanation for this interesting correlation.

The fact that, for low bulk concentrations, the initial part of the experimental $\Gamma$-$t^{1/2}$ curve is straight, indicates that this stage of the adsorption is described by some diffusion process. However, the meaning of the diffusion coefficients derived from the initial slope of this curve using Eq. 4 (also indicated in Table 4) is limited. At high bulk concentration ($\geq 10^{-2}$ g/l), the initial linear part of the $\Gamma$-$t^{1/2}$ curve cannot be observed at all by our technique.

At first sight, the finding that, for the lower concentrations, the $\Gamma$-$t^{1/2}$ curve remains straight up to $\Gamma$-values of 1 mg/m² is surprising. For most proteins half of the saturation value of the first layer is reached at that surface concentration. So it is expected that the probability for newly arriving molecules to find an empty patch to adsorb at the interface has decreased considerably. As during the adsorption process equilibrium exists between the sub-surface and the adsorbed layer, the straight $\Gamma$-$t^{1/2}$ curve up to 1 mg/m² means that a surface concentration of 1mg/m² is in equilibrium with an extremely low sub-surface concentration. This is an extra indication for the high affinity character of protein adsorption.

The results in Table 4 and Figure 11 indicate that with ovalbumin the adsorption rate shows a maximum at the I.E.P. (pH=4.6 for ovalbumin). This cannot be attributed to electrostatic repulsion forces between charged adsorbing molecules and a charged layer of adsorbed molecules at pH≠I.E.P., as this charged layer is not present at the initial stage of the adsorption process. Norde (6) described a similar pH dependency of protein adsorption at solid surfaces. This effect was explained by assuming that excess of either positive or negative charge, at pH≠I.E.P, leads to intramolecular repulsion and therefore promotes a more expanded structure. It is likely that the diffusion coefficient of this expanded structure is lower. However, the pH-effects on the diffusion coefficient as given in Table 4 are somewhat more pronounced than expected (87).

For all proteins examined, the adsorption rate decreases at long times and eventually vanishes when $\Gamma$ has reached its equilibrium value, whether or not there is an adsorption barrier.

2.7.2 Time dependence of the surface pressure.

We now consider the experimental $\Pi$-$t^{1/2}$ curves shown in Figures 2b-7b. At low bulk concentrations ($\leq 10^{-1}$g/l), an induction period was observed during which the tension was almost constant, i.e. surface pressure $\Pi$ remained very low ($\leq 1$mN/m). Such a period has also

been observed by others (40,59,98,104,112-115). For all proteins examined it was found that this period shortens rapidly with increasing protein concentration. As soon as $\Pi$ exceeds ca. 1mN/m, it starts to increase sharply with time. Curves of $\Pi$-$t^{1/2}$ show points of inflection at $\Pi \approx 4$ mN/m, after which the rate of change decreases and reaches zero after long adsorption times.

Due to lack of direct information about the surface concentration, this induction period in the $\Pi$- t or $t^{1/2}$ curves has often been misinterpreted. According to Tornberg (40) and Ward et al. (104), the induction period which they observed, was due to an artifact caused by the method they used for measuring the surface tension. They employed the drop-volume method, which involves the drop enlarging its surface during formation, and they thought that this would cause $\Pi$ to remain low at the initial stage of the adsorption. This explanation is not correct, since we find that the same phenomenon is observed with the static Wilhelmy plate method, for which the surface area remains constant during the entire experiment. Others attributed this period to an adsorption barrier (95) or to very slow unfolding (112,113) of already adsorbed protein molecules. The real reason is quite different: it is simply the consequence of the fact that the surface pressure for proteins does remain low (not measurably different from zero) until a considerable amount has been adsorbed. This is illustrated in Fig.16 which summarises the $\Pi$-$\Gamma$ relationships for all proteins given in Figs. 10a-f. Figure 16 shows that for all proteins, even at equilibrium, a certain minimum level of adsorbed protein is required before the surface pressure starts to deviate measurably from zero. This minimum level depends on protein type and increases from 0.5mg/m$^2$ for β-casein to 1.1 mg/m$^2$ for lysozyme. In the early stage of the adsorption process, therefore, the tension can not be noticeably different from that for of pure water. The underlying physical reason will be discussed in section 2.7.4 "The surface equation of state".

Fig. 16 also indicates that it is impossible to obtain any information about the evolution of adsorption, especially the initial part, by only measuring $\Pi$-t curves. Attempts to do so (40,95,116) were based on the assumption that $\Pi$ is related to $\Gamma$ by the ideal surface equation of state:

$$\Pi = RT\Gamma = RT/A \qquad (8)$$

In equation (8), $\Gamma$ is the adsorption in Mol/m$^2$, T is the absolute temperature, R is the Gas constant, and A is the area available per adsorbed Mol. Combining equations (4) and (8) gives

$$\Pi = 2RTc_0(Dt/\pi)^{1/2} \qquad (9)$$

However, the assumption underlying Eq. (8) is not valid as can be seen from Fig. 16 by

38

comparing the measured curves with the calculated line according to this equation. It is clearly shown that for all proteins examined, $\Pi$ is not proportional to $\Gamma$, certainly not for $\Pi > 1$ mN/m, and hence the proteins do not exhibit ideal surface behaviour for $\Pi \geq 1$ mN/m. This same conclusion was arrived at by Bull (117) and Hansen (14), who carefully studied $\Pi(A)$ curves of proteins spread at the air water interface. Bull found that, even at surface pressures as low as $10^{-2}$ mN/m, proteins do not behave ideally.

It follows from the above, that reliable information about the relationship between $\Pi$ and $\Gamma$ is essential for interpreting the time-dependence of surface pressures in terms of the underlying physical processes. For this purpose several investigators (14,17) have made use of the $\Pi(A)$ curves of spread proteins. Using this method it is implicitly assumed that the surface equation of state is the same for spread and adsorbed protein layers. The correctness of this assumption can be estimated from Figs. 15a-d in which we have compared the $\Pi(\Gamma)$ curves determined using our ellipsometric method, with $\Pi(\Gamma)$ curves that were determined by compression of a spread protein layer. The spread $\Pi(\Gamma)$ curves were obtained from $\Pi(A)$ curves given in literature for β-casein (98), BSA (102), ovalbumin(96) and lysozyme (97). For the first three proteins the agreement between spread and adsorbed curves is generally good, especially where the experiments were performed at similar pH and ionic strength (see also section 2.7.4. "surface equation of state"). With lysozyme the similarity is only semi qualitative over the whole curve, probably because the spread curve for this protein was determined at a considerably higher ionic strength. An effect of ionic strength on the adsorption is not unlikely here, because of the high positive charge on lysozyme at pH=6.7 (see section 2.6.5).

This good agreement between spread and adsorbed $\Pi(\Gamma)$ curves also supports the relevance of adsorption studies by performing surface pressure measurements (14). In these studies surface pressure values were related to $\Gamma$-values using the $\Pi(\Gamma)$ curves obtained by compression of a spread layer (14). However, about the initial part of adsorption process, up to the surface concentration where the surface tension starts to deviate measurable from zero, no information could be obtained.

The adsorption kinetic sections (2.7.1 and 2.7.2) can be summarised as follows:

1. In most cases the initial stage of the adsorption is diffusion controlled. This allows the conclusion that the characteristic time of step 2, $\tau_2$,(Fig. 1) is considerably smaller than the characteristic time of the diffusion process.

2. The apparent induction period of surface pressure is a direct consequence of the shape of the surface equation of state of proteins and is not caused by an adsorption barrier.

3. The characteristic time of reconformation at the interface $\tau_3$, (step 3 in Fig. 1) is < 10 min. as will be shown in section 2.7.4 .

4. A more precise determination of the limits of $\tau_2$ and $\tau_3$ will be possible with the aid of the dynamic interfacial properties as will be shown in chapter 3.

2.7.3 Adsorption isotherms.

True equilibrium adsorption does not seem to be possible with proteins: even after two or three days the surface concentration slowly continuous to increase. The origin of these very slow changes is not known, but possible candidates are: denaturation, evaporation/drying, changes in intermolecular interaction (Chapter 5, Surface shear properties of adsorbed proteins layers). The consequence of these slow changes is that it is impossible to determine the real equilibrium adsorption isotherms. Therefore we considered the surface concentration measured after 24 hours as the pseudo-equilibrium value. Using these data the apparent adsorption isotherms given in Fig. 9 were constructed. We see from this figure that all adsorption isotherms are of the high-affinity type which is characteristic for macromolecules, i.e. high adsorbed amounts even at very low concentrations. In the concentration range $10^{-4}$-$10^{-3}$ g/l a finite initial slope is indicated. This is in line with the finding of Norde (6) who stated that with compact molecules a finite initial slope is not an exception. The borderline between real high-affinity isotherms and isotherms with a finite initial slope is of course, quantitative, rather than qualitative.

Table 5        The "equilibrium" adsorption at high bulk concentrations compared to data calculated on the basis of monolayer coverage and molecular dimensions.

| protein type | shape/size of molecule | Γcalc. (mg/m²) | Γmeasured (mg/m²) | thickness (nm) |
|---|---|---|---|---|
| κ-casein | ? | | 6.0 | 13.0 |
| Na-caseinate | ? | | 3.4 | 6.0 |
| β-casein | random coil | | 4.4 | 8.0 |
| ovalbumin | sphere radius: 2.9 nm | 2.2 | 1.8 (pH=3.6) 6 (pH=4.6) 1.6 (pH=6.4) | 2.5 7.5 2.0 |
| lysozyme | ellipsoid: 4.5*3.0*3.0 nm | 1.8 (side on) 2.7 (end on) | 4.6 | 6.0 |
| BSA | ellipsoid: 14*3.8*3.8 nm | 2.5 (side on) 6 (end on) | 2.0-3.0 | 2.5 |

In Table 5 equilibrium adsorption data (Γmeasured) are compared with values calculated for monolayer coverage, based on the molecular dimensions in bulk solution (= Γcalc). This table

also gives the ellipsometric thickness of the adsorbed layer. Although for the caseins reliable molecular dimensions are lacking, it is likely that especially in the cases of κ-casein and β-casein multilayer adsorption has taken place. Outside the IEP region ovalbumin just seems to reach monolayer coverage, but at the IEP ovalbumin reaches multilayer coverage especially at relatively high concentrations. Lysozyme also gives multilayers especially at high bulk concentrations. Multilayer adsorption of lysozyme was also observed by other investigators (33,99), and related to the tendency of the molecules to associate in solution. The slight turbidity of ovalbumin solution at the IEP and high concentrations supports this. This means that multilayer adsorption is caused by attractive forces between the first and the second adsorbed layer (6). These attractive forces may be related to structural rearrangements in the adsorbed protein molecules (118,119).

The tendency of protein molecules to associate and the slight turbidity at higher concentrations suggests solution non-ideality, which is in line with the finding that in the plateau range most of the isotherms show a constant surface pressure over a considerable concentration range. This constant surface pressure is also expected in case of multilayer adsorption, because the effect of a second layer on $\Pi$ will be small.

The adsorbed amounts given in this table are determined at the highest protein concentration that was investigated. The adsorption isotherms (Figures 9 and 17) indicate that especially for systems that show multilayer adsorption, it is likely that for higher protein concentration even higher adsorbed amounts have to be expected.


2.7.4 The surface equation of state.


The $\Pi$-$\Gamma$ relationship at equilibrium is called the surface equation of state. Surface equations of state are phenomenological, thermodynamic expressions. For a molecular interpretation one could try to relate the surface pressure to the (excess) surface concentration $\Gamma$, the distributions and the forces acting amongst the segments and molecules within the surface layer. These forces are affected by the spatial orientation or conformation of the adsorbed molecules. With low-molecular-weight surfactants, molecular reorientation is fast; the time-scale is of the order of the molecular rotation time ($\leq 10^{-3}$ s) (120). This means that the orientation of surfactant molecules, and consequently the measured surface pressure, is completely determined by $\Gamma$ over the experimental time-scale. That is, there is internal equilibrium within the surface layer even when the layer is not (yet) in equilibrium with the bulk solution. With macromolecules, however, adjustment of the conformation of the adsorbed molecules to the local surface force field may proceed much more slowly. This will be particularly the case for proteins, where reconformation requires breaking of weak intramolecular interactions between various groups of amino-acid residues. It is therefore

41

expected that the protein surface pressure will depend not only on $\Gamma$, but also on time, and that $\Pi$ may change with time at constant $\Gamma$ (18,13). Contrary to such expectations, we find that at given T, within experimental error, $\Pi$ is a unique, protein specific, function of $\Gamma$ for all proteins studied here (see Figures 10a-f). This means that either the reconformation time after adsorption is much shorter than the time-scale of our experiments (minutes to many hours), or reconformation does not occur at all. The second explanation is quite unlikely, as it would mean that adsorbed molecules have the same conformation as those in bulk solution, independent of time. This is at variance with the observation that many proteins denature on adsorption (26,121) or for that matter significantly change their conformation (21).

Therefore, our finding, that for each protein $\Pi$ is uniquely determined by $\Gamma$ strongly indicates, that the time-scale of the reconformation process is shorter than the experimental time-scale of the ellipsometric technique, i.e. less than ca. 10 minutes. Evidence for a relaxation time of the reconformation process of proteins varying between a few seconds and a few minutes has been deduced from dynamic experiments at adsorbed protein layer, as will be discussed in Chapter 3. During periodic compressions and expansions at higher surface concentrations ($>1$ mg/m$^2$) and higher frequencies, it was observed that the surface pressure changes do not follow the equilibrium $\Pi(\Gamma)$ curve. This indicates that adaptations of the conformation (=changes in molecular size or shape) to the one that is in equilibrium with the surface pressure cannot be established within the timescale of the applied periodic deformation. Note that this finding applies to conformational changes in sofar as they affect the surface pressure. From these results we cannot exclude the possibility that there are conformational changes acting at a much longer timescale, but having little or no effect on the surface pressure.

The finding that the measured $\Pi(\Gamma)$ relationship is a unique function for each protein, provided there is enough time for conformational changes after adsorption, is supported by the agreement between spread and adsorbed $\Pi(\Gamma)$ curves (see Figs. 15a-d).

In Figure 16 the surface equations of state of all proteins examined are collected. The shapes of the $\Pi(\Gamma)$ curves for the globular proteins BSA, ovalbumin and lysozyme are similar. Below a certain $\Gamma$ value (0.8 - 0.9mg/m$^2$) the surface pressure does not deviate measurably from zero. Above a slightly higher value, 1 mg/m$^2$ for BSA and ovalbumin and 1.2 mg/m$^2$ for lysozyme, the surface pressure steeply increases with increasing $\Gamma$. For $\kappa$-casein the surface concentration where the surface pressure starts to deviate from zero is also about 0.8 mg/m$^2$, but compared to the globular proteins is more gradual. For $\beta$-casein, $\Pi$ starts to deviate measurably from zero at a significantly lower surface concentration (0.5 mg/m$^2$) and increases also more gradually with a further increase of $\Gamma$. For comparison, the surface equation of state of the synthetic polymer PVA is also given. With PVA the surface pressure starts to deviate from zero at a surface concentration of about 0.3mg/m$^2$, which is significantly lower than with

β-casein. The differences between the shape of the $\Pi(\Gamma)$ curves of the various proteins seems to correlate with the differences in flexibility or rigidity of the protein molecules. PVA and β-casein have flexible and almost random coil molecules, which can easily expand at the interface after adsorption. Consequently, the surface will already be almost fully occupied with a thin layer of these molecules at a relatively low surface concentration. From this surface concentration onward the surface pressure starts to deviate from zero, because of increasing adsorption and increasing interaction forces between the adsorbed molecules. With the flexible molecules this increase of the surface pressure is gradual because compression of these expanded molecules will require little energy as these changes are mainly entropic. The more rigid globular molecules hardly expand upon adsorption, so with these molecules the surface becomes fully occupied at a significantly higher surface concentration. However, once the surface is nearly fully packed with these rigid molecules, a further increase of the surface concentration will cause a much steeper increase of the surface pressure.

The characteristics of the measured $\Pi(\Gamma)$ curves can be summarized as follows :

(i) Up to a certain minimum value of the surface concentration, $\Gamma_{min}$, the surface pressure does not measurably deviate from zero. Depending on protein type $\Gamma_{min}$ varies between 0.5-1.0 mg/m$^2$.

(ii) A steep increase of $\Pi$ at surface concentrations exceeding $\Gamma_{min}$. The steepness depends on protein type.

(iii) At surface concentrations corresponding to around monolayer coverage, the $\Pi(\Gamma)$ curve flattens.

In principle the very low value of $\Pi$ up to $\Gamma_{min}$ can be explained by treating the adsorbed protein molecules as a two dimensional ideal gas. The calculated line, $\Pi = RT\Gamma$ (Eq.8), is plotted in figure 16.

The S-shape of the curves at higher surface concentrations can be qualitatively described by the Soft Particle Model (38), which is a modification of the scaled-particle theory of Helfand et al. (122). The latter theory is derived for "hard" particles without interactions and results in,

$$\Pi = \frac{RT\Gamma}{(1-\Theta)^2} \qquad (10)$$

where $\Theta = \pi R_p^2 \Gamma$, with $R_p$ the particle radius in the plane of the surface. The Soft Particle Model uses the same expression, but considers the particles (=protein molecules) as deformable ("soft"). This means that the radius $R_p$ may be continuously variable as a function of $\Gamma$. Although such an assumption is not consistent with the assumptions underlying Eq. (10), it does furnish a qualitative description of the measured $\Pi(\Gamma)$ curves on the basis of differences in deformability/rigidity. Upon adsorption protein molecules tend to deform in

43

Figure 15 Comparison between spread and adsorbed Π – Γ curves.
Adsorbed from fig. 10 ; spread from literature
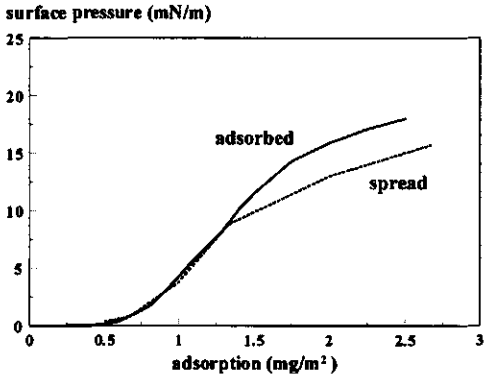


Figure 15a β-casein
adsorbed and spread: pH=7 ; I=0.1M
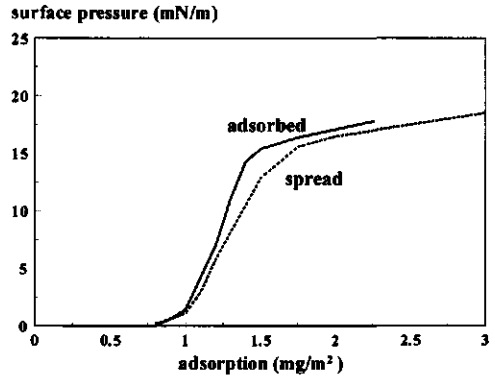
Figure 15 b BSA
adsorbed: pH=6.7 ; I=0.03M
spread: pH=7.3 ; 0.15 M NaCl
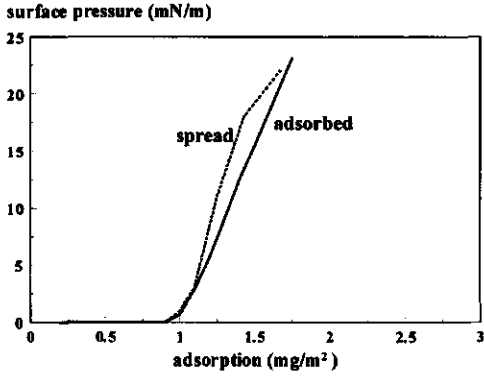
Figure 15 c Ovalbumin
adsorbed: pH=6.4 ; I=0.02M
spread: pH=neutral ; 1M Na₂SO₄
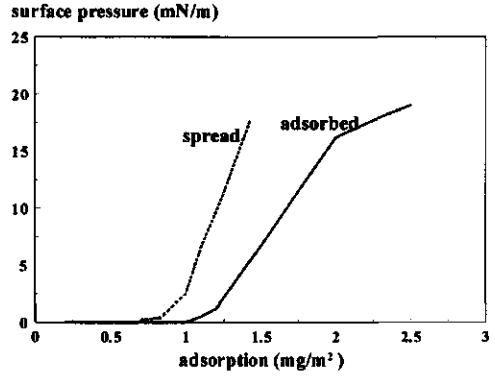
Figure 15 d Lysozyme
adsorbed: pH=6.4 ; I=0.02M
spread: pH=neutral ; 1M KCl

Figure 16 Surface equation of state of proteins and PVA.



44
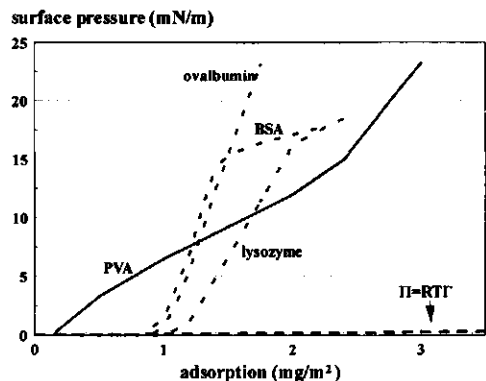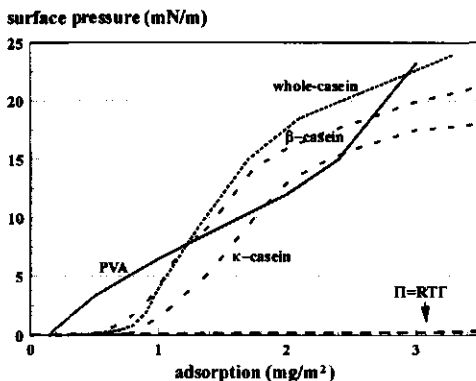
such a way that the free energy of the system is minimized. At low $\Gamma$ the effect will be that the adsorbed molecules are flattened at the surface, resulting in an increase of the area covered by an adsorbed molecule. The deformation of the adsorbed protein molecules by the surface force field is counteracted by an internal mechanical force, due to intramolecular bonds. We therefore expect that the internal mechanical force will increase with increasing number and strength of the intramolecular bonds (e.g. hydrophobic interaction and disulphide bridges) and with increasing deformation, and that it may (partially) relax with time. In concentrated monolayers steric repulsive forces may become operative resulting in a decrease of $R_p$. Applying this model to the experimental data, the apparent decrease of molar radius (R) with increasing $\Gamma$ is a factor 1.7 for the flexible $\beta$-casein molecule, a factor 1.3 and 1.4 for the rigid globular molecules BSA and ovalbumin, respectively and only a factor of 1.1 for the very rigid lysozyme molecule (see Table 1, Chapter 6). These values, obtained by substituting measured values of $\Pi$ and $\Gamma$ into Eq (10), appear to be physically reasonable but have not been independently confirmed.

A different model, applied only recently to adsorbed protein layers, is the two dimensional solution model (49,55). This model considers both entropy and enthalpy in first order, for a solvent and a protein with constant molecular areas, $\omega_1$ and $\omega_2$, respectively, where $1/\omega_i$ can be equated to the saturation adsorption $\Gamma_i^\infty$. In this model, the surface pressure $\Pi$ depends on the degree of surface coverage $\Theta$ ($=\omega_2\Gamma_2$) according to

$$\frac{\Pi\omega_1}{RT} = -\ln(1-\Theta) - (1-1/S)\Theta - \frac{H}{RT}\Theta^2 \qquad (11)$$

where the size factor, S ($=\omega_2/\omega_1$), is the factor by which the protein's molar area exceeds that of the solvent, and $H\Theta^2$ is the partial molar heat of mixing of a Frumkin-type model or regular surface mixture. Positive values of H represent a domination of attractive interactions between like molecules over those between unlike. For an ideal surface mixture of equally sized molecules (H=0; S=1), Eq (11) is equivalent to the Langmuir equation; non-zero values of the second and third terms express the non-ideal entropy of a mixture of small and large molecules and the enthalpy of mixing, respectively. Using realistic values for S and H, $\Pi(\Gamma)$ curves up to about 75% monolayer coverage can be described. To explain the flattening of the $\Pi(\Gamma)$ curves, which is characteristic for all proteins examined, a decrease of protein molar area, $\omega_2$, with increasing $\Pi$ can be introduced, similar to the Soft Particle model. Other explanations for this phenomenon are multilayer formation or collapse.

Both the Soft Particle Model and the Two Dimensional solution model, including their ability to account for the dynamic interfacial properties, will be described in detail in Chapter 6.

45

2.7.5 Effect of pH and ionic strength.

In section 2.6.1 the effect of pH on the adsorption rate, as established for ovalbumin, was discussed. The highest rate was found at the I.E.P., possibly because, away from the I.E.P., the diffusion coefficient is lower due to a more expanded molecular structure. The explanation in terms of electrostatic repulsion forces between charged adsorbing molecules and a charged layer of adsorbed molecules at pH≠I.E.P. is less plausible.This effect can operate only at finite adsorption values, not in the limit of vanishingly small adsorption in the initial stage of the adsorption process.

From Figure 12 it can be seen that the pH (and consequently the charge of the protein molecules) significantly affects the equilibrium adsorption ($\Gamma_{eq}$) with $\Gamma_{eq}$ being a maximum at the I.E.P.. As expected, this effect of pH on adsorption is affected by the ionic strength. When the pH differs more than 2 units from the I.E.P. $\Gamma_{eq}$ increases with increasing ionic strength. However, $\Gamma_{eq}$ decreases with increasing ionic strength for the pH range near the I.E.P.

Qualitatively the same behaviour ($\Gamma$ vs. pH and the flattening effect of increasing ionic strength on this pH effect) was observed for HSA adsorbed at solid surfaces (123,124). The maximum adsorption at the I.E.P. can be explained by the absence lateral of repulsive forces between charged adsorbed molecules (26). However, the reduction of equilibrium surface concentration at either side of the I.E.P. may also be due to structural rearrangements in the adsorbing molecules. Away from the I.E.P. a more expanded structure is found (6). As electrostatic repulsion is reduced by increasing salt concentration, one would expect that the influence of pH on $\Gamma_{eq}$ reduces with increasing ionic strength of the solution. The experimental results shown in figure 12 support this electrostatic repulsion explanation. In addition to the direct effect of electrostatic repulsion between the protein molecules at the interface, the charge of the molecules (and hence the pH) may also indirectly affect the surface concentration: the pH of the solution affects the solubility of the protein molecules, which is lowest near the I.E.P. In general, the surface activity increases with decreasing solubility. For ovalbumin close to the I.E.P. the solubility is low: for c=5 g/l at pH=4.6 and ionic strength ≈ 0.0075 m/l the solution is turbid, implying that agglomerates are present in the solution. The influence of the ionic strength on $\Gamma_{eq}$ (Fig. 12) could also be caused by a change of the solubility: from NMR measurements, Kleibeuker et al. (125) concluded that ovalbumin has an increased tendency to agglomerate when the salt concentration is increased. The slight decrease of $\Gamma_{eq}$ with increasing ionic strength for pH=I.E.P. could then be attributed to the fact that close to the I.E.P. the solubility increases with increasing ionic strength. The correctness of this hypothesis requires more experimental information about the effect of ionic strength on the solubility of ovalbumin. A similar effect was observed by van

Figure 17
Adsorption isotherm of ovalbumin at different pH values



47
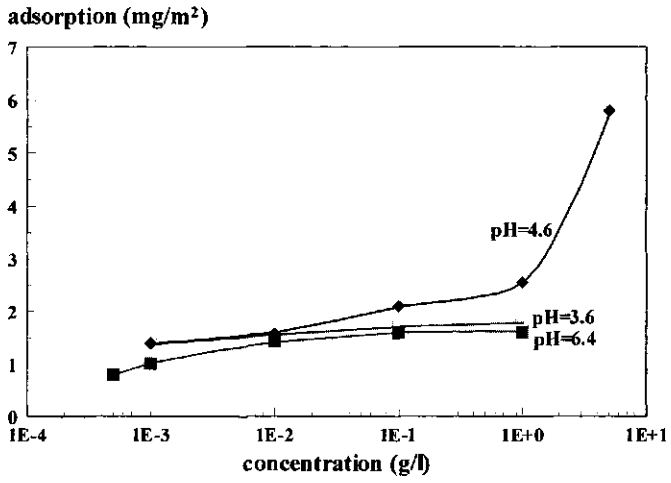
der Scheer (124). He explained the effect by assuming that at the I.E.P. the protein molecules have a more compact shape at low ionic strength. However, the conformation of ovalbumin is hardly affected by pH in the range considered by us (125). An interesting point is that, within the experimental error, the $\Pi(\Gamma)$ plots, as obtained in the pH-range 4.6-7.7 coincide (Figure 13). This means that although in this pH-range the surface concentration is significantly affected by pH (and so is the charge and structure of the protein molecules), it does not notably affect the surface pressure. A similar small effect of pH on the $\Pi(\Gamma)$ curve in the pH range from 5-7 was observed for BSA (113). Qualitatively, one would expect repulsion forces to increase $\Pi$ at given $\Gamma$. For small molecules, there have been attempts to explain and quantify this effect in terms of double-layer theory (126). Experimental values of the repulsion effect on $\Pi$, however, were much smaller than theoretically predicted.

At more extreme pH values (3.6 and 10.3) a significant effect on the $\Pi(\Gamma)$ curve was observed. Surprisingly, depending on the sign of the charge the shift of this curve is to more expanded at pH=10.3 and to more condensed at pH=3.6. This indicates that changes in pH also affect intermolecular interactions which are not simply related to charge.

The adsorption isotherms of ovalbumin as illustrated in Figure 17 show that, for pH=3.6 and pH=6.4, the equilibrium surface concentration only slightly increases with increasing bulk concentration, with $\Gamma_{eq}$ reaching a plateau value for $c \geq 10^{-1}$ g/l. As already discussed in section 2.7.3 the level of this plateau value indicates monolayer adsorption. For pH=4.6 at higher bulk concentrations ($c > 10^{-1}$ g/l), both $\Gamma_{eq}$ and the thickness of the adsorbed layer steeply increase with increasing concentration (see Fig. 17 and Table 5), indicating multilayer adsorption. In general, multilayer adsorption for macromolecules is expected when, in bulk solution, the molecules tend to agglomerate (127). This is in agreement with the observation that higher ovalbumin concentrations at pH=4.6 are slightly turbid.


2.8. Conclusions


1.      All proteins examined show high affinity adsorption, i.e. strong adsorption at low concentrations in the solution.

        With proteins it is almost impossible to attain true equilibrium adsorption at the air-water interface. Even after 24 hours the adsorbed amount keeps increasing.

2.      Surface concentrations determined by ellipsometry show that the initial stage of adsorption of all proteins examined is well described by the simplified diffusion equation (4), at least for very low concentrations. At higher concentrations adsorption proceeds too fast for our method to follow the onset of the process. In the later stages, equation (4) no longer holds but this does not necessarily mean that parts of the

process are no longer diffusion-controlled. The diffusion coefficients that can be derived from the initial stage do not always perfectly agree with literature data due on bulk diffusion.

3.   It is also demonstrated that diffusion control does not imply linearity of $\Pi$-$t^{1/2}$ curve. This is because such an interpretation would require the assumption that the surface behaves like an ideal gas [equation(8)], and our experiments indicate that such ideality does not hold over any measurable range of surface pressure. Hence, any linearity in an experimental plot of $\ln(d\Pi/dt)$ versus $\Pi$ gives no indication as to whether or not there is an adsorption barrier at the surface. In fact, analysis of surface pressure measurements alone cannot lead to any conclusion about the relative rates of physical processes (diffusion, attachment, reconformation, etc.) taking place in or near the surface.

We find that the surface pressures of all proteins examined are protein specific, but otherwise unique time-independent functions of $\Gamma$. Otherwise stated, for each protein a unique surface equation of state has been obtained.

4.   The $\Pi(\Gamma)$ curve of a protein reflects the flexibility/rigidity of the protein molecule. Main features to classify the proteins on this curve are (i) the minimum surface concentration ($\Gamma_{min}$) where $\Pi$ starts to deviate measurably from zero (ii) the steepness of the increase of the surface pressure upon further increasing the surface concentration. For flexible molecules like $\beta$-casein and PVA, $\Gamma_{min}$ is low and from this point onward the surface pressure increases gradually with increasing surface concentration. For rigid globular proteins (BSA, ovalbumin and lysozyme), $\Gamma_{min}$ is higher and with a further increase of the surface concentration the surface pressure increases steeply.

5.   Effects of pH and ionic strength were studied with ovalbumin. Both the adsorption rate and the surface concentration reach a maximum at the IEP of the protein. These maxima can be explained by a more compact molecular structure at the IEP due to the absence of intra-molecular electrostatic repulsive forces. The maximum at the IEP is less pronounced at increased ionic strength, because the repulsive forces are reduced. The compact structure at the IEP results in multilayer adsorption at high protein concentration.

Surprisingly perhaps, the surface equation of state of ovalbumin is only slightly affected by pH and ionic strength in the pH-range 4-8, indicating that electrostatic intermolecular repulsive forces do not contribute much to the surface pressure. Effects of pH on this curve become apparent only at more extreme pH values.

6.   At higher protein concentrations and long adsorption times, for most proteins multilayer adsorption takes place.

49

2.9 REFERENCES.

1.      F.M. Ascherson. Archives of Anatomical Physiology., (1840) 44-68

2.      H. Neurath, H.B. Bull. The Surface Activity of Proteins, Chemical Review. $\underline{23}$ (1938) 391

3.      I.R. Miller, D.Bach. Biopolymers at Interfaces. Surface and Colloid Science, ed. E. Matijevic (Wiley. New York) $\underline{6}$ (1973) 185

4.      F. MacRitchie. Proteins at Interfaces. Advances in Protein Chemistry. $\underline{32}$ (1978) 283

5.      F. MacRitchie. Spread Monolayers of Proteins. Advances in Colloid and Interface Science. $\underline{25}$ (1986) 341.

6.      W. Norde. Adsorption of Protein from Solution at the Solid-Liquid Interface. Advances in Colloid and Interafce Science. $\underline{25}$ (1986) 267

7.      P.M. Claesson, E. Blomberg, J.C. Fröberg, T. Nylander, T. Arnebrant. Protein Interactions at Solid Surfaces. Advances in Colloid and Interface Science. $\underline{57}$ (1995) 161

8.      Th.A. Horbett, J.L. Brash, eds. Proteins at Interfaces 2, Fundamentals and Applications. ACS Symp. Ser. $\underline{602}$ (1995). Chapter 1

9.      A.Sadana, Protein Adsorption and Inactivation on Surfaces. Influence of Heterogeneities. Chem Rev. $\underline{92}$ (1992) 1799.

10.     E. Dickinson, Y. Matsumura, Proteins at Liquid Interfaces: Role of the Molten Globule State. Colloids and Surfaces B: Biointerfaces $\underline{3}$ (1994) 1

11.     C.H. Haynes, W. Norde. Globular Proteins at Solid/Liquid Interfaces. Colloids and Surfaces B: Biointerfaces, $\underline{2}$ (1994) 517

12.     J. Benjamins, J.A. de Feijter, M.T.A. Evans, D.E. Graham, M.C. Phillips. Dynamic and Static Properties of Proteins Adsorbed at the Air/Water Interface. Faraday Discussions of the Chemical Society, $\underline{59}$ (1975) 218

13.     D.E. Graham, M.C. Phillips. Proteins at Liquid Interfaces. Journal of Colloid and Interface Science, $\underline{70}$ (1979) 403

14.     F.K. Hansen, R. Myrvold. The Kinetics of Albumin Adsorption to the Air/Water Interface Measured by Automatic Axisymmetric Drop Shape Analysis. Journal of Colloid and Interface Science $\underline{176}$ (1995) 408.

15.     J. Lyklema. Proteins at Solid-liquid Interfaces; A Colloid-Chemical Review. Colloids and Surfaces, $\underline{10}$ (1984) 33

16.     M. Shimizu, A. Ametani, S. Kaminogawa, K. Yamauchi. The Topography of $\alpha_{s1}$-casein Adsorbed to an Oil/Water Interface: an analytical approach using proteolysis. Biochemica Biophysica Acta. $\underline{869}$ (1986) 259

17.     F. MacRitchie, A.E. Alexander. Kinetics of Adsorption of Proteins at Interfaces.

Journal of Colloid Science 18 (1963) 453

18.   G. Serrien, G. Geeraerts, L. Ghosh, P. Joos. Dynamic Properties of Adsorbed Protein Solutions. Colloids and Surfaces. 68 (1992) 219

19.   F. MacRitchie. Protein Adsorption/Desorption at Fluid Interfaces. Colloids and Surfaces. 41 (1989) 25

20.   J.C. Dijt, M.A. Cohen Stuart, G.J. Fleer. Kinetics of Polymer Adsorption and Desorption in Capillary-flow. Macromolecules. 25 (1993) 5416

21.   W. Norde, F. MacRitchie, G. Nowicka, J. Lyklema. Protein Adsorption at Solid-Liquid Interfaces: Reversibility and Conformation Aspects. Journal of Colloid and Interface Science. 112 (1986) 447

22.   M. A. Cohen Stuart. G. J. Fleer, J. Lyklema, and J.M. H. M. Scheutjens, Adsorption of Ions, Polyelectrolytes and Proteins. Advances in Colloid Interface Science.,34 (1991) 477

23    W. Norde, J.P. Favier. Structure of Adsorbed and Desorbed Proteins. Colloids and Surfaces. 64 (1992) 87

24    W. Norde, A.C.I. Anusiein. Adsorption, Desorption and Readsorption of Proteins on Solid-Surfaces. Colloids and Surfaces. 66 (1992) 73

25.   I. Jönsson, I. Rönnberg, M. Malmqvist. Flow-Injection Ellipsometry - An in situ Method for the Study of Biomolecular Adsorption and Interaction at Solid Interfaces. Colloids and Surfaces. 13 (1985) 333

26.   C.A. Haynes, W. Norde. Structures and Stabilities of Adsorbed Proteins. Journal of Colloid and Interface Science. 169 (1995) 313

27.   A.F.H. Ward and I. Tordai. Time Dependence of Boundary tensions of solutions. Journal of Chemical Physics. 14 (1946) 453

28.   A.G. Walton, M.E. Soderquist. Behaviour of Proteins at Interfaces. Croatica Chemica Acta 53 (1980) 363

29.   R.L. Beissinger, E.F. Leonard. Sorption Kinetics of Binary Protein Solutions: General Approach to Multicomponent Systems. Journal of Colloid and Interface Science. 85 (1982) 521

30.   I. Lundström. Models of Protein Adsorption on Solid Surfaces. Progress in Colloid & Polymer Science. 70 (1985) 76

31.   P. Schaaf, J. Talbot. Surface Exclusion Effects in Adsorption Processes. Journal of Chemical Physics. 91 (1989) 4401

32.   R.Z. Guzman, R.G. Carbonell, P.K. Kilpatrick. The Adsorption of Proteins at Gas-Liquid Interfaces. 114 (1986) 536

33.   J.R. Hunter, P.K. Kilpatrick, R.G. Carbonell. Lysozyme Adsorption at the Air/Water Interface. Journal of Colloid and Interface Science. 137 (1990) 462

34. J.R. Hunter, P.K. Kilpatrick, R.G. Carbonell. β-casein Adsorption at the Air/Water Interface. Journal of Colloid and Interface Science. 142 (1991) 429

35. R.Douillard, J. Lefebvre. Adsorption of Proteins at the Gas-Liquid Interface: Models for Concentration and Pressure Isotherms. Journal of Colloid and Interface Science 139 (1990) 488

36. T.A. Horbett, J.L. Brash. Proteins at Interfaces, Physicochemical and Biochemical Studies. J.L. Brash, T.A. Horbett. eds. ACS Symp. Ser. 343 (1987). Chapter 1.

37. A.V. Makievski, V.B. Fainerman, M. Bree, R. Wüstneck, J. Krägel, R. Miller. Adsorption of Proteins at the Liquid/Air Interface. J. Phys. Chem. B 102 (1998) 417

38. J.A. de Feijter, J. Benjamins.Soft-Particle Model of Compact Macromolecules at Interfaces. Journal of Colloid and Interface Science 90 (1982) 289

39. F. MacRitchie, L. E. Alexander. Kinetics of Adsorption of Proteins at Interfaces II. Journal of Colloid and Interface Science. 18 (1963) 458

40. E. Tornberg. The Application of the Drop Volume Technique to Measurements of The Adsorption of Proteins at Interafces. Journal of Colloid and Interface Science. 64 (1978) 391

41. F. MacRitchie. Desorption of Proteins from the Air/Water Interface. Journal of Colloid and Interface Science. 105 (1985) 119

42. J.W. Gibbs. On the Equilibrium of Heterogeneous Substances. Trans. Connecticut Acad., III: 108 343 (1878). Reprinted in: The scientific papers of J.Willard Gibbs, Volume 1, Dover Publications Inc., New York. p.55.

43. G. Gonzalez, F. MacRitchie. Equlibrium Adsorption of Proteins. Journal of Colloid and Interface Science. 32 (1970) 55

44. J.A. de Feijter, J. Benjamins. Adsorption Behaviour of PVA at the Air-Water Interface. Journal of Colloid and Interface Science. 81 (1981) 91

45. G.J. Fleer, M.A. Cohen Stuart, J.M.H.M. Scheutjens, T. Cosgrove, B. Vincent. Polymers at Interfaces. Chapman & Hall, London (1993)

46. A. Schmitt, R. Varoqui, S. Uniyal, J.L. Brash, C. Pusineri. Interaction of Fibrinogen with Solid Surfaces of Varying Charge and Hydrophobic-Hydrophilic Balance. Journal of Colloid and Interface Science. 92 (1983) 25

47. J.L. Brash, Q.M. Samak. Dynamics of Interactions between Human Albumin and Polyethylene Surface. Journal of Colloid and Interface Science. 65 (1978) 495

48. W.J. Dillman, I.F. Miller. On the Adsorption of Serum Proteins on Polymer Membrane Surfaces. Journal of Colloid and Interface Science. 44 (1973) 221

49. E.H. Lucassen-Reynders. Competitive adsorption of emulsifiers. Colloids and Surfaces. 91 (1994) 79

50. A. Silberberg. Theoretical Aspects of the Adsorption of Macromelecules. Journal of

Polymer Science. 30 (1970) 393

51. C.A.J. Hoeve. Theory of Polymer Adsorption at Interfaces. Journal of Polymer Science. 34 (1971) 1

52. S.J. Singer. Note on an Equation of State for Linear Macromolecules in Monolayers. Journal of Chemical Physics 16 (1948) 872

53. H.L. Frisch, R. Simha. Monolayers of Linear Macromolecules. Journal of Chemical Physics 24 (1956) 652

54. A.M. Altschul. "Proteins". Chapman and Hall, London, chapter 2 (1965)

55. E.H. Lucassen-Reynders and J. Benjamins. Dilational Rheology of Proteins Adsorbed at Fluid Interfaces. in E. Dickinson and J. Rodríguez Patino (Editors), Food Emulsions and Foams: Interfaces, Interactions & Stability, Special Publication No. 227, p 195-206 (Royal Society of Chemistry, London, 1999)

56. E. Dickinson, D.S. Horne, J.S. Phipps, R.M. Richardson. A Neutron Reflectivity Study of the Adsorption of β-Casein at Fluid Interfaces. Langmuir 9 (1993) 242

57. A. Eaglesham, T.M. Herrington, J. Penfold. A Neutron Reflectivity Study of a Spread Monolayer of Bovine Serum Albumin. Colloids and Surfaces. 65 (1992) 9.

58. D.E. Graham, M.C. Phillips. Proteins at Liquid Interfaces II. Journal of Colloid and Interface Science. 70 (1979) 415

59. S. Xu, S. Damodaran. Comparative Adsorption of Native and Denatured Egg-White, Human and T4 Phage Lysozymes at the Air-Water Interface. Journal of Colloid and Interface Science. 159 (1993) 124

60. S. Xu, S. Damodaran. Kinetics of Adsorption of Proteins at the Air-Water Interface from a Binary Mixture. Langmuir. 10 (1994) 472

61. T. Sengupta, S. Damodaran. Role of Dispersion Interactions in the Adsorption of Proteins at Oil-Water and Air-Water Interfaces. Langmuir 14 (1998) 6457

62. D.J.Adams, M.T.A. Evans, J.R.Mitchell, M.C. Phillips, P.M. Rees. Adsorption of Lysozyme and some Acetyl Derivates at the Air-Water Interface. Journal of Polymer Science: Part C. 34 (1971) 167

63. M.E. Soderquist, A.G. Walton. Structural Changes in Proteins Adsorbed on Polymer Surfaces. Journal Colloid Interface Science 75 (1980) 386

64. V. Hlady, R.A. van Wagenen, J.D. Andrade. in "Surface and interfacial aspects of biomedical polymers", J.D. Andrade, Ed., Vol. 2 " Protein Adsorption", Plenum Press, New York, (1985) 81

65. M. Coke, P.J. Wilde, E.J. Russell, D.C. Clark. The Influence of Surface Composition and Molecular Diffusion on the Stability of Foams formed from Protein/Surfactant Mixtures. Journal Colloid Interface Science. 138 (1990) 489

66. C.G. de Kruif, R.P. May. Kappa-casein Micelles - Structure, Interactions and Gelling

Studied by Small-Angle-Neutron-Scattering. Eurpean Journal of Biochemistry. <u>200</u> (1991) 431

67.   Y.L. Cheng, B.K. Lok, C.R. Robertson, in "Surface and interfacial aspects of biomedical polymers", J.D. Andrade, Ed., Vol. 2 " Protein Adsorption", Plenum Press, New York, Ch. 2, (1985) 121

68.   A.C. Hall. A Century of Ellipsometry. Surface Science <u>16</u> (1969) 1

69.   A. Vasicek. Optics of Thin Films, North Holland, Amsterdam (1960)

70.   E.Passaglia, R.R. Stromberg, J.Kruger, Eds. Ellipsometry in the Measurement of Surfaces and Thin Films. Natl. Bur. Stand. U.S. Misc. Publ. 256, Washington, D.C. (1964)

71.   N.M. Bashara, A.B. Buckman, A.C. Hall, Eds. Surface Science <u>16</u> (1969)

72.   J.J. Ramsden. Experimental Methods for investigating Protein Adsorption Kinetics at Surfaces. Quaterly Reviews of Biophysics <u>27</u> (1993) 41

73.   T. Nylander. Proteins at the Metal/Water Interface - Adsorption and Solution Behaviour Thesis, University of Lund. Lund, Sweden. (1987)

74.   M. Malmsten. Ellipsometry Studies of Protein Layers Adsorbed at Hydrophobic Surfaces. Journal of Colloid and Interface Science <u>166</u> (1994) 333

75.   P.A. Cuypers, J.W. Corsel, M.P. Janssen, J.M.M. Kop, W. Th. Hermens, H.C. Hemker. Journal Biology and Chemistry. <u>258</u> (1983) 2426.

76.   J.A. de Feijter, J. Benjamins, F. Veer. Ellipsometry as a Tool to Study the Adsorption Behaviour of Synthethic and Biopolymers at the Air-Water Interface. Biopolymers. <u>17</u> (1978) 1759

77.   F.L. McCrackin, E.Passaglia, R.R. Stromberg, H.L. Steinberg. J. Res. Natl. Bur. Stand. Sect. A, <u>67</u> (1963) 363

78.   H.J. Trumit. A Theory and Method for the Spreading of Protein Monolayers. Journal of Colloid Science. <u>15</u> (1960) 1

79.   A.D. Nisbet, R.H. Saundry, A.J.G. Moir, L.A. Fothergill and J.E. Fothergill. The Complete Amino-Acid-Sequence of Hen Ovalbumin. European Journal of Biochemistry. <u>115</u> (1981) 335

80.   Aftab A. Ansari, R. Ahmad, A. Salahuddin. The Native and Denatured States of Ovalbumin. Biochemical Journal. <u>126</u> (1972) 447

81.   C. C. F. Blake, D. F. Koenig, G. A. Mair, A. C. T. North, D. C. Phillips, V. R. Sarma. Structure of Hen Egg-White Lysozyme. Nature. <u>206</u> (1965) 757

82.   H.E. Swaisgood. Chemistry of the Caseins. In Advanced Dairy Chemistry, Volume 1 Proteins. P.F. Fox ed.; Elsevier Applied Science.  (1992) 63

83.   D.C. Carter, J.X. Ho. Structure of Serum Albumin. Advances in Protein Chemistry <u>45</u> (1994) 153

84. R. Cecil. The Proteins: Composition, Structure and Function. ed. H. Neurath. V1, Academic Press, New York, (1963)

85. B.D. Fair, A.M. Jamieson. Studies of proteins on Polysterene Particles. Journal of Colloid and Interface Science. 77 (1980) 525

86. A.J. Luft, F.L. Lorscheider. Structural Analysis of Human and Bovine α-Fetoprotein by Electron Microscopy, Image Processing, and Circular Dichroism. Biochemistry. 22 (1983) 5978

87. Y. T. Su, B. Jirgensons. Further Studies on Detergent-Induced Conformational Transitions in Proteins. Archives of Biochemistry and Biophysics 181 (1977) 137

88. M. Paulsson. Thermal Denaturation of Whey Proteins and Adsorption at the Air/Water Interface. Thesis, University of Lund. Lund, Sweden. (1990)

89. C. Tanford. Physical Chemistry of Macromolecules. Wiley, New York, 1961, Chap.6.

90. L.J. Gosting. Measurements and Interpretation of Diffusion Coefficients of Proteins. Advances in Protein Chemistry. Academic Press Inc., New York (1956) 429

91 D.E. Kuehner, C. Heyer, C. Rämsch, U.M. Fornefeld, H.W. Blanch, J.M. Prausnitz. Interactions in Concentrated Electrolyte Solutions from Dynamic Light Scattering. Biophysical Journal. 73 (1997) 3211

92 A.K. Gaigalas, J.B. Hubbard, M. McCurley, S. Woo. Diffusion of Bovine Serum Albumin in Aqueous Solutions. J. Phys. Chem. 96 2355 (1992)

93. J.R. Whitaker, S.R. Tannenbaum. Food Proteins. AVI Publishing Company. (1977)

94. Toshio Ishii, Mitsuo Muramatsu. Spreadibility of Ovalbumin Monolayers at Air-Water Interface. Bulletin of the Chemical Society of Japan. 43 (1970) 2364

95. M. Blank, B. B. Lee, J. S. Britten. Adsorption Kinetics of Ovalbumin Monolayers. Journal of Colloid and Interface Science. 50 (1975) 215

96. H. B. Bull. Adsorbed Surface Films of Egg Albumin. Journal of Colloid and Interface Science. 41 (1972) 305

97. T. Yamashita, H. B. Bull. Films of Lysozyme Adsorbed at the Air-Water Interface. Journal of Colloid and Interface Science. 27 (1968) 19

98. M.T.A. Evans, J. Mitchell, P.R. Musselwhite, L. Irons. The effect of the modification of protein structure on the properties of proteins spread and adsorbed at the air-water interface. Surface Chemistry of Biological Systems. ed. M. Blank, Plenum N.Y. (1970) 1

99. D.E. Graham, M.C. Phillips. Proteins at Liquid Interafaces III. Journal of Colloid and Interface Science. 70 (1979) 427

100. B.S. Murray. Adsorption Kinetics of Nonradiolabeled Lysozyme via Surface Pressure-Area Isotherms. Langmuir 13 (1997) 1850

101. J.A de Feijter, J. Benjamins. Adsorption Kinetics of Proteins at the Air-Water

Interface. In Food Emulsions and Foams, E. Dickinson ed.; Royal Society of Chemistry: London, (1987) 72

102. F. MacRitchie, L. Ter-Minassian Saraga. Concentrated Protein Monolayers: Desorption Studies With Radiolabelled Bovine Serum Albumin. Colloids and Surfaces. 10 (1984) 53

103. M. Paulsson, P. Dejmek. Surface Film Pressure of β-Lactoglobulin, α-Lactalbumin, Bovine Serum Albumin at the Air/Water Interface studied by Wilhelmy plate and Drop Volume. Journal of Colloid and Interface Science. 150 (1992) 394

104. A.J.I. Ward, L.H. Regan. Pendant Drop Studies of Adsorbed Films of Bovine Serum Albumin. Journal of Colloid and Interface Science. 78 (1980) 389

105. N. Puff, A. Cagna, V. Aguié-Béghin, R. Douillard. Effect of Ethanol on the Structure and Properties of β-Casein Adsorption Layers at the Air/Buffer Interface. Journal of Colloid and Interface Science. 208 (1998) 405

106. M. B. Huglin. Light Scattering from Polymer Solutions, Academic Press, London, (1972) 277

107. J.R. Lu, T.J. Su, R.K. Thomas, J.Penfold, J. Webster. Structural Conformation of Lysozyme layers at the Air/Water Interface studied by Neutron Reflection. Journal of the Chemical Society -Faraday Transactions. 94 (1998) 3279

108. T.J. Su , J.R. Lu, R.K. Thomas, Z.F. Cui, J. Penfold. The Effect of Solution pH on the Structure of Lysozyme Layers Adsorbed at the Silica-Water Interface studied by Neutron Reflection. Langmuir. 14 (1998) 438

109. J.R. Lu, T.J. Su, R.K. Thomas. Binding of Surfactants onto Preadsorbed Layers of Bovine Serum Albumin at the Silica-Water Interface. Journal of Physical Chemistry B 102 (1998) 10307

110. T. Kull, T. Nylander, F. Tiberg, N.M. Wahlgren. Effect of Surface Properties and Added Electrolyte on the Structure of β-Casein Layers Adsorbed at the Solid/Aqueous Interface Langmuir 13 (1997) 5141

111. M.R. Bruzessi, E. Chiacone, E. Antonini. Association-Dissociation Properties of Lysozyme. Biochemistry. 4 (1965) 1796

112. A.A. Trapeznikov, V.G. Vins, T.Y. Shirikova. Kinetics of the Reduction of Surface Tension in Protein Solutions. Colloid Journal of USSR. 43 (1981) 262

113. D. Cho, G. Narsimham, E.I. Franses. Adsorption Dynamics of Native and Pentylated Bovine Serum Albumin at Air-Water Interfaces: Surface Concentration/Surface Pressure Measurements. Journal of Colloid and Interface Science 191 (1997) 312

114. A.P. Wei, J.N. Herron, D. Andrade. in "From Clone to Clinic" (D.J.A. Crommelin and A. Schellekens, Eds.), Kluwer, Dordrecht, (1990) 309

115. M. Subirade, J. Gueguen, K.D Schwenke. Effect of Dissociation and Conformational

Changes on the Surface Behaviour of Pea Legumin. Journal of Colloid and Interface Science 152 (1992) 442

116. J.G.M. Lankveld, J. Lyklema. Adsorption of Polyvinyl Alcohol on the Paraffin-Water Interface. Journal of Colloid and Interface Science. 41 (1972) 454

117. H.B. Bull. Spread Monolayers of Protein. Advances in Protein Chemistry. 27 (1947) 95

118. P. Bagchi, S.M. Birnbaum. Effect of pH on the Adsorption of Immunoglobulin G on Anionic Poly(vinyltoluene) Model Latex Particles. Journal of Colloid and Interface Science. 83 (1981) 460

119. B.W. Morrissey, C.A. Fenstermaker. Conformation of Adsorbed $\gamma$-globulin and $\beta$-Lactoglobulin. Effect of Surface Concentration. Trans. Am. Soc. Artif. Int. Organs. 22 (1976) 278

120. M. van den Tempel, E.H. Lucassen-Reynders. Relaxation Processes at Fluid Interfaces. Advances in Colloid Interface Science. 18 (1983) 281

121. A.F. Henson, J.R. Mitchell, P.R. Musselwhite. The surface coagulation of proteins during shaking. Journal of Colloid and Interface Science. 32 (1970) 162

122. E. Helfand, H.L. Frisch, J.L. Lebowitz. Theory of Two- and One-Dimensional Rigid Sphere Fluids. Journal of Chemical Physics. 34 (1961) 1037

123. P.van Dulm W. Norde. The Adsorption of Human Plasma Albumin on Solid Surfaces, with Special Attention to Kinetic Aspects. Journal of Colloid and Interface Science. 91 (1983) 248

124. A. v.d. Scheer; Adsorption of Plasma Proteins. Thesis, Twente, the Netherlands (1978)

125. J.F. Kleibeuker, R. Schaier. Unpublished results (1978)

126. E.H. Lucassen-Reynders. Surface Equation of State for ionized Surfactants. Journal of Physical Chemistry. 70 (1966) 1777

127. A. Siberberg. Multilayer Adsorption of Macromolecules. Journal of Colloid and Interface Science. 38 (1972) 217

# 3    DYNAMIC BEHAVIOUR OF ADSORBED PROTEINS UNDER SURFACE COMPRESSION AND EXPANSION.

## 3.1 Introduction

Proteins can be very effective in producing and stabilizing foams and emulsions. To a degree, their role is similar to that of low molecular weight surface active molecules: both types of molecules adsorb at air/water (foams) and oil/water (emulsions) interfaces. The primary effect of such molecular adsorption is that it reduces the tension of the interface. However, the reduction of the interfacial tension cannot in itself explain the formation of emulsions and foams with more than transient stability. If this were the case, it should be possible to prepare emulsions and foams in the absence of surface active solutes, from pure low tension liquids. In practice it is impossible to obtain emulsions with any degree of stability.

Lowering of the interfacial tension by surface active substances is only a first step in the production of a stable foam or emulsion. A low interfacial tension facilitates break-up into smaller droplets. However, break-up requires rapid and substantial stretching of bubbles or drops and consequently the interfacial tension may be far from equilibrium. This is one reason for an investigation into the dynamic interfacial properties of adsorbed protein layers.
A more important reason, why information about the dynamic properties of adsorbed layers is needed, is related to their stabilizing function during emulsification. In many emulsifying machines, conditions of flow are such that zones of low shear exist adjacent to highly sheared regions. After break-up in a high shear region, droplets almost always spend some time in zones where they can recoalesce if their dynamic stability is low. Emulsifiers retard or prevent recoalescence because, due to their presence in the interface, gradients in interfacial tension can arise which enable the interface to resist tangential stresses from the adjoining flowing liquids (1). Figure 1a illustrates how such gradients can produce a resistance against local thinning of a liquid film separating two emulsion droplets or foam bubbles, and so prevent or retard coalescence. Similar interfacial tension gradients (see Figure 1b) arise if two emulsion droplets are forced towards each other by liquid flow. In this case the gradient is caused by the drainage of the liquid out of the film between the droplets. In turn the gradient will retard the further drainage. Without such a gradient any two drops just formed would be liable to re-coalescence during the emulsification process.
Consequently, information about the behaviour under static conditions is not sufficient to understand the role of surface active agents during foaming and emulsification. Extra information is needed  about the response of adsorbed layers to deformations.

Figure 1a
Result of surface disturbance in thin liquid layer separating two emulsion drops or foam bubbles.
Arrows: flow of surface and bulk liquid.

**Local Extension of Interface**
▽
**Lower Adsorption**
▽
**Higher Interfacial Tension**
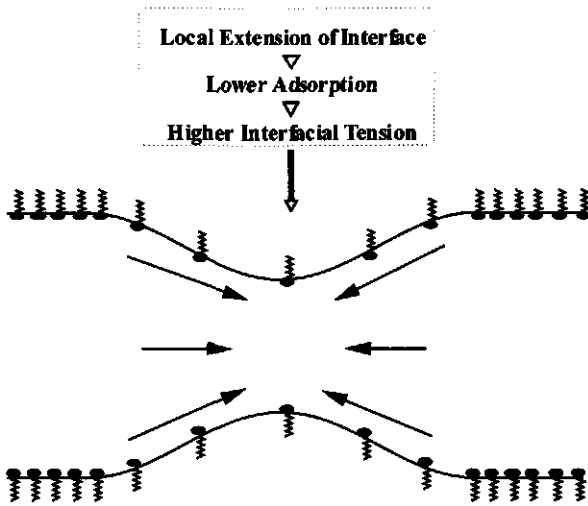


Figure 1b
Marangoni effect in the liquid layer separating two emulsion drops.

oil    $\Delta\gamma$

water

oil
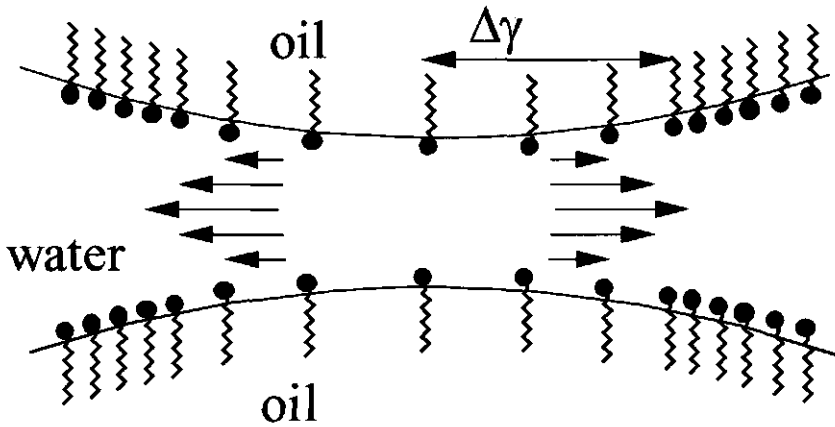
The magnitude and rate of these deformations depend on the process under consideration. Large and fast deformations are relevant to the break-up process (2), while slower deformations are important for the study of film drainage and stabilisation (3). The relevant timescale of the break-up process in a homogeniser was estimated to be $10^{-3}$ sec or even faster (3). The time scale of recoalescence during emulsification is of the same order of magnitude. However for long term stability the relevant timescale is of course considerably longer.

Dynamic interfacial properties or interfacial rheology can be measured in two types of deformation:

(i) surface compression/dilation, which measures the response to changes in area at constant shape of a surface element. These form the subject of this chapter.

(ii) surface shear, which measures the response of the surface to changes in shape at constant area. (see chapter 5)

In principle a third type of deformation, interfacial bending, can be distinguished. This type of deformation is likely to be only relevant in strongly curved systems, such as microemulsion droplets, but not in the fairly coarse low curvature emulsions considered here. Both measurements can be performed at small periodical deformations as well as under continuous expansion (4,5,6) or shear (7,8). For extensive reviews see refs. (9,10). Results generally depend on extent and rate of the surface deformation applied. The advantage of small periodical deformations compared to continuous ones, is that the former type enables us to study relaxation phenomena without full knowledge of the surface equation of state. Another advantage is that in periodic experiments only one time scale is involved (11). Rheological coefficients obtained at small and large deformation can be interrelated only in special cases where both relaxation mechanism and equation of state are known quantitatively (12).

Recently, significant progress has been made in the measurement of dynamic interfacial processes at short time scales as upon rapid expansion of drops (13,14) or at high frequencies ($10^{+2}$-$10^{+3}$ Hz) of compression/expansion (15,16).

For low molecular weight surfactants the dynamic behaviour is more or less fully understood and can often be explained in terms of the surfactant parameters, e.g. their diffusion coefficient and surface-equation-of-state parameters (12). For proteins it has not yet been possible to build a comprehensive model in spite of many recent experimental data (8,17-22). Bottlenecks for building such a model from literature data are: (i) the same proteins from different sources will sometimes give different results, especially if the molecules have been modified, e.g., in radio tracer probing, (ii) the experimental techniques that have been used are not always compatible, and (iii) model building is hampered because it is unclear how the

apparent "irreversibility" of protein adsorption is reflected in the dynamic behaviour. This apparent "irreversibility" is related to the multiple states of unfolding and their charateristic times (23).

The aim of the present chapter is to contribute to the understanding of dynamic properties of adsorbed protein layers under compression/dilation. These properties will be related to the equilibrium adsorption properties that were presented in the previous chapter (chapter 2) and the molecular properties of the protein.

3.2 The surface dilational modulus

The suface dilational modulus is defined by the expression originally proposed by Gibbs (24) for the surface elasticity of a soap-stabilised liquid film as the increase in surface tension for a small increase in area of a surface element:

$$\epsilon = \frac{d\gamma}{d\ln A} \qquad (1)$$

where $\gamma$ is the surface tension and A the area of the surface element. In the simplest case, the modulus is a pure elasticity with a limiting value, $\epsilon_0$, to be deduced from the surface equation of state, i.e., from the equilibrium relationship between surface tension and surfactant adsorption, $\Gamma$:

$$\epsilon_0 = \left( \frac{-d\gamma}{d\ln\Gamma} \right)_{eq} \qquad (2)$$

The limiting value is reached only if, in the timescale of the experiment, there is no exchange of surfactant with the adjoining bulk solution ( $\Gamma$xA is constant), and if, moreover, the surface tension adjusts instantaneously to the equilibrium value of the new adsorption. Deviations from this simple limit occur when relaxation processes in or near the surface affect either $\gamma$ or $\Gamma$ within the time of the measurement. In such cases, the modulus $\epsilon$ is a surface viscoelasticity, with an elastic part accounting for the recoverable energy stored in the interface and a viscous contribution reflecting the loss of energy through any relaxation process occurring at or near the surface. Elastic and viscous contributions can be measured simultaneously by subjecting the surface to small periodic compressions and expansions at a given frequency. In such experiments the viscoelastic modulus $\epsilon$ is a complex number, with a real part $\epsilon'$ (the storage modulus) equal to the elasticity, $\epsilon_d$, and the imaginary part $\epsilon''$ (the loss modulus) given by the product of viscosity, $\eta_d$, and the imposed angular frequency, $\omega$,

of the area variations:

$$\epsilon = \epsilon' + i\epsilon'' = \epsilon_d + i\omega\eta_d \tag{3}$$

Experimentally, the imaginary contribution $\epsilon''$ to the modulus $\epsilon$ is reflected in a phase difference $\phi$ between stress $(d\gamma)$ and strain $(dA)$. The elastic and viscous contributions are given by:

$$\epsilon' = |\epsilon|\cos\phi \qquad ; \qquad \epsilon'' = |\epsilon|\sin\phi \tag{4}$$

respectively, where $|\epsilon|$ is the absolute value of the complex modulus and $\phi$ is the phase angle.

## 3.3 Experimental methods

### 3.3.1 Longitudinal wave method.

Convenient techniques for measuring surface dilational moduli are derived from the longitudinal wave method developed by Lucassen and van den Tempel (4). In this method, the surface is periodically expanded and compressed, usually but not invariably by a barrier which oscillates in the plane of the surface, and the response of the surface tension is monitored by a probe, e.g., a Wilhelmy plate, some distance away from the barrier. A problem here is that the amplitude of the area variations generated by the barrier may be substantially damped when the area disturbance reaches the probe (e.g. plate). The area variation generated by the barrier travels over the surface as a longitudinal wave, with characteristics derived and measured by Lucassen and van den Tempel (25). The wave characteristics, wavelength $(\lambda)$ and damping coefficient $(\beta)$, were found to depend far more strongly on the surface dilational modulus than is the case for transverse capillary waves or ripples.

The equations describing small-amplitude surface waves can be obtained by solving the hydrodynamic equations of motion of the adjoining bulk phases, using the boundary condition that the viscous drag exerted by the surface on the adjoining bulk phases is compensated by a surface tension gradient, in the absence of appreciable resistance to surface shear. Three regimes must be distinguished depending on the damping coefficient of the wave and the effective length (L, see Section 3.3.2) of the trough. Experimentally most convenient is the

limiting case where the wavelength ($\lambda$) is much greater than L and the damping coefficient is much smaller than 1/L. In this region the wave is reflected back and forth between the walls of the trough and the barrier. As a result of these multiple reflections, the surface undergoes a practically uniform deformation, without the wave character being apparent from variations in phase and amplitude with distance. This region is characterised by very high values of the wave propagation number W defined by Lucassen and Barnes (26) as the ratio of the distance at which the wave is damped to 1/e of its original amplitude ($=1/\beta$) to the effective length of the trough ($=L$). In view of the dispersion equation of the wave (25), W can be expressed by:

$$W = \frac{1}{\beta L} = \frac{|\epsilon|^{1/2}}{L\omega^{3/4}\left(\sqrt{\eta\rho} + \sqrt{\eta'\rho'}\right)^{1/2} \sin(\pi/8 + \phi/2)} \tag{5}$$

where $\eta$ and $\rho$ are liquid viscosity and density, respectively, and primed symbols refer to the upper fluid phase. In cases where $W \gg 1$, the viscoelastic modulus simply can be obtained from the surface tension variation ($\Delta\gamma$) measured anywhere on the surface and from the amplitude of the overall area change ($\Delta A$):

$$|\epsilon| = \left[(\epsilon')^2 + (\epsilon'')^2\right]^{1/2} = \frac{A\Delta\gamma}{\Delta A} \tag{6}$$

At the other extreme, the surface wave is fully damped before it has travelled the distance L. In this case the viscoelastic modulus $|\epsilon|$ and the viscous phase angle $\phi$ can be determined by measuring wave number $\kappa$ ($=2\pi/\lambda$) and damping coefficient $\beta$ (25):

$$|\epsilon| = \frac{\omega^{3/2}\left(\sqrt{\eta\rho} + \sqrt{\eta'\rho'}\right)}{\kappa^2 + \beta^2} \tag{7}$$

$$\phi = 2\arctan(\beta/\kappa) - \pi/4 \tag{8}$$

In this region the wave propagation number W is very small ($W \ll 1$, i.e., $\beta L \gg 1$).

In the intermediate region, where W is of order 1, no explicit expressions exist for the calculation of modulus and phase angle $\phi$ from measured values of $\Delta\gamma$ and phase difference as a function of distance from the oscillating barrier. The only way to determine required data in this region is to compare the curve of the measured $\Delta\gamma$ and phase difference with a set of predicted curves (26). This procedure is laborious; it is advisable to avoid this region by

63

adapting trough length and/or frequency.

3.3.2 Conventional method

The conventional apparatus, schematically drawn in Figure 2, consists of a rectangular shallow trough with one or two movable teflon bar(s) as barrier(s) compressing and expanding the interface, and a Wilhelmy plate for monitoring the response of the interfacial tension. For a water vapour interface to be investigated, the trough is filled up to the rim with the aqueous solution, and the barriers are placed on top. The interfacial area between the teflon bars is compressed and expanded by a sinusoidal movement of one or both end bars. This sinusoidal movement is generated by an eccentric, driven by a constant-speed motor attached to a gear system. The change of the interfacial tension $d\gamma$ produced by the change of the interfacial area $dA$ is measured by a properly positioned Wilhelmy plate attached to a force transducer. The Wilhelmy plate can be situated anywhere on the surface if the deformation of the interface is uniform, i.e., if the wavelength $\lambda$ of the compression/expansion wave generated by the barrier movement is much larger than the length of the trough (W>>1; see Section 3.3.1).
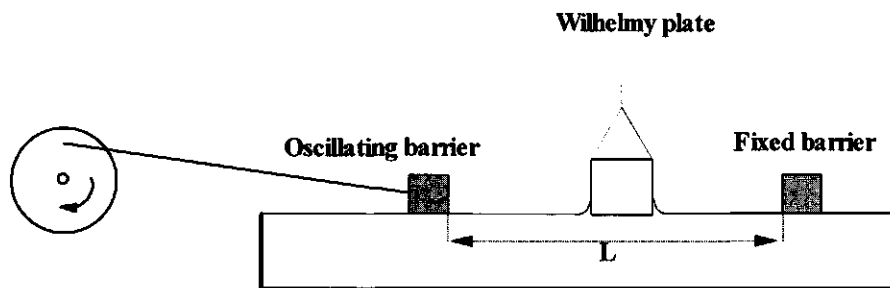


Figure 2. Longitudinal wave apparatus for measuring surface dilational properties.

3.3.3 Surface Shear, a complicating factor in the traditional longitudinal wave method.

The above conventional method has proven to be very suitable to investigate the dilational properties and relaxation mechanisms of many surfactants adsorbed at the air/water interface (4,25,27,28). Occasionally, however, when applied to some macromolecules (29,30) the

Figure 3a
Results of the longitudinal wave experiment on a surface of whey.
$\gamma$ =47 mN/m, $\omega$ =0.042 s$^{-1}$, trough length = 32 cm, $\Delta$ lnA=0.026
Surface tension variations vs. distance from the barrier.

**log $\Delta\gamma$ ($\gamma$ in mN/m)**
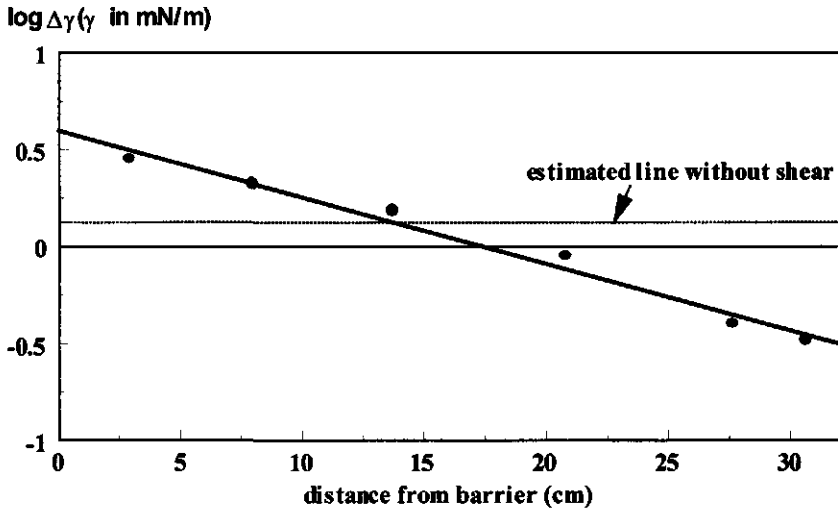


Figure 3b
Surface tension variations during longitudinal wave experiments with a spread monolayer of $\beta$-lactoglobulin.
Trough length= 32 cm, $\omega$ =0.042 s$^{-1}$, $\Delta$ lnA=0.026

**log $\Delta\gamma$ ($\gamma$ in mN/m)**
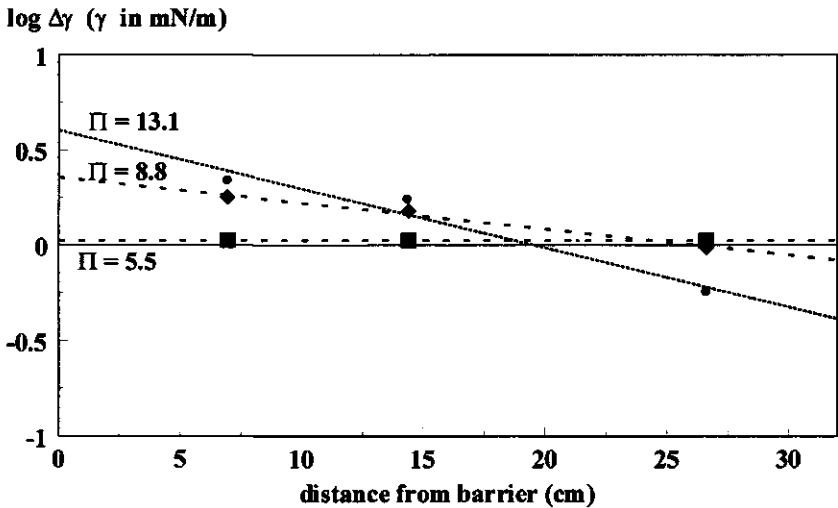
Figure 4a
The effect of shear resistance during visco-elasticity measurements.
Surface displacement pattern without shear (a) and with shear (b).
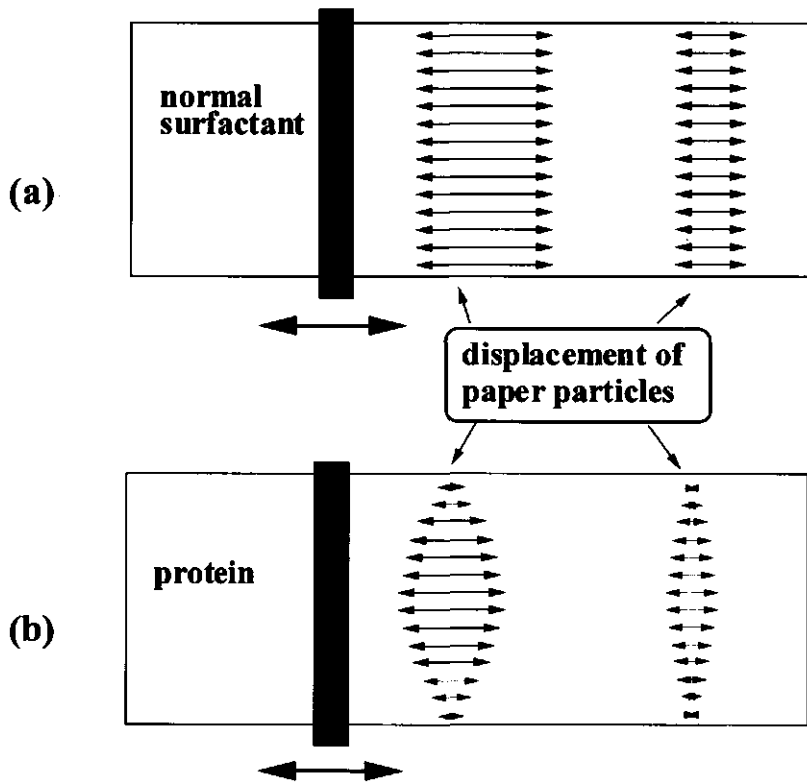
method yielded results that could not be explained with a theory for systems with negligible shear resistance. In the latter study the longitudinal wave method was applied to adsorbed layers of whey protein. In figure 3a the surface tension variations are given as a function of the distance to the barrier. Apparently, the surface deformation is far from uniform, i.e., the wave propagation number W is not >> 1. Indeed, calculations of Lucassen and Barnes (26) show a similar decrease of $\Delta \gamma$ with distance for $W \approx 1$. However, according to Eq. 5 such low values of W can only correspond to very low values of $|\epsilon|$. For the experimental conditions given in Figure 3, this would be the case for $|\epsilon| < 2$ mN/m, i.e., $\Delta \gamma < 0.05$ mN/m., which is considerably lower than the measured values. With spread layers of $\beta$-lactoglobulin similar deviations from theory became obvious at surface pressures > 5 mN/m for BLG (see Fig. 3b) (30). This paradox indicates that the conditions of the simple wave theory were not obeyed in these systems. The decrease of the tension variations with distance from the oscillating barrier, which is a result of decreasing area variations, points to a damping mechanism additional to that in isotropic deformation.

The presence of non-isotropic deformation could be visualized by monitoring the displacement of small paper particles floating on the surface. In fig.4a slightly idealized pictures of the displacement patterns, found for low molecular weight surfactants and proteins are given. For low molecular weight surfactants usually the displacement is uniform across the width of the trough and decreases with increasing distance from the barrier. Provided the modulus is sufficiently high and/or frequency is sufficiently low, this results in an isotropic deformation over the trough (26). For proteins sometimes the pattern is different. The displacement of the particles increases with increasing distance from the side walls. Across the width of the trough a parabolic displacement profile was observed, with the maximum in the middle of the trough. As with low molecular weight surfactants, the displacement decreases with increasing distance from the barrier. However, this decrease is not linear, consequently the deformation over the length of the through is not uniform. The paper particles were only found to be displaced in the length direction of the trough, displacements perpendicular to this direction were not observed, but the experimental accuracy was perhaps not sufficient to detect these.

The non-uniform deformation over the length and width of the trough is in line with the non-uniformity of the surface tension variations, which was found to depend not only on distance from the oscillating barrier, but also on distance from the side walls. The results indicate that shear effects are not negligible here and point to a high shear modulus of the protein-covered surface. Surface shear, which is manifested by a parabolic flow profile of the surface across the width of the trough on compression or expansion was also found for polymers (31) and polypeptides (32).

The parabolic flow profile of the surface is caused by the fact that the surface sticks to the sidewalls of the trough (zero displacement at the sidewalls). Thus, the anomalous damping

of the longitudinal wave should be eliminated when sticking of the surface layer to the sidewalls would be prevented. For ovalbumin solutions this could be achieved by using sidewalls with an electrical charge of the same sign as that of the protein (33). As expected, it was found that the extra damping of the longitudinal wave could be completely eliminated, thus supporting the correctness of the description given above.

In general, eliminating stick of the surface layer to the sidewalls is not very convenient, because it is only effective under special conditions (e.g., pH of the protein solution), which imposes undesirable restrictions on the protein solutions to be investigated.

In principle the longitudinal wave theory can be extended to include the effect of surface shear deformations (34,35,36). However, the interpretation of the data then requires extra experimental input, such as a detailed analysis of the surface movement or independent measurement of the surface shear properties.

A more practical alternative is to change the experimental set-up in such a way that surface shear deformations are avoided, i.e. making the surface deformation purely dilational. This problem was solved by constructing an apparatus in which the surface area is changed isotropically.

3.3.4 Modified method

An isotropic dilational deformation of the surface, without interference of shear, can be achieved using the device shown in Fig.4b . It consists of a shallow, square glass vessel with surface area 19×19 cm and depth 4 cm which contains the solution to be investigated. The area to be subjected to compression/expansion is isolated from the rest of the surface by a square of elastic rubber bands (1 cm high) placed vertically in the surface. In the zero position the dimensions of the sequestered square are 15×15 cm. At the corners of this square, the rubber bands are attached to metal gliders using stainless steel clamps, which can move synchronously in the direction of the square's diagonals. Through flexible metal wires the gliders are connected to an eccentric which is driven by an electromotor; the rotation by the electromotor is thus converted in a synchronous, sinusoidal movement of the corners of the square in the direction of the diagonals of the square. The deformation of the surface within the square is isotropic (purely dilational). It is also uniform provided the conditions (values of $\epsilon$, $\omega$ and L) are such that the wave propagation number W>>1 (see section 3.3.1). In this four-sided compression/expansion set-up L is half the length of the square. Using equations 5, 7 and 8 it is found that in our case this condition is fulfilled when $|\epsilon|>$ 3 mN/m for $\omega=$ 1 rad/sec and $|\epsilon|>$ 0.1 mN/m for $\omega=$ 0.1 rad/sec.

In our device the cycle frequency $\omega$ can be varied between $10^{-3}$ and 1 rad/sec by using an electromotor supplied with a gear box. The amplitude $\Delta\ln A$ of the sinusoidal change of the

Figure 4b
Modified longitudinal wave set-up.
1, rubber bands; 2, metal wire; 3, glass vessel; 4, wheels; 5, eccentric driver system; 6
Wilhelmy plate.
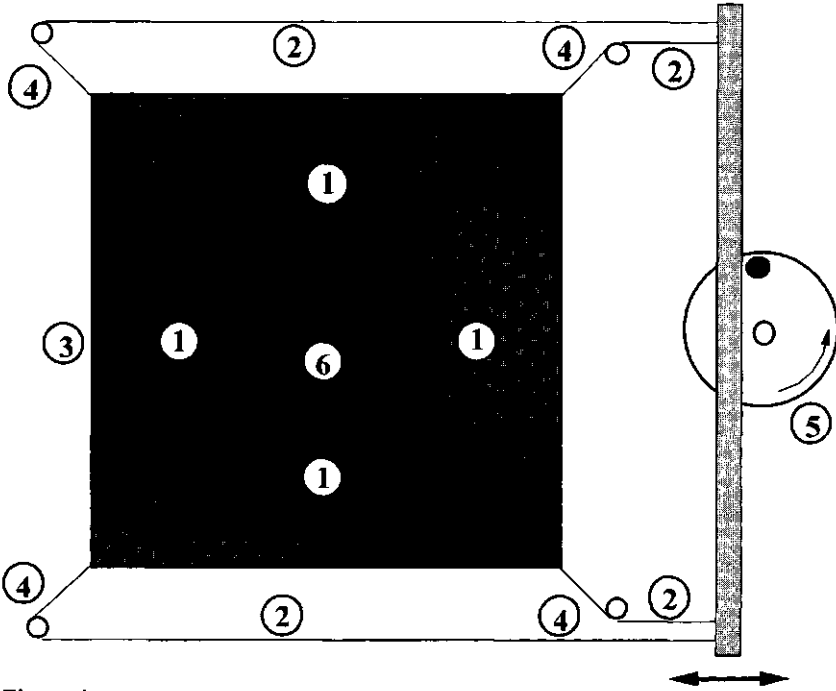


Figure 4c.
Schematic illustration of sinusoidal area variations and corresponding tension variations, for
purely elastic and viscoelastic surface behaviour.
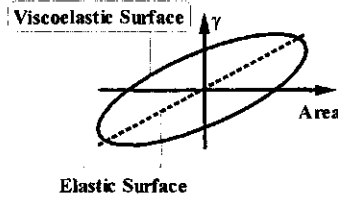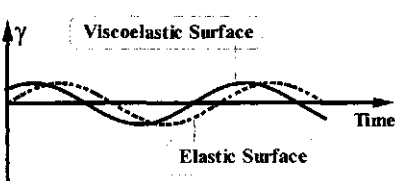
surface area A can be varied between 0 and 0.25 by adjusting the degree of eccentricity of the eccentric system.

To avoid surface contamination of the rubber bands by surface active substances, the bands were first rinsed several times with a soap solution and subsequently washed for several days with distilled water. With the bands thus cleaned no detectible decrease of the surface tension of water ($\Delta\gamma < 0.1$ mN/m) was found after a period of three days.

The sinusoidal oscillation of the surface tension produced by the sinusoidal surface area change is measured in the centre of the square with the Wilhelmy plate attached to an electrobalance. Both $d\gamma$ and $dA/A$ are converted into electrical signals and plotted on the axes of an xy-recorder. This results in a straight line for purely elastic behaviour of the interface, while viscoelastic interfaces produce an ellipse (illustrated in fig 4c). The phase angle $\phi$ is then calculated from the eccentricity of the ellipse written by the xy-recorder. Equipment-induced phase angles were avoided.

The elastic component $\epsilon'$ and the viscous component $\epsilon''$ are calculated from the maximum change of the surface tension, $\Delta\gamma$, and the maximum change of the surface area, $\Delta A$, and from the phase angle $\phi$ using equations 4 and 6.

This modified longitudinal wave device eliminated the anomalous damping of the longitudinal wave found for protein solutions using the standard set-up. The surface tension variations $\Delta\gamma$ and the phase angle $\phi$ were found to be independent of the location of the Wilhelmy plate in the surface.


3.3.5 Modified method versus traditional methods and alternatives.


The advantage of the modified method is that the complicating effects of shear are fully eliminated. However, the use of elastic rubber bands in this set-up necessitates more careful and extensive cleaning. This is a good reason to use this method only if necessary.

The modified method produces more reliable results with surface layers of proteins, polymers and other surfactants that develop a high surface shear modulus. The improvement becomes visible above a certain surface concentration, e.g for $\beta$-lactoglobulin if $\pi > 5$mN/m

Alternative methods that have been developed to cope with this problem can be grouped as follows:

(i)     Methods that do not fully eliminate but sufficiently reduce the shear effect.
        In this type of experimental set ups the traditional Langmuir trough is used. The only adaptations are a wider and shorter trough and two-sided compression and expansion (27). In this set up especially the effect of shear on the Wilhelmy plate is diminished by placing this plate half-way between the oscillating barriers.

(ii)    Methods that fully eliminate shear effects. They include:

a) the method described by Thiessen and Scheludko (37) in which cylindrical transverse waves are generated by excitation of the cylindrical container of the solution. However, transverse waves are not very suitable for the determination of the dilational modulus (11)

b) the ring trough method (38) in which isotropic compression and expansion is ensured, because the surface area deformation is caused by moving a cylindrical glass ring vertically in the liquid surface.

c) the oscillating bubble method (39,40) where isotropic deformation of the surface area is caused by small volume oscillations of the bubble. The resulting surface tension variations are determined from bubble pressure variations. Until now this method has been used only at the air/water surface, for low molecular weight surfactants (low shear) and at high frequencies of the compression/expansion cycle. However, there is no reason to expect difficulties with high shear interfaces at low frequencies.

d) a recently developed dynamic drop tensiometer, which is especially suitable for oil/water interfaces (41). As in the previous method, the area oscillations are induced by volume oscillations. The resulting surface tension variations are determined using drop shape analysis. This method will be described in more detail in chapter 4.

e) simplified modifications of the method with the square rubber band as described above include procedures where only the side-walls of the trough are rubber bands, which are connected to the moving barrier and the opposite wall (35,42). This method can also be combined with the Lucassen-Giles method (27) by connecting the rubber bands to both barriers.

3.4 Results of modulus measurements with modified method.

The surface dilational modulus measurements described below were performed with the same protein samples and under the same experimental conditions as the ellipsometric adsorption measurements presented in chapter 2. Both experiments also involved the measurement of the surface pressure. This enables us to link the measured moduli via the surface pressure to the surface concentration. In Figure 5 a-f, for a flexible protein, a globular protein and a synthetic polymer, modulus, surface pressure and adsorbed amount are plotted as a function of the adsorption time (43). In each case results for two concentrations are given. These figures illustrate the slow equilibration of the surfaces of very dilute macromolecular solutions, reflected in a steady increase of modulus, adsorbed amount and surface pressure as a function of the adsorption time. As expected, the modulus of the higher protein concentrations starts to increase after a shorter adsorption time. However, the modulus at near-equilibrium (i.e. after 21 hours) does not significantly increase with increasing concentration in most cases.

Figure 5a-f.
Surface dilational modulus, adsorption and surface pressure as a function of adsorption time.
for two protein concentration. Frequency: 0.84 rad/s; pH=6.7; $\Delta A/A=0.07$
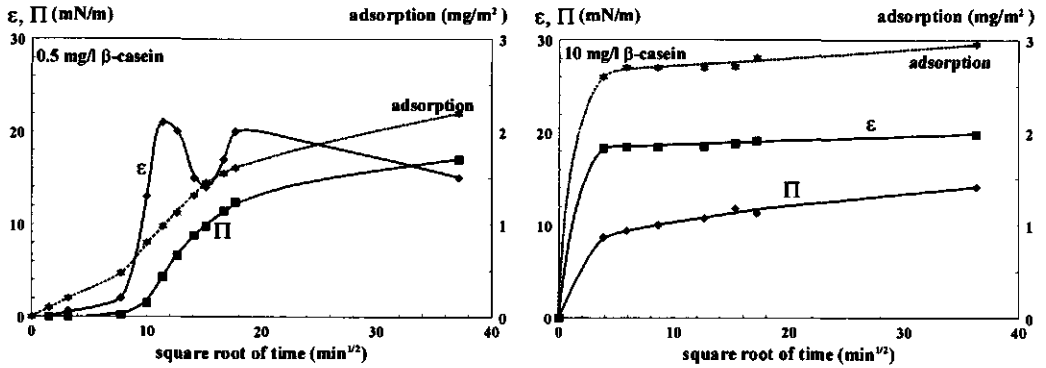


Figure 5a and 5b β-casein
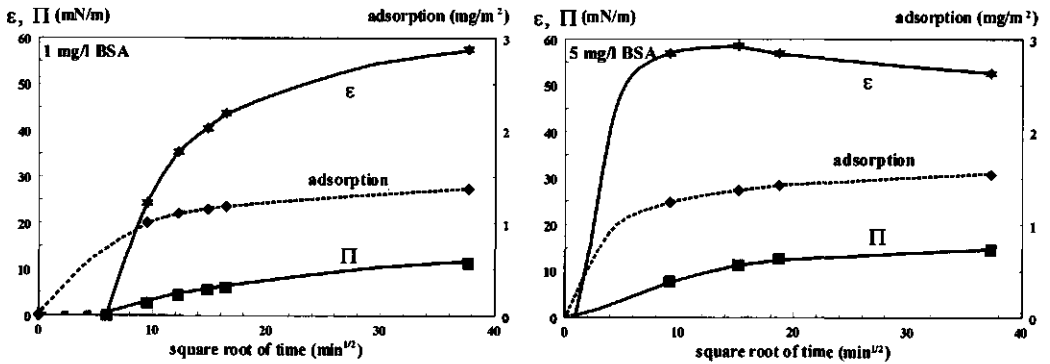


Figure 5c and 5d BSA
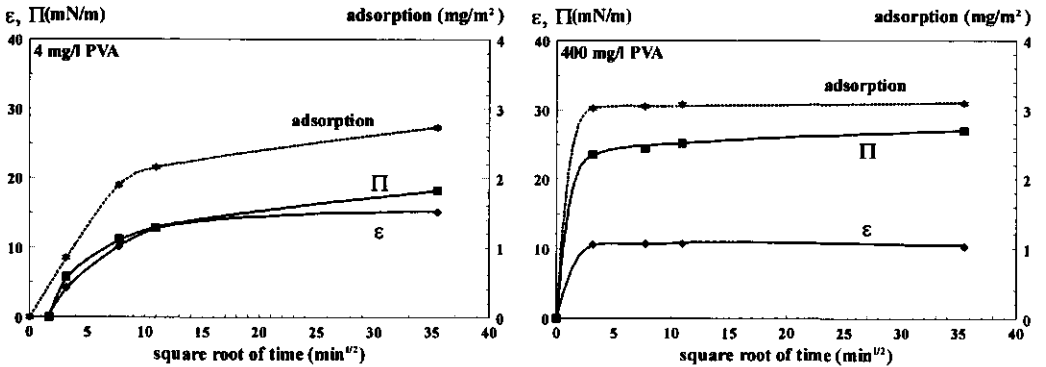


Figure 5e and 5f PVA

This is illustrated in Table 1, which also gives the the corresponding surface pressures and adsorptions.

At all concentrations in this work, modulus values were found to be almost independent of frequency (in the range of $0.01 < \omega < 1$ rad/s) in the region of surface pressures up to around 10 mN/m. At higher surface pressures, i.e., at higher adsorbed amounts, moduli generally did decrease somewhat with decreasing frequency. In this region, viscoelastic surface behaviour was found, indicating the occurrence of relaxation processes in close-packed protein surfaces. Table 2 summarises viscous phase angles and moduli for each of the proteins and the polymer at low, medium and high surface pressures, and at different frequencies.

Table 1
The dilational modulus at near-equilibrium (after 21 h) for different protein concentrations. Frequency : 0.84 rad/s.

| Protein | Molecular Weight (Da) | Concentration. (g/l) | Surface Pressure (mN/m) | Adsorption (mg/m$^2$) | Modulus (mN/m) |
|---|---|---|---|---|---|
| β-casein | 24,000 | 0.0005<br>0.003<br>0.01 | 17<br>19<br>19.8 | 2.2<br>2.95<br>2.95 | 17<br>16<br>16.4 |
| κ-casein | 19,000 | 0.0008<br>0.008<br>0.3 | 13.4<br>17.7<br>18.5 | 1.95<br>3.1<br>4.6 | 22<br>58<br>80 |
| Na-caseinate | 23,000 | 0.0002<br>0.0005<br>0.3 | 12.2<br>19<br>25 | 1.55<br>2.15<br>3.3 | 29<br>24.2<br>20.6 |
| BSA | 69,000 | 0.001<br>0.005<br>0.1 | 11.3<br>14.6<br>17.8 | 1.37<br>1.54<br>1.95 | 59<br>56<br>69 |
| Ovalbumin | 45,000 | 0.1 | 16.3 | 1.52 | 75 |
| PVA | 42,000 | 0.001<br>0.004<br>0.4 | 13.3<br>18.2<br>27 | 2.2<br>2.73<br>3.1 | 11.1<br>15.5<br>11 |

The slow changes with time of the dilational modulus and the viscous phase angle at maximum "plateau" adsorption are illustrated in Fig. 6a and 6b respectively.

Figure 6
The effect of age of the adsorbed layer on modulus (6a) and phase angle (6b) at the highest
concentration investigated (0.01-0.4g/l), at frequency 0.084 rad/s.

6a



6b
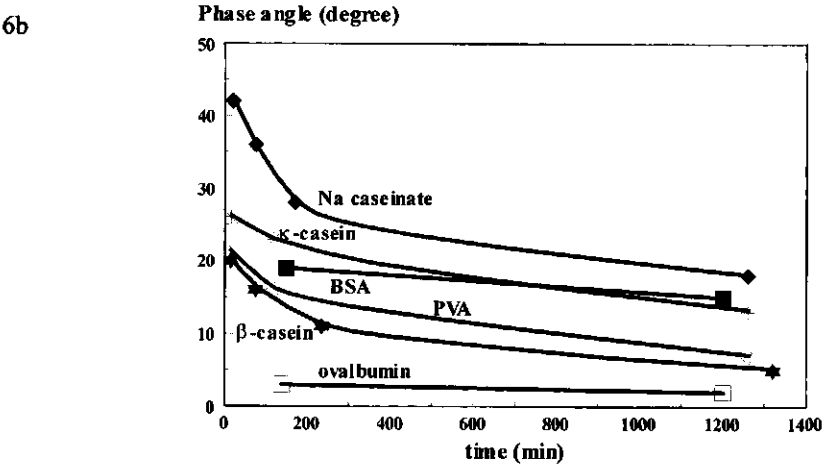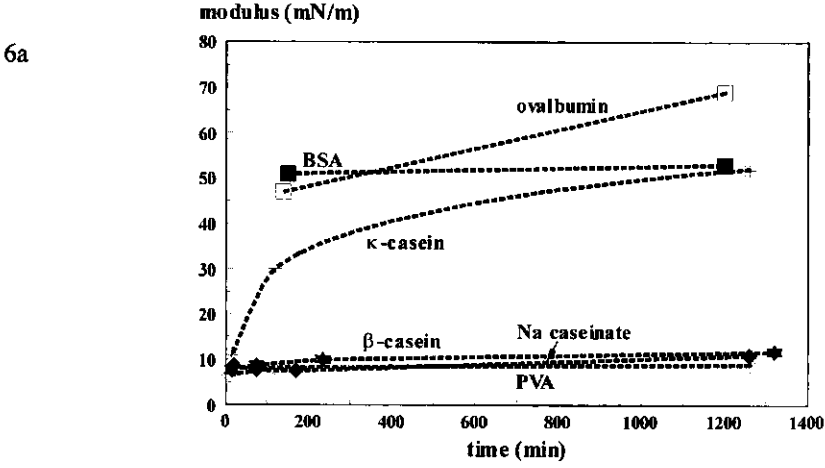
Table 2.
The viscous phase angle and modulus at low, medium and high surface pressure for all proteins examined and PVA.

| surface pressure (mN/m) | adsorption (mg/m²) | viscous phase angle | | | modulus (mN/m) | | |
|---|---|---|---|---|---|---|---|
| frequency (rad/s.) --> | | 0.84 | 0.033 | 0.0084 | 0.84 | 0.033 | 0.0084 |
| β-casein | | | | | | | |
| 4.3 | 0.98 | 0 | 0 | | 24 | 22 | |
| 9.8 | 1.45 | 0 | 0 | | 14 | 14 | |
| 19 | 2.95 | 0 | 6 | 8 | 16 | 11.8 | 10 |
| κ-casein | | | | | | | |
| 3.2 | 1.2 | 0 | 0 | | 14 | 13 | |
| 9.2 | 1.65 | 0 | 0 | | 24 | 22 | |
| 18.2 | 3.2 | 0 | 16 | 17 | 82 | 57 | 42 |
| Na caseinate | | | | | | | |
| 4.2 | 1.05 | 0 | 0 | | 19.7 | 19.2 | |
| 9.5 | 1.3 | 0 | 0 | | 27.8 | 25.2 | |
| 22 | 3.3 | 12 | 42 | | 19.7 | 8.6 | |
| BSA | | | | | | | |
| 6.1 | 1.18 | 0 | 0 | | 44.3 | 43.2 | |
| 11.3 | 1.37 | 0 | 0 | | 61.3 | 58.5 | |
| 16.9 | 1.83 | 7 | 19 | | 66 | 51 | |
| Ovalbumin (pH=6.7) | | | | | | | |
| 5.9 | 1.2 | 0 | 0 | | 44 | 35 | |
| 9.4 | 1.3 | 0 | 3 | | 50 | 47 | |
| 14.5 | 1.45 | 0 | 4.5 | | 78 | 70 | |
| PVA 205 | | | | | | | |
| 4.3 | 0.65 | 0 | 0 | | 4.5 | 4 | |
| 11.2 | 1.9 | 0 | 16 | | 10.7 | 9.7 | |
| 23.5 | 3.0 | 0 | 21 | | 12.2 | 6.5 | |

The effect of pH on the modulus of adsorbed Ovalbumin is given in Figure 7 and Table 3. In figure 7 the modulus data at different pH are plotted as a function of the surface concentration. In Table 3 the effect of pH on the dilational modulus at equilibrium surface concentration (21 hours) is given.

Figure 7
The moduli of an adsorbed ovalbumin layer at different pH's vs. surface concentration.
Determined during equilibration

modulus (mN/m)



surface concentration (mg/m$^2$)
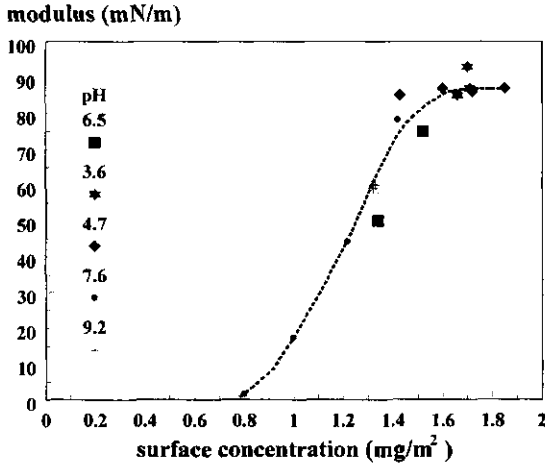
Figure 8
The effect of the deformation on the modulus.
Proteins: BSA and Ovalbumin.

modulus (mN/m)



deformation (%)
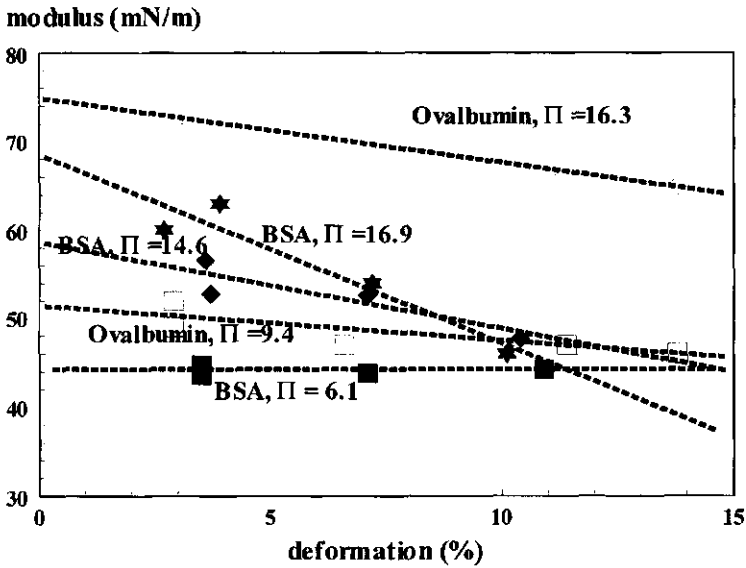
Table 3
The effect of pH on the modulus of an adsorbed ovalbumin layer at a protein concentration of 0.1 g/l.
Modulus at equilibrium adsorption(21 hours), frequency=0.84 rad/sec.

| pH | surface pressure (mN/m) | surface concentration (mg/m$^2$) | modulus (mN/m) |
|---|---|---|---|
| 3.6 | 20.5 | 1.71 | 87 |
| 4.7 (≈IEP) | 23.4 | 1.85 | 87 |
| 6.5 | 16.3 | 1.52 | 75 |
| 7.6 | 14.5 | 1.42 | 78 |
| 9.2 | 11.4 | 1.33 | 60 |

In Figure 8 the effect of the amplitude of the surface area deformation on the modulus is given. This effect was determined at different surface pressures for the proteins BSA and Ovalbumin.

Summarising, the visco-elastic modulus of adsorbed layers of the proteins Na-caseinate, β-casein, κ-casein, BSA and ovalbumin has been studied as a function of adsorption time and concentration and frequency. Results are compared with those obtained for PVA. In addition, effects of surface age, pH and amplitude of the area deformation are determined.

3.5 Discussion

3.5.1 Effect of adsorption time and protein concentration.

One of the main conclusions in chapter 2 was that for each protein at given adsorption values the surface pressures were virtually independent of bulk concentration and surface age. Thus, the surface pressure is uniquely related to the surface concentration during the adsorption process. So, via the surface pressure the measured moduli can be linked to the surface concentration. Typical examples of how the modulus evolves during the adsorption process are given in figure 5 for β-casein, BSA and PVA 205. In these figures the square root of the adsorption time was chosen merely to accommodate both short and long times and thus get a better survey over the whole process. It is seen that initially the modulus, the adsorbed amount and the surface pressure all gradually increase with time.

For lower protein concentration a time lag is observed during which the modulus is too small to be measured with sufficient accuracy. This time lag more or less corresponds with the time lag that was observed in the surface pressure versus time curves (see Figs. 2b-7b in chapter 2). This indicates that a minimum adsorbed amount, characteristic for each protein, is not only

77

needed to make the surface pressure differ measurably from zero, but also the dilational modulus. This correlation is of course not unexpected because at least a certain minimum value of the surface pressure is needed above which detectable variations in $\Pi$ and $\epsilon$ on compression and expansion are possible. In this study we did not try to accurately determine the time or adsorbed amount at which the modulus starts to deviate measurably from zero. It is difficult to determine these quantities by simply measuring the surface tension as a function of time, as this requires a very stable base line of the electrical signal. Such an experiment would be possible by measuring a tensio-elastogram, the response of the surface pressure to a continuous sinusoidal area oscillation, as described in ref. (44).

In most cases the initial gradual increase of the modulus with time continues until a certain maximum value is reached. Only in the case of 0.0005 g/l β-casein is the modulus vs. time curve irregular. In this situation the modulus first increases steeply, followed by a significant decrease and again an increase to a certain plateau value. A similar irregular shape can be deduced from results with [1-$^{14}$C]Acetylated β-casein (45). The origin of this irregular shape can be deduced from the shape of the surface pressure versus adsorption curve as will be shown below (3.5.2).

For adsorbed protein layers real equilibrium values of the interfacial parameters are seldom found : the surface pressure, the adsorbed amount and the dilational modulus continue to change even after an adsorption time of over 21 hours. Nevertheless, as in the case of adsorption and surface pressure, after 21 hours the moduli are regarded as reflecting quasi equilibrium. In most cases, these quasi- equilibrium values are virtually independent of the protein concentration (see Table 2), so they do characterize the adsorbate. This finding can be explained considering the high affinity character of protein adsorption. Even at very low concentrations the adsorption already approaches full monolayer coverage (Table 3, Chapter 2). PVA, a synthetic polymer which also exhibits high affinity adsorption, also produced an almost constant value of the equilibrium modulus with increasing concentration.

Somewhat unexpectedly, in some cases the modulus decreases with concentration beyond full monolayer coverage (see also Figure 10). Only with κ-casein does the final modulus significantly increase with increasing concentration. This corresponds with a significant increase of the adsorption in this concentration range for this protein.

3.5.2 The relation between modulus and surface pressure.

From Fig. 5 it follows that the increase of the modulus with time parallels that for the surface pressure up to 5 - 10 mN/m. This suggests a correlation between these two characteristics. This is further illustrated in figure 9. The symbols in these plots indicate different protein concentrations and angular frequencies of the sinusoidal surface area deformation. Not only

78

Figure 9. The dilational modulus against the surface pressure for β-casein (a), κ-casein (b), whole casein (c) BSA (d), Ovalbumin (e), PVA (f)
Solid line is mean curve through the experimental data. Dashed curve is $\varepsilon_0$.
Closed symbols higher frequency; open symbols lower frequency



9a, β-casein
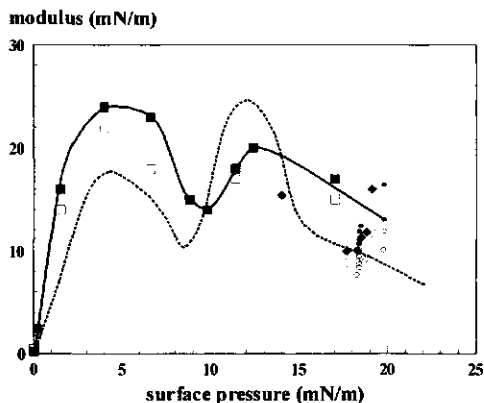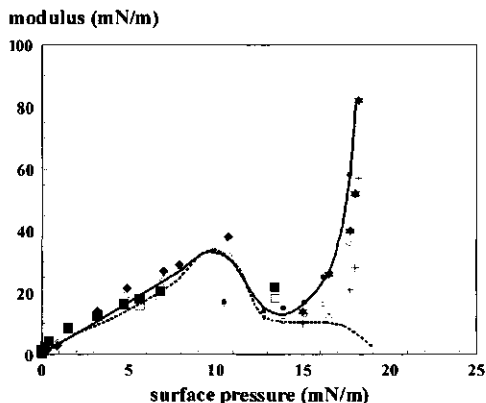


9b, κ-casein
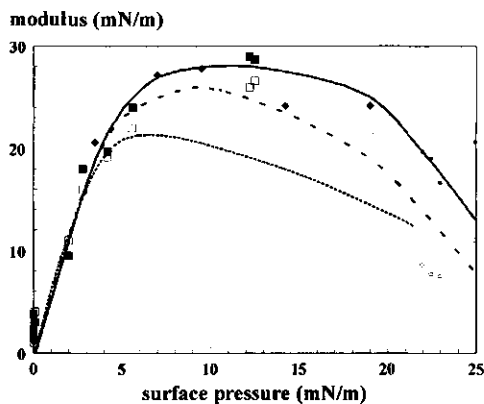


9c, whole casein
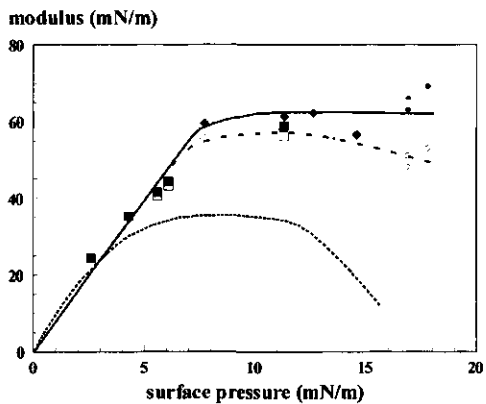


9d, BSA
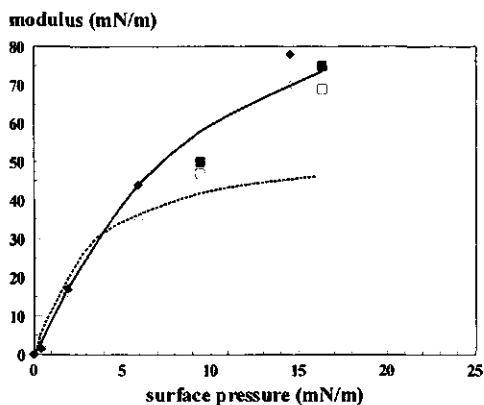


9e, ovalbumin



9f, PVA

79
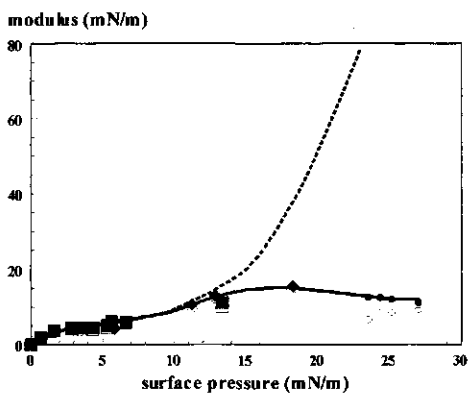
are the equilibrium results given but all data measured during the adsorption process. In the same plots the limiting value of the modulus ($\epsilon_0$) is given. This limiting value is calculated according to Eq.2 from the surface equation of state, i.e., from the equilibrium relationships between surface tension and surface concentration, which were presented in the previous chapter.

For all systems investigated it is evident that, especially at not too high surface pressures, the measured points merge into one single curve indicated by the solid line. This curve appears to be characteristic for each particular protein. The initial part of this curve is linear, passing through the origin. It represents purely elastic behaviour depending only on the momentary value of the surface pressure during the establishment of equilibrium between surface and subphase. This indicates that, within the timescale of the modulus measurements, equilibrium within the adsorbed layer is maintained. At higher surface pressures the modulus starts to become somewhat dependent on concentration and frequency. In Fig. 11 the characteristic curves for the different proteins are collected in one graph. From this figure it is inferred that, apart from the initial linear part, the curves for the caseins ($\beta$- and $\kappa$-) are relatively irregular. With BSA (Fig. 9d) the modulus increases with increasing surface pressure to a maximum value at a surface pressure between 8 and 10 mN/m. Upon further increase of the surface pressure the modulus remains constant or even decreases somewhat, especially at lower frequencies. With Ovalbumin (Fig. 9d) no real maximum is found. Perhaps the experiments with this protein were not performed at a sufficiently high concentration (turbid solution at high concentrations) to show a similar decrease as found with BSA.

For $\beta$-casein, the curve representing $\epsilon_0$ vs. surface pressure showed a similar irregular shape as the curve of the measured moduli. This means that this irregular shape is related to the inflection in the equilibrium pressure-area curve at a surface pressure of about 8 mN/m. This inflection has been attributed to a transition of an all-trains configuration, in which flexible polypeptide chains lie fully unfolded in the surface, to a trains-and-loops configuration where some segments protrude as loops into the aqueous phase (45). In this surface pressure range loop formation has also been deduced from enzymatic action on adsorbed $\beta$-casein molecules by Leaver and Dalgleish (46). In the frequency range of our experiments the phase angles are zero, which means that the characteristic time scale of this process of loop formation is smaller than 1 sec. (See also section 3.5.6)

Modulus vs surface pressure curves, determined while adsorption proceeded, being independent of protein concentration were also found by Joos (47) and Giles and Lucassen (48) for the proteins $\beta$-lactoglobulin and BSA, respectively.

The initial slopes determined from the plots in Figure 9a-f for the different proteins are given in Table 4, and compared to initial slopes obtained from literature data. For some proteins few data for adsorbed layers are available in the literature; therefore, we also include literature

data obtained from spread monolayers. The slopes from the present work are similar to the literature data. However, in the case of β-casein, where radio-labelled casein was used (49), the value is considerably lower. This is likely to be due to the fact that with this labelled casein the pressure vs surface concentration curve is less steep. The data available at present do not allow a statement about effects of experimental conditions on this slope.

Table 4.
Comparison between the linear range (d$\epsilon$/d$\Pi$ and extent) determined in this work and literature data.

| protein | this work | | literature data | | |
|---------|-----------|--|-----------------|--|--|
| | d$\epsilon$/d$\Pi$ | extent (mN/m) | d$\epsilon$/d$\Pi$ (ref) | extent (mN/m) | method |
| β-casein | 9 | 3 | 3 (49) 6 (50) 7 (51) | 5 3 3 | adsorption ,, ,, |
| κ-casein | 4 | 7 | | | |
| BSA | 8 | 7 | 9 (52) 9 (18) 8 (48) | 5 6-7 | spreading ads.pH=4.9 adsorption |
| Ovalbumin | 12 | 4 | 8 (52) | 5 | spreading |
| β-lactoglobulin | - | - | 7.5 (47) | 5 | spread/ads |
| PVA205 | 2 | 2 | | | |

It is not possible to relate the initial slope in a simple way to the structure of the protein molecule. Had that been the case, the lowest value for the slope would have been found with β-casein. From our results, however, it appears that the initial slope for the flexible β-casein is in the same range as it is for the globular proteins. Differences between the different proteins become more evident if we compare the surface pressure ranges in which the line remains straight; the linear range. Compared to globular proteins, β-casein produces linear behaviour over a relatively short range of surface pressures.

Compared to the proteins, the relation between dilational modulus and surface pressure for the synthetic polymer PVA 205 is significantly different. For PVA the slope d$\epsilon$/d$\Pi$=2, while for the proteins this slope ranges from 4-12. However, as with β-casein the linear region is small. Due to flexibility of the adsorbed molecule the linear range seems to be shortened.

At very low adsorptions, all known equations of state reduce to the two-dimensional analogue of the ideal gas, which predicts a slope of +RT for the $\Pi$ vs $\Gamma$ curve and a slope of +1 for the $\epsilon_0$ vs $\Pi$ curve (53). A striking feature of Figures 9a-f is that there is no observable trace of

such a limiting slope in any of the present systems. All exibit severely non-ideal behaviour at very low surface pressures, which reduces the range where $d\epsilon/d\Pi=1$ to the point of invisibility. Such non-ideality, of course, is also apparent from the quite high adsorptions (half saturation coverage) needed to produce any measurable surface pressure. At such high surface concentrations lateral interactions between adsorbed molecules are likely to occur.

Modulus versus surface pressure plots were first published by Blank et al. (52). Their experiments were performed with spread layers, which enabled them to compare the measured moduli with the limiting value of the moduli ($\epsilon_0$) calculated from the pressure-area curve using equation 2. They found a good agreement between the measured and calculated values. We have checked this finding for our results by calculating $\epsilon_0$ from the surface pressure-adsorption curves that were given in the previous chapter. The curve of $\epsilon_0$ versus surface pressure (figs 9a-f) almost coincides with the curve of the measured (dynamic) moduli, especially in the surface pressure range where the measured modulus increases linearly with increasing surface pressure (the initial part) almost independent of the frequency of the deformation. Such coincidence of measured and calculated moduli ($\epsilon_0$) indicates that, in this range, the surface pressure adjusts instantaneously to the changing surface concentration during the compression expansion cycle. This offers the possibility to calculate at least the first part of the surface pressure versus adsorption curve from dilational modulus measurements if the coordinates of one point on the curve are known. This procedure has been applied successfully by Lucassen-Reynders et al. (44) for a low molecular weight surfactant.

In Chapter 2 it was shown that for all proteins examined the surface pressure is for each protein uniquely related to the adsorbed amount. Therefore, the characteristic dynamics of a protein can also be expressed by plotting the modulus versus the adsorbed amount. In figure 10a-f the relationship between the dilational modulus and the adsorption is shown for all proteins examined. In these plots $\epsilon_0$ is also given for comparison. These curves show a great similarity with the modulus versus pressure curves in figure 9. The main difference is that the modulus versus surface concentration curve does not pass through the origin. Of course, the modulus can reach measurable values only if $\Pi$ does so, i.e. at a surface concentration between 0.5 and 1 mg/m$^2$ ($\Gamma_{\Pi>0}$).

A common feature of the modulus versus surface concentration curves (Fig.10) is that at surface concentrations exceeding $\Gamma_{\Pi>0}$ the modulus increases very steeply with increasing surface concentration. This steep increase is a result of an increase of the interaction between the adsorbed molecules because in this range $d\epsilon/d\Pi >>1$ (see Table 4). To compare the different proteins the solid curves in figure 10a-f are combined in one plot (Figure 12). The steepness of the increase of the modulus with increasing surface concentration appears to be related to the molecular structure of the protein molecule. For the rigid globular molecules

82

Figure 10. Surface dilational modulus as a function of surface concentration for β-casein (a), κ-casein (b), whole casein (c), BSA (d), Ovalbumin (e) and PVA (f).
Drawn line: results at highest frequency. Dashed line is $\varepsilon_0$.
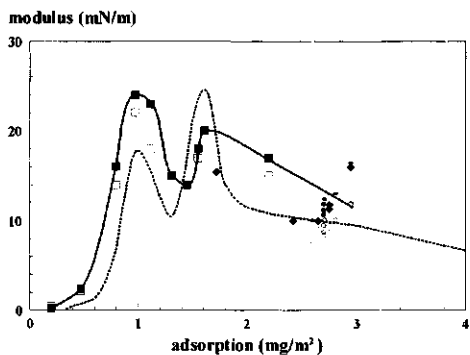


Fig.10a. β-casein
closed symbols: ω=0.84 rad/s
open symbols: ω=0.033 rad/s
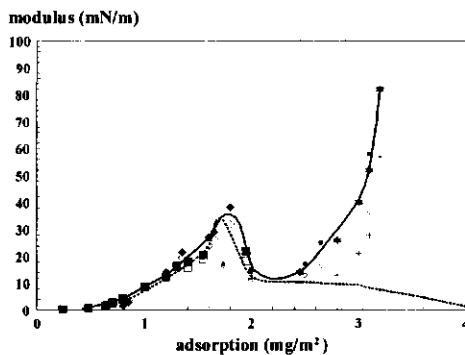
Fig. 10b. κ-casein
closed symbols: ω=0.84 rad/s
open symbols: ω=0.033 rad/s
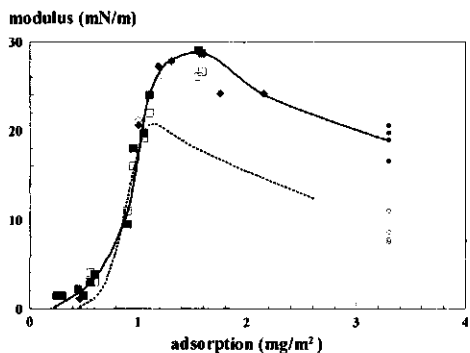


Fig.10c. whole casein
closed symbols: ω=0.84 rad/s
open symbols: ω=0.033 rad/s
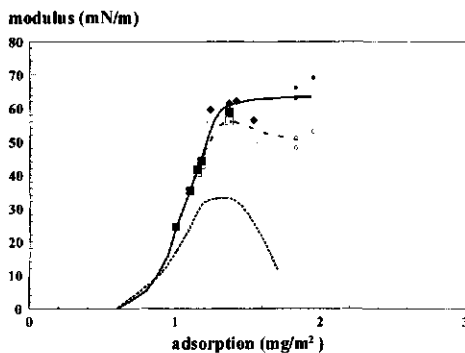
Fig. 10d. BSA
closed symbols: ω=0.84 rad/s
open symbols: ω=0.084 rad/s
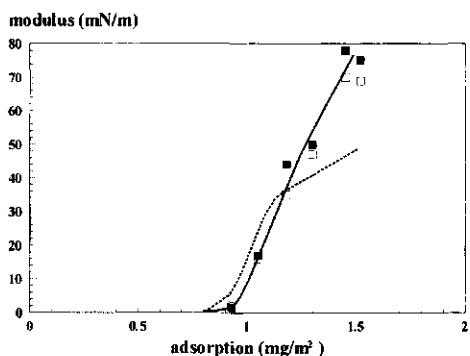


Fig.10e. ovalbumin
closed symbols: ω=0.84 rad/s
open symbols: ω=0.084 rad/s
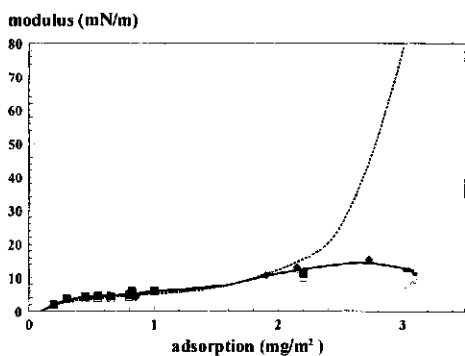
Fig. 10f. PVA
closed symbols: ω=0.84 rad/s
open symbols: ω=0.084 rad/s

83

Figure 11
Modulus versus surface pressure, at the highest frequency (0.84 rad/s).
Combined plot of all proteins examined.
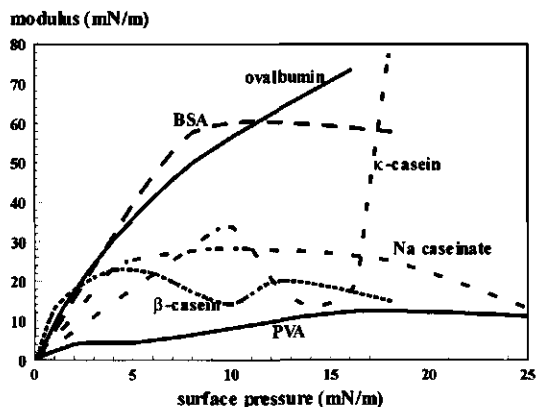
modulus (mN/m)



Figure 12
Modulus versus surface concentration, at the highest frequency (0.84 rad/s).
Combined plot of all proteins examined.
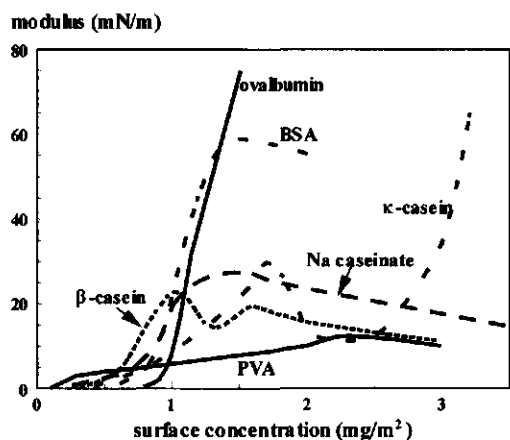
modulus (mN/m)



Figure 13
Comparison of experiment and theory for ovalbumin at the air/water interface

modulus (mN/m)



84
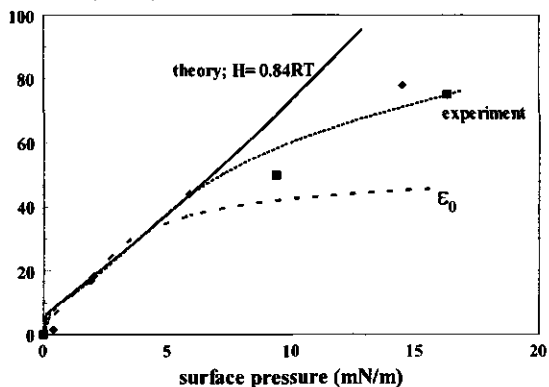
(BSA, Ovalbumin) this increase is steeper than for the more flexible caseins. This indicates that the modulus is not only determined by the interaction between the adsorbed molecules, but that the internal structure of the adsorbed molecule also plays an important role. The conclusion that molecular structure is important to understand the interfacial behaviour was also drawn from the surface pressure-surface concentration curves of the different proteins (Chapter 2). For most proteins we observe that above a certain surface concentration (1-2 mgr/m$^2$) the steep increase is halted, the modulus curve flattens off, and in some cases even decreases with a further increase of the surface concentration. At the point of inflexion we often observe the transition from purely elastic behaviour to visco-elastic behaviour, with $\phi>0$. Here the moduli become frequency dependent (Fig 10), the upper branch representing the moduli for high frequencies, the lower branch those for low frequencies. This means that a mechanism of surface tension relaxation, with a characteristic time within the timescale of the area oscillations, has become operative. In section 3.5.6. the origin of this relaxation process will be discussed further.

### 3.5.2.1. Comparison with theory

It is seen that the curve of $\epsilon_0$ versus surface pressure (figs 9a-f) almost coincides with the curve of the measured (dynamic) moduli, especially in the range of surface pressures up to at least 5 mN/m where the measured modulus increases linearly with increasing surface pressure. This result indicates that within this range of protein concentration and frequency, a surface equation of state can be used to predict the dynamic interfacial behaviour. This also offers the possibility to compare measured moduli with those calculated according to the models for a surface equation of state as presented briefly in the previous chapter.

A first attempt to check the applicability of one of these models was given in ref. (54). The model is a 2-D solution model, which considers both entropy and enthalpy in first order, for a solvent and a protein with constant molecular areas, $\omega_1$ and $\omega_2$, respectively, where $1/\omega_i$ ($\omega_i$ not to be confused with $\omega$, the angular frequency of the oscillation) can be equated to the saturation adsorption, $\Gamma_i^*$. In this model, the surface pressure $\Pi$ depends on the degree of surface coverage $\Theta$ ($=\omega_2\Gamma_2$) according to

$$\frac{\Pi\omega_1}{RT} = -\ln(1-\Theta) - (1-1/S)\Theta - \frac{H}{RT}\Theta^2 \qquad (9)$$

where the size factor, S ($=\omega_2/\omega_1$), is the factor by which the protein's molar area exceeds that of the solvent, and $H\Theta^2$ is the partial molar heat of mixing of a Frumkin-type model or regular surface mixture. Positive values of H represent an excess of attractive interactions between like molecules over those between unlike molecules. A key element in this model

is therefore the possibility of phase separation, starting at very low values of surface pressure and surface concentration, which can result in a near-zero surface pressure up to surface concentrations > 0.5 mg/m$^2$. The limiting modulus $\epsilon_0$ according to this model is given by

$$\frac{\epsilon_0 \omega_1}{RT} = \frac{\Theta}{1 - \Theta} - (1 - 1/S)\Theta - \frac{2H}{RT}\Theta^2 \tag{10}$$

Numerical examples of the effects of S and H on the modulus vs. pressure relationship have been presented earlier (43). Interestingly, it is only the combination of entropy and enthalpy (54) that produces the steep linear ascent of the modulus at moderately high surface coverage observed experimentally. Figure 13 illustrates that Eq. 10 describes a large range of the experimental data for ovalbumin quite well assuming S=245 and a relatively high value of the interaction enthalpy H=0.84RT, which, at the chosen value for the size factor S, predicts phase separation in the surface and a very steep increase of $\epsilon_0$ at near-zero $\Pi$ (see chapter 6). As in the Soft Particle model, the flattening of the $\Pi$-$\Gamma$ curves, which is characteristic for all proteins examined, can be described by a decrease of protein molar area, $\omega_2$, with increasing $\Pi$. Other possible explanations for this phenomenon are multilayer formation or collapse.

Summarising, the dilational properties of adsorbed protein layers are satisfactorily explained by the equilibrium pressure-area curve for surface concentrations from 0 to roughly 1.5 mg/m$^2$. Surface behaviour is purely elastic at a time scale of 1 sec. for all proteins considered. The equality of measured and calculated moduli ($\epsilon_0$) in this range implies that equilibrium in the surface is established within the time scale of the compression/expansion, i.c., within approximately 1 sec.. Surface pressures and dilational moduli are negligibly small up to a surface concentration of 0.5 mg/m$^2$ ; at higher surface concentrations, up to 1.5 mg/m$^2$, the modulus increases sharply and linearly with surface pressure. Such a steep increase of the elasticity points to a severely non-ideal surface equation of state, with an overriding influence of intra or lateral intermolecular interactions.

The great advantage of the modulus versus surface pressure plot is that measurement of surface pressure is far less problematic than that of the surface concentration, especially at oil/water interfaces (see chapter 4).


3.5.3 Comparison with literature data.


Reliable published data of dilational moduli for proteins measured after adsorption from solution are relatively scarce compared to results obtained with spread monolayers. Under static conditions, surface behaviour as expressed in the surface pressure vs. surface concentration curve is generally found to be similar for adsorbed and spread layers (see

Chapter 2). For this reason, we include results obtained with spread layers, to compare with the present results.

As the methods, concentrations and nature of the buffered solutions were never fully identical to the conditions in this study, we have to decide first how to compare the different results. In Chapter 2 we found that differences between pressure-area curves are small, if the conditions in solution (pH, ionic strength) are not too different. Hence, although in principle results should be compared at equal surface concentration and equal age, for practical purposes it is admissible to use the surface pressure as a reference for equal surface layer conditions. For spread layers this is the preferred way, as we know that due to spreading and subsequent compression, some protein can be lost in the sub phase. This is in fact the only comparison possible in the case of results obtained with adsorbed layers where only the surface pressure is measured.

For β-casein, modulus values were reported by Graham and Phillips (45), Serien et al. (18), Williams and Prins (55), Mellema et al. (51) and Puff et al. (50) with adsorbed layers, while spread layers were used by Gau et al. (19) and van Aken and Merks (20,56). These results are shown in Figure 14 as a function of the surface pressure, together with the results from Figure 9a, represented by the drawn line. For BSA, similarly, Figure 15 collates data from adsorbed layers (14,45) and spread layers (Blank et al. (52); van Aken and Merks (20,21); Boury et al. (22)) with the present data from Figure 9c. In Figure 16 a similar plot for ovalbumin is given comparing the present results with the results published by Blank et al. (52) and Neurath (57) obtained with spread layer.

In some of this work (20,22,56) the area variations were step-wise rather than sinusoidal; we present only data showing fully elastic behaviour, i.e., no relaxation after the area change. Inevitably, methods, materials and conditions used in these studies were in no case fully identical to the conditions in the present work. Apart from any differences between adsorbed and spread layers, other possible reasons for discrepancies are:

(i) Most published studies used uniaxial compression and monitored the surface tension changes in the middle of a long and narrow trough, assuming isotropic deformation. A careful analysis of the available information indicates a significant non-isotropy of the deformation in the work of Graham and Phillips (45), as recognised by the authors, and the data by van Aken and Merks (20,56). Such non-isotropy can cause surface shear effects within the deformed protein layer that adheres to the side-walls. Under these conditions reliable data can only be obtained by determining the local area change. The presented data from these references were calculated using the measured surface tension change and the area change assuming uniform area deformation. This results in moduli that are somewhat too low at

87
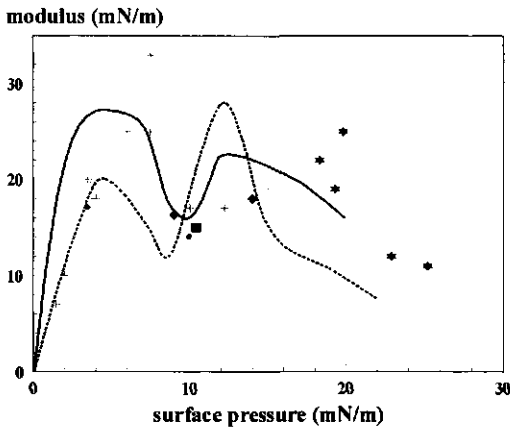
Figure 14. Surface dilational modulus as a function of surface pressure for β-casein; data from various sources. Drawn and dashed lines as in figure 10a. Points: ✕ ref.45, + ref.50, ●, ■ ref. 19, ◆ refs.20,56, ✳ref.51, ✿ ref.55
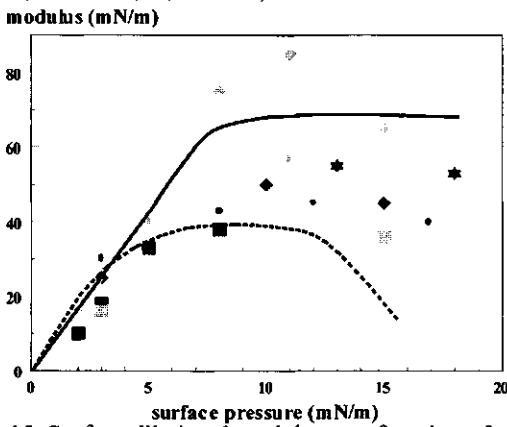


Figure 15. Surface dilational modulus as a function of surface pressure for BSA; data from various sources. Drawn and dashed lines as in figure 10d. Points:■ ref.52, ▣ ref.20, ◆ ref.21, ◆ ref.18, ● ref.45, ✳ ref.22, ◉ ref.27
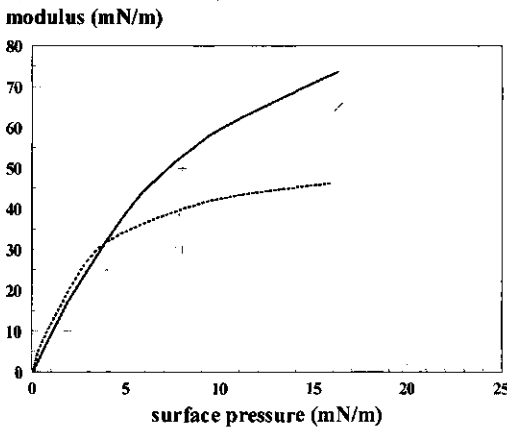


Figure 16. Surface dilational modulus as a function of surface pressure for ovalbumin; data from various sources. Drawn and dashed lines as in figure 10e. Points: ✕ ref.57, + ref.52

higher surface pressures.Williams and Prins (55), Mellema et al. (51) and van Aken and Merks (21) used a ring trough designed to produce purely dilational deformation. Puff et al. (50) used the Dynamic Drop Tensiometer (see also Chaper 4), a method that also produces purely dilational deformation.

(ii) The proteins used by Graham and Phillips (45) were radio-labelled. For such proteins the initial increase of the pressure-adsorption curve is less steep, and consequently $\epsilon_0$ and $\epsilon$ are smaller at low surface pressures compared to the unlabelled proteins.

(iii) The frequencies used by Gau et al. (19) were in the kHz range, i.e., much higher than ours. In this high frequency range, the authors observed a transition from purely elastic to visco-elastic, indicating a relaxation mechanism with characteristic time-scale in this high frequency range. As a result, one would expect their high-frequency moduli to be rather higher than ours. Surprisingly, the agreement is found to be quite good. A relaxation mechanism at a time-scale of $10^{-3}$sec. points to fast conformational changes (58).

In spite of these significant differences in methods and in experimental conditions, the results obtained in this work for most part agree rather well with the earlier studies in which the deformation was non-isotropic. This also proves that a comparison of the rheological characteristics of interfacial layers of proteins can be made reliably at equal surface pressures. We conclude that interference by shear induced only minor errors in the present systems where the dilational modulus exceeds the shear modulus (see also chapter 5).

3.5.4. The effect of deformation amplitude.

The moduli discussed above were determined at a fixed amplitude of the surface deformation ($\Delta A/A=0.07$). To check whether this level of deformation is small enough to produce a linear response of the system, with the modulus independent of the deformation, we determined the extent to which the modulus depends on the deformation by varying $\Delta A/A$ between 0.025 and 0.13.

From the modulus vs. deformation plot (Fig. 8) it can be seen that below about 50 mN/m the moduli do not depend on the extent of the area deformation. However, higher moduli increase significantly with decreasing deformation. This behaviour was found for the two rigid globular molecules BSA and ovalbumin. For β-caseins this behaviour was not investigated, but as the modulus of this protein is always below 40 mN/m no effect of the deformation is to be expected. With PVA (modulus< 20mN/m) and PMMApe (modulus < 50mN/m) the modulus is constant over the whole deformation range examined.

The modulus increases almost linearly with decreasing deformation, which enables us to extrapolate to zero deformation. We have not made use of this possibility in the results

discussed above, because the corrections to be obtained in this way are relatively small. The phenomenon is interesting, but its origin is not fully understood. The results indicate that this behaviour is related to irreversible breaking of intermolecular interactions, due to the deformation. This can be concluded from the finding that by measuring at increasing deformation first, followed by a measurement at the initial low deformation, the modulus was also lower than initially at the same deformation. This breaking of bonds seems to be determined by the extent of the deformation only and not by the deformation rate, because the slope of the modulus vs. deformation line is not much affected by the frequency.

The phase angles increase somewhat with increasing deformation, which indicates that surface tension relaxation may be partly explained by (ir)reversible breaking of the intermolecular bonds.

3.5.5 The effect of pH.

In Chapter 2 it was found that for ovalbumin the surface concentration versus pH shows a maximum near the I.E.P. of the protein. This maximum was explained by the more extended structure of the protein molecule outside the I.E.P. region, due the repulsive effects of equally charged parts of the molecule (55) or by lateral repulsive forces between adsorbed molecules. Table 3 shows that the modulus increases if the pH decreases from high pH to the iso-electric region. This is in line with the generally found increase of the modulus with increasing surface concentration. Table 3 further indicates that at pH< I.E.P. the modulus remains at the level that is reached at the I.E.P.. This is not surprising, because at pH 3.6 the surface concentration remains at a level where the modulus no longer increases upon further increase of the surface concentration (see Fig. 7).

As illustrated above (see 3.5.3) interfacial data are best compared at equal surface pressure or equal surface concentration. Therefore we have plotted in Fig. 7. the modulus versus surface concentration at different pH's. Because of the fast adsorption near the I.E.P at high protein concentration only moduli at high surface pressures are available in this pH region. Consequently there is only little overlap between data at high and low pH. However, all measured points in this plot, once again, more or less collapse into one single modulus vs. surface concentration curve. This further illustrates that the major part of the effect of pH on the modulus can be related to the effect of pH on the surface concentration.

Near the I.E.P. the interface becomes more viscous, which is in line with the general trend that the viscous component of the modulus increases with a further increase of the surface concentration. It is not very likely that this small viscous component ($\phi$<9 deg). is related to multilayer adsorption, because the surface concentration does not exceed 2 mg/m$^2$.

3.5.6 Relaxation phenomena in protein layers.

Relaxation of the surface tension by diffusion is the most common relaxation mechanism in surfactant stabilized emulsions and foams. If relaxation occurs purely through diffusional exchange of molecules with the surfactant solution a quantitative description is available (4). Additional relaxation mechanisms may also affect the interfacial tension and the viscoelastic properties of an interface depending on the time scale considered. Examples of relaxation processes that may occur in time scales ranging from $10^{-2}$ to $10^{+3}$ seconds were reviewed by van den Tempel and Lucassen-Reynders (60) and include (i) retardation of adsorption by an adsorption "barrier"; (ii) slow re-orientation of molecules after adsorption; (iii) complex formation and phase transitions in the surface; (iv) formation or destruction of 3-D structures. These can occur either in the surface, e.g. in collapsed monolayers or in solution, e.g., micelles. Generally these relaxation phenomena occur in combination with diffusion. Information about these mechanisms has been obtained mainly from investigations with low molecular weight surfactants. About the mechanisms that are operative in polymer/protein systems less conclusive experimental evidence is available. Recently Serrien et al. (18) developed a relaxation mechanism for proteins involving diffusion and a dynamic equilibrium between two adsorbed states (native and denatured) of protein molecules. This mechanism was derived from the behaviour of a low molecular weight surfactant (sulfosuccinate) that clearly showed a time-dependent reorientation in the interface. Another generally accepted mechanism for relaxation in protein surface layers assumes conformational changes or changes in size and shape (45,61,62,63). These are changes that are similar to the molecular rearrangements that occur during adsorption. At low surface concentrations, molecules are supposed to expand upon adsorption. However, at higher surface concentrations, they will become compressed to their native size or even further. If the time required for these molecular rearrangements is of the same order as the timescale of the oscillations, visco-elastic behaviour will be observed. Under conditions where multilayer adsorption is found, a kind of diffusional exchange between e.g. first and second layer is proposed (55,61).

Below we will discuss, on the basis of the experimental evidence, which relaxation mechanism or combination of mechanisms is most probable. First the probability of a contribution of diffusion to the surface tension relaxation will be considered. In Figure 10 the dynamic modulus and the limiting value of the modulus ($\epsilon_0$), based on the pressure-area curve using Equation 2, are given. It is seen that, especially at low surface concentrations the measured moduli almost coincide with the curve that represents the limiting modulus vs. surface concentration. This indicates that in this adsorption range and within this frequency range the protein layer behaves as being insoluble, supporting the idea that protein adsorption is irreversible. The fact that above this surface concentration visco-elastic behaviour is

observed does not necessarily mean that reversibility comes into play. However, at very long time scales we cannot exclude this possibility. McRitchie (61) found that at longer time scales and only at surface pressures exceeding the level that can be obtained by adsorption, a slow desorption could take place for various proteins e.g. BSA, β-lactoglobulin.

Hunter et al. (64) found for β-casein full exchangeability between adsorbed and non-adsorbed molecules at a timescale of hours. The surface concentration in these experiments was well above monolayer coverage (3 mg/m$^2$). On the basis of the reported data it is difficult to estimate whether this means that also at timescales of minutes (our frequency range) this will occur to an extent that viscoelasticity will be found. It is interesting to note that for the compact rigid molecule lysozyme this exchangeability was not observed. This is probably related to conformational changes (lower α-helix content) upon adsorption (65).

Purely diffusional relaxation for a single surfactant is characterised by a frequency dependency of the modulus, $|\epsilon|$, and the viscous phase angle, $\phi$, decribed by (4)

$$|\epsilon|/\epsilon_0 = [1 + 2(\omega \tau_{diff})^{-1/2} + 2(\omega \tau_{diff})^{-1}]^{-1/2} \tag{11}$$

and

$$\tan\phi = \frac{1}{1 + \sqrt{\omega \tau_{diff}}} \tag{12}$$

respectively. For diffusion-controlled relaxation the characteristic time scale, $\tau_{diff}$, is defined by

$$\tau_{diff} = \frac{2}{D}\left(\frac{d\Gamma}{dc}\right)^2 \tag{13}$$

where D is the diffusion coefficient of the surfactant, and dΓ/dc measures the penetration depth of the diffusion which is determined by the slope of the adsorption isotherm (Fig. 9, Chapter 2). This characteristic time scale ($\tau_{diff}$) can also be calculated from our modulus measurements using equation (12).

A comparison between calculated and measured characteristic time scales of the relaxation process is presented in Table 5. From this Table it is inferred that such a diffusional relaxation process operates at frequencies some orders of magnitude faster than considered in our experiments. This way of calculating the timescale of this process is of course sensitive to the slope of the adsorption isotherm at the relevant concentrations. However, slopes needed to match the experimental data are up to four orders of magnitude higher. This is not very likely because in most cases treated in the table the highest possible value of the slope was chosen.

Table 5 Comparison between experimental and calculated characteristic timescales for $\tau_{diff}$ assuming diffusion controlled relaxation.

| protein | conc. (wt%) | freq. exp (rad/s.) | phase angle (°) | $\tau_{diff}$, eq.12 (s) | $d\Gamma/dc$ ($10^{-6}$m) | D ($10^{-10}$m$^2$s$^{-1}$) | $\tau_{diff}$, eq. 13 (s) |
|---------|-------------|--------------------|-----------------|--------------------------|---------------------------|------------------------------|----------------------------|
| β-casein | 0.001 | 0.033 | 20<br>5 | 93<br>3300 | 3.6 | 0.6 | 0.4 |
| κ--casein | 0.03 | 0.033 | 26<br>13 | 34<br>340 | 2.5 | 0.7 | 0.2 |
| Na-caseinate | 0.03 | 0.033 | 42<br>18 | 0.4<br>131 | 3.6 | 0.7 | 0.4 |
| BSA | 0.01 | 0.084 | 19<br>15 | 43<br>89 | 0.37 | 0.7 | 0.004 |
| BSA | 0.05 | 0.0033 | 25<br>21 | 392<br>770 | 0.62 | 0.7 | 0.01 |
| PVA | 0.04 | 0.084 | 21<br>7 | 31<br>610 | 1 | 0.5 | 0.04 |

A further indication that diffusional transport is not responsible for the frequency dependency that we have observed, is demonstrated in Figure 17. Eqns (11) and (12) imply that the frequency spectrum of the reduced modulus and the viscous phase angle as a function of the dimensionless frequency, $\omega\tau_{diff}$, are represented each a by single curve for any surfactant at any concentration: the characteristics of individual surfactants are reflected in the numerical values of $\tau_{diff}$ and $\epsilon_0$, but not in the shape of the curve. Therefore, the frequency spectrum of the viscous loss angle and also that of the reduced modulus, $|\epsilon|/\epsilon_0$, can be used as a master curve to identify diffusional relaxation. These master curves for diffusional relaxation so far have been applied to small-molecule surfactants, but they are equally valid for any other surface active agents. Macromolecules have lower values of D and different adsorption isotherms, but changing the values for these two factors merely produces a horizontal shift of the lines for $|\epsilon|/\epsilon_0$ and tan $\phi$ in Figure 17, not a change in its shape. Whether or not the viscous loss of fairly close-packed protein layers is due to diffusional interchange with the solution is checked by also plotting in Fig. 17 measured data obtained for BSA at concentrations ranging from 0.001 - 0.5 g/l and at a frequency range from 0.3 - 0.003 rad/s. We tried to fit the measured curves to the mastercurves by adjusting the values for $\tau_{diff}$ and $\epsilon_0$. It must be noted that the chosen value of 100 for $\tau_{diff}$ is several orders of magnitude larger than the calculated ones in Table 5. But even with this value the slope of modulus vs. frequency is too small and also the measured phase angle curve fails to follow the
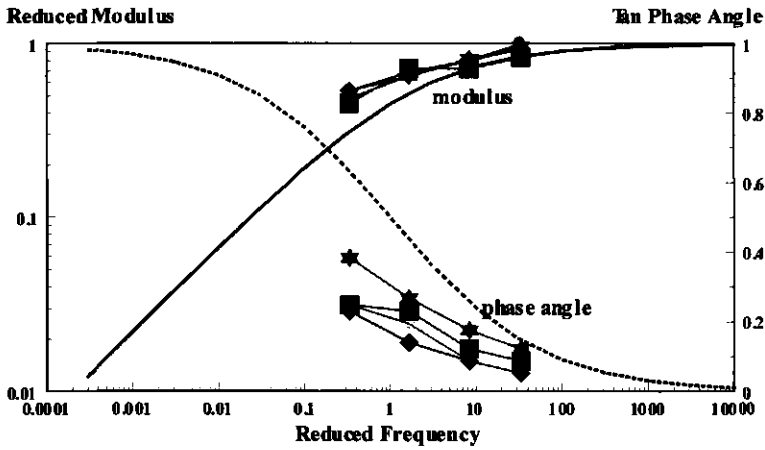
Figure 17
Characteristic spectra for diffusional relaxation. Reduced modulus from Eq. (11) , viscous
phase angle from Eq. (12).
Measured curves: BSA, ◆ 0.001 g/l, ■ 0.005 g/l, ● 0.1 g/l, ✿ g/l
$\tau_d$ = 100 s and $\varepsilon_0$ = 60 mN/m

characteristic diffusional spectrum. The absence of an effect of the bulk concentration on the frequency dependency is a further indication that diffusion-controlled relaxation cannot explain this behaviour.

An extra argument against diffusional relaxation is the finding that with all proteins examined $\epsilon \geq \epsilon_0$ (Figs. 9 and 10). If diffusional exchange occurs the opposite ought to be found.

Another feature of diffusional relaxation is that the modulus versus concentration passes through a maximum caused by increasing diffusional interchange between interface and solution at the higher concentration. With proteins this maximum is absent (Table 2), except at lower frequencies where with some of the proteins (BSA), a slight decrease after a maximum is observed. However, this is in the surface concentration region where the limiting modulus $\epsilon_0$ even decreases more steeply. So in this case this maximum is not an indication for diffusion relaxation.

We conclude that the viscous phase angles measured in time scales above 1 sec. (i.e., frequencies below 1 rad/s) cannot be explained by diffusional relaxation: an additional relaxation mechanism is necessary.

A mechanism, generally accepted as important for relaxation in protein surface layers, is related to slow molecular reconformation (18,45,61-63). In the model proposed by Serrien et al. (18), this reconformation is the transfer between the two distinct adsorbed states, however, for proteins the number of adsorbed states is not necessarily limited to two. Reconformation can only contribute to surface tension relaxation if it affects the surface tension. If this is not the case this mechanism also requires diffusional exchange to obtain surface tension relaxation.

If the time required for these molecular rearrangements is of the same order as the timescale of the oscillations, these rearrangements will result in a transition from purely elastic to visco-elastic behaviour with decreasing frequency. For the more rigid globular proteins we can think of limited conformational changes, such as, changes in secondary structure (decrease of $\alpha$-helix content), changes in size and shape, changes in orientation (end-on or side-on) and minor changes in the number of contacts with the interface. With flexible random coil molecules, like β-casein and PVA, the conformational changes may also involve changes in loops and trains (66). Interesting in this respect is the irregular shape of the modulus versus surface pressure curves for β-casein (see Fig. 9). This shape is also found for the $\epsilon_0$ curves, which means that the origin is related to the inflection in the pressure-area curve (Chapter 2). This inflection at surface pressures between 8 and 10 mN/m has been attributed to a transition of an all-trains configuration, in which the flexible polypeptide chains lie fully unfolded in the surface, to a trains-and-loops configuration where some segments protrude as loops into the aqueous phase (45). Loop formation was also deduced from enzymatic action on adsorbed

95

β-casein molecules (46). In the frequency range of our experiments the phase angles are zero, which means that the characteristic time scale of this process of loop formation is significantly smaller. This is in line with the results described by Gau et al. (19) who observed visco-elastic behaviour above 1 mg/m$^2$ at much higher frequencies (100Hz).

At high surface concentrations, in the region where some proteins show multilayer adsorption, another relaxation mechanism may come into play: the exchange between first and second layers (61,64). Multilayers will provide a reservoir of protein close to the interface and the protein molecules in it should be able to readily interchange with the interface as the area is varied (55). Thus one would expect quite fast relaxation from this mechanism, which is most likely to apply to the caseins. The data presented in Figure 9 for β-casein give little indication of exchange with multilayers as phase angles are very small at all frequencies over the whole surface concentration range. However, higher viscous phase angles were reported (55) for high concentrations (>0.1 g/l) of β-casein in a time scale of 10 sec. and qualitatively ascribed to such an exchange in combination with diffusion from the bulk of the solution.

The results discussed above indicate an increasingly viscous modulus with increasing surface concentration (see Fig.10). However, from experiments where the "plateau" level of these high surface concentrations was reached fast (high protein concentration), we observe a decrease of the phase angle with time for all proteins as well as for PVA (Fig.6b). At these high concentrations the surface concentration has reached its equilibrium value within 15 min. So with time this surface concentration remains constant or increases only slightly. As the modulus is mainly determined by the surface concentration, it should remain fairly constant with time. This is indeed the case for most proteins except for κ-casein and ovalbumin (Fig 6a). The decrease of the phase angle with time indicates that upon aging the adsorbed protein layer becomes less viscous.

Which phenomenon will reduce the ability of the surface tension to relax? One possibility is the stronger adsorption of the molecules due to the increase of the number of sites per molecule in direct contact with the interface (only in the case of diffusional relaxation). If this is the correct explanation, this interpretation implies that, due to a high adsorption rate at high protein concentrations, lateral forces between adsorbed molecules would prevent rapid adaptation of the equilibrium conformation of the adsorbed molecule. Another explanation could be that with time the molecules form an increasing number of intermolecular bonds which obstruct relaxation due to conformational changes.

Various attempts have been made to describe the relaxation process (for a brief survey see ref. 43), due to changes of the adsorbed molecules with time, as a first-order kinetic model. However, such an approximation cannot distinguish between particular models for surface reactions, e.g. re-orientation, unfolding, aggregation and collapse. For instance, the linear model as used by Veer and van den Tempel (67) to describe the effect of exchange of

96

medium-chainlength aliphatic alcohol molecules with collapsed particles on the modulus, was subsequently applied by Kitching et al. (68) to "reorientation/reconformation" of polymeric surfactants. Similar first-order models in terms of surface pressure were applied to protein relaxation (18,20,69,70). However, due to lack of quantitative knowledge about the specific relaxation mechanism, these models have not advanced far beyond the stage of curve fitting with a number of adjustable parameters.

Summarising, we conclude that diffusion-controlled relaxation plays a minor role in the dynamic behaviour of adsorbed protein layers. Viscoelasticity of adsorbed protein layers is more likely to be due to slow molecular reconformation, molecular interaction or collapse-type phenomena (exchange between first and second layer).
The available knowledge about these relaxation mechanisms is insufficient to build meaningful models.

3.6 Conclusions

1.    An improved method for the measurement of the surface dilational modulus of adsorbed protein layers has been developed. This method ensures isotropic deformations, and, consequently fully eliminates the complicating shear effects that became apparent with adsorbed layers of proteins.

2.    The dilational modulus of an adsorbed protein layer is mainly determined by the surface concentration, as is the surface pressure. The protein concentration only plays a role as far as it determines the time needed to reach a certain surface concentration. Due to the high affinity character of protein adsorption, very high moduli are obtained at very low protein concentrations ($10^{-4}$wt%).
       For all proteins examined at frequencies in the range from 0.01 to 1 rad/s, the initial part of the modulus versus surface pressure plot is a steep straight line going through the origin. The slope of the initial part is not much affected by protein type: similar values are found for the flexible caseins and the more rigid globular proteins (BSA, ovalbumin). A much smaller slope is found only with PVA, which has a random coil molecule without any internal structure. However, the range of this linear part is smaller for the flexible molecules (casein, PVA).

3.    In the linear range, the measured moduli coincide with the limiting values of the modulus, calculated from the quasi-equilibrium data. This indicates that the surface pressure adjusts "instantaneously" to the changing adsorption during the compression

97

expansion cycle in timescales ranging from 1 to 100 sec.: the modulus is purely elastic, i.e. effects of relaxation phenomena are negligible.

In this elastic range, differences between individual proteins are related to different degrees of non-ideality, reflected in the surface equation of state. An adequate description of the characteristic features of the elastic region is obtained from a simple equation-of-state model combining non-ideal entropic and enthalpic effects. The measured steep increase of the elasticity points to an overriding influence of attractive intermolecular interactions.

4.  The modulus increases in the order: PVA < $\beta$-casein < BSA < ovalbumin < $\kappa$-casein. For the first four molecules the flexibility of the molecule decreases in the same order. The very high modulus in the case of $\kappa$-casein cannot be attributed to the rigid molecular structure, but is probably caused by the very high surface concentration or due to intermolecular interaction (S-S bridges).

5.  The effect of pH on the modulus can mainly be attributed to the effect of pH on the surface concentration.

6.  At increasing amplitude of compression/expansion, the modulus of the globular proteins (BSA, ovalbumin) was found to decrease. This effect must be attributed to irreversible (within the timescale of the experiment) breaking of intermolecular interactions.

7.  Comparison of the rheological characteristics of interfacial layers of proteins can be made reliably at equal surface pressures.

8.  The relaxation mechanism that becomes operative at higher surface concentrations is most probably not caused by diffusional exchange between surface and solution during the compression expansion cycle ($\omega$ ranging from 0.84 to 0.0033 $s^{-1}$). Relaxation due to conformational changes is the most plausible mechanism. In the viscoelastic region $\epsilon \geq \epsilon_0$ for all proteins examined. This is an extra argument against diffusional exchange. At high surface concentrations the modulus becomes more elastic with time, probably caused by slow molecular rearrangements or by formation of intermolecular bonds.

## 3.7 References

1.  M. van den Tempel. The function of stabilizers during emulsification. 3rd Int. Congress Surface Active Agents (Colonge). Volume II (1960) 345.

2.  H.P. Grace. Dispersion Phenomena in High Viscosity Immiscible Fluid Systems and application of Static Mixers as Dispersion Devices in such systems. Chemical Engineering Communication. 14 2257 (1982)

3.  P. Walstra, I. Smulders. Making Emulsions and Foams: An Overview. in "Food Colloids; Proteins, Lipids and Polysaccharides". E. Dickinson and B. Bergenstahl Editors (1997) 367

4:  J. Lucassen, M. van den Tempel. Dynamic Measurements of Dilational Properties of a Liquid Interface. Chemical Engineering Science 27 (1972) 1283

5.  F. van Voorst Vader, T.F. Erkens, M. van den Tempel, Measurement of Dilational Surface Properties. Transactions Faraday Sociey, 60 (1964) 1170

6.  D.J.M. Bergink Martens, H.J. Bos, A. Prins. Surface Dilation and Fluid-Dynamical Behaviour of Newtonian Liquids in an Overflowing Cylinder.2. Surfactant Solutions. Journal of Colloid and Interface Science 165 (1994) 221

7.  J.A.de Feijter and J.Benjamins, The Propagation of Surface Shear Waves. Journal of Colloid and Interface Science. 70 (1979) 375.

8.  E. Dickinson, B.S. Murray, G. Stainsby. Coalescence Stability of Emulsion-sized Droplets at a Planar Oil-water Interface and the Relationship to Protein Film Surface Rheology. Journal Chemical Society Faraday Transactions1, 84 (1988) 871

9.  E.H. Lucassen-Reynders. Dynamic Interfacial Properties and Emulsification. The Encyclopedia of Emulsion Technology, Volume 4, P. Becher, ed. (1996)

10. R. Miller, P. Joos, V.B. Fainerman. Dynamic Surface and Interfacial Tensions of Surfactant and Polymer Solutions. Advances in Colloid and Interface Science. 49 (1994) 249

11. E.H. Lucassen-Reynders. Surface Elasticity and Viscosity in Compression/Dilation, in Anionic Surfactants; Physical Chemistry of Surfactant Action ; E.H. Lucassen-Reynders, ed. Dekker, New York (1981) 173

12. E.H. Lucassen-Reynders, J. Lucassen. Surface Dilational Viscosity and Energy Dissipation. Colloids and Surfaces A. 85 (1994) 211

13. C.A. MacLeod, C.J. Radke. A Growing Drop Technique for Measuring Dynamic Interfacial tension. Journal of Colloid and Interface Science. 160 (1993) 435

14. V.B. Fainerman, R. Miller, P. Joos. The Measurement of Dynamic Surface Tension by the Maximum Bubble Pressure Method. Colloid & Polymer Science. 272 (1994) 731

15. K.D. Wantke, K. Lunkenheimer, C. Hempt. Calculation of Elasticity of Fluid Boundary Phases with the Oscillating Bubble Method. Journal of Colloid and Interface Science. 159 (1993) 28

16. D. Langevin (Ed.), Light Scattering by Liquid Surfaces. Surfactant Science Series. Marcel Dekker, New York, Chapters 11 and 16 (1991)

17. D.E. Graham, M.C. Phillips. Proteins at Liquid Interfaces. Journal of Colloid and Interface Science. 70 (1979) 403

18. G. Serrien, G. Geeraerts, L. Ghosh, P. Joos. Dynamic Properties of Adsorbed Protein Solutions: BSA, Casein, Buttermilk. Colloids and Surfaces. 68 (1992) 219

19. C-S. Gau, H. Yu, G. Zografi. Surface Viscoelasticity of β-Casein Monolayers at the Air/Water Interface by Electrocapillary Wave Diffraction. Journal of Colloid and Interface Sci. 162 (1994) 214

20. G.A. van Aken, M.T.E. Merks. Dynamic Surface Properties of Milk Proteins. Progress in Colloid Polymer Science. 97 (1994) 001

21. G.A. van Aken, M.T.E. Merks. Dynamic Interfacial Tensiometry as a Tool for the Characterization of Milk Proteins and Peptides. Spec. Publ. no 113 of the Royal Society of Chemistry, E. Dickinson, ed. (1993) 402

22. F. Boury, Tz. Ivanova, I. Panaïotov, J.E. Proust. Dilational Properties of Poly(D,L-lactic acid) and Bovine Serum Albumin Monolayers Formed from Spreading an Oil-in Water Emulsion at the Air/Water Interface. Langmuir 11 (1995) 2131

23. Th.A. Horbett, J.L. Brash. eds. Proteins at Interfaces : Current Issues and Future Prospects. ACS Symp. Ser. 343 (1987). Chapter 1

24. J.W. Gibbs, Collected Works (Longmans, Green, New York), 1 (1928) 302

25. J. Lucassen, M. van den Tempel. Longitudinal waves on Visco-Elastic Surfaces. Journal of Colloid and Interface Science. 41 (1972) 491

26. J. Lucassen, G.T. Barnes. Propagation of Surface Tension Changes over a Surface with Limited Area. Journal of Chemical Society, Faraday Transactions. 68 (1972) 2129

27. J. Lucassen, D. Giles. Dynamic Surface Properties of Nonionic Surfactant Solutions. Journal of Chemical Society, Faraday Transactions 1, 71 (1975) 217

28. L.Ting, D.T. Wasan, K. Miyano. Longitudinal Surface Waves for the study of Dynamic Properties of Surfactant Systems III, Liquid-liquid Interface. Journal of Colloid and Interface Science 107 (1985) 345

29. J.Th.G. Böhm, Adsorption of Polyelectrolytes at Liquid-liquid Interfaces and its Effect on Emulsification. Thesis, Wageningen, The Netherlands. (1974)

30. J. Benjamins, M.A.T. Loeve, F.A. Veer. unpublished results (1972)

31. M.A. Cohen Stuart, J.T.F. Keurentjes, B.C. Bonekamp, J.G.E.M. Fraaye. Gelation of

Polymers Adsorbed at the Water-Air Interface. Colloids and Surfaces. <u>17</u> (1986) 91

32.    B.R. Malcolm. The Flow and Deformation of Synthetic Polypeptide Monolayers during Compression. Journal of Colloid and Interface Science <u>104</u> (1985) 520

33.    J.C. van de Pas, A. Prins. unpublished results (1973)

34.    J.A. de Feijter, J. Benjamins. unpublished results (1975)

35.    A. Snik. Study of Physical Properties of Monolayers, Application to Physiology. Thesis, Eindhoven, The Netherlands (1983)

36.    D.A. Edwards, H. Brenner, D.T. Wasan. Interfacial Transport Processes and Rheology. Butterworth-Heinemann, Boston (1991).

37.    D. Thiessen, A. Scheludko. Kolloid-Zeitschrift und Zeitschrift zur Polymeren. <u>218</u> 139 (1967)

38.    J.J. Kokelaar, A.Prins, M. de Gee. A new Method for Measuring the Surface Dilational Modulus of a Liquid. Journal of Colloid and Interface Sci. <u>146</u> (1991) 507

39.    K.D. Wantke, K. Lunkenheimer, C. Hempt. Calculation of Elasticity of Fluid Boundary Phases with the Oscillating Bubble Method. Journal of Colloid and Interface Science. <u>159</u> (1993) 28

40.    K.D. Wantke, H. Fruhner, J. Fang, K. Lunkenheimer. Measurement of the Surface Elasticity in Medium Frequency Range using the Oscillating Bubble Method. Journal of Colloid and Interface Science. <u>208</u> (1998) 34

41.    J. Benjamins, A. Cagna, E.H. Lucassen-Reynders. Viscoelastic Properties of Triacylglycerol/Water Interfaces Covered by Proteins. Colloids and Surfaces <u>114</u> (1996) 245

42.    A.A.H. Boonman, P.M.C. Gieles, C.H. Massen, J. Egberts. Dynamic Surface-Tension Measurements on Surface Active Materials: part II. Thermochemica Acta, <u>152</u> (1989) 165

43.    J. Benjamins, E.H. Lucassen-Reynders, in "Proteins at Liquid Interfaces", D. Mobius and R. Miller, Editors, Elsevier Science, Amsterdam, the Netherlands (1998) 341

44.    E.H. Lucassen-Reynders, J. Lucassen, P.R. Garrett, D. Giles, F. Hollway. Dynamic Surface Measurements as a Tool to Obtain Equation-of-State Data for Soluble Monolayers. Advances in Chemistry Series, No 144 Monolayers. E.D. Goddard, Ed. (1975)

45.    D.E. Graham, M.C. Phillips. Proteins at Liquid Interfaces; IV. Dilational Properties. Journal of Colloid Interface Science. <u>76</u> (1980) 227

46.    J. Leaver, D.G. Dalgleish. Variations in the Binding of β-casein to Oil-Water Interfaces Detected by Trypsin-Catalysed Hydrolysis. Journal of Colloid Interface Science. <u>149</u> (1992) 49

47.    P. Joos. Approach for an Equation of State for Adsorbed Protein Surfaces. Biochemica

et Biophysica Acta. $\underline{375}$ (1975) 1

48.    D. Giles, J. Lucassen. Dynamic Surface Properties of Adsorbed Films of Bovine Plasma Albumin. unpublished results (1971)

49.    J. Benjamins, J.A. de Feijter, M.T.A. Evans, D.E. Graham, M.C. Phillips. Dynamic and Static Properties of Proteins Adsorbed at the Air/Water Interface. Faraday Discussions of the Chemical Society. $\underline{59}$ (1975) 218

50.    N. Puff, A. Cagna, V. Aguie-Beghin, R. Douillard. Effect of Ethanol on the Structure and Properties of b-casein Adsorption layers at the Air/Buffer Interface. Journal of Colloid and Interface Science. $\underline{208}$  (1998) 405

51.    M. Mellema, D.C. Clark, F.A. Husband, A.R. Mackie. Properties of β-casein at the Air/Water Interface as supported by Surface Rheological Measurements. Langmuir. $\underline{14}$ (1998) 1753

52.    M. Blank, J. Lucassen, M. van den Tempel. The Elasticities of Spread Monolayers of Bovine Serum Albumin and Ovalbumin. Journal of Colloid Interface Science. $\underline{33}$ (1970) 94

53.    E.H. Lucassen-Reynders. Interactions in Mixed Monolayers. Part I; Assessment of Interactions between Surfactants. Journal of Colloid Interface Science. $\underline{42}$ (1973) 563

54.    E.H. Lucassen-Reynders and J. Benjamins. Dilational Rheology of Proteins Adsorbed at Fluid Interfaces. in E. Dickinson and J. Rodríguez Patino (Editors), Food Emulsions and Foams: Interfaces, Interactions & Stability, Special Publication No. 227, Royal Society of Chemistry, London. (1999) 195

55.    A. Williams and A. Prins, Comparison of the Dilational Behaviour of Adsorbed Milk Proteins at the Air-water and Oil-water Interfaces. Colloids and Surfaces, $\underline{114}$ (1996) 267

56.    G.A. van Aken, M.T.E. Merks. Oppervlakte-actieve Eigenschappen van Melkeiwitten. Voedingsmiddelentechnologie. $\underline{27}$ (1994) 11

57.    H. Neurath, H.B. Bull. The Surface Activity of Proteins. Chemical. Review. $\underline{23}$ (1938) 391

58.    R.D. Ludescher. Molecular Dynamics of Food Proteins: Experimental Techniques and Observations. Trends in Food Science & Technology. $\underline{1}$ (1990) 145.

59.    W. Norde. Adsorption of Proteins at Solid-Liquid Interfaces. Advances in Colloid and Interface Science. $\underline{25}$ (1986) 267

60.    M. van den Tempel, E.H. Lucassen-Reynders. Relaxation Pprocesses at Fluid Interfaces. Advances in Colloid Interface Science. $\underline{18}$ (1983) 281

61.    F. MacRitchie. Spread Monolayers of Proteins. Advances in Colloid Interface Science. $\underline{25}$ (1986) 341

62.    R. Maksymiw, W. Nitsch. Catalase Monolayers at the air/water Interface. Journal of

Colloid and Interface Science. 147 (1991) 67

63.  G. van Aken. A Phenomenological Model for the Dynamic Interfacial Behaviour of Adsorbed Protein Layers. Food Macromolecules and Colloids; Spec. Publ. no 156 of the Royal Society of Chemistry, E. Dickinson, D. Lorient, ed. (1995) 43

64.  J.R. Hunter, P.K. Kilpatrick, R.G. Carbonell. $\beta$-casein Adsorption at the Air/Water Interface. Journal of Colloid and Interface Science. 142 (1991) 429

65.  W. Norde, J.P. Favier. Structure of Adsorbed and Desorbed Proteins. Colloids and Surfaces. 64 (1992) 87

66.  F. MacRitchie. Equilibria between Adsorbed and Displaced Segments of Protein Monolayers. Journal of Colloid Interface Science. 79 (1981) 461

67.  F.A. Veer and M. van den Tempel. Surface Tension Relaxation in a Surface containing Surfactant Particles. J. Colloid Interface Sci., 42 (1973) 418

68.  S. Kitching, G.D.W. Johnson, B.R. Midmore and T.M. Herrington. Surface Rheological Data for a Polymeric Surfactant using a Pulsed Drop Rheometer. Journal of Colloid Interface Science. 177 (1996) 58

69.  V.B. Fainerman. Kolloidnyi Zhurnal., 40 (1978) 530

70.  A.A. Trapeznikov, V.G. Vins and T.Y. Shirokova. Kinetics of the Reduction of Surface-Tension in Protein Solutions. Colloid Journal USSR. 43 (1981) 262

## 4 VISCOELASTIC PROPERTIES OF PROTEINS ADSORBED AT OIL/WATER INTERFACES

### 4.1 Introduction

The dynamic interfacial properties of protein layers adsorbed at the air/water interface, expressed in the dilational modulus, $\varepsilon$, have been discussed in the previous chapter. The experimental determination of this modulus, defined in equation 1 of Chapter 3, usually involves monitoring the response of the interfacial tension to small-amplitude oscillations of the interfacial area. In classical experiments (1-4, for a brief survey see Chapter 3), surface waves have been generated by barriers oscillating in the surface, while monitoring the interfacial tension by a Wilhelmy plate, positioned at some distance from the barrier. Such experiments have greatly increased our knowledge and understanding of interfacial dynamics, especially at the *air*-water surface. The applicability of the barrier-and-plate technique is limited by a number of problems which occur at any interface (5), but which are aggravated at *oil*-water interfaces. This will be discussed in section 4.2.

In this chapter a new technique will be described which does not suffer from those problems. The new set-up is a Dynamic Drop Tensiometer in which a small drop (of a few mm diameter) is subjected to sinusoidal oscillations of its volume. The corresponding area changes produce tension changes, which are evaluated from measurements of the fluctuating shape of the drop, using the Young-Laplace equation. The interfacial tension measurement is based on the well-known method of axisymmetric drop shape analysis (6-10). This set-up permits us to determine the interfacial rheological properties in compression/expansion at different amplitudes and frequencies of the area oscillations.

The method was first used to investigate the dynamic interfacial behaviour of proteins adsorbed at the triacylglycerol/water interface. For a better understanding of this behaviour these results will be compared with those obtained at the air/water and tetradecane/water interface.

The molecular structure of the proteins used varied from almost random coil to globular, as in Chapter 3.

### 4.2 The Dynamic Drop Tensiometer: a solution for specific problems at oil/water interfaces.

In section 3.3.1 it was discussed that, when using the traditional longitudinal wave method, the most convenient experimental regime is the limiting case where the wavelength ($\lambda$) is much greater than L, the effective length of the trough, and the damping coefficient is much smaller than 1/L. In this region the wave is reflected back

and forth between the wall of the trough and the barrier. As a result of these multiple reflections, the surface undergoes a practically uniform deformation, without the wave character being apparent from variations in phase and amplitude with distance. This condition is easily met when studying dynamic interfacial properties at the air/water interface. However, the much higher viscosity of triacylglycerol-oil, in comparison to air or water, greatly increases wave damping and hinders wave propagation. Consequently, oil/water interfaces require smaller effective trough lengths L for the condition of uniform deformation (W>>1, see section 3.3.1) to be met. Under these conditions, in principle, it should be possible to apply the damped-wave method. However, damping will occur over distances that become small compared to the size of the Wilhelmy plate.

A second problem that also becomes more serious in the case of oil/water interfaces is leakage of surface-active material past the moving barrier. Several solutions for this problem have been described in the literature: (i) connecting the moving barrier to the side wall with a teflon tape (11), (ii) using the ring trough method (12) in which the surface is deformed by moving a cylindrical glass ring, acting as the wall of the trough, vertically in the liquid surface and (iii) using a rhombus-shaped trough, the sides of which acting as barriers (13). In the last set-up the surface is deformed by driving together the two opposite corners. These modifications to the traditional methods fully eliminated leakage, but no attention has been paid to the size reduction needed, because of the increased wave damping in oil/water systems.

The Dynamic Drop Tensiometer, to be described in this chapter, fully solves both the leakage and the damping problem. It differs from the barrier-and-plate technique in that the oscillations in area and tension are measured on one and the same small interfacial area. Here, the role of the oscillating barrier is played by the rim of the capillary against which the interface is being alternately compressed and expanded. For an external diameter of the capillary of 2 mm, the distance over which the wave can travel over the drop is only a few mm, i.e., much smaller than the effective trough length in the conventional set-up. Therefore, homogeneity of deformation of the area is far more easily ensured. For example, when using a triacylglycerol oil with a viscosity of 100 mPas and an oscillating frequency of 1 rad/s, this condition is met even for adsorbed layers with a modulus as low as 1 mN/m.

4.3 Experimental

4.3.1 Dynamic Drop Tensiometer

An experimental set-up for measuring interfacial viscoelasticity requires two elements. (i) a possibility to sinusoidally oscillate the interfacial area and (ii) a method for measuring the resulting interfacial tension oscillations. Both elements are combined in the Dynamic Drop Tensiometer, which is a modified version of the Automatic Drop

Tensiometer developed by Labourdenne et al. (10). First results of the use of this technique have been published in ref. (11).

The interfacial area to be investigated is the area of a droplet, of which the volume oscillates by moving back and forth the piston of the syringe from which the droplet is formed, see fig. 2.

The interfacial tension measurements are based on the axisymmetric drop shape analysis. According to this method the drop shape is processed starting from the fundamental Laplace equation

$$\frac{1}{x}\frac{d}{dx}(x\sin\Theta) = \frac{2}{b} - cz \tag{1}$$

applied to the drop profile z(x) (14,15), which is obtained as described below (see Figure 1), where x and z are the cartesian co-ordinates at any point of the drop profile, b the curvature radius of the drop at its apex, $\Theta$ is the angle of the tangent to the slope of the drop profile, dz/dx, and c is the capillarity constant (equal to $(g\Delta\rho)/\gamma$, where $\Delta\rho$ is the difference between the densities of the two liquids and g is the acceleration of gravity).

Figure 2 shows a diagram of the experimental set-up. An integrating sphere light source (2), a thermostatted cuvette (3) containing the oil drop within a water phase and a CCD camera attached to a telecentric lens (5) are aligned on an optical bench (1). A drop of liquid (e.g. oil) is delivered from a syringe (4), controlled by a DC motor drive, into a thermostatted optical glass cuvette (1x2x4.3 cm) containing the other liquid (e.g. the aqueous phase) (3). The syringe is attached, through a Luer-lock device, to a stainless steel laboratory pipetting canula with a flat-cut tip having an external and internal diameter of 2 and 1 mm respectively. Depending on the specific gravity difference between the two liquids, the drop is rising or pending. In the first case this canula is U-shaped. The materials in contact with both liquids must be carefully cleaned in order to prevent any contamination by surface-active agents. The absence of contamination can be verified by interfacial tension measurements with pure liquids: the tension should remain constant with time and upon compression.

The drop profile, required to determine the interfacial tension, is obtained by analysing the profile of the droplet using a CCD camera coupled to a video image profile digitiser board connected to a personal computer (9). All points of the measured profile are used to determine the profile curve. The curve that obeys best the theoretical Laplace curve is determined by means of a least square method as indicated in figure 3 (14), where the $E_i$ (coordinates $x_i$ and $z_i$) indicate the experimental points and $P_i$ their orthogonal projection on the theoretical curve. By using optimised software and a fast computer, several times per second the three characteristic parameters of the drop, i.e., volume, area and interfacial tension are calculated. This enables us to determine continuously, during the volume oscillation of the droplet, the oscillating area and the resulting sinusoidal interfacial tension oscillations.

106

Figure 1
Profile of pendant drop analysed according to Eqn. (2).
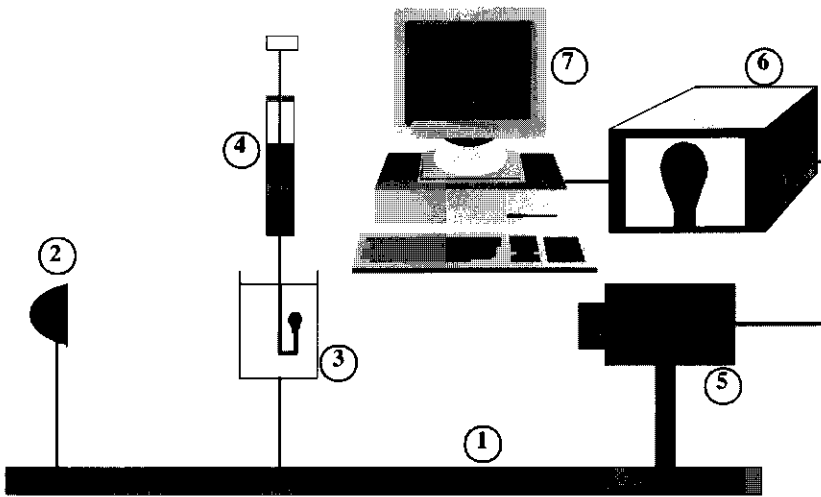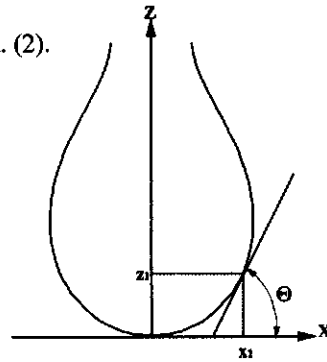
Figure 2
Dynamic Drop Tensiometer :(1) optical bench, (2) integrating sphere light source, (3) drop formation device inside thermostatted cuvette (contains water phase), (4) syringe containing drop forming liquid (oil); piston is driven by DC motor (not shown), (5) CCD camera, (6) video monitor and (7) personal computer.:

Figure 3
Illustration of the least square method to determine the optimal drop shape with respect to the Laplace curve $E_i$ indicate experimental points.
$P_i$ indicate their orthogonal projection on the theoretical curve.

107
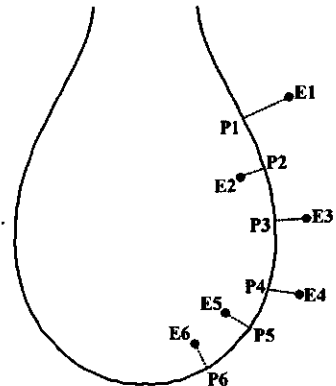
The software also analyses, by means of the Fourier Transform method, the measured sinusoidal area changes and the resulting sinusoidal tension changes in terms of interfacial viscoelastic parameters. Both the absolute value of the complex modulus, $|\varepsilon|$, and the phase angle $\phi$ between the changes in interfacial tension and the changes in interfacial area are determined. In the simple case of homogeneous deformation of the entire area, the absolute value $|\varepsilon|$ is directly related to the amplitude of the oscillating interfacial tension, $\Delta\gamma$, and interfacial area, $\Delta A$, by Eqn (2):

$$|\varepsilon| = A(\Delta\gamma / \Delta A) \qquad (2)$$

The elastic component $\varepsilon'$ and the viscous component $\varepsilon''$ are calculated from $|\varepsilon|$ and the phase angle $\phi$ by Eqns (3) and (4):

$$\varepsilon' = |\varepsilon|\cos\phi \qquad (3)$$

$$\varepsilon'' = |\varepsilon|\sin\phi \qquad (4)$$

Several experimental procedures are possible, depending on the information that is required:

(i) first the oil droplet is formed within a few seconds; immediately after formation of the droplet, the interfacial tension measurement starts.

(ii) the sinusoidal area oscillation for the dilational modulus measurement can be started directly after the droplet formation. In this way the evolution of the modulus starting with an almost clean interface up to a fully covered interface can be obtained.

(iii) the area oscillations can be applied continuously, but can also be stopped and restarted as required. In this way the disturbance of the adsorbed layer is minimized.

The lower limit of the amplitude, $\Delta A/A$, is about 0.01. The frequency of the oscillation can be varied between 0.5 and 0.001Hz.

An extra regulation mode of the software enables us to superimpose sinusoidal area oscillations on the transient change in area of a growing drop from the early stages of its life onwards. In this way the interfacial conditions of an emulsion droplet elongated in a shear field can be simulated.

4.3.2 Materials

The triacylglycerol (TAG-oil) used in this investigation was sunflower seed oil, ex Union Merksem, was silica-treated to remove any surface-active impurities (e.g. monoglycerides and fatty acids).

Tetradecane, ex Fluka, was treated in the same way.

Sufficient removal of these impurities was checked by interfacial tension measurements (right and constant value).

Information about the proteins Na-caseinate, $\beta$-casein, BSA, ovalbumin is given in Chapter 2. In the case of $\beta$-casein a commercial sample, ex Eurial, instead of the laboratory-prepared sample was used. In the present study the globular milk protein $\beta$-

lactoglobulin (MW= 18.000; 5 cystein/M; 10 % α-helix, 50 % β-sheet (16)) is also investigated (BLG, ex Sigma Chemicals)

All proteins were dissolved in buffered solutions made from twice-distilled water. The chemicals used for preparing the buffers (phosphate buffer (I=0.03M) at pH=6.7) were all of analytical grade.

The interfacial protein layer is formed by adsorption.

All experiments were performed at 25°C.

4.4 Results

The Dynamic Drop Tensiometer (DDT-method) and the Barrier-and-Plate (longitudinal wave) method, the two techniques used for determining the interfacial dilational modulus, both measure the response of the interfacial tension to periodic changes in interfacial area. Thus, the two methods are similar in principle, but quite different in the experimental set-up. Experimental results are likely to be similar, but a more detailed comparison of results obtained with the two methods is needed to judge whether agreement is quantitative.

In Fig 4 the modulus vs. surface pressure data for the nonionic surfactant $C_{12}$ $E_6$ (E=$OCH_2CH_2$) obtained by both methods are compared. The good agreement in the case of this simple surfactant indicates that, as expected, the DDT method is a reliable method to determine dilational moduli.

**modulus (mN/m)**
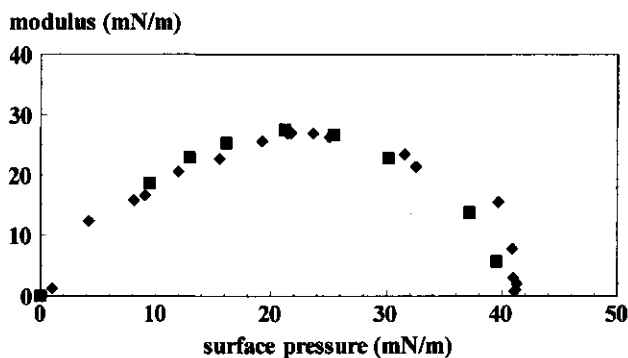


Figure 4

Comparison between DDT, ♦(17) and Barrier-and-Plate, ■(2) method for the nonionic surfactant $C_{12}$ $E_6$ . (Surface pressure, $\Pi=\gamma_0-\gamma$), frequency = 0.1 Hz
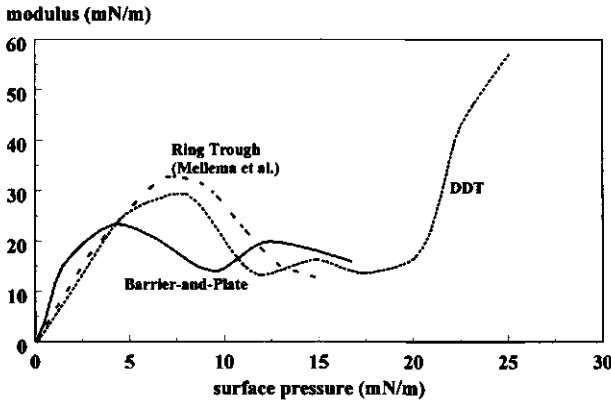
Figure. 5a β-casein
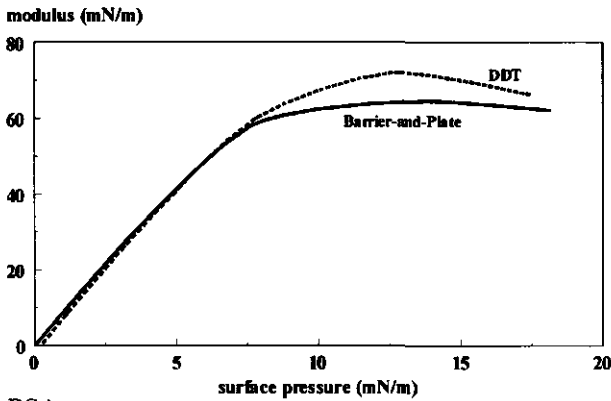


Figure 5b BSA
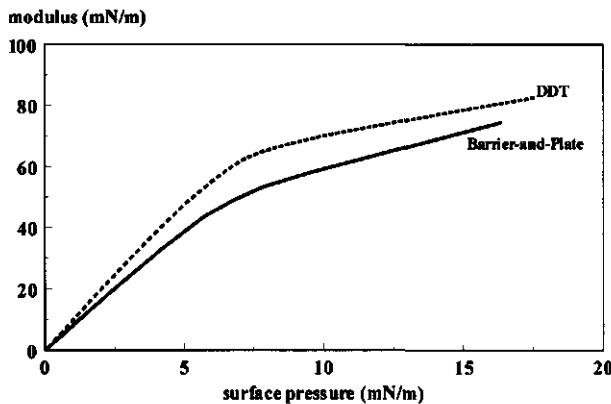


Fig 5c Ovalbumin

Figure 5
Comparison between DDT-method and Barrier-and-Plate method for determining the dilational modulus at the air/water interface, for β-casein (a), BSA (b), ovalbumin (c).
Frequency = 0.1 Hz

For proteins adsorbed at the air/water interface we have made a comparison between results obtained with the DDT-method and those determined with the square-elastic-band-method as described in Chapter 3. This comparison is visualised in terms of dilational modulus vs. surface pressure plots for β-casein (Fig. 5a), BSA (Fig. 5b) and Ovalbumin (Fig. 5c).

For the TAG-oil/water interface a comparison is presented in Table 1. In this case it was not possible to use the square-elastic-band-method because the oil interacts with these bands as could be concluded from considerable swelling. Therefore a modified Barrier-and-Plate set-up was constructed in which leakage of adsorbed material was prevented by connecting the moving barrier to the sidewall with a teflon tape (11). To satify the condition of homogeneous deformation (W>>1) the length of this trough was only 10 cm. For TAG-oil, with viscosity of 100 mPas and an oscillating frequency of 0.1 rad/s, this condition is met for adsorbed layers with a modulus as low as 10 mN/m. With the DDT this condition is even met for 1 rad/s and 1 mN/m.

Figure 5 indicates good agreement between the two methods. Only in the case of β-casein the differences are significant. However, these differences are most likely due to difference in protein sample.

In Table 1 the moduli measured by both methods were compared at equal interfacial pressures for the proteins Na-caseinate, BSA and ovalbumin, adsorbed at the TAG-oil/water interface.

Table 1. Elastic moduli at equal surface pressures measured with the Dynamic Drop Tensiometer and the Trough-with-Barrier-and-Plate method, for three proteins at the TAG-oil/water interface.
Frequency of the compression/expansion: 0.1 Hz.

| protein | concentration g/l | interfacial pressure mN/m | modulus; drop mN/m | modulus; trough mN/m |
|---|---|---|---|---|
| Na-caseinate | 5 | 17 | 5 | 6 |
| BSA | 0.01 | 14.2 | 23 | |
| | 0.1 | | 18 | 16 |
| | 1 | | 18 | |
| | 0.1 | 15.2 | 14 | 15 |
| | 1 | | 15 | |
| ovalbumin | 0.01 | 5 | 10-12 | 10 |
| | 0.01 | 7 | 14-17 | 15 |
| | 0.01 | 9.1 | 18 | |
| | 0.1 | | 23 | 26 |
| | 1 | | 22 | |
| | 0.1 | 10.7 | 26 | 30 |
| | 1 | | 26 | |
| | 0.1 | 12.4 | 30 | 30 |
| | 1 | | 29 | |

Figure 6
Example of the time dependence of the modulus (freq. = 0.1 Hz) and the interfacial pressure for 0.003g/l and 0.01g/l
BSA adsorbed at the tetradecane/water interface.
Filled symbols: modulus ; open symbols : interfacial pressure
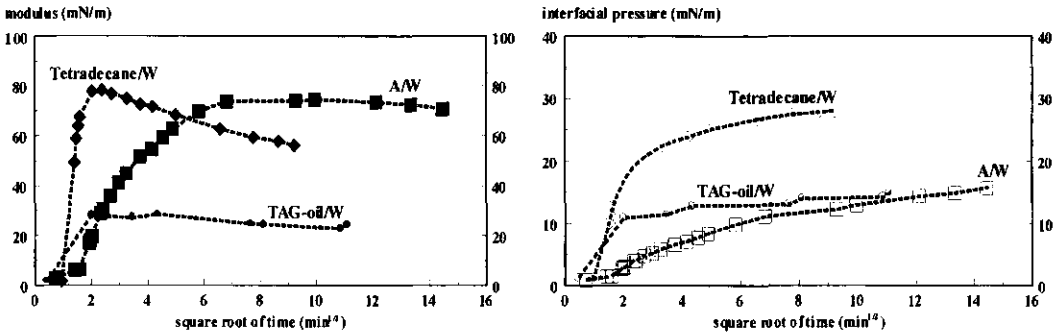


Figure 7a 0.01g/l BSA
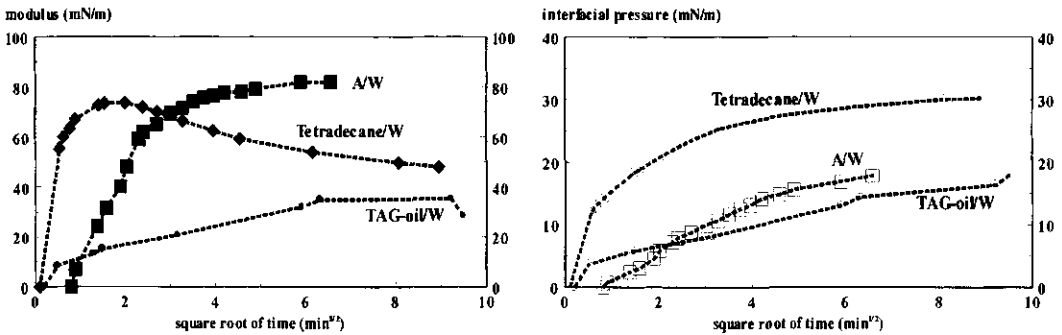


Figure 7b 0.1g/l ovalbumin

Figure 7
Time dependence of the modulus and the interfacial pressure for 0.01g/l BSA (7a) and 0.1g/l ovalbumin (7b) at the three interfaces.
Frequency = 0.1 Hz

112

Using the DDT the viscoelastic modulus of four proteins, β-casein, BLG, BSA and ovalbumin was studied in detail at three interfaces, air/water, TAG-oil/water and tetradecane/water. The experiments were performed at various protein concentrations and as a function of time after formation of the droplet, i.e., at different age of the interface. After droplet formation protein adsorption starts and after a certain time, the induction time, at a certain level of adsorption the interfacial pressure (Π) starts to deviate measurably from zero and generally increases with increasing adsorbed amount (3,18 and chapter 2). From this point the viscoelastic modulus also starts to increase with time. Figure 6 gives an example of the time dependence of the modulus and the interfacial pressure for 0.003g/l and 0.01g/l BSA. In Figure 7 the time dependence of the modulus and the interfacial pressure for 0.01g/l BSA (7a) and 0.1g/l ovalbumin (7b) at the three interfaces is given. Combining these data for different protein concentrations in a modulus vs. pressure plot makes them collapse into a single curve. Examples of those curves are presented in Figures 8a-c for BLG at air/water, β-casein at tetradecane/water and ovalbumin at TAG-oil/water, respectively. The curve in each plot is the combined result of experiments with the different protein concentrations, indicated by different symbols, at different interfacial ages. The results with the different protein concentrations form a master curve which is characteristic for each protein.

In Figure 9 these characteristic curves for the four proteins are compared at the three different interfaces; the air/water (9a), tetradecane/water (9b) and TAG-oil/water (9c).

In Figure 10 the effect of interface type on the modulus vs. pressure plot of each protein is given; β-casein (10a), BLG (10b), BSA (10c) and ovalbumin (10d).

Depending on the frequency of the area oscillations and the relaxation mechanisms involved, the interfacial layer behaves either as purely elastically, with $\phi=0$ in Eqn (3), or viscoelastically, with $\phi>0$ and increasing with decreasing frequency. Measured phase angles $\phi$ are collected in Tables 2 and 3, where an increasing phase angle represents an increasing viscous contribution to the modulus according to Eqn (4).

In Table 2 the viscoelastic behaviour of adsorbed protein layers is given at increasing interfacial pressure. The results for the different proteins are compared at the three interfaces; air/water, tetradecane/water and TAG-oil/water. In this table the results at the lower concentrations (0.01- 0.1 g/l) are given. At higher concentrations the phase angles are initially somewhat higher, however, with time (=age of the interface) a decrease to the level as presented in this table was observed.

In Table 3 the effect of the oscillation frequency on the viscoelastic behaviour for the proteins BSA and ovalbumin at the tetradecane/water and the TAG-oil/water interface is given.

Especially for BSA at the TAG-oil/water interface a considerable increase of the phase angle with decreasing frequency is observed. Ovalbumin behaves as purely elastic at both interfaces in this frequency range.

modulus (mN/m)
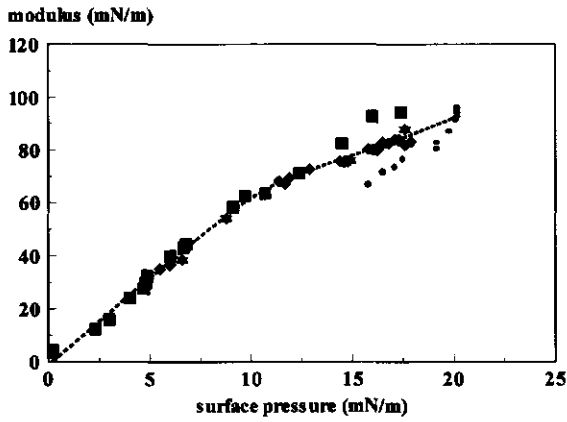


Figure 8a: 0.01 g/l (■) , 0.1 g/l (✿,♦), 1 g/l (●)

modulus (mN/m)
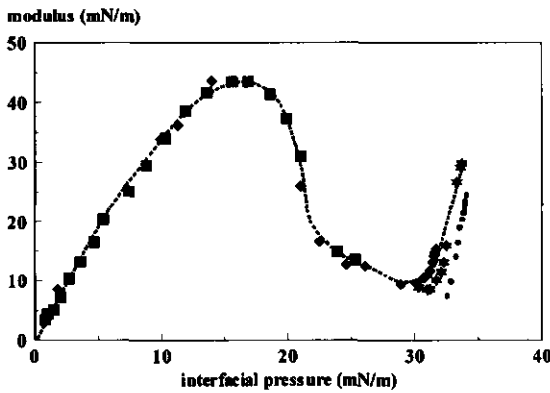


Figure 8b: 0.003 g/l (■) , 0.01 g/l (♦), 0.1 g/l (✿), 1 g/l (●)
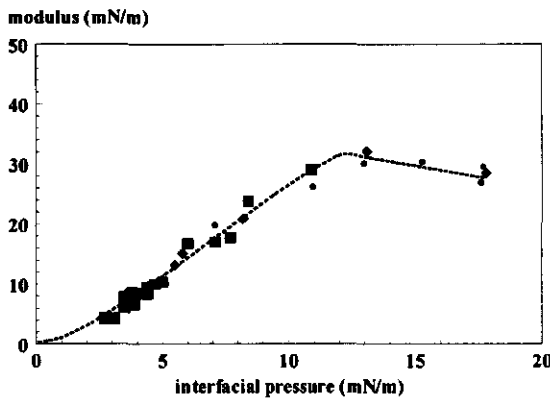
modulus (mN/m)



Figure 8c: 0.01 g/l (■) , 0.1 g/l (♦), 1 g/l (●)

Figures 8
Modulus vs. interfacial pressure curves for BLG at air/water (Fig.8a), β-casein at
tetradecane/water (Fig.8b) and ovalbumin at TAG-oil/water (Fig.8c).
Frequency = 0.1 Hz

114
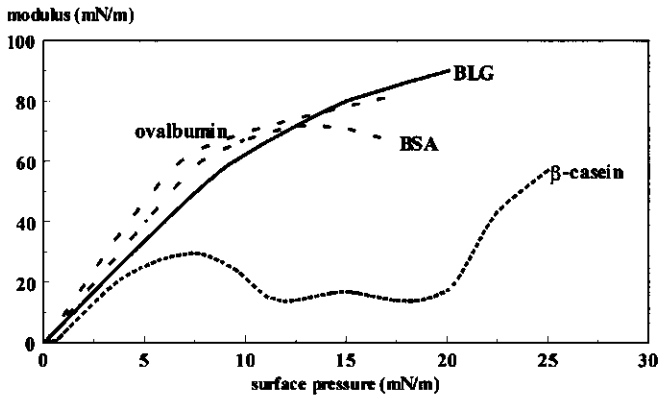
Figure 9a air/water
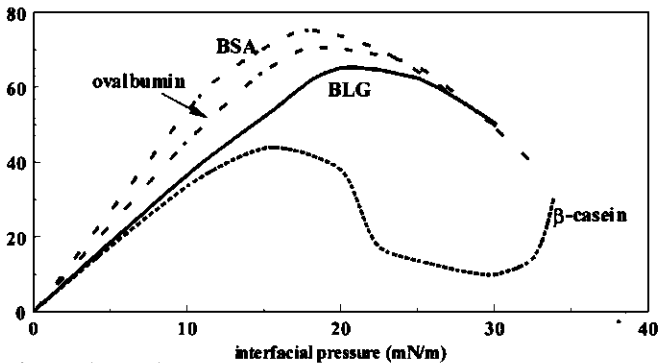


Figure 9b tetradecane/water
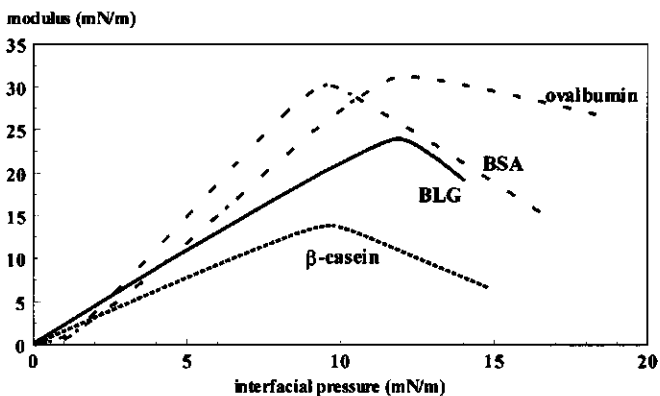


Figure 9c TAG-oil/water

Figure 9
Modulus vs. interfacial pressure curves of four proteins compared at the three different interfaces; air/water (Fig.9a), tetradecane/water (Fig.9b) and TAG-oil/water (Fig.9c).
Frequency = 0.1 Hz
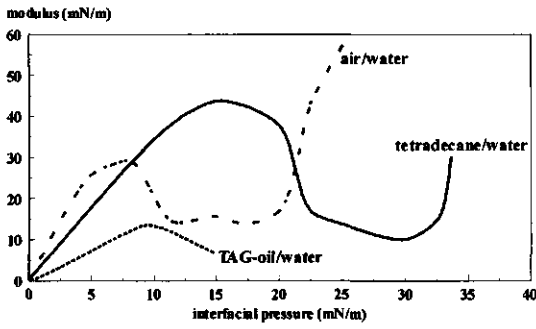
Figure 10a β-casein
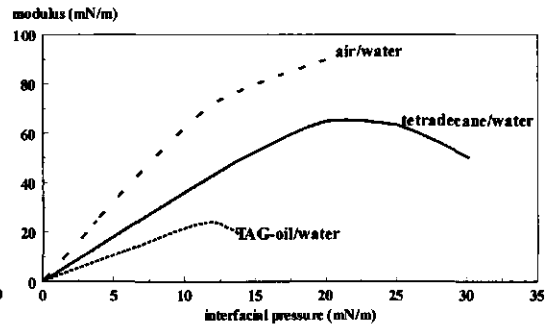
Figure 10b BLG
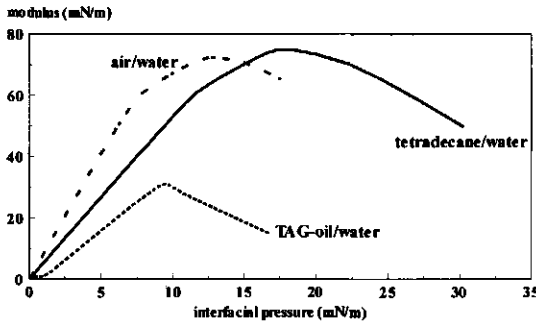
Figure 10c BSA
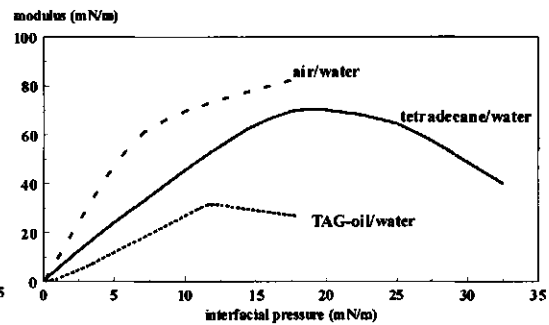
Figure 10d ovalbumin

Figure 10
The effect of interface type on the modulus vs. pressure curve of each protein; β-casein (Fig.10a), BLG (Fig.10b), BSA (Fig.10c) and ovalbumin (Fig.10d).
Frequency = 0.1 Hz

Table 2. Viscoelastic behaviour of adsorbed protein layers as indicated by the phase angle φ at increasing interfacial pressure.
The frequency of the area oscillation is 0.1Hz.

| protein | interfacial pressure mN/m | air/water | | tetradecane/water | | TAG-oil/water | |
|---|---|---|---|---|---|---|---|
| | | modulus mN/m | Phase angle (degrees) | modulus mN/m | Phase angle (degrees) | modulus mN/m | Phase angle (degrees) |
| Nacaseinate | 15 | | 0 | | | 8.5 | 0 |
| | 16.5 | | | | | 8.1 | 3 |
| | 17 | | | | | 5.7 | 14 |
| | 17.5 | | 12 | | | 5.4 | 9 |
| β-casein | 10 | 15 | 4 | 34 | 3 | | |
| | 15 | 16 | 6 | 44 | 4 | | |
| | 20 | 18 | 20 | 26 | 9 | | |
| | 25 | 57 | 32 | 13 | 10 | | |
| | 30 | | | 10 | 16 | | |
| BLG | 10 | 62 | 7 | 40 | 3 | | |
| | 15 | 82 | 7 | 50 | 5 | 15 | 8 |
| | 20 | 91 | 11 | 65 | 4 | 17 | 7 |
| | 25 | | | 62 | 4 | | |
| | 30 | | | 55 | 4 | | |
| BSA | 7.5 | 44 | 3 | 29 | 4 | 26.2 | 16 |
| | 11 | 64 | 6 | 60 | 4 | 28 | 16 |
| | 15 | 87 | 6 | 69 | 3 | 17.3 | 18 |
| | 16.5 | 94 | 5 | 72 | 4 | 17.3 | 23 |
| | 20 | 91 | 11 | | | | |
| | 26.8 | | | 49 | 11 | | |
| Ovalbumin | 11 | 71 | 5 | 56 | 6 | 30 | 0 |
| | 13 | 77 | 5 | 60 | 6 | 30 | 0 |
| | 18 | 82 | 6 | 73 | 4 | 29 | 2 |
| | 25 | | | 66 | 4 | | |
| | 30 | | | 48 | 2 | | |

Table 3. Viscoelastic behaviour of adsorbed protein layers as indicated by the phase angle φ at increasing frequency.

| interface | protein | interfacial pressure mN/m | frequency (Hz) | modulus mN/m | Phase angle degrees |
|---|---|---|---|---|---|
| Tetradecane/water | BSA | 30.6 | 0.01 | 38 | 14 |
| | | | 0.1 | 48 | 8 |
| | | | 0.5 | 51 | 2 |
| TAG-oil/water | | 15 | 0.01 | 9.7 | 23 |
| | | | 0.1 | 17.3 | 18 |
| | | | 0.5 | 22.3 | 0 |
| Tetradecane/water | ovalbumin | 33.3 | 0.01 | 34 | 1 |
| | | | 0.1 | 36 | 0 |
| | | | 0.5 | 37 | 0 |
| | | | 1 | 40 | 0 |
| TAG-oil/water | | 18 | 0.01 | 25 | 5 |
| | | | 0.1 | 29 | 2 |

4.5 Discussion

4.5.1 Comparison between the Dynamic Drop Tensiometer and the Barrier-and-Plate method

In principle, three reasons can be put forward to account for differences between the results of the two methods: (i) wave propagation effects, since barrier and plate in the trough are some distance apart, (ii) effects of shearing deformation on top of the isotropic compression/expansion, and (iii), only in the case of tetradecane or TAG-oil, the very much lower volume ratio of drop phase to reservoir phase (oil and water in the present work) in the Drop Tensiometer, which might result in a different sensitivity to oil-soluble impurities between the two methods. Wave propagation effects, due to too low values of the wave propagation number W, could lower the moduli in trough experiments (see section 4.2). Shearing deformation is expected to be larger in the trough than in the drop experiment; it might hamper the propagation of the deformation if the shear modulus is high enough. Both effects are expected to result in lower moduli in the case of the barrier and plate method. The effect of shearing deformation is expected to be small as can be deduced from section 3.3.3 (Chapter 3). As to the third possible effect, we do not regard this as important in our case as the oil had been purified, but specific displacement effects cannot be ruled out completely especially at low protein concentration.

From Figure 4 in which the two methods are compared for the nonionic surfactant $C_{12}E_6$, adsorbed at the air/water interface, it can be concluded that the DDT method is reliable.

For proteins adsorbed at the air/water interface, the results obtained with the DDT are compared with those determined by using the square elastic band method, described in Chapter 3. It can be seen from Figure 5 that, especially in the case of BSA and ovalbumin and at low surface pressures, the differences are very small. At higher pressures the differences between the two methods increase somewhat, but, they never exceed 10 %. In the case of β-casein (Fig. 5a) the overall shape of the curve is similar, exhibiting two maxima in the pressure range <20 mN/m. However, the modulus values and the surface pressures at these maxima differ somewhat. These differences are most likely due to small differences in the protein samples: home-made sample in Chapter 3 and a commercial sample in the DDT experiments. This sample-nature effect is supported by a comparison between the DDT results with those obtained with the ring-trough experiments (19) with a protein sample from the same supplier.

For the TAG-oil/water interface, the results obtained with the DDT-method are compared with those obtained with the modified Barrier-and-Plate set-up (11). The results, presented in Table 1, indicate that, when compared at equal interfacial pressures, the differences between the two methods are comparable to duplicate experiments with the same method.

118

The above results indicate that the above-mentioned causes for possible differences between the two methods only play a minor role and strongly support the reliability of the new Dynamic Drop Tensiometer for measuring interfacial viscoelasticity.

4.5.2   The effects of adsorption time and protein concentration.

In Fig. 6, as a representative example of the time dependence of the modulus and the interfacial pressure, the results for 0.003 g/l and 0.01 g/l BSA, adsorbed at the tetradecane/water interface are given. After droplet formation protein adsorption starts and at a certain level of adsorption, after a certain age of the interface, the interfacial pressure (Π) starts to deviate measurably from zero. From that time onward, generally, the interfacial pressure further increases with increasing adsorbed amount (3,18 and Chapter 2). From this point the viscoelastic modulus also starts to increase with time. In Fig. 6 this induction time is 4 and 1 min for 0.003 g/l and 0.01 g/l, respectively. Especially the initial parts of pressure and modulus curves show a great similarity.

These modulus vs. time curves also show a great advantage of the DDT-set-up, compared to the conventional Barrier-and-Plate method, viz. the very short time, 10 to 20 s, between formation of the interface and the first modulus measurement. Such a short response time makes it possible to determine the changes in viscoelasticity during fast increasing adsorption as occurs initially with higher protein concentrations.

From Fig. 7a,b, in which the time dependence of modulus and interfacial pressure for BSA and ovalbumin at the three different interfaces are compared, it can be seen that there are three aspects in which these curves are different (i) "induction" time (t $_{Π>0}$), (ii) steepness of pressure and modulus increase with time and (iii) the maximum value of the modulus. The induction time increases in the sequence TAG-oil < Tetradecane< air. The increase is steepest at the tetradecane/water interface for both proteins. At all interfaces the protein adsorbs from the solution in water, consequently in the low interfacial pressure range the adsorption rate will be the same. So, a shorter t $_{Π>0}$ combined with a steeper increase of the pressure, indicates a significantly different pressure vs. surface concentration curve as will be discussed in section 4.5.3.

In Figures 8a-c for BLG at air/water, β-casein at tetradecane/water and ovalbumin at TAG-oil/water, respectively, the modulus is plotted as a function of the interfacial pressure. The line given in each plot is the combined result of experiments with the different protein concentrations, indicated by different symbols, at different interfacial ages. The results with the different protein concentration collapse into one modulus vs. pressure curve, especially so for the lower concentrations. In Chapter 3 the same finding was dealt with for protein layers adsorbed at the air/water interface. Thus, equilibration within the surface is very much faster than between surface and bulk solution. Consequently, with respect to interfacial viscoelasticity, the interfacial pressure fully characterises the adsorbed layer. It also indicates that the time for a protein molecule needed to change its conformation from the dissolved to the adsorbed state is small

compared to the characteristic time of the measurement ($\approx$ 1 min.). However at higher protein concentrations we see some deviation from the modulus vs. pressure curve determined at lower concentrations. In this case the modulus is initially lower than expected, however, with increasing pressure and consequently increasing time/age, it re-approaches the curve for the lower concentrations. This effect is illustrated best in Fig. 8a (BLG at A/W). The explanation is that at high protein concentrations adsorption is so fast that the time needed to fully saturate the interface is of the same order as the time needed for conformation change after adsorption. As soon as this reconformation is nearly finished $\varepsilon(\Pi)$ data of the high bulk concentration will also follow the low concentration curve. This finding indicates that, for high protein concentrations, during the first minutes after adsorption a situation exists that differs from the one that exists when the adsorbed layer obeys the equilibrium pressure vs. surface concentration curve.

4.5.3. The effect of protein type and nature of the interface.

The effect of protein type on the viscoelasticity is given in Figure 9, in which the characteristic curves of the four proteins are compared at the three different interfaces; the air/water (9a), tetradecane/water (9b) and TAG-oil/water (9c). At the air/water interface (9a) we observe that for the globular proteins the $\varepsilon(\Pi)$ are very similar. An almost linear increase is found for $\varepsilon(\Pi)$ up to pressures of about 7 mN/m. At higher pressures the curves flatten. With BSA, at $\Pi > 10$ mN/m, $\varepsilon$ even tends to decrease with further increasing $\Pi$. Compared to the globular proteins, the shape of the $\varepsilon(\Pi)$ curve of $\beta$-casein, a protein with an almost random coil molecule, is clearly different. Only the steepness of the initial part of the $\varepsilon(\Pi)$ is similar. The curve is linear only up to $\Pi = 5$ mN/m. With a further increase of $\Pi$ maxima are observed at $\Pi = 7.5$ and 15 mN/m. At $\Pi > 20$ mN/m the modulus again increases considerably. This increase is most likely due to multilayer formation or collapse phenomena (20) at higher pressures. Qualitatively for $\beta$-casein and almost quantitatively for the BSA and ovalbumin, these curves are similar to the ones presented in Chapter 3. Differences can be attributed to differences in experimental method (Barrier-and-Plate vs. DDT) and differences in protein sample.

At the tetradecane/water interface (9b) we also find qualitatively the same difference between the globular proteins and $\beta$-casein. Compared to air/water, the linear range extends to higher pressures for all proteins, especially for $\beta$-casein. In the case of $\beta$-casein the second maximum is absent and replaced by a pressure region with a more or less constant value of the modulus. For all proteins at $\Pi > 15$-20 mN/m a significant decrease of the modulus with a further increase of pressure is found.

A clear maximum in the $\varepsilon(\Pi)$ as found for the tetradecane/water interface was also present in the $\varepsilon(\Pi)$ curves at the TAG-oil/water interface. The linear range at the latter interface is up to pressures in between those found for the two other interfaces.

At all three interfaces globular proteins show a higher maximum value for the modulus than β-casein. However, these maxima are considerably affected by the type of interface as can be seen from Figure 10 for β-casein (10a), BLG (10b), BSA (10c) and ovalbumin (10d) respectively. For BLG and ovalbumin the behaviour at different interfaces is similar, Figs. 10b vs. 10d , the same values for the maxima of the modulus and the same sequence of the maxima; air/water > tetradecane/water > TAG-oil/water. If we compare maxima of the globular proteins at tetradecane/water and air/water we observe that the differences decrease in the sequence BLG > ovalbumin > BSA. The characteristic features of the proteins at the three different interfaces are summarised in Table 4.

Table 4
Initial slope, dε/dΠ, and extent of linear range of the proteins at the three interfaces

| protein | air/water | | tetradecane/water | | TAG-oil/water | |
|---------|-----------|--|-------------------|--|---------------|--|
| | dε/dΠ | Extent mN/m | dε/dΠ | Extent mN/m | dε/dΠ | Extent mN/m |
| β-casein | 5 | 5 | 3.4 | 10 | 1.5 | 8 |
| BLG | 6.2 | 9 | 3.8 | 11 | 2.0 | 8 |
| BSA | 8.5 | 7 | 5.5 | 12 | 3.5 | 8 |
| Ovalbumin | 9.4 | 7 | 4.4 | 14 | 3.0 | 10 |

In the limiting case of purely elastic behaviour (high frequency) the modulus can be derived from the surface equation of state according to equation 2 of Chapter 3. So, the elastic modulus vs. pressure curve generally reflects the surface equation of state of the adsorbed material at the given interface, and it is a particularly sensitive tool to assess non-ideal behaviour in the surface layer (21). In the absence of any interactions, whether intramolecular or intermolecular, the initial slope in these plots would have been +1, as predicted by the two-dimensional analogue of the ideal-gas law. The data collected in Table 4 imply severe non-ideality for all proteins at the three interfaces and at all interfacial pressures, including the very lowest. At the air/water and tetradecane/water not a trace of such a low-slope region was observed, even at pressures Π<<1 mN/m. For the TAG-oil/water interface the initial slopes of the ε(Π) curves, at pressures Π<1 mN/m, are very low. Lack of reliable data at these very low pressures probably obscures the +1 slope. So, in contrast to what was found at the air/water surface and the tetradecane/water interface, here the gaseous region may extend up to pressures of about 1 mN/m.

At the TAG-oil/water interface, at pressures slightly higher than 1 mN/m, a steeper linear part follows with a slope ranging from 1.5 to 3.5 depending on protein type. At air/water these slopes are considerably higher (range: 5 to 9.4 ), in fair agreement with data published elsewhere (see table 4 Chapter 3). For the tetradecane/water interface the

values for the slopes are in between. Consequently, the intra- and intermolecular interactions in adsorbed protein layers decrease in the sequence air/water> tetradecane/water > TAG-oil/water.

At the three interfaces investigated the following trend is observed: the initial slope and the pressure range of this steep linear behaviour increases with decreasing flexibility of the protein molecule. β-casein is the most flexible molecule and ovalbumin is the most compact one. In this linear range, the modulus is purely elastic, and should be equal to the value of $\varepsilon_0$ evaluated from the equilibrium pressure *vs.* adsorption curve. Such equality was confirmed for adsorbed protein layers at the air/water interface (22 and Chapter 3). At present, however, it is not possible to confirm this equality for the TAG-oil/water and tetradecane/water interfaces because reliable adsorption data over a sufficient range of interfacial pressures are lacking.

Pressure-area curves of BSA and BLG spread at the tetradecane/water interface (23) indicate a more expanded structure at the tetradecane/water interface compared to air/water. This is in line with what has often been observed with small surface-active molecules, where it is attributed to reduced van der Waals cohesion of hydrophobic chains in oil, which is a better solvent for the chains than air or water. Both Graham and Phillips (24) and Murray (23) apply this argument to the hydrophobic polypeptide chains of globular proteins, which can unfold into loops in the oil phase. Such reduced cohesion results in a higher pressure at oil/water at low surface coverage. However, the flexible protein β-casein exhibits the opposite behaviour, as it was found to be more expanded at air/water(23). The author explains this by arguing that the unhindered loop formation which is possible only for flexible macromolecules, results in a smaller number of segments in the surface, i.e., a smaller molecular area and, therefore a smaller degree of coverage (Θ) and a lower surface pressure at the same value of Γ. This second, positive, effect on the surface pressure overrides the negative effect of the van der Waals cohesion of the hydrophobic chains.

If the above explanation for the more expanded structure at the tetradecane/water interface is right, globular molecules will behave more flexible/ β-casein like at this interface. Consequently, one should expect lower moduli at the tetradecane/water interface. For the globular proteins this is indeed the case, especially in the lower pressure range up to pressures of about 10 mN/m, depending on protein type. The maxima do not always differ so much; with BSA they were even found to be equal. For β-casein this trend is only observed in the pressure range up to 5 mN/m and the first maximum of the modulus at the tetradecane/water interface is even considerably higher.

At the TAG-oil/water interface all characteristic features, such as initial slope, length of the linear range and especially the maximum value of the modulus, are considerably lower than at the tetradecane/water interface. This indicates an even more expanded structure of the protein at the TAG-oil/water interface, which would result in lower adsorbed amounts at this interface. Available adsorption data at TAG-oil/water indeed suggest a lower adsorption for β-casein but for BLG differences were found to be small

(25). The reason for a further expansion at the TAG-oil/water interface compared to tetradecane/water may be the possibility that, due to the less apolar character of this oil, more hydrophobic amino acids experience the TAG-oil as a better solvent.

Adsorption of proteins involves molecular reconformation including unfolding of the protein molecules at the interface, which is expected to be easiest for the most flexible protein, β-casein, resulting in a less cohesive, more compressible film with a low elasticity modulus. For globular proteins, the extent of reconformation upon adsorption is considered to be much less. The present results indicate that at all interfaces these molecular reconformations take place fairly rapidly. The fact that the characteristic ε(Π) curve is not affected by protein concentration led to the conclusion (section 4.5.2) that the time for a protein molecule needed to change its conformation from the dissolved to the adsorbed state is short compared to the characteristic time of the measurement ($\approx 1$ min.). The time scale of reconformation of already adsorbed molecules during a modulus measurement, in the low interfacial pressure range, is even smaller, $< 1$ s, since the modulus at a frequency of 0.1 Hz. is purely elastic as is indicated by low phase angles. During an oscillation at this frequency the adsorbed molecule is able to adopt its conformation continuously to the changing interfacial pressure along the equilibrium Π(Γ) curve.

In the range of higher interfacial pressures, after the linear region, phase angles are no longer negligible (see Table 2) and the modulus becomes frequency dependent (see Table 3). Remarkable effects are (i) the very low phase angles with ovalbumin at all interfaces, even in the pressure range where the modulus decreases with increasing pressure (ii) the relatively high phase angles with BSA and significant frequency dependency of the modulus, especially at TAG-oil/water and (iii) the high phase angles with β-casein at air/water in the pressure range >20 mN/m. The measured viscous phase angles cannot be explained in terms of diffusional exchange with the bulk solution (see Chapter 3). Other relaxation mechanisms as discussed in Chapter 3, slow reconformations, collapse phenomena and, in the case of flexible proteins, exchange with protein molecules adsorbed in a second or higher are more likely to play a role.

We also observe that all ε(Π) curves pass through a maximum and then decline with increasing pressure. This decline is less clear at the air/water interface where in most cases only a flattening is observed. For low molecular weight surfactants (see Fig. 4) this decrease must be attributed to faster tension relaxation caused by diffusional exchange between interface and solution. For proteins, which do not desorb in the time-scale of the oscillations (see Chapter 3), the relaxation mechanisms mentioned before may cause this decrease. However, it is by no means clear why these should be facilitated at the tetradecane/water and TAG-oil/water interface.

In section 4.5.2 it was mentioned that the "induction" time for pressure and modulus is shorter for tetradecane/water and TAG-oil/water interface compared to the air/water
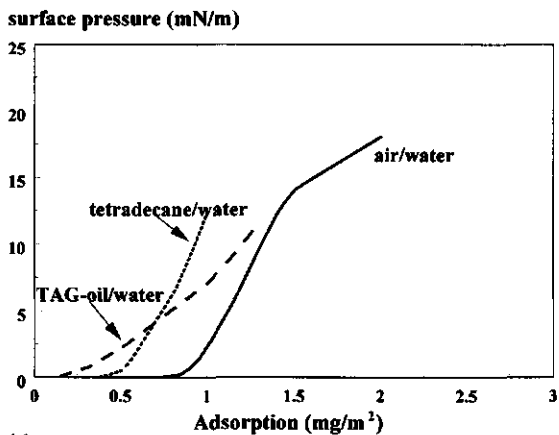
Figure 11
Estimated Π(Γ) curves for BSA adsorbed at Tetradecane/water and TAG-oil/water interface compared to the measured curve at the air/water interface.
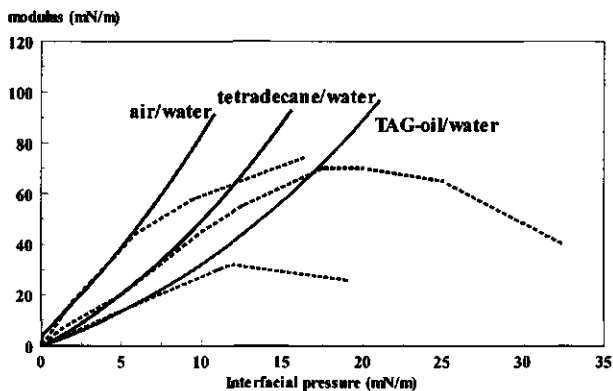


Figure 12
The two-dimensional solution theory applied to adsorbed ovalbumin layers at the air/water, Tetradecane/water and TAG-oil/water interface.
Dotted lines= measured curves, solid lines = theoretical curves.

interface. Assuming a similar initial adsorption rate, this shorter induction time is an extra indication for a more expanded structure. The consequence for the $\Pi(\Gamma)$ curve is a measurable $\Pi$ at lower $\Gamma$ compared to air/water. However, this does not mean that the $\Pi(\Gamma)$ curves for tetradecane/water and TAG-oil/water are the same. Assuming, that in the linear range, the modulus is equal to the value of $\varepsilon_0$ evaluated from the equilibrium pressure *vs.* adsorption curve, a steeper slope indicates a steeper increase of $\Pi$ with increasing $\Gamma$. On the basis of this view an estimation is made of the $\Pi(\Gamma)$ curves for BSA at the tetradecane/water and TAG-oil/water interface and compared with a measured $\Pi(\Gamma)$ plot of BSA at the air/water interface (Fig. 11).

### 4.5.4. Comparison with theory.

In Chapter 3 a two dimensional solution theory was applied to ovalbumin adsorbed at the air/water interface. Best fits were obtained for $S = 245$ and $H = 0.84RT$. Positive values of H mean that like molecules attract each other more than unlike molecules; high enough values of H lead to phase separation into a solute-rich surface phase and a solvent-rich one. Applying this theory to the modulus vs. pressure curve of ovalbumin at tetradecane/water and TAG-oil/water (Figure 12) we obtain values for the interaction parameter H of 0.45RT and 0 respectively, assuming the mentioned value for S. So, this theory also indicates increasing interaction in the sequence TAG-oil/water< tetradecane/water< air/water. This finding is probably related to the decrease of the solvent quality of the interface for the more hydrophobic amino acids which decreases in the same sequence.

It may be argued that S should be higher for the first two interfaces because of the more expanded structure, however, also the size of the solvent molecule is expected to increase for these interfaces because it consists of a mixture of oil/tetradecane and water.

### 4.6 Conclusions

- The Dynamic Drop Tensiometer is a reliable instrument for the measurement of the viscoelastic modulus in compression/expansion. The set-up is particularly suited for liquid/liquid interfaces, because interfacial leakage is fully eliminated. Due to the small size of the interfacial area, uniform deformation is ensured even if one of the liquids is a viscous oil. An additional advantage of the method is the short response time.
- At the three interfaces investigated, the modulus vs. surface pressure curve does not depend on protein concentration. This indicates that equilibration within the surface is much faster than between surface and bulk solution. The characteristic time for reconformations of protein molecules upon adsorption is less than one minute.

At high protein concentrations (>0.1g/l), during the first minutes after adsorption a situation exists that differs from the equilibrium pressure vs. surface concentration curve.

- The time scale of reconformations during a modulus measurement, in the low interfacial pressure range, is <1 s since the modulus at a frequency of 0.1 Hz. is purely elastic and, for the air/water interface (see Chapter 3) equal to the limiting modulus.

- The non-ideality of the adsorbed protein layer increases in the sequence TAG-oil < tetradecane < air. A 2-dimensional solution theory indicates a considerable increase of the interaction parameter H in the same sequence. This finding is probably related to the decrease of the solution quality for the more hydrophobic amino acids which decreases in the same sequence.

- At all interfaces non ideality and the maximum of the modulus increase in the sequence β-casein<BLG<BSA<ovalbumin. In this sequence the molecular structure changes from flexible to compact/rigid.

- The decline of the ε(Π) curve at higher interfacial pressures is most probably caused by collapse. It is not clear why this effect is more pronounced at the TAG-oil/water and tetradecane/water interface, than at air/water.

- At high interfacial pressures the modulus acquires a viscous component (measurable phase angles and frequency dependency). This effect is most pronounced for BSA at the TAG-oil/water interface but absent at all interfaces with ovalbumin.

- A first estimate of the Π(Γ) curve of proteins adsorbed at an oil/water interface, can be deduced by combining the effect of interface type on the induction time (t$_{\Pi>0}$) with the differences in intitial slope of the ε(Π) curve.

4.7 References

1    J. Lucassen, M. van den Tempel, Dynamic Measurements of Dilational Properties of Liquid Interfaces. Chemical Engineering. Science. 27 (1972) 1283.

2    J. Lucassen, D. Giles, Dynamic Surface Properties of Nonionic Surfactant Solutions. Journal of the Chemical. Society., Faraday Transactions. 1, 71 (1975) 217.

3    J. Benjamins, J.A. de Feijter, M.T.A. Evans, D.E. Graham and M.C. Phillips. Dynamic and Static Properties of Proteins Adsorbed at the Air/Water Interface. Faraday Discussions of the Chemical Society. 59 (1975) 218

4    L. Ting, D.T. Wasan, K. Miyano, Longitudinal Surface Waves for the Study of Dynamic Properties of Surfactant Systems III. Journal of Colloid and Interface Science. 107 (1985) 345.

5    E.H. Lucassen-Reynders, Surface elasticity and viscosity in compression/dilation, in E.H. Lucassen-Reynders (Ed.), Anionic Surfactants,

Physical Chemistry of Surfactant Action, Marcel Dekker, New York, 1981, p. 173

6       Y. Rotenberg, L. Boruvka and A.W. Neumann, Journal of Colloid and Interface Science. 93 (1983) 169

7       C.A. McLeod and C.J. Radke, A Growing Drop Technique for measuring dynamic Interfacial Tension. Journal of Colloid and Interface Science. 160 (1993) 435

8       R. Nagarajan, K. Koczo, E. Erdos and D.T. Wasan, AIChE Journal, 41 (1995) 915

9       R. Miller, P. Joos and V.B. Fainerman, The Measurement of Dynamic Surface Tension by the Maximum Bubble Pressure Method. Advances in Colloid and Interface Science, 49 (1994) 249

10      S. Labourdenne, N. Gaundry-Rolland, S. Letellier, M. Lin, A. Cagna, G. Esposito, R. Verger, C. Rivière, The Oil-Drop Tensiometer: Potential Application for Studying the Kinetics of (phopho)Lipase Action. Chemistry and Physics of Lipids. 71 (1994) 163

11      J. Benjamins, A. Cagna, E.H. Lucassen-Reynders, Viscoelastic Properties of Triacylglycerol/Water Interfaces covered by Proteins. Colloids and Surfaces 114 (1996) 245

12      J.J. Kokelaar, A. Prins, M. de Gee, A new Method for measuring the Surface Dilational Modulus of a Liquid. Journal of Colloid and Interface Science. 146 (1991) 507

13      B. S. Murray, P. V. Nelson. A Novel Langmuir Trough for Equilibrium and Dynamic Measurements on Air-Water and Oil-Water Monolayers. Langmuir. 12 (1996) 5973

14      Patent WO 92/16824

15      G. Faour, M. Grimaldi, J. Richou, A. Bois. Real-Time Pendant Drop Tensiometer Using Image Processing with Interfacial Area and Interfacial Tension Control Capabilities. Journal of Colloid and Interface Science. 181 (1996) 385

16      M. Paulson. Thermal Denaturation of Whey Proteins and Adsorption at the Air/Water Interface. Thesis, University of Lund. Lund, Sweden. (1990)

17      A. Cagna. Unpublished results (1999)

18      J.A. de Feijter and J.Benjamins, Adsorption Kinetics of Proteins at the Air-Water Interface. Food emulsions and foams, E. Dickinson (Ed.), Special publication no. 58, Royal Society of Chemistry. (1987) 72

19      M. Mellema, D.C. Clarck, F.A. Husband, A. R. Mackie. Properties of β-Casein at the Air/Water Interface as Supported by Surface Rheological Measurements. Langmuir. 14 (1998) 1753

20    F. A. Veer, M. van den Tempel. Surface Tension Relaxation in a Surface containing Surfactant Particles. Journal of Colloid and Interface Science. 42 (1972) 418

21    E.H. Lucassen-Reynders, J. Lucassen, P.R. Garrett, D. Giles and F. Hollway, Dynamic Surface Measurements as a Tool to Obtain Equation of State Data for soluble Monolayers. Advances in Chemistry Series (E.D. Goddard, Ed.) 144 (1975) 272.

22    J. Benjamins, E. H. Lucassen-Reynders. Surface Dilational Rheology of Proteins Adsorbed at Air/Water and Oil/Water Interfaces, in "Proteins at liquid Interfaces", D. Mobius and R. Miller, Editors, Elsevier Science, Amsterdam, the Netherlands (1998) 341

23    B. S. Murray. Equilibrium and Dynamic Surface Pressure-Area Measurements on Protein films at Air-Water and Oil-Water Interfaces. Colloids and Surfaces A. 125 (1997) 73

24    D. E. Graham, M. C. Phillips, Proteins at Liquid Intefaces, III. Molecular Structures of Adsorbed Films. Journal of Colloid and Interface Science. 70 (1979) 427

25    D. G. Dalgleish. Proteins on the Surfaces of Food Emulsions: Adsorption, Structure and Emulsion Stability. Bioprocess Technology. 23 (1996) 447

# 5 SURFACE SHEAR PROPERTIES OF ADSORBED PROTEIN LAYERS

## 5.1 Introduction.

Interfacial rheology describes the functional relationship between stress, deformation and rate of deformation of a surface in terms of surface-elasticity and surface-viscosity. If we ignore changes in curvature of the surface, two different types of deformation of plane surface elements are possible:

(i) surface shear, i.e., changes in shape of surface elements at constant area.

(ii) surface compression/dilation, i.e. changes in area at constant shape.

Measurements of the stresses produced by these deformations result in two sets of different rheological parameters, i.e. dilational and shear properties.

The surface dilational properties of adsorbed protein layers were dealt with extensively in Chapter 3. This investigation demonstrated that these layers can also show a considerable resistance against shear deformation. This was in line with experimental evidence that proteins and other macromolecules, after being adsorbed, may form a two-dimensional visco-elastic network. Such a network formation influences the shear-rheological properties of the interface (1-7). Some investigators (8-10) assume that these surface shear properties play a dominant role in foam and emulsion formation and stability. This role of the surface shear properties was explained as being similar to that of dilational properties: a high resistance against shear deformation will oppose droplet deformation and consequently break-up. For the same reason a high resistance against shear was assumed to retard droplet coalescence. However, the evidence is not at all conclusive; there are also indications to the contrary, for instance, from experiments in which break-up of drops covered with β-lactoglobulin was not at all hindered by any resistance against shear (11)

Information about intra- and intermolecular interaction of the adsorbed molecules forming a 2D network, and about the structure of this network, can be derived from the dynamic response of the interface to periodic deformations with an externally imposed frequency, which are sufficiently small to leave the network intact (12). The surface-rheological quantities that control this response are the dilational modulus and the shear modulus of the interface. A method for measuring the surface dilational modulus of surfaces that also have appreciable shear moduli has been described in Chapter 3. The present chapter deals with the development of a convenient method for measuring the surface shear modulus as a function of the deformation frequency. Combining these results with the information on dilational properties and surface concentration will lead to a more complete understanding of the inter- and intramolecular interactions occurring in adsorbed protein layers. The surface concentration

and an estimate of the thickness of the adsorbed layer were obtained by ellipsometry (13, Chapter 2).

The development of a new experimental set-up was needed because none of the existing methods fully met the requirements for determining the required shear visco-elastic properties. The shortcomings of the existing procedures, the new technique and results obtained are the subject matter of this chapter.

5.2 Review of available experimental methods.

Reviews on interfacial rheology (1,14-17) illustrate that, compared to surface dilational rheology, surface shear rheology is very popular. However, this popularity did not result in standardisation of the methods, as can be concluded from the wide variety of experimental techniques that have been used.

Main emphasis has been on methods that are only suitable for measuring interfacial shear viscosity. Examples are various double ring and Couette-type surface viscometers in which the surface is continuously deformed at a constant rate of shear (18,19). Such approaches are only suitable to investigate interfacial layers of low molecular weight adsorbates, because only such layers show almost purely viscous behaviour. For protein monolayers these methods are not appropriate, because such layers are visco-elastic: continuous deformation at constant shear rate will at least partly destroy the protein network at the interface. In analogy to the behaviour of bulk viscoelastic materials, this phenomenon is expected to lead to inhomogeneity of the monolayer (20). The effective surface shear viscosity measured by any of these methods then reflects some average over these local values, and contains an elastic contribution.

Indirect methods include measurements with the canal viscometer(1) and the deep-channel viscometer (21). In the canal viscometer the surface viscosity is determined from the surface flow caused by an imposed surface pressure gradient. Due to the way in which this pressure gradient is applied, shear flow is mixed with dilational motion. An additional disadvantage is poor control of slip at the wall. Non-Newtonian behaviour of protein monolayers, already concluded from canal surface viscometer measurements (22), makes the interpretation troublesome. In principle, the deep-channel viscometer allows for the determination of both the real (elastic) and the imaginary (viscous) parts of the surface shear modulus as a function of frequency (21). With this method it was also attempted to correct for the viscous interaction between the flowing monolayer and the bulk substrate (23). However, the technique is difficult to apply to interfaces between two liquid bulk phases and the evaluation of the surface parameters is cumbersome.

Other methods suffer from the problem that the surface deformation is ill-defined (24,25). Additional disadvantages are that the hydrodynamic coupling between the motion at the surface and in the underlying solution is often not considered (1,3,26) and that the mathematics can be handled only by assuming that the surface shows Newtonian behaviour (1,27), which is not likely for adsorbed protein layers.

A method, especially suitable for measuring surface yield stresses, is the low-shear plate viscometer as designed by Van Vliet et al. (28) for bulk rheology and applied to study gelation properties of adsorbed polymers (4,6).

Recently, a number of torsion-pendulum methods have been described (26,29-31). These are, in principle, suitable to determine the visco-elastic modulus as a function of frequency. In these methods interaction between interfacial layer and substrate liquid can be taken into account (32,33). A disadvantage of the damped pendulum is that the measurements can only be performed at certain fixed frequencies, determined by the torsion system and the rheological characteristics of the interface. The evaluation requires a certain rheological model, e.g. the Voigt model (30,26). The parameters needed to fit the damped oscillation curves, have to be introduced into the viscoelastic model to yield the (complex) modulus and viscosity. As the Abraham method (26) also allows for the possibility of measuring stress-strain curves using the cup-rotation procedure, a quasi-static shear modulus can be determined from the initial part of this curve. A second mode in the Lee method (31) also allows oscillation of the vessel, the vessel wall acting as the outer ring.

An alternative technique that has been developed and tested, was based on determining the properties of surface shear waves (34,12). While allowing for full evaluation of the surface shear modulus, this method requires large amounts of solution and can be used only over a restricted range of shear moduli. However, as insight into the properties of the surface shear waves is essential for a full analysis of the double-ring surface rheometer, to be described below, the theoretical and experimental features of the surface shear wave will be given first.

The technique presented here is a modification of the double ring surface viscometer (35). A similar geometry has been applied by Sheriff and Warburton (36) and Burgess and Sahin (37). However, the instruments of these authors do not allow frequency control, which, of course, is a serious disadvantage.

## 5.3 Surface shear waves.

A liquid surface or an interface between two liquids can carry two different types of waves: compression/expansion waves, which can be transverse or longitudinal, and shear waves.

131

Transverse waves, where the surface has a velocity component normal to the direction of the propagation and to the plane of the undisturbed surface, can be divided into capillary waves or ripples (small wavelength, surface tension-dependent) and gravity waves (long wavelength) (38,39,40). Longitudinal waves are characterized by the fact that the motion of the surface is in the direction of the propagation of the wave. The properties of this type of wave depend mainly on the ability of the surface to support surface tension gradients (41,42) (see also Chapter 3).

The theoretical description of a third type of wave, the surface shear wave, has been presented in ref. 34 and verified experimentally in ref. 12. Surface shear waves are characterized by the fact that, as with the capillary waves, the surface motion is normal to the propagation direction but, in contrast to the capillary waves, this motion is in the plane of the surface as illustrated in Fig. 1a for a shear wave produced by a rod oscillating in the interface in the direction of its axis.

For a surface at rest (Fig. 1b), the stress in the surface is completely determined by the isotropic surface tension $\sigma_0$. When a surface element is subjected to shear, the surface stress may become anisotropic with the shear stress components $\sigma_{xy}$ and $\sigma_{yx}$ being non-zero. In general, monolayers have viscoelastic properties, implying that $\sigma_{xy}$ and $\sigma_{yx}$ depend on both the magnitude and the rate of the shear deformation. For small periodic deformations, in the linear region where the shear stress is proportional to the strain according to:

$$\sigma_{xy}(t) = \sigma_{yx}(t) = \mu_s s(t) = \mu_s \left( \frac{\delta \xi^s}{\delta y} \right) \tag{1}$$

where $s(t) = \tan a(t)$ is the strain and $\xi^s$ is the displacement in the x direction of a material point from its equilibrium position (Fig. 1b). $\mu_s$ is the complex surface shear modulus, which can be written as:

$$\mu_s = \mu_s' + i\mu_s'' = |\mu_s|(\cos\Phi + i\sin\Phi) = |\mu_s|\exp(i\Phi) \tag{2}$$

where $\mu_s'$ is the storage modulus which defines the component of the stress that is in phase with the strain, and $\mu_s''$ is the loss modulus which defines the stress component that is in phase with the rate of strain and $\Phi$ is the phase angle between stress and strain:

$$|\mu_s| = \left[ \left(\mu_s'\right)^2 + \left(\mu_s''\right)^2 \right]^{1/2} \quad \text{and} \quad \tan\Phi = \mu_s''/\mu_s' \tag{3}$$

This surface shear modulus is the two-dimensional analogue of the shear modulus of a visco-elastic bulk material (43, 44).

When a liquid surface is subjected to a periodic shear motion, the bulk liquid exerts a viscous drag on the surface. When the liquid and the surface have a velocity component in the x direction only, and when surface tension gradients are absent ($\delta\sigma_{xx}/\delta x=0$), the stress boundary condition for the surface reads:

$$\left(\frac{\delta\sigma_{yx}}{\delta y}\right)dxdy=\eta\left(\frac{\delta v_x^1}{\delta z}\right)_{z=0}dxdy \tag{4}$$

where $\eta$ is the viscosity and $v_x^1$ is the velocity component of the liquid; the viscous drag exerted on the surface by the vapour phase can in general be neglected. Using Eq. (1)], the stress boundary condition at the surface takes the form:

$$\mu_s\left(\frac{\delta s}{\delta y}\right)=\mu_s\left(\frac{\delta^2\xi^s}{\delta y^2}\right)=\eta\left(\frac{\delta v_x^1}{\delta z}\right)_{z=0} \tag{5}$$

Eq. [5] shows that the shear deformation cannot be homogeneous when the contacting liquid phase exerts a viscous drag on the surface. The strain then has a gradient in the y direction (Fig 1a). As a consequence, the displacement $\xi^s$ of a material point in the x direction is no longer a linear function of y.

The resistance of the surface against deformation (Eq.1) acts as restoring force. The resulting motion of the surface creates a motion of the liquid underneath (Eq.5). This coupling between shear stress-induced surface motion and viscosity-controlled liquid motion results in a damped wave in the surface and a damped wave in the liquid (34). Hence, a rod oscillating in the interface generates a momentum transport into the liquid, leading to a three dimensional transverse wave as visualized in fig.1a.

According to the surface shear wave theory (34), $|\mu_s|$ and $\Phi$ (Eq.3) can be calculated from the wave parameters $\beta_s$, the damping coefficient, and $\kappa_s=2\pi/\lambda_s$, the wave number, of the surface shear waves, where $\lambda_s$ is the wavelength (see $\lambda_y$ in fig.1a). For sufficiently high $|\mu_s|$, the theory reduces to the following simple forms:

$$|\mu_s|=(\omega^3\eta\rho)^{1/2}/(\kappa_s^2+\beta_s^2) \tag{6}$$

and

$$\tan\left(\frac{\pi}{8}+\frac{\Phi}{2}\right)=\beta_s/\kappa_s \tag{7}$$

where $\omega$ is the frequency of the oscillation and $\rho$ is the density of the liquid phase.

133
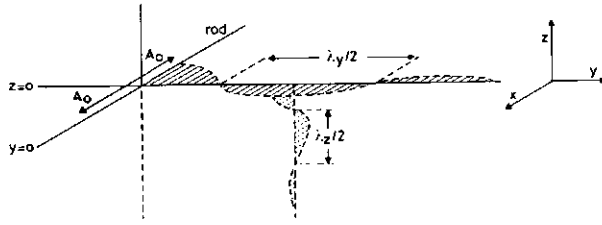
Fig. 1a. Plane transverse wave generated in the surface and the liquid by an oscillating rod at y=0. $A_0$ = amplitude of the displacement of the rod; $\lambda_y$= wavelength of the surface shear wave; $\lambda_z$ =wavelength of the ensuing bulk shear wave. (perspective view)
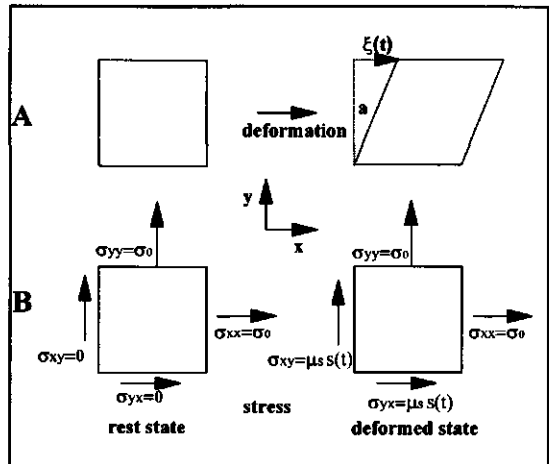


Fig. 1b. Simple shear deformation of a surface element (A) and stress components exerted on the sides of a square surface element (B). (top view)
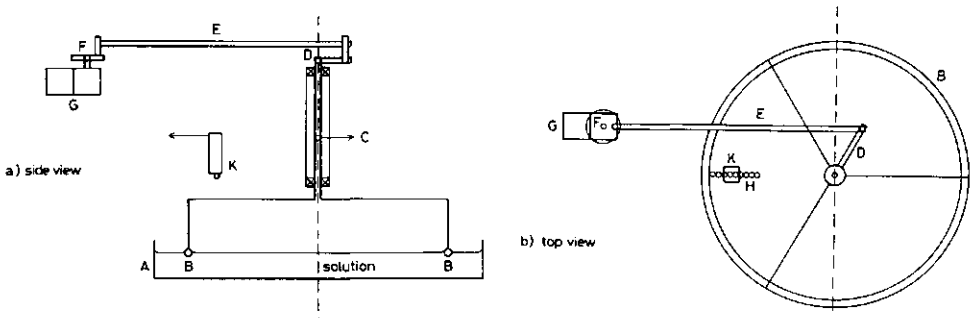


Fig. 2 Schematic picture of the surface shear wave rheometer with oscillating ring.
A=basin, B=oscillating ring, C=rotatable axis, D=horizontal arm, E=metal bar, F=wheel.
G=electromotor with gear box, H=tracer particles, K=video camera

There is a close formal analogy with the longitudinal wave theory (41,42), which will also be illustrated in section 5.5.2 and has been met before in Chapter 3, section 3.3.1 equations (7) and (8).

For experimental verification a circular geometry was chosen, because the use of an oscillating rod in a liquid surface with finite dimensions will give rise to periodic compressions and expansions at the sides of the surface. It is expected that the concomitant surface tension gradients will affect the propagation properties of the shear wave and this problem should be maximally avoided.

The surface shear wave theory was tested using the surface shear wave rheometer (Fig. 2) in which circular surface shear waves are generated by a large ring (R=49.5 cm), which oscillates sinusoidally around its centre in the plane of the liquid surface (12). The motion of the liquid surface is made visible by means of small paper particles (H) having diameters of 1 mm. They are placed on the surface along a radius at intervals of about 2 cm. The motion of these paper particles (amplitude of the angular motion, A(r), and phase lag, $\delta$, between ring and paper particle) is registered by video recording and analyzed.

For circular geometry theory predicts (34) that in the range of $(\omega\eta^3/\rho)^{1/2} << |\mu_s| << (\omega^3\eta\rho r^4)^{1/2}$ the amplitude of the surface motion of the outer part of the liquid surface within the ring is described by:

$$\ln\frac{A(r)r^{1/2}}{A_o R^{1/2}} = -\beta_s(R-r) \qquad (8)$$

Here $A_o$ is the amplitude of the ring oscillation. The phase lag $\delta$ is a linear function of the distance R-r from the ring (r is the distance from the centre of the surface):

$$\delta(r) = -\kappa_s(R-r) \qquad (9)$$

So plots of $\delta$ vs. (R-r) and ln [A(r). $\sqrt{r}$] vs. (R-r) should provide straight lines with slopes $\kappa_s$ and $\beta_s$, respectively.

The propagation properties of the shear waves were investigated on surfaces of aqueous protein solutions, because adsorbed protein layers are known to display viscoelastic shear (see Chapter 3). The proteins used in this investigation were Na-caseinate, bovine serum albumin (BSA) and ovalbumin (all at 0.01 wt% aqueous solutions). The angular frequencies ranged from 0.17- 0.84 s$^{-1}$. For Na-caseinate and BSA solutions, the surface motion shows the features of a transverse wave, thus demonstrating the existence of surface shear waves. The variation of the phase lag $\delta(r)$ and the amplitude A(r) with distance from the ring is described fairly well by equations 8 and 9. Consequently, the surface motion of adsorbed protein layers

135

in our apparatus was satisfactorily described by the surface shear wave theory (12).

The surface shear parameters, as derived from the wave parameters $\kappa_s$ and $\beta_s$, are presented in Table 1.

Table 1

Surface shear properties of some proteins measured with the surface shear wave method. Protein concentration is 0.1 g/l

|  | $\omega$ (rad sec$^{-1}$) | $\|\mu_s\|$ (mNm$^{-1}$) | $\Phi$ (degrees) | $\mu_s{}'$ (mNm$^{-1}$) | $\mu_s{}''$ (mNm$^{-1}$) |
|---|---|---|---|---|---|
| Sodium caseinate surface age 4hr, $A_0$=6.2 cm | 0.17 | 2.1±0.5 | 56±6 | 1.2±0.3 | 1.7±0.4 |
| | 0.42 | 3.1±0.6 | 39±5 | 2.4±0.5 | 2.0±0.5 |
| | 0.84 | 3.4±0.6 | 26±5 | 3.1±0.6 | 1.5±0.5 |
| BSA surface age 1hr $A_0$=7.0 cm | 0.17 | 3.3±0.8 | 77±5 | 0.7±0.3 | 3.2±0.8 |
| | 0.42 | 4.0±1.0 | 57±6 | 2.2±0.6 | 3.4±0.8 |
| | 0.84 | 4.5±1.0 | 48±6 | 3.0±0.8 | 3.3±0.8 |
| Ovalbumin surface age 1hr $A_0$=7.0 cm | 0.17 | >6 | | | |
| | 0.84 | >90 | | | |

For the experimental set-up that was used and for aqueous solutions with $\eta = 10^{-3}$ Pa.s and $\rho = 10^3$ kg/m$^3$, the limits of the shear wave method are: $10^{-3} << |\mu_s| << 90$ mN/m for $\omega$=1 rad/s and $10^{-4} << |\mu_s| << 3$ mN/m for $\omega$=0.1 rad/s. For $\omega$=0.17 rad/s the upper limit is 6 mN/m. The surface of the ovalbumin solution behaves as a rigid disk (no damping or phase differences) , which indicates, according to the limits of the wave method that $|\mu_s| > 6$-90 mN/m (depending on frequency).

The results given in Fig.5 of Ref. 12 indicate that, at small shear deformations, adsorbed layers of sodium caseinate and bovine serum albumin show linear viscoelastic behaviour. The surface shear resistance increases in the sequence sodium caseinate<BSA<ovalbumin. It is concluded that, within the window given, the present surface shear wave technique can be used to study the shear properties of viscoelastic liquid interfaces. In practice the method has two disadvantages (i) it requires large amounts of solution because the diameter of the basin must be sufficiently large to show a damped shear wave and (ii) the method can only be used over a restricted range of shear moduli and/or frequencies.

5.4 Experimental.

The major part of the experiments to be described in this chapter were performed using the "concentric ring surface shear rheometer". This is a newly built instrument that allows measurements of the viscous and elastic part of the surface shear modulus as a function of frequency and deformation. Preliminary experiments were performed with the "stress-strain" surface shear rheometer. The results obtained with this latter set-up were used as a first check of the reliability of the "concentric ring surface shear rheometer".

5.4.1 "Stress-strain" surface shear rheometer

The principle of the "stress-strain" surface shear rheometer (Couette type) is shown in Fig. 3a. The outer ring is the cylindrical wall of the glass vessel ($r_o = 7.3$cm) containing the solution. The inner cylinder is a hollow glass ring with inner radius 6.2cm (radius of the hollow glass tube is 0.75mm) and suspended from a torsion wire. To the torsion wire a mirror is rigidly fixed. The inner ring is positioned just in contact with the surface of the solution. After aging the solution for a certain time in the viscometer, the stationary shear modulus is measured by rotating the glass vessel at a constant low angular speed ($1 \times 10^{-3} s^{-1}$). Due to the rotation the adsorbed surface layer is deformed and exerts a stress on the inner ring. This stress is determined from its rotation which can be quantified from the displacement of a small light spot that is reflected by the mirror. This displacement is, in turn, monitored by a recorder. At small deformations ($s_m(R_i)=0.01$-$0.02$) the stress increases linearly with the deformation. In this linear region the modulus has been determined from the slope of the stress versus deformation line.

5.4.2 Concentric ring surface shear rheometer.

The surface shear rheometer (Fig.3b) consists of two concentric glass rings which lie flat in the interface. The opposing faces of the rings were roughened to suppress slip. The outer ring oscillates periodically around its axis with a small amplitude ($\approx 0.05$ rad). The inner ring, which is stationary, is connected to a torque-measuring device consisting of an air bearing and a capacitive rotation transducer. A small rotation ($\approx 10^{-4}$ rad) of this transducer is coupled back automatically by a torque motor. The voltage on the torque motor, required to prevent motion of the inner ring, measures the torque exerted on this ring. The relation between this voltage and the torque was calibrated by replacing the rings by two concentric cylinders and measuring the torque transferred by liquids of known bulk viscosity. The relation was linear with a proportionality constant of $3.75*10^{-5}$ Nm/V. The motion of the outer ring was

137

converted into an electric signal by placing a wedge-shaped blade, attached to the outer ring, in the light path between a lamp and a photomultiplier. The amplitude of the outer ring and, hence, the deformation of the surface, can be varied by adjusting the eccentricity of the driver system. On the axis of the outer ring a small mirror was mounted. From this mirror a light beam was reflected to the wall of the room. From the amplitude of the displacement of the light spot on the wall and the distance between the axis and the wall the amplitude of the outer ring was calculated. The angular frequency ($\omega$) of this ring can be varied between 0.008 and 0.4 rad/s by means of a synchronous electric motor with a gear box. The electrical signals of the outer ring motion and of the torque on the inner ring were recorded on an X-Y recorder. The phase angle $\Phi$ is calculated from the eccentricity of the resulting ellipse according to a procedure described by Lucassen et al. (45)

The protein solutions were poured into the measuring vessel using a separating funnel. During the filling of the vessel the tip of the funnel was kept just touching the surface in order to ensure that the surface was fresh at the start of each experiment. The vessel was filled until the two concentric rings were completely in contact with the surface.

The modulus $\mu_s$ and the viscous phase angle $\Phi$, were determined for a number of proteins at various concentrations and ages of the surface. The reproducibility was tested by determining $\mu_s$ and $\Phi$ for different solutions of a given protein at chosen concentrations and the same surface ages. We also varied the gap width L between the rings, the amplitude of the shear deformation at the inner ring $s_m(R_i)$ and the oscillation frequency $\omega$.

The rheometer was placed in a box of plastic foil to prevent surface contamination by dust and to minimize water evaporation. As the instrument was very bulky, the latter objective was only partly met.

5.4.3 Materials.

The proteins used in this investigation are sodium-caseinate ex DMV, bovine serum albumin (BSA fraction IV) ex Sigma and ovalbumin (grade V) ex Sigma and ovalbumin ex Brocades. The polymers PMApe; a copolymer of methacrylic acid and its methylester (molar ratio 2:1), Rohagit S ex Röhm AG and PVA 205 ($M_{visc.}$ =42000) ex Kurashiki were used for comparison. Doubly distilled water was used from a thoroughly leached glass distillation apparatus. All solutions were stored in cleaned glass vessels. Unless indicated otherwise, the measurements were performed in a phosphate buffer (pH 6.7) containing 0.99 g/l $Na_2HPO_4.2\ H_2O$ and 1.76 g/l $KH_2PO_4$. The temperature was 23±1 °C.
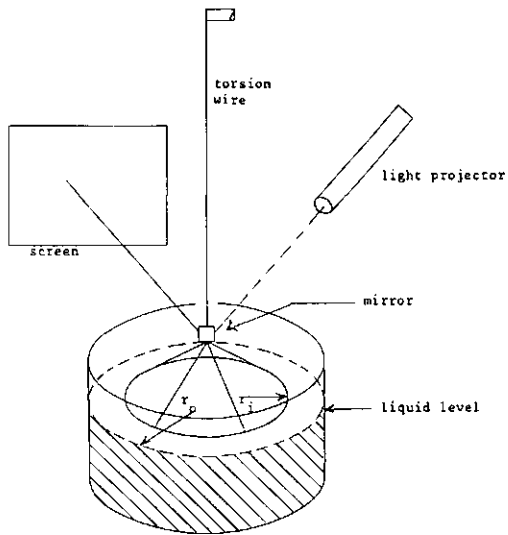
Fig. 3a "Stress-strain" surface shear rheometer.
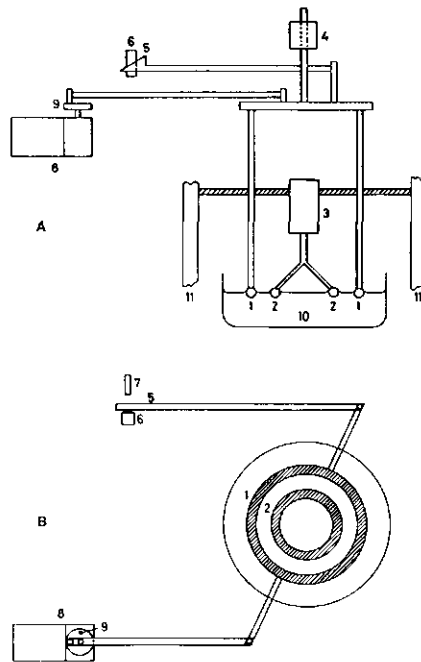


Fig. 3b Schematic representation of the concentric ring surface rheometer.
1= outer ring, 2=inner ring, 3=torque measuring device, 4=mirror, 5=wedge, 6=
photomultiplier, 7=lamp, 8=electromotor with gear box, 9= eccentric driver system, 10=
solution, 11=support

## 5.5 Evaluation of the measurements with the concentric ring surface shear rheometer.

### 5.5.1 Stress on the inner ring as a result of the oscillatory motion of the outer ring.

The outer ring (inner radius $R_o$) in the surface shear rheometer oscillates sinusoidally around its axis, which is mounted normal to the plane of the surface. If its amplitude is $A_o$ and the angular frequency is $\omega$, its motion is described by:

$$X(R_o,t) = A_o \exp(i\omega t) \qquad (10)$$

where $X(R_o,t)$ is the displacement, in the direction indicated by the arrow alongside the outer ring (see Fig.4), of a point on inner side of the ring from its zero position.

The periodical motion of the outer ring generates a periodic shear deformation $s(r,t)$ in the surface between the rings, which is given by:

$$s(r,t) = r.\frac{d[X(r,t)/r]}{dr} = s_m(r)\exp\{i[\omega t + \delta(r)]\} \qquad (11)$$

where $s_m(r)$ is the amplitude of $s(r,t)$ (i.e. its maximum value during a cycle), $\delta(r)$ is the phase lag between the periodic surface shear deformation at r and the displacement of the outer ring and $X(r,t)$ is the displacement of a material point in the surface from its zero position in the direction of the arrow (see Fig. 4).

The shear stress exerted on the stationary inner ring (outer radius $R_i$) is measured as a periodic torque $T(R_i,t)$ which equals:

$$T(R_i,t) = T_m(R_i)\exp[i(\omega t + \alpha)] \qquad (12)$$

where $T_m(R_i)$ is the maximum value, i.e. the amplitude, of $T(R_i,t)$ during a cycle and $\alpha$ is the phase difference between the torque and the displacement of the outer ring. In our apparatus, both $T_m(R_i)$ and $\alpha$ are measured. Because in this set-up the bulk solution and the inner ring are both stationary, the viscous drag exerted by the solution on the inner ring is negligible, even for surface shear moduli as small as 0.1 mN/m (see section 5.5.2). Hence, the torque exerted on the inner ring is entirely caused by the shear stress in the surface originating from the oscillation of the outer ring. This greatly facilitates the interpretation of the experimental parameters $T_m(R_i)$ and $\alpha$ in terms of the shear properties of the surface and also improves the sensitivity of our technique as compared to instruments in which the inner ring is not stationary (30,31,33).
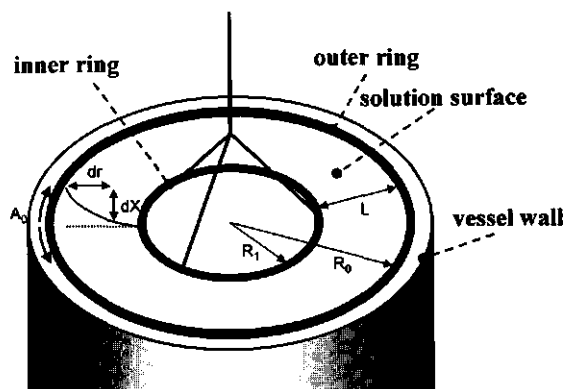
Fig. 4 Shear deformation in the concentric ring surface rheometer.
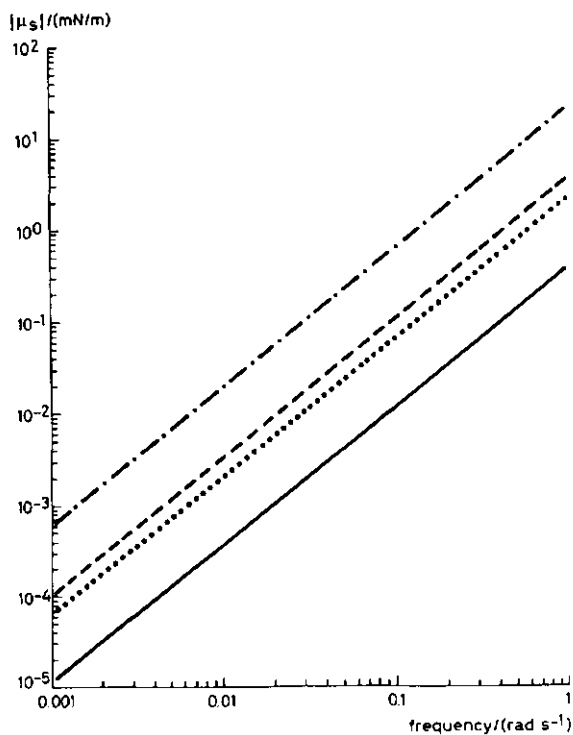


Fig. 5 Minimum value of $|\mu_s|$ at which the deformation between the rings is homogeneous ( · ) L=0.01 m, $\Phi = 0°$, (---) L=0.03 m, $\Phi = 0°$; (......) L =0.01 m, $\Phi = 90°$; (_ . _ ) L =0.03 m, $\Phi = 90°$.

For small periodic deformations, $T(R_i,t)$ is related to the surface shear deformation at the inner ring, $s(R_i,t)$, and the surface shear modulus, $\mu_s$, by

$$T(R_i,t) = 2\pi R_i^2 \mu_s s(R_i,t) \tag{13}$$

For viscoelastic surfaces, the surface shear modulus is a complex quantity as expressed in Eq. 2. For a purely elastic surface, $\mu''_s = 0$, $\Phi = 0$ and $\mu_s = |\mu_s| = \mu'_s$, while for a purely viscous surface $\mu'_s = 0$, $\Phi = \pi/2$ and $\mu_s = i|\mu_s| = i\mu''_s$. Substitution of Eqns. (11), (12) and (2) into Eq. (13) gives:

$$T(R_{i,t}) = 2\pi R_i^2 |\mu_s| s_m(R_i) \exp(i[\omega t + \Phi + \delta(R_i)]) = T_m(R_i)\exp[i(\omega t + \alpha)] \tag{14}$$

from which

$$T_m(R_i) = 2\pi R_i^2 |\mu_s| s_m(R_i) \tag{15}$$

$$\alpha = \Phi + \delta(R_i) \tag{16}$$

Eqns (15) and (16) allow calculation of $|\mu_s|$ and $\Phi$ from the experimental parameters $T_m(R_i)$ and $\alpha$ provided the amplitude $s_m(R_i)$ and the phase lag $\delta(R_i)$ of the surface shear deformation at the inner ring are known.

5.5.2 The wave character of oscillatory shear deformations and the consequences for the deformation and stress at the inner ring.

Due to hydrodynamical coupling between surface and solution in contact with it (see section 5.3 and ref.34), the oscillatory motion of the outer ring generates a damped transverse shear wave in the surface as illustrated in Fig 1a. The amplitude $s_m(r)$ and the phase lag $\delta(r)$ will therefore in general depend on the distance from the oscillating ring.

Moreover, a wave generated by the outer ring induces multiple reflection between the two rings, thus affecting both $s_m(r)$ and $\delta(r)$, as in the case with longitudinal waves. For the latter, the effect in a trough of finite dimensions has been analyzed (46). It was found that neglecting the deviations from uniformity of deformation leads to an error of less than 1% in both the dilational modulus and in the viscous phase angle, provided the length of the trough (L) is much smaller than the propagation length of the wave, given by the inverse of damping coefficient $\beta$. For such small trough lengths, the wave propagation number W

142

defined as $1/\beta L$ is large enough for the deformation to be practically uniform across the gap. Because of the close formal analogy between surface shear waves and longitudinal waves (34), these results can be directly applied to surface shear waves. For surface shear waves, the damping coefficient $\beta_s$ is given by:

$$\beta_s = \omega^{3/4}(\eta\rho/|\mu_s|^2)^{1/4}\sin(\pi/8 + \Phi/2) \tag{17}$$

where $\eta$ the bulk viscosity and $\rho$ the density of the solution.

From the results of Lucassen and Barnes (46) it then follows that in our double ring surface rheometer the deviation from uniformity can be ignored when $L.\beta_s < 0.2$, where $L = R_o - R_i$ is the gap width between the two rings. On combining this inequality with Eq.(17), it follows that this approximation is justified provided

$$|\mu_s| > 25L^2\omega^{3/2}(\eta\rho)^{1/2}\sin^2(\pi/8 + \Phi/2) \tag{18}$$

The required minimum value of $\mu_s$ therefore increases with gap width L and angular frequency $\omega$. Fig.5 shows $\mu_s$ vs. $\omega$ plots for aqueous solutions, calculated from Eq.(18) for various values of $\Phi$ and for the values L = 0.01 m and 0.03 m, used in our experiments. For $\omega = 0.084$ s$^{-1}$, the inequality shown in Eqn (18) is satisfied even for $\Phi = 90°$ when $|\mu_s| > 0.5$ mN/m. For the proteins discussed below, $\mu_s$ is usually larger than 1 mN/m: for solutions showing a lower value, the value of $\Phi$ was also small. Hence Fig. 5 indicates that the deviations from uniformity of the deformation can be neglected when $\omega < 0.1$ s$^{-1}$ and L< 0.03 m. For $\mu_s < 0.5$ mN/m either the damped shear wave method can be used, or the measurements must be performed at lower frequencies or at a smaller L.

5.5.3 Calculation of the shear modulus from experimental parameters.

If the conditions for Eq. 18 are satisfied, the surface shear stress and deformation can be calculated from the parameters $A_o$ (see Eq. (10)), $T_m(R_i)$ (see Eq. (12)), $R_o$ and $R_i$. Mechanical equilibrium requires that, when the viscous drag exerted on the surface by the solution can be ignored, the net torque exerted on a ring of the surface between r and r+dr must be zero ($R_i \le r \le R_o$); hence, $dT(r,t)/dr=0$. Eq. (13) then indicates that:

$$T(r,t) = 2\pi r^2 \mu_s s(r) = 2\pi r^2 \mu_s rd(X/r)/dr = T(t) \tag{19}$$

where T(t) is independent of r. Integration of Eq. (19) leads to

$$X/r = -T(t)/(4\pi\mu_s r^2) + C(t) \qquad (20)$$

where $C(t)$ is independent of r. Insertion into Eq. (20) of the boundary conditions:

$r = R_o$ : $X = A_o \exp(i\omega t)$

$r = R_i$ : $X = 0$ (inner ring is stationary)

gives the torque exerted on the inner ring:

$$T(R_i, t) = T(t) = 4\pi\mu_s \frac{A_o R_o^2 R_i^2}{R_o(R_o^2 - R_i^2)} \exp(i\omega t) \qquad (21)$$

Combination of Eqns (11), (13) and (21) gives the surface shear deformation at the inner ring:

$$s(R_i, t) = s_m(R_i)\exp\{i[\omega t + \delta(R_i)]\} = \frac{2A_o R_o}{(R_o^2 - R_i^2)} \exp(i\omega t) \qquad (22)$$

Hence, the amplitude of the surface shear deformation at the inner ring equals:

$$s_m(R_i) = 2A_o R_o/(R_o^2 - R_i^2) \qquad (23)$$

Eq. (22) indicates that the phase lag between the surface shear deformation at the inner ring and the motion of the outer ring, $\delta(R_i)$, is zero. Eq. (16) then shows that:

$$\alpha = \Phi \qquad (24)$$

Eqs. (23) and (24) are valid if deviations from uniformity are negligible, in which case the effect of the hydrodynamic coupling between the surface and the bulk solution is also negligible. Combination of Eqns. (2), (14) and (21) leads to:

$$|\mu_s| = T_m(R_i) \cdot \frac{(R_o^2 - R_i^2)}{4\pi A_o R_o R_i^2} \qquad (25)$$

144

Eqs. (24) and (25) show that when Eq. (18) applies, the surface shear storage modulus $\mu'_s$ and the surface shear viscous modulus $\mu''_s$ can be determined by measuring the maximum torque on the inner ring, $T_m(R_i)$, the amplitude imposed on the outer ring, $A_o$, the radii of the rings, the phase lag $\alpha$ between the torque on the inner ring and the oscillation of the outer ring. The values obtained for $\mu_s$ and $\Phi$ can be written in terms of the elastic and viscous surface shear moduli $\mu'_s$ and $\mu''_s$ by means of the equations:

$$\mu'_s = |\mu_s|\cos\Phi \qquad (26)$$

$$\mu''_s = |\mu_s|\sin\Phi \qquad (27)$$

## 5.6 Results and discussion.

### 5.6.1 Reproducibility of the measuerements.

In Table 2 the reproducibility of the shear modulus measurements is illustrated. In this table the results with *two different solutions* of BSA and ovalbumin are compared at increasing age of the surface. The solutions were prepared less than one hour before use. The protein bulk concentrations range from $1*10^{-3}$g/l to $1*10^{-1}$g/l for BSA and is $3*10^{-1}$g/l for ovalbumin. With our apparatus $\mu_s$ values as small as 0.2 mN/m can be detected. The reproducibility of $\mu_s$ and $\Phi$, as obtained from different deformation cycles at *the same surface*, was respectively 10% and 5° for $\mu_s$ = 1 mN/m and 5% and 5° for $\mu_s$ = 10 mN/m.

The data shown in Table 2 for two different solutions of BSA and of ovalbumin, each at the same concentration and surface age, indicate that the values of $\mu_s$ may differ by 10 to 50%. The differences in $\Phi$ may even be larger. These differences are far beyond the accuracy of the apparatus (see above) and are apparently due to irreproducibility of the surface formation at the start and aging. Lack of reproducibility of the surface shear modulus, for different solutions of a given protein, has been found earlier (47), and might be caused by e.g. a too slow establishment of stationary humidity above the surface after filling the trough. When the surface was sucked off after filling the vessel with a BSA solution (which involves air circulation close to the surface), the values of both $\mu_s$ and $\Phi$ were significantly affected.

Table 2

Reproducibility of shear modulus measurements; $\omega = 0.084 s^{-1}$, $R_o - R_i = 1.2$ cm, $s_m(R_i) = 0.07$

| system | age of surface (hours) | Solution I | | Solution II | |
|---|---|---|---|---|---|
| | | $|\mu_s|$ (mN/m) | $\Phi$ (deg.) | $|\mu_s|$ (mN/m) | $\Phi$ (deg.) |
| 0.001 g/l BSA | 4 | 2.7 | 36 | 4.4 | 21 |
| | 21 | 4.7 | 21 | 6.3 | 24 |
| 0.005 g/l BSA | 1 | 1.6 | 66 | 2.8 | 46 |
| | 4 | 5.9 | 30 | 7.8 | 25 |
| | 21 | 5.9 | 32 | 7.0 | 28 |
| 0.03 g/l BSA | 1 | 7.4 | 22 | 6 | 25 |
| | 3 | 9.3 | 18 | 7 | 25 |
| | 21 | 9.6 | 16 | 8.5 | 20 |
| 0.1 g/l BSA | 1 | 3.1 | 48 | 8.1 | 28 |
| | 4 | 4.9 | 57 | 9.9 | 23 |
| | 21 | 6.3 | 35 | 9.5 | 16 |
| 0.3 g/l Ovalbumin | 3 | 13.2 | 19 | 13.6 | 20 |
| | 21 | 32 | 18 | 29.5 | 18 |

Likewise, a comparison of the data for BSA solutions given in Table 2 suggests that even after sufficient time for equilibration (21h) the value of $\mu_s$, when measured at separately prepared surfaces, may show differences of up to 5mN/m. Other factors probably affecting the reproducibility are (i) very small amounts of adventitious surface active admixtures, (ii) inhomogeneous layer/structure formation by unintentional disturbances in the surface layer during the preparation stage or (iii) irreproducible adherence of surface layer to the glass rings. Considering the very radical cleaning procedure and the precautions taken to prevent dust particles falling on the surface, the risk of such surface active pollution playing an important role looks rather small at first sight. However, profound structure-decreasing effects of very small amounts of low molecular weight surfactants have been described (48-50). A major structure-disturbing action is creating the interface and establishing contact between the interface and the rings. Consequently, irreproducible disruption of the structure is likely to occur already at the start of an experiment. This is in line with the finding that differences between duplicates are already clearly noticeable from the very first measurement. For the lower protein concentrations (0.001 and 0.0005 g/l) the surface concentration at this stage of an experiment is estimated to be between 0.2 and 0.5 mg/m². At these very low surface concentrations no surface structure is detectible yet (see 5.6.4). At higher bulk concentrations the surface concentration during the start-up of a measurement is sufficient for a measurable structure. As there is little difference in reproducibility between low and high concentrations,

146

one can argue that disturbances during the start of the experiment are not a major factor causing the poor reproducibility. One also could argue that even at a low surface concentration, where the structure is very weak, a structure-disturbing action causes partial breakdown which is not fully reversible within the timescale of an experiment (24 hours). It will be shown in section 5.6.3 that especially at larger deformations, structure breakdown can occur which recovers rather slowly .

Adherence of the surface layer to the glass rings was promoted by roughening the parts of the rings that are in contact with the surface layer. In this respect no irregularities were observed visually. From the above, it is evident that the reproducibility of the measurements must be improved in order to obtain accurate values for the surface rheological parameters, e.g. by using instruments of a more compact design that allow a closer control of the air humidity after filling. In such a design accidental disturbances by air flow and vibrations can be better eliminated. The problem of inhomogeneous deformation or slip at the rings can be prevented by using toothed rings in analogy with ribbed cylinders that are in use in Couette-type bulk rheometers.

In steady state shear viscosity measurements at the oil/water interface similar irreproducibility was not observed (51), perhaps because surface shear viscosity measurements involve major structure breakdown, making it impossible to observe irreproducibility in the building of the structure. In the case of an oil/water interface humidity problems, mentioned above as a probable cause for poor reproducibility at the air/water interface, will not play a role.


5.6.2 Comparison with literature data.


As already mentioned in the introduction of this chapter, numerous experimental techniques are in use in surface shear rheology. Each instrument has its own geometry, way and extent of deformation and method of preparation of the monolayer. Moreover, different assumptions and models are used to analyse the experimental data. To obtain some feeling for the state of affairs, in Tables 3A and 3B a comparison has been made between our results and those obtained from literature. Considering substantial differences in experimental conditions and preparation of the monolayer, the agreement with respect to the modulus (Table 3A) is satisfactory, even semi-quantitatively. This is in the first place the case for the ranking order of the maximum values of the surface shear modulus (Na-caseinate< BSA< Ovalbumin). The only result that disagrees completely with our results and those of others, is the very low modulus of HSA, 0.01mN/m, reported by Krägel et al. (30). In that work a very sophisticated automated oscillating disc rheometer was used. The reason for this exception is not clear. Burgess (37) reported considerably higher values for the shear modulus of BSA. However, these high values were only found for high protein concentrations. There are indications that

with high protein bulk concentrations the thickness of the adsorbed layer increases considerably probably by the formation of multilayers (Chapter 2). The trend of increasing shear modulus at higher concentrations was also found in the present work (see Table 3 BSA and ovalbumin).

Table 3A
Comparison with literature data
The shear modulus data in this table are determined after adsorption equilibrium has been established

| protein | shear modulus (mN/m) | method (ref) | angular freq.(s$^{-1}$) |
|---|---|---|---|
| β-casein | <0.1 | creep (2) | |
| | low visc. | creep (52) | |
| | <1 | osc.ring (53) | |
| Na-caseinate | 2.1 (0.1 g/l) | shear wave (table 1) | 0.17 |
| | 0.5 (0.3 g/l) | this work (stress-strain) | 0.001 (def. rate) |
| | 0.2 (0.3 g/l) | this work (osc.) | 0.084 |
| κ-casein | high visc. | creep (52) | |
| | 6 (0.3 g/l) | this work (osc.) | 0.42 |
| β-lactoglobulin | 5-10 (spread layer) | creep (52) | |
| BSA | 8 (spread layer) | creep (54) | |
| | 5 (0.05 g/l) | creep (2) | |
| | 12 (1 g/l), 237 (10 g/l) | osc.ring (37) | |
| | 30 (1 g/l) | osc.disk (29) | 66 |
| | 3.3 (0.1g/l) | shear wave (table 1) | 0.17 |
| | 12 (0.3 g/l) | this work (stress-strain) | 0.001 (def. rate) |
| | 14.5 (0.1 g/l) | this work (osc.) | 0.42 |
| | 17 (0.3 g/l) | ,, | 0.42 |
| HSA | 3 (0.005 g/l), 12 (1 g/l) | osc. disc (55) | |
| | 0.01 (0.1 g/l) | osc. disc (30) | |
| Lysozyme | 5 (spread layer) | osc. disc (55) | |
| Ovalbumin | 27-60 (1 g/l) | osc.disc (29) | 66 |
| | 20 (0.3 g/l) | this work (stress-strain) | 0.001 (def. rate) |
| | 19 (0.1 g/l) | this work (osc.) | 0.42 |
| | 40 (0.3 g/l) | ,, | |
| PMMA | 10 (Π=20-25mN/m) | stress-strain (56) | def. rate? |
| | 21 (α=0.1; Π=9mN/m)* | this work (osc.) | 0.42 |

* α=degree of neutralization

148

The shear moduli determined according to the shear wave method (Table 1) clearly deviate from the values obtained by the other methods in this work. This is most probably caused by the fact that for the shear wave experiments less pure protein samples were used, because this method requires large amount of solution. The pH was somewhat lower, 5.5 instead of 6.7, because these solutions were not buffered.

The agreement for the shear viscosity data (Table 3B) is poorer, probably due to large differences in deformation rate, which were difficult to infer from the publications.

Table 3B Comparison with literature data, continued.
The shear viscosity data in this table are determined after adsorption equilibrium has been established

| protein | shear viscosity (mN.s/m) | method (ref) | angular freq. ($s^{-1}$) |
|---|---|---|---|
| β-casein | <1 | creep (2) | |
| | 1 | creep (52) | |
| Na-cas | 2.3(0.3 g/l) | this work (osc.) | 0.084 |
| κ-casein | 2 | creep (52) | |
| | 4.6(0.3 g/l) | this work (osc.) | 0.42 |
| β-lactoglobulin | 0($\Gamma$=1.5), 500($\Gamma$=2) (spread layer) | creep (52) | |
| | 0.01(0.02 g/l) | osc. disc (57) | |
| BSA | 13.4($\Pi$=16) | osc. needle (58) | |
| | 0($\Gamma$=1), 3000($\Gamma$=1.5) | creep (54) | |
| | 10($\Gamma$=1.6), 200($\Gamma$=4) | creep (2) | |
| | 1($\Gamma$=1.1), 37($\Gamma$=2) (spread) | (1) | |
| | 0.3($\Pi$=3), 16($\Pi$=16) | osc. disc (59) | |
| | 0.06 | osc.disc (29) | 66 |
| | 2.9($\Gamma$=1.2), 7.9($\Gamma$=1.9) | this work (osc.) | 0.42 |
| | 129($\Gamma$=1.9) | ,, | 0.21 |
| HSA | 0.06(0.1 g/l) | osc. disc (30) | |
| Ovalbumin | 18.1($\Pi$=14.6) | osc. needle (58) | |
| | 15.5(0.1 g/l) | this work (osc.) | 0.42 |
| | 19.5(0.3 g/l) | ,, | |

$\Gamma$= surface concentration in mg/m$^2$

5.6.3 Effect of deformation and frequency.

In order to obtain the surface shear modulus for the undisturbed structure of the adsorbed protein film, the deformation must be so small that $|\mu_s|$ no longer depends on the magnitude of the deformation. It was verified whether our measurements satisfied this condition by determining $\mu_s$ and $\Phi$ for different values of $s_m(R_i)$ ranging from 0.012 to 0.25. For both BSA and ovalbumin, at all protein concentrations, surface ages and angular frequencies, we found $|\mu_s|$ to increase and $\Phi$ to decrease with decreasing deformation. Only for $|\mu_s| < 5$ mN/m, which is the case at low protein concentration and at the initial stage of the adsorption process (low surface ages), $|\mu_s|$ was found to be more or less constant over the whole deformation range (Fig. 6). Fig.7 shows the equilibrium result (21h) for BSA concentrations ranging from 0.005g/l to 0.3g/l and ovalbumin at 0.3g/l.

Each set of experiments was performed on the same solution surface, using a series of increasing values of $s_m(R_i)$. The slope of $|\mu_s|$ versus $s_m(R_i)$ appears to increase with increasing $|\mu_s|$. The increase of $|\mu_s|$ and decrease of $\Phi$ with decreasing shear deformation, necessitates an extrapolation to $s_m(R_i) \rightarrow 0$ in order to optimally approach the unperturbed structure of the surface layer. Within the deformation range of the present measurements both $|\mu_s|$ and $\Phi$ appear to be linear functions of $s_m(R_i)$, which facilitates the extrapolation. This procedure is only allowed if the linear range $[s_m(R_i)lin]$ is very small, $0 < s_m(R_i)lin \leq 0.012$. However, even if $|\mu_s|$ and $\Phi$ became constant immediately below the lowest deformation point measured, the relative errors in the extrapolated surface shear storage moduli remain less than 10% and so are commensurate with the overall accuracy of the measurements. Unless stated otherwise, all values of $\mu'_s$ and $\mu''_s$ reported in this chapter have been calculated by this extrapolation using Eqns (26) and (27).

The clear deformation dependency of the modulus suggests breaking of bonds that are responsible for the structure. In all experiments where $|\mu_s|$ and $\Phi$ were determined as a function of $s_m(R_i)$ the experiments were performed at increasing deformation followed by an experiment at the initial first small deformation. This latter mentioned modulus is always lower than on the way up, which supports this idea. It further indicates that restoring these bonds takes at least 0.5 hour, being the time needed for a set of experiments at the different frequencies at one deformation.

From bulk rheology of protein gels a linear region up $s_m(R_i) \geq 0.025$ was found (60). Assuming it is allowed to consider the adsorbed protein layer as a thin gel layer of protein, a similar linear region would be expected for surface shear rheology. A considerably smaller linear region points to inhomogeneities in the adsorbed layer. Due to these inhomogeneities the local deformation can be much larger than the mean applied deformation.
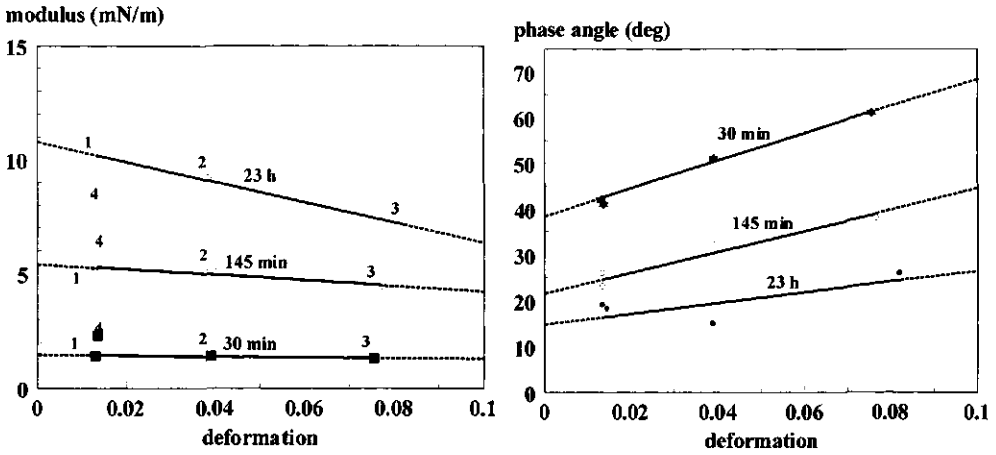
Figure. 6
Shear modulus and phase angle vs. deformation at increasing adsorption time.
BSA : 0.005 g/l, $\omega = 0.42$ s$^{-1}$.
The numbers indicate the sequence of the measurements.
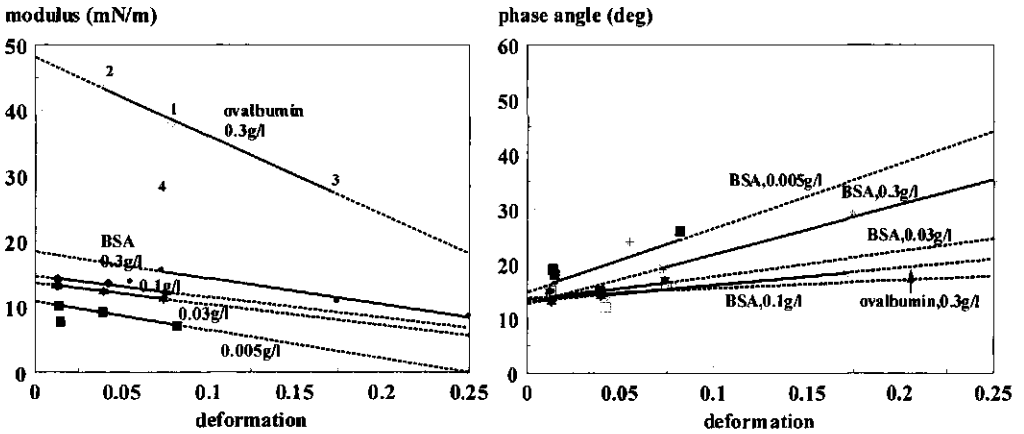


Figure 7
The shear modulus and the phase angle vs. deformation for BSA and Ovalbumin.
Age of the surface = 21 h (equilibrium surface concentration), $\omega = 0.42$ s$^{-1}$.
The numbers indicate the sequence of the measurements.

151

modulus (mN/m)
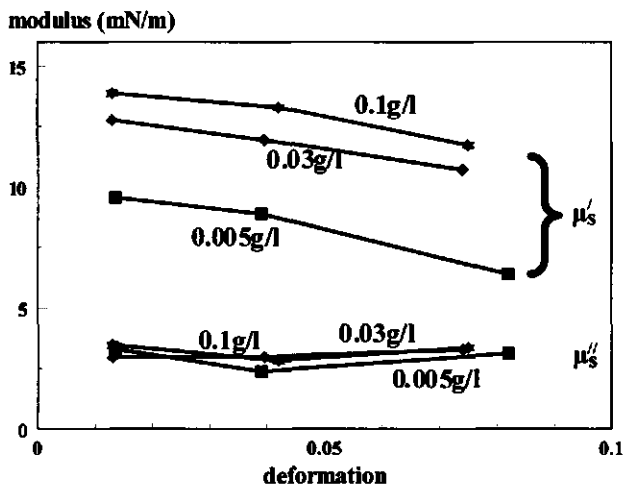


Figure 8
$\mu'_s$ and $\mu''_s$ vs. deformation for adsorbed layers of BSA obtained from solutions containing
0.005g/l, 0.03 g/l and 0.1 g/l.
Age of the surface = 21 h (equilibrium).

modulus (mN/m)
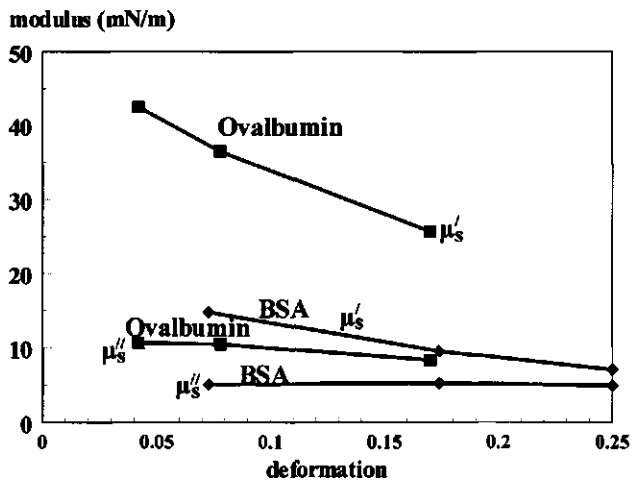


Figure 9
$\mu'_s$ and $\mu''_s$ vs. deformation for BSA and Ovalbumin.
Bulk concentration = 0.3 g/l;
Age of the surface = 21 h (equilibrium).

**modulus (mN/m)**
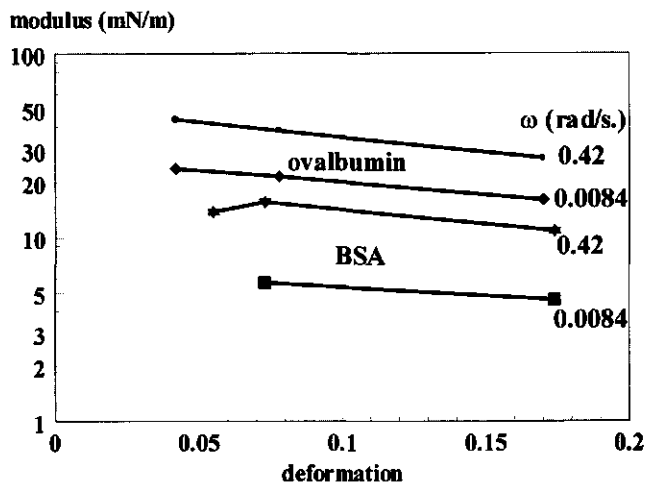


Figure 10a
The effect of frequency on the deformation dependency of the modulus. A comparison between
BSA and Ovalbumin. Bulk concentration = 0.3 g/l; Age of the surface = 21 h (equilibrium).

**modulus (mN/m)**
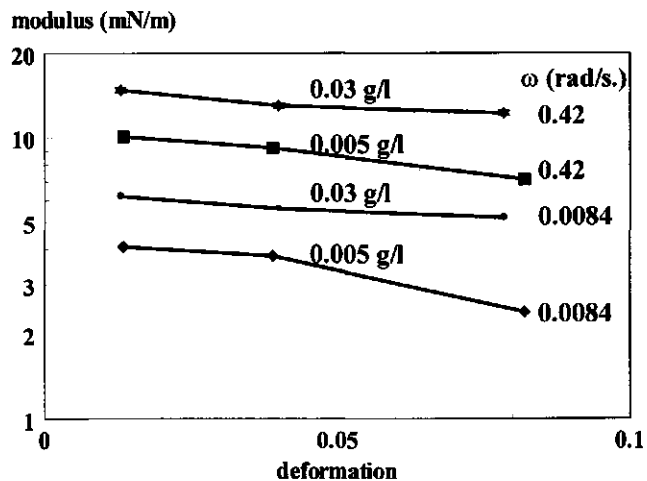


Figure 10b
The effect of frequency on the deformation dependency of the modulus for adsorbed layers of BSA.
Age of the surface = 21 h (equilibrium).

153

**modulus (mN/m)**
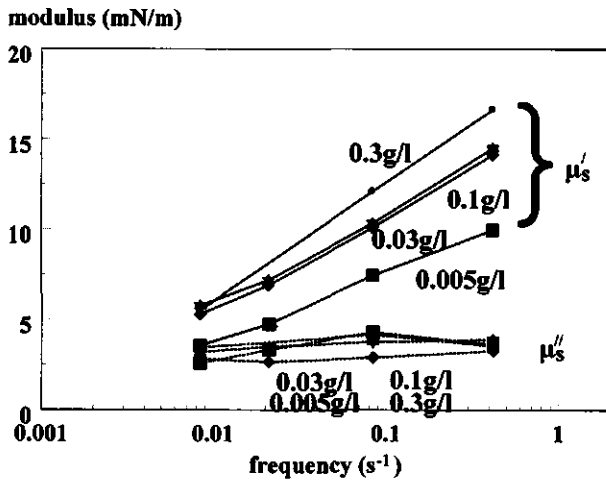


Figure 11
Frequency dependence of the shear modulus for adsorbed layers of BSA.
Bulk concentration is indicated. Age of the layer = 21 h (equilibrium).

**modulus (mN/m)**
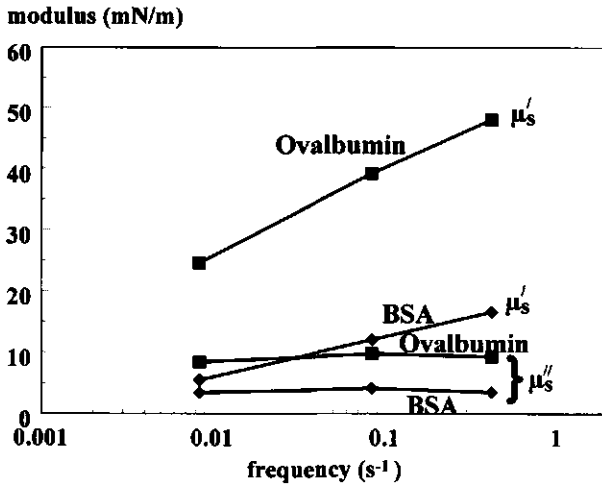


Figure 12
Shear modulus vs. frequency. A comparison between BSA and ovalbumin.
Protein concentration 0.3 g/l. Age of the layer = 21 h (equilibrium).

154

In Figures 8 and 9 the surface shear storage modulus $\mu'_s$ and the surface shear loss modulus $\mu''_s$ of the adsorbed protein layers are plotted versus $s_m(R_i)$. The data were calculated from the values of $|\mu_s|$ and $\Phi$ at different values of $s_m(R_i)$ using Eqns (26) and (27). While $\mu'_s$ decreases in all cases linearly with increasing value of $s_m(R_i)$, $\mu''_s$ appears to be nearly independent of the deformation. Consequently, the type of bonds that are broken at large deformations and slowly restore, do not contribute to $\mu''_s$.

The effect of the frequency on the deformation dependency of the modulus is illustrated in Fig. 10. In this figure the modulus vs. deformation is plotted semi-logarithmically for different frequencies. It is clear from this plot that the frequency hardly affects the slope. Consequently, the increase of the modulus with increasing frequency, does not affect the deformation dependency. Comparison of these results (BSA) with surface pressure, surface concentration and dilational modulus measurement as described in the previous chapters, shows that $|\mu_s|$ becomes deformation dependent at $\Pi \approx 3$-$5$ mN/m and $\Gamma \approx 1$-$1.1$ mg/m$^2$. Above these values the dilational modulus also becomes deformation dependent. However, the deformation dependency of the dilational modulus is significantly smaller (see Chapter 3).

As already mentioned above, the modulus generally increases with increasing frequency. The effect of the frequency $\omega$ on $\mu'_s$ and $\mu''_s$ is shown in Figs 11 and 12 for BSA solutions ranging from 0.005g/l to 0.3g/l. $\mu'_s$ strongly increases with increasing frequency, while $\mu''_s$ only weakly depends on $\omega$. A similar result was found for ovalbumin.

The usual trend for the frequency dependence of elastic and viscous moduli in bulk rheology (61), also applying to surface dilational rheology (62) over a much broader frequency range is shown in Fig. 13. The elastic modulus increases with increasing frequency, until at high frequencies a maximum is reached. In the frequency range with the steepest increase of the elastic modulus a maximum value of the viscous modulus is found. Our general observation of an increasing $\mu'_s$ at about constant $\mu''_s$ is qualitatively in line with this trend if we assume that our experiments apply to a frequency range around $\omega = \tau^{-1}$ for the two decades investigated. Constancy of the viscous modulus over a wide frequency range is likely if several, closely related relaxation mechanisms are involved.

So, if this wide frequency range of almost constant $\mu''_s$ can be applied to Figs. 11 and 12 a relaxation time of 10 - 100 sec. can be estimated. This time-scale suggests collective behaviour of several parts of a molecule. Restoration of intermolecular bonds would occur at a much shorter time-scale. The almost constant value of $\mu''_s$ over the whole frequency range indicates that the surface shear viscosity ($\eta_s = \mu''_s / \omega$ (static viscosity)) decreases with increasing frequency. Occurence of shear thinning was also inferred from interfacial shear viscosity measurements at protein layers adsorbed at the tetradecane/water interface (63). Their

explanation is that intermolecular interactions (probably hydrogen bonding) are easily disrupted by shearing.
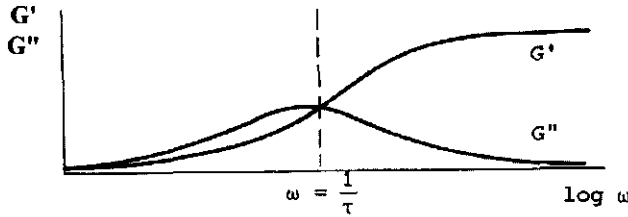


Figure 13
The elastic and viscous part the modulus, in bulk rheology, as a function of frequency (61).

These results again show the importance of controlling the frequency at which the measurements are performed.

5.6.4. Effect of surface age and adsorbed amount on the shear modulus.

In Figs. 14 and 15 two examples are given of the increase of $\mu'_s$ and $\mu''_s$ as a function of the age of the surface ($t_s$). For all data points in these plots, measurements at increasing deformations $s_m(R_i)$ were performed from which the values of $\mu_s$ and $\Phi$ at $s_m(R_m) \rightarrow 0$ were determined by extrapolation as discussed in section 6.6.3. The values of $\mu'_s$ and $\mu''_s$ were calculated using Eqns (26) and (27). In nearly all experiments it was observed that the elastic and viscous shear moduli of adsorbed BSA and ovalbumin increase considerably with increasing age of the surface. A similar effect has been observed for adsorbed layers of gelatin (47), gelatin and human serum albumin (30), and polymethacrylic acid (64). This behaviour had a certain similarity with the increase of the shear modulus with time as observed for a photopolymerisation reaction in an interface (65). From surface shear viscosity measurements a similar effect of the surface age was concluded (7,66).
In Fig. 16 this increase of the shear modulus with time is compared with the time dependency of the adsorption and the dilational modulus. This comparison indicates that the shear modulus continues to increase when the dilational modulus is already constant (or even

156

modulus (mN/m)
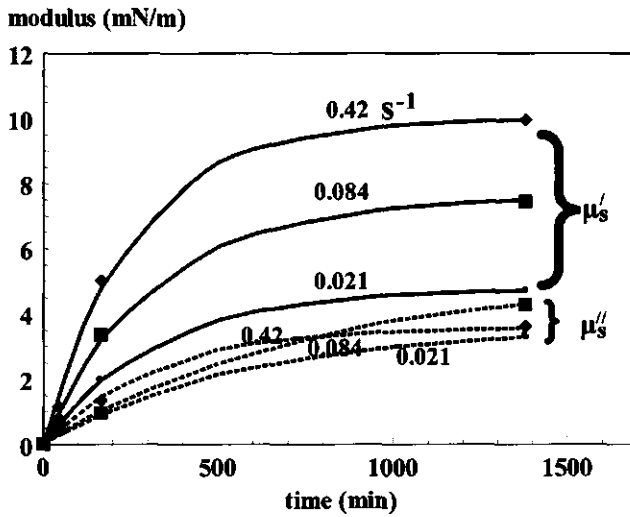


Figure 14
The increase of the shear moduli, $\mu_s'$ and $\mu_s''$, with age of the surface for 0.005 g/l BSA.
The frequency of the deformation is indicated.
The lines represent the best fits according to Eq. 28.

modulus (mN/m)
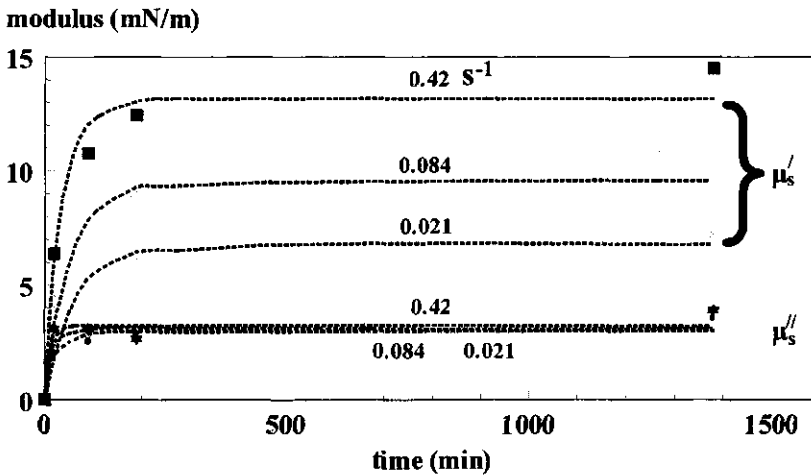


Figure 15
The increase of the shear moduli, $\mu_s'$ and $\mu_s''$, with age of the surface for 0.03 g/l BSA.
The frequency of the deformation is indicated.
The lines represent the best fits according to Eq. 28.

157

decreases, depending on frequency, not indicated in this plot). In this surface age region the adsorption increases still somewhat. Consequently, the increase of $\mu_s$ with time may at least be due to two different time-dependent contributions being; (i) increase of the adsorbed amount and (ii) increase of bond formation between adsorbed molecules.

In most investigations described in the literature detailed information about adsorption and surface pressure is lacking. Consequently, the time-dependent increase of the shear modulus is loosely interpreted as caused by a structure formation process. For instance, in Ref. 64 bond formation between neighbouring macromolecules according to a first order reaction was postulated but the possibility of an increase of adsorption was ignored. The modulus then should increase with time according to:

$$\mu_s(t_s) = \mu_s(\infty)[1 - \exp(-t_s/\tau)] \qquad (28)$$

where $\mu_s(\infty)$ represents the final value of the modulus and $1/\tau$ is the rate constant of the surface structure formation. Our measured curves can be fitted fairly well with this equation (Figs. 14,15). For all protein concentrations the results of this fitting procedure are summarised in Table 4.

As expected, the frequency hardly affects $\tau$, being the characteristic time of this structure formation process, for $\mu'_s$, whereas the characteristic time for $\mu''_s$ increases somewhat with decreasing frequency. At low concentrations similar values of the characteristic times are found for $\mu'_s$ and $\mu''_s$ whereas at high concentrations significantly lower values were found for the characteristic time of the structure formation process as far as it affects the viscous modulus.

The results in table 4 also indicate that $\tau$ is different for different protein concentrations. At low concentrations $\tau$ is about 300 minutes, whereas at higher concentrations about 40 minutes is found. The main difference between low and high concentrations with respect to structure formation is the rate of adsorption. Especially at low concentrations, where within the time-scale of the experiment the surface concentration ($\Gamma$) considerably increases, it is likely that the adsorption process interferes with that of structure formation.

Consequently, a first order reaction model for the structure formation can be applied only under conditions where the surface concentration is constant.

In Fig. 17a $|\mu_s|$ is plotted as a function of the surface concentration for different BSA concentrations. For the sake of comparison the dilational modulus vs. surface concentration curve ( $|\epsilon|(\Gamma)$) is also given. The adsorption data were obtained by ellipsometry, not at the same surfaces, but under identical experimental conditions. The adsorption time was used to link adsorbed amount to the shear modulus. The data in this plot were obtained by measuring

| conc. (g/l) | freq. (s⁻¹) | $\mu'_s(\infty)$ (mN/m) | $\tau'$ (min) | $\mu''_s(\infty)$ (mN/m) | $\tau''$ (min) |
|---|---|---|---|---|---|
| BSA 0.001 | 0.42 | 6.1 | 266 | 2 | 206 |
| | 0.084 | 4.5 | 275 | 2 | 246 |
| 0.005 | 0.42 | 10 | 253 | 3.7 | 319 |
| | 0.084 | 7.5 | 301 | 5 | 723 |
| | 0.021 | 4.8 | 309 | 3.6 | 559 |
| 0.03 | 0.42 | 13 | 37 | 3.3 | 5.6 |
| | 0.084 | 9.6 | 53 | 3.1 | 11.7 |
| | 0.021 | 6.8 | 63 | 3 | 18.8 |
| 0.1 | 0.42 | 14.8 | 22 | 3.8 | 2.5 |
| | 0.084 | 11.3 | 32 | 3.3 | 2.4 |
| | 0.021 | 6.9 | 43 | 2.9 | 17.9 |
| ovalbumin 0.3 | 0.42 | 49.3 | 339 | 9.4 | 207 |
| | 0.084 | 39.7 | 274 | 9.8 | 199 |

Table 4

The calculated parameters $\mu_s(\infty)$ and $\tau$ (calculated from the best fits using Eq. 28) for BSA at various concentrations and Ovalbumin.
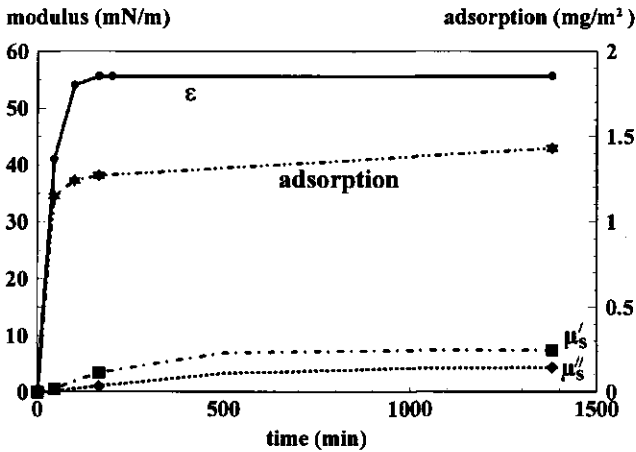


Fig. 16

Shear modulus $\mu_s$, dilational modulus $|\epsilon|$, and adsorbed amount as a function of the age of the surface. BSA conc. 0.005 g/l, frequency = 0.084 s⁻¹.

the shear modulus in the course of the adsorption process, consequently at increasing surface ages. So equal adsorptions for different concentrations mean higher surface ages for the lower concentration. If the formation of intermolecular bonds is slow compared to the rate of adsorption, moduli determined at equal adsorptions, but at different protein concentrations, would be higher for the lower concentration. However, the results with the different concentrations seem to merge into one master curve of $|\mu_s|(\Gamma)$. **Consequently, (i) not the intermolecular bond formation step, but the adsorption rate controls the increase of the shear modulus with time and (ii) the adsorbed amount dominates the value of shear modulus.**

This conclusion also implies that the formation of bonds between adsorbed molecules (the structure formation process) is fast compared to the adsorption process. Whether this is also true for much higher concentrations than those studied in this investigation, (initially much faster adsorption) is questionable. These findings justify the conclusion that within the frame of experimental conditions examined, the surface shear modulus is uniquely determined by the adsorbed amount and surface pressure. In Chapter 3 the same conclusion was drawn about the dilational modulus. However, in contrast with the dilational modulus, the elastic component of the shear modulus is affected by the frequency over the entire adsorption range. Due to the rather poor reproducibility of the shear modulus measurements, the accuracy of the shape of $|\mu_s|(\Gamma)$ curve is less than that of the $|\epsilon|(\Gamma)$ curve. The results, however, justify the conclusion that, compared to $|\epsilon|$, a higher adsorption is required to produce a non-zero value of the shear modulus. The resistance against shear deformation becomes measurable at about half saturation adsorption. In this adsorption region $|\epsilon|$ is already half way its maximum value. With a further increase of the adsorption the shear modulus increases rather steeply. The relative slopes of the increase of $|\epsilon|$ and $|\mu_s|$ versus adsorption are comparable. The finding that the shear modulus becomes measurable at higher adsorbed amount than the dilational modulus is in line with the different behaviour of the shear modulus with respect to surface age as shown in Fig. 16.

In Fig. 17b $|\epsilon|$ and $|\mu_s|$ are plotted versus the surface pressure. This plot shows that above a critical value of the surface pressure, $2 \leq \Pi \leq 5$ mN/m, the shear modulus starts to deviate from zero. This in contrast to the dilational modulus, which linearly increases with increasing surface pressure as soon as $\Pi$ deviates from zero. A critical value for the surface pressure was also found for viscosity measurements by Joly (1). Above this critical value, for BSA 4 mN/m, the shear became non-Newtonian.

The above picture applies to BSA at relatively low concentrations, indicated in Figs. 13-17 and Table 4. For ovalbumin only measurements at higher concentrations are available. For those conditions the shear modulus continues to increase with surface age whereas the

**modulus (mN/m)**
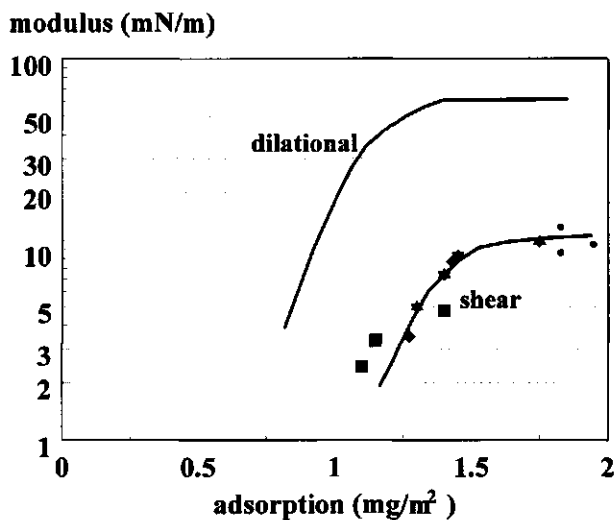


Figure 17a

The shear modulus $|\mu_s|$ and the dilational modulus $| \epsilon |$ (Chapter 3) as a function of the adsorbedamount. Both curves are the combined result of various BSA concentration at increasing surface age.

BSA conc. ■ 0.001 g/l, ◆ 0.005 g/l, ✳ 0.03 g/l, ● 0.1 g/l.
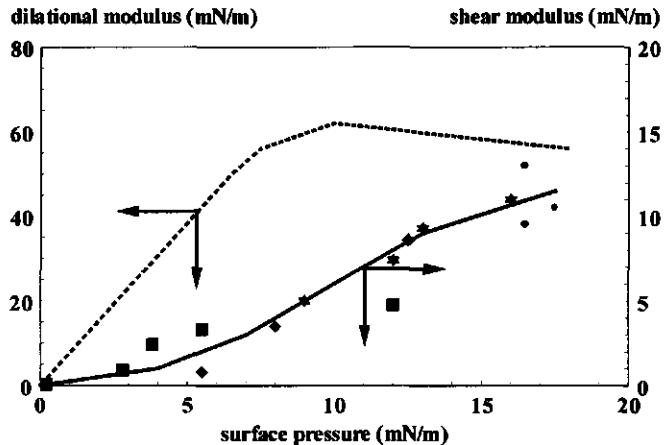


Figure 17b

The shear modulus $|\mu_s|$ and the dilational modulus $| \epsilon |$ (Chapter 3) as a function of the surface pressure. Both curves are the combined result of various BSA concentration at increasing surface age.

BSA conc. ■ 0.001 g/l, ◆ 0.005 g/l, ✳ 0.03 g/l, ● 0.1 g/l.

Note the different scales for $|\mu_s|$ and $| \epsilon |$.

161

adsorption only slightly increases (0.1g/l, ovalbumin ex Sigma, Table 5) and the thickness of the adsorbed layer points to multilayer adsorption (0.3g/l, ovalbumin ex Brocades, Table 6). Formation of thick coherent layers with ovalbumin could also be deduced from the finding that adsorbed surface layers could be torn off from the water (67). Van Aken (68) observed that upon compression of a spread layer of BSA crack formation and sudden drops of pressure occur. This also points to the formation of a thick and coherent layer prior to the area deformation. Cracks are formed at weak spots in such a layer.

## 5.6.5. Further comparison of dilational and shear moduli.

### 5.6.5.1 Summary of observed similarities and differences.

In this section a comparison will be made between the surface shear moduli determined by the double ring surface rheometer and surface dilational moduli dealt with in Chapter 3. The following similarities and differences become apparent.

(i) For both moduli a minimum surface coverage has to be surpassed to obtain a non-zero value. This critical surface coverage is higher for the shear modulus. Both moduli increase with further increase of the surface concentration. At a certain surface concentration, depending on protein type, the dilational modulus shows a clear plateau or maximum value, attributed to reconformation or collapse type phenomena. In the shear modulus, the existence of plateau or maximum value is less pronounced probably due to increased thickness of the adsorbed layer as a result of multilayer formation.

(ii) Both moduli become deformation-dependent at about the same, relatively high surface concentration. At these surface concentrations the dilational modulus has already reached about its maximum value, whereas the shear modulus is still very low.

(iii) For all proteins at surface concentrations up to about half saturation the dilational modulus was almost purely elastic. Only at higher surface concentrations (depending on protein type) the dilational modulus acquires a minor viscous contribution. In the same surface concentration range the shear modulus strongly increases with increasing frequency, but the relatively high viscous part of the shear modulus is almost constant over the whole frequency range, indicating a decrease of the surface shear viscosity with increasing frequency (= shear thinning).

(iv) The increase of both moduli with time is primarily a surface concentration effect. Effects of surface age at constant surface coverage have never been found for the dilational modulus. Only with protein layers adsorbed from higher bulk concentrations (0.1-1g/l), does the dilational modulus of the layer become somewhat more elastic with time (Chapter 3). For the shear modulus increase with time at constant surface coverage cannot be ruled out

162

completely (ovalbumin at concentrations $\geq 0.1$ g/l).

5.6.5.2 Provisional model for shear properties of adsorbed protein layers.

The thin layer of interacting adsorbed protein molecules can be considered as a very thin three-dimensional protein gel. For the shear properties of such a layer two elements are supposed to play a role, (i) the internal rheological properties of the protein molecule and (ii) the intermolecular interaction. The internal rheological properties of the protein molecule are determined by the strengths and number of intramolecular bonds (hydrophobic interactions, H-bridges and covalent bonds, e.g. S-S bridges). The intermolecular interactions will be determined by the number and type of the adsorbed protein molecules and are probably much weaker.

According to the above picture two models to obtain an adsorbed layer with a high resistance against shear can be imagined (see Fig. 18); (i) a layer of basically flexible molecules with a high number of strong crosslinks between the molecules (rubberlike structure), (ii) a layer of molecules, each having a strong internal structure (rigid molecules). With the latter model the required intermolecular interaction depends on the surface concentration. At low surface concentration the molecules must interact strongly to obtain high resistance against shear (model iia), however, at high adsorbed amount interaction becomes less important. With a close-packed monolayer the individual rigid molecules must deform due to shearing (model iib).

An adsorbed layer according to model (i) will be mainly elastic because mostly deformation of the chains between the crosslinks takes place. An adsorbed layer according to model (iia) will also be mainly elastic when the interaction between the molecules is strong, because upon shearing, the molecules have to deform. An adsorbed layer according to model (iib) allows the molecules to move along each other if the individual molecules deform to a certain extent. This moving of the molecules will be accompanied by breaking and restoring of



model (i)                    model (iia)                    model (iib)
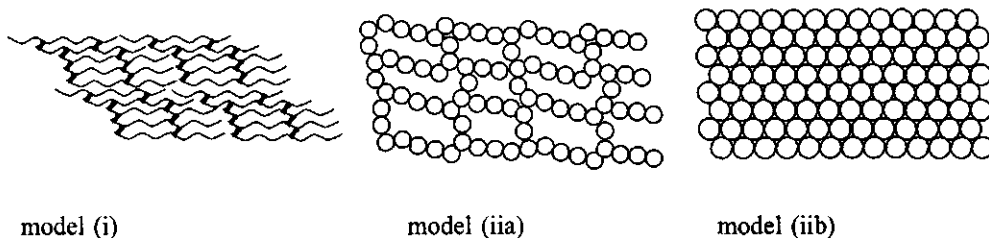
Fig. 18 Possible structures of an adsorbed protein layer.

intermolecular bonds. Consequently, a layer according to this model will be visco-elastic. The balance between viscous and elastic part will be determined by the nature of intra-molecular bond. A high viscous part will be caused by weak intermolecular interactions which break and re-form during deformation.

5.6.5.3 Relation between dilational and shear modulus.

According to the provisional model described in 5.6.5.2 it is likely that the shear modulus is determined by a thin 3-D network of protein molecules. In three-dimensional rheology (69), the shear modulus measured in extension of an incompressible system is three times higher than the modulus measured in *simple* shear. This means that dilational deformation of a surface carrying such a 3-D network should result in a dilational modulus, $\epsilon$, that is at least equal to three times the surface shear modulus, $\mu_s$:

$$\epsilon \geq 3\mu_s \qquad (29)$$

if we assume the volume of the adsorbed layer to remain unchanged during the deformation. Table 5 compares the values of $\mu_s$ and $\epsilon$ for BSA, ovalbumin and PMApe at various concentrations, frequencies and surface ages. Values of $\epsilon/\mu_s > 3$ indicate extra contributions to $\epsilon$, as indicated by $\Delta\epsilon$ (= $\epsilon$-$3\mu_s$) in Table 5. It is clear that only a minority of the experimental data come anywhere near the ratio of three for $\epsilon/\mu_s$. An upper limit of 51 is found for experiments with the lowest concentration of BSA, where the ratio never exceeds the limiting value according to Eqn. (29). This limiting value of 3 for the ratio was not reached either for BSA concentrations up to 0.1 g/l. At the other end of the scale, with PMApe, $\alpha$=0.5, $\mu_s$ is even twice the value of $\epsilon$. According to Eqn (29) a ratio of three can be explained by assuming an adsorbed surface layer that behaves as a homogeneous gel layer, where $\mu_s$ and $\epsilon$ are determined by the same interactions between the adsorbed molecules. The most likely extra positive contribution would seem $\epsilon_{ideal}$, determined by changes in surface pressure only due to changes in surface concentration in an ideal monolayer (70). The shear modulus can be assumed to depend only on stresses caused by changes in conformations and interactions. According to Eqn 10 of Chapter 6, $\epsilon_{ideal}$ can amount to quite high values depending on the degree of coverage, $\Theta$. From table 5 it can be seen (0.005 g/l BSA) that $\Delta\epsilon$ decreases with increasing time and consequently increasing surface concentration. At high surface concentration $\epsilon_{ideal}$ will decrease, because the adsorbed molecules can no longer be considered as separate kinetic units. At higher protein concentrations (BSA $\geq$ 0.3g/l and ovalbumin 0.3g/l) the limiting value of three for $\epsilon/\mu_s$ is reached and in some cases even passed. With PMApe,

164

$\alpha=0.5$ $\mu_s$ becomes even twice the value of $\epsilon$. Values of $\epsilon/\mu_s<3$ were only found under conditions when multilayers are formed (BSA, ovalbumin) or with systems that form extremely thick layers (PMApe, $\alpha=0.5$) (see table 6). These results suggest that only the first layer, which is in direct contact with the surface, affects the dilational modulus. In the adsorption region where multilayer adsorption takes place, the dilational modulus has reached a maximum value or even decreases somewhat. In Chapter 3 it was suggested that a second layer may affect the dilational modulus by providing the possibility of molecules to interchange between first and second layer. Such a mechanism will be responsible for the

Table 5
The ratio $\epsilon/\mu_s$ for BSA, ovalbumin and PMApe at various concentrations, frequencies and surface ages.

| protein | conc.(g/l) | age (h) | freq. (s⁻¹) | $|\mu_s|$ (mN/m) | $|\epsilon|$ (mN/m) | $\epsilon/\mu_s$ | $\Delta\epsilon$ |
|---|---|---|---|---|---|---|---|
| BSA | 0.005 | 0.75 | 0.42 | 1.4 | 41 | 29 | 37 |
| | | | 0.084 | 0.8 | 41 | 51 | 38 |
| | | 2.75 | 0.42 | 5.2 | 56 | 11 | 40 |
| | | | 0.084 | 3.5 | 56 | 16 | 45 |
| | | 23 | 0.42 | 10.6 | 59 | 6 | 27 |
| | | | 0.084 | 8.6 | 56 | 7 | 30 |
| BSA | 0.03 | 23 | 0.42 | 15 | 59 | 3.9 | 14 |
| | | | 0.084 | 11 | 49 | 4.4 | 16 |
| BSA | 0.1 | 23 | 0.42 | 14 | 70 | 5 | 28 |
| | | | 0.084 | 10 | 53 | 5.3 | 23 |
| BSA | 0.3 | 23 | 0.42 | 17 | 50 | 2.9 | -1 |
| | | | 0.084 | 13 | 46 | 3.5 | 7 |
| BSA | 0.5 | 1.5 | 0.42 | 15.8 | 54 | 3.4 | 7 |
| | | | 0.084 | 10.3 | 42 | 4.1 | 11 |
| | | 23 | 0.42 | 24.8 | 58 | 2.3 | -16 |
| | | | 0.084 | 18.5 | 48 | 2.6 | -7 |
| Ovalbumin | 0.1 | 2 | 0.42 | 11 | 80 | 7.3 | 47 |
| | | 23 | 0.42 | 19 | 82 | 4.3 | 25 |
| Ovalbumin | 0.3 | 23 | 0.42 | 49 | 80 | 1.6 | -67 |
| | | | 0.084 | 40.5 | 71 | 1.7 | -50 |
| PMA,$\alpha=0.1$ | 0.1 | 23 | 0.42 | 20 | 63 | 3.1 | 3 |
| | | | 0.084 | 6.6 | 36 | 5.4 | 16 |
| PMA,$\alpha=0.5$ | 0.1 | 23 | 0.42 | 56 | 29 | 1.9 | -139 |
| | | | 0.084 | 31 | 21 | 1.5 | -72 |

decrease of the dilational modulus in this surface coverage region, especially at low frequencies (0.01 rad/s.). The effect of a second layer on the shear modulus is obvious, the deformed gel layer has become thicker.

In Table 6 a comparison has been made between the dilational and shear modulus of various proteins and polymers. In this table effects of protein denaturation on both surface rheological parameters is included. This table also presents the main parameters that characterize the adsorbed surface layer, i.e., surface pressure, adsorption and layer thickness.

This table shows that a low $\epsilon$ combined with a low $\mu_s$ is linked to adsorbed layers of flexible (random coil) molecules viz. Na caseinate and PVA. Adsorbed layers of rigid globular molecules viz. BSA and ovalbumin show a high $\epsilon$ combined with a high $\mu_s$. The same result was found for PMA, $\alpha=1$. This finding supports the idea that $\epsilon$ and $\mu_s$ are governed by the same molecular parameters. Exceptions to this rule that $\epsilon$ and $\mu_s$ both are low or high are adsorbed layers of $\kappa$-casein and PMA, $\alpha=0.5$. These molecules have in common that they form very thick layers.

The idea that the rigidity of the molecular structure determines to a large extent the magnitude of both moduli is supported by the finding that in the presence of a denaturing agent (6M urea) the moduli of BSA and ovalbumin decrease to the value of Na caseinate.

Table 6

Comparison between shear- and dilational moduli for proteins and polymers. For some proteins the effect of denaturation agents is included.

surface age= 21hour, freq.=0.42s$^{-1}$

| protein | conc. (g/l) | surface pressure (mN/m) | layer thickness (nm) | adsorption (mg/m$^2$) | $\|\epsilon\|$ (mN/m) | $\|\mu_s\|$ (mN/m) |
|---|---|---|---|---|---|---|
| Na-caseinate | 0.3 | 23 | 6 | 3.2 | 21 | 0.2 |
| idem+6M urea | 0.3 | 23.5 | | | 19 | 0.02 |
| κ-casein | 0.3 | 18.5 | 13 | 6 | 80 | 6 |
| BSA,Fraction V | 0.1 | 18 | 2.5 | 2.3 | 56 | 14.5 |
| idem+6M urea | 0.1 | 28 | | | 29 | 0.1 |
| BSA,Fraction IV | 0.3 | 24 | 11 | 6.2 | 50 | 17 |
| Ovalbumin,Sigma | 0.1 | 22.5 | 2.5 | 1.9 | 82 | 19 |
| idem +6M urea | 0.1 | 26.5 | | 1.7 | 36 | 0.02 |
| Ovalbumin,Brocades | 0.3 | 24 | 16 | 9.7 | 80 | 48 |
| PMA,α=0.1 | 0.1 | 9.8 | 11 | 2.4 | 63 | 21 |
| PMA,α=0.5 | 0.1 | 6.6 | 25 | 1.5 | 29 | 56 |
| PVA | 0.4 | 26.5 | 10 | 3.1 | 11 | <0.1 |

From ellipsometry the ellipsometric thickness and concentration of the adsorbed layer can be inferred. This offers the possibility to compare the rheology of the adsorbed layer with the rheological behaviour of protein solutions at equal concentration (6). The results discussed in Ref. 6 indicate that, even if we take into account the rather large experimental uncertainties, the shear modulus of the adsorbed layer is some orders of magnitude higher than that of the bulk solution. A possible explanation is that in the adsorbed layer the adsorbed molecules do not only interact in the same way as in a concentrated solution, but that due to the fact that the adsorbed segments form anchor points to the surface which act as extra crosslinks, the structure becomes more rigid. Another explanation is that due to conformational changes upon adsorption the interaction between the molecules and the rigidity of the molecules have changed.

5.6.6   Rheological behaviour of adsorbed protein layers; trends and views as deduced from the present investigation.

From the results presented and discussed above, the following trends and views with respect to the rheological behaviour of adsorbed protein layers can be extracted.
(i) At given $\Gamma$, both the elastic surface dilational moduli and the elastic surface shear moduli increase in the sequence PVA< Na-caseinate < BSA < ovalbumin. This suggest that essentially the same molecular properties are responsible for the magnitudes of both moduli. Two properties of the polymer/protein molecule increase in the same sequence: (a) rigidity of the molecule (PVA/Na caseinate are flexible random coils, whereas BSA and ovalbumin are rigid globules), (b) number of S-S bridges. This result is in line with earlier findings (2) that the resistance against shear, as well as dilation, increases when the protein becomes more rigid. The results with κ-casein and PMA do not completely fit into this sequence. Both components build very thick adsorbed layers.
(ii) For both moduli, the increase with time is primarily a surface coverage effect.
(iii) From the results presented in Chapters 3, 4 and the present chapter, it was concluded that adsorbed protein molecules strongly interact. This interaction is responsible for the steep slope (about 8) of $\epsilon(\Pi)$. Together with the level of molecular flexibility/rigidity, this interaction also determines the maximum value of the dilational modulus. It is plausible that the same interaction and molecular structure parameters are responsible for the shear modulus. A strong interaction however, was not only found for BSA and ovalbumin, which are globular/rigid proteins, but also for casein. However, with the latter protein the shear modulus is very low (see Table 6). Consequently, a strong interaction, as deduced from the slope of the dilational modulus vs. surface pressure plot, is not sufficient for a high shear modulus. In the case of casein these interactions take place between flexible, easily deformable molecules; the

167

intermolecular bonds are stronger than intramolecular ones. With BSA and ovalbumin the intermolecular bonds are the weakest part of the network. So for both moduli the internal rigidity of the molecule is more important for the magnitude of the modulus. This conclusion is supported by the finding that addition of urea, an agent that turns rigid globular protein molecules into flexible more random coil molecules, decreases both the dilational and the shear modulus of BSA and ovalbumin to the level of those for casein. This points again to a dominant contribution of molecular structure to the value of both moduli.

The origin of the interactions between adsorbed protein molecules may be caused by electrostatic, hydrogen bridge or covalent bonds. The first two types of bonds will be formed almost instantaneously, the extent being determined by protein type and adsorbed amount. The rate of covalent bond formation can be controlled by the slow conformation changes that may occur in the adsorbed layer. If these intermolecular chemical bonds between adsorbed molecules (e.g. S-S bridges) contribute to the shear modulus, the characteristic time for the formation of these bonds must be of the order of minutes. Time-dependent polymerization (formation of dimers, trimers and tetramers) of BLG through disulphide bonds at oil/water interface was found by Dickinson (71). In that work the time-dependent polymerization correlates with a time dependent increase of shear viscosity .

(iv) A high surface concentration is required for a non-zero value of the shear modulus and the steep increase of $|\mu_s|(\Gamma)$ at this high surface coverage (almost full packed monolayer) suggests that the low deformability of the individual molecules dominates the shear modulus. The molecules of globular proteins can be considered as rigid spheres. At sufficiently high surface concentrations these rigid molecules are closely packed (Fig. 18, model iib) Due to shearing the (rigid, elastic) molecules deform to allow them to flow along each other. This indicates visco-elastic behaviour, which is only possible if relatively weak, non-chemical bonds determine the intermolecular interaction. This explains the relatively high viscous part of the shear modulus.

Both moduli become deformation-dependent at about the same surface concentration. Deformation dependency of the modulus at small deformations points to inhomogeneities in the structure. The results with the shear modulus at larger deformations indicate breaking of bonds which restore slowly (0.5 h) (see section 5.6.3). The effect of large deformations on the dilational modulus also indicates breaking of bonds. However, this effect is much less pronounced.

(v) The shear modulus increases with increasing thickness of the adsorbed layer. For proteins this increase becomes evident in the case of multilayer adsorption (e.g. ovalbumin). The contribution of the first and following layers will be similar. For macromolecules like PMA, the effect of increase of thickness is due to long loops or tails.

(vi)The difference between the dilational and shear moduli with increasing surface

concentration is obvious. With increasing surface concentration $|\epsilon|$ changes from purely elastic at low $\Gamma$ to slightly viscoelastic at high $\Gamma$. The counterpart is found for $|\mu_s|$, which was found to begin almost purely viscous at low $\Gamma$, to become more elastic at high $\Gamma$. Different frequency dependencies of $\epsilon$ and $\mu_s$ suggest that inter- and intra-molecular interactions work out differently with respect to stress relaxation for the different types of deformation.

5.7 Conclusion.

The method described in this chapter provides a characterization of the shear properties of spread and adsorbed protein layers. Measured trends agree with those determined by others, despite large experimental differences. However, the reproducibility of the measurements must be improved before they allow an accurate evaluation of the surface parameters.

(i) The surface shear wave theory was used to determine the consequences of the coupling between the motion of the surface and the flow in the adjoining bulk phases for a proper evaluation of measurements with the concentric ring method. It is shown that for layers at the air/water interface the damped wave character of the deformation as a result of this coupling can often be neglected provided the moduli are not too low and the frequencies are not too high. These limits of moduli and frequency can be shifted somewhat by adjusting Ro-Ri.

(ii) The influence of the magnitude of the shear deformation on the values of the moduli has been analyzed. As it affects markedly the value of $\mu'_s$, an extrapolation procedure is required to asses the shear properties of the undisturbed surface.

(iii) As both $\mu_s$ and $\Phi$ depend upon the magnitude of the amplitude used for their measurement, interpretation of literature results obtained by methods requiring a large deformation of the interface (e.g. 32) should be reconsidered.

(iv) As the technique allows the frequency to be varied over a broad range, it can provide information on the nature of the relaxation processes occurring in the interface layer and also improves the basis for comparison between the surface properties of different protein solutions. This is an advantage over some earlier instruments (36).

(v) The elastic surface dilational moduli and the elastic surface shear moduli both increase in the sequence PVA< Na-caseinate < BSA < ovalbumin. This suggests that essentially the same molecular properties are responsible for magnitude of both moduli.

(vi) Adsorbed BSA and ovalbumin, which are globular proteins, strongly interact. Judging from the slope of the dilational modulus vs. surface pressure curve, the interaction between casein molecules is similar. In the case of casein these interactions take place between flexible, easily deformable molecules; these interactions are stronger than the intramolecular

structure. With BSA and ovalbumin the interacting bonds are the weaker part of the network. So for both moduli the rigidity of the molecule is the dominating characteristic.

(vii) Modelling the adsorbed protein layer as a thin homogeneous gel layer seems to be realistic as can be concluded from the finding that $\epsilon/\mu_s \geq 3$ for most systems. At low to medium surface concentrations a significant ideal monolayer contribution to $\epsilon$ was found.

(viii) The shear modulus increases with increasing thickness of the adsorbed layer. For proteins this increase is due to multilayer adsorption (e.g. ovalbumin). For macromolecules the effect of increase of thickness is due to long loops or tails (e.g. PMA) .

ACKNOWLEDGMENT.

5.8 References.

1.      M. Joly. Rheological Properties of Monomelecular Films. Part II: Experimental Results. Theoretical Interpretation. Applications. In: E. Matievié (Ed.), Surface and Colloid Science, vol.V, Wiley-Interscience, New York, (1972)79.

2.      D.E. Graham and M.C. Phillips, Proteins at Liquid Interfaces. V. Shear Properties. Journal of Colloid and Interface Science. 76 (1980) 240.

3.      V.I. Izmailova, G.P. Yampolskaya and B.D. Summ. Poverkhnostnie Yavleniya i Belkovykh Sistemakh (in Russian) , Chimia, Moscow. (1988) 93

4.      M.A. Cohen Stuart, J.T.F. Keurentjes, B.C. Bonekamp, J.G.E.M. Fraaye. Gelation of Polymers Adsorbed at the Water-Air Interface. Colloids and Surfaces. 17 (1986) 91

5.      H.J. Holterman, E.J. 's-Gravenmade, H.A. Waterman, J. Mellema, C. Blom. Flow curves of an Adsorbed Protein Layer at the air-saliva Interface. Colloid & Polymer Science 268 (1990) 1036

6.      F.J.G. Boerboom, A.E.A. de Groot-Mostert, A. Prins, T. van Vliet. Bulk and Surface Rheological Behaviour of Aqueous Protein Solutions. A Comparison. Netherlands Milk & Dairy Journal. 50 (1996) 183

7.      J. Castle, E. Dickinson, B. Murray, G. Stainsby. Mixed-Protein Films Adsorbed at the Oil-Water Interface. ACS Symposium Series No 343. Proteins at Interfaces: Physicochemical and Biochemical Studies. J.L. Brash and T.A. Horbett, eds. (1987).

8.      E. Dickinson, B.S. Murray, G. Stainsby. Coalescence Stability of Emulsion-Sized Droplets at a Planar Oil-Water Interface and the Relationship to Protein Film Rheology. Journal of the Chemical Society, Faraday Transactions 1. 84 (1988) 871

9.      M. Coke, P.J. Wilde, E.J. Russell, D.C. Clark. The Influence of Surface Composition

and Molecular Diffusion on the Stability of Foams Formed from Protein/ Surfactant Mixtures. Journal of Colloid and Interface Science. 138 (1990) 489

10.    E. Dickinson. Protein-Stabilized Emulsions. Journal of Food Engineering. 22 (1994) 59

11.    A. Williams, J.J.M. Janssen, A. Prins. Behaviour of Droplets in Simple Shear Flow in the presence of a Protein Emulsifier. Colloids and Surfaces A. 125 (1997) 189.

12.    J.A. de Feijter and J. Benjamins. The Propagation of Surface Shear Waves. Journal of Colloid Interface Science. 70 (1979) 375.

13.    J.A.de Feijter, J. Benjamins and F.A. Veer. Ellipsometry as a Tool to Study the Adsorption Behaviour of Synthethic and Biopolymers at the Air-Water Interface. Biopolymers 17    (1978) 1759.

14.    R. Miller, R. Wüstneck, J. Krägel, G. Kretzschmar. Dilational and Shear Rheology of Adsorption Layers at Liquid Interfaces. Colloids and Surfaces A 111 (1996) 75

15.    B. Warburton. Interfacial Rheology. Current Opinion in Colloid Interface Sci. 1 (1996) 481

16.    B.S. Murray, E. Dickinson. Interfacial Rheology and the Dynamic Properties of Adsorbed Films of Food Proteins and Surfactants. Food Science and Technology, Int. 2(3) (1996) 131

17.    D.A. Edwards, H. Brenner, D.T. Wasan. Interfacial Transport Processes and Rheology. Butterworth-Heinemann, Boston (1991).

18.    F.C. Goodrich, L.H. Allan, A.K. Chatterjee. The Theory of Absolute Surface Shear Viscosity. III. The Rotating Ring problem. Proceedings of the Royal Society. London. A320 (1971) 537.

19.    F.C. Goodrich, L.H. Allan. A New Surface Viscometer of High Sensitivity. III. Stearic Acid at the Oil/Water Interface. Journal of Colloid and Interface Science. 75 (1980) 590

20.    V.G. Vinogradov, G.B. Froishteter and K.K. Trilisky. Generalized Theory of Flow of Plastic Dispersed Systems with Account of Wall Effects. Rheologica Acta. 17 (1978) 156.

21.    R.J. Mannheimer, R.S. Schlechter. The Theory of Interfacial Viscoelastic Measurements by the Viscous-Traction Method. Journal of Colloid and Interface Science. 32 (1970) 225.

22.    M. Joly. Viscosité Superficielle et Structure Moléculaire des Couches de Protéines. Biochimica et Biophysica Acta. 2 (1948) 624

23.    R.J. Mannheimer, R.A. Burton. A Theoretical Estimation of Viscous-Interaction Effects with a Torsional (Knife-Edge) Surface Viscometer. Journal of Colloid and Interface Science. 32 (1970) 73

24. L. Fourt. Lateral Cohesion in Protein Monolayers. Journal of Physical Chemistry. 43 (1939) 887

25. W.E. Ewers, R.A. Sack. The Surface Viscosity of Soluble Films. Australian Journal of Chemistry. 7 (1953) 40.

26. B.M. Abraham, K. Miyano, J.B. Ketterson. An Instrument for measuring the Static and Dynamic Response to Shear at the Air/Water Interface and of Insoluble Monolayers: Some New Insights into Two-Dimensional Phases. Industrial & Engineering Chemistry. Product Research and Development. 23 (1984) 245.

27. L. Gupta, D.T. Wasan. Surface Shear Viscosity and Related Properties of Adsorbed Surfactant Films. Industrial & Engeering Chemistry. Fundamentals. 13 (1974) 26.

28. T. van Vliet, A.E.A. de Groot-Mostert, A. Prins. A Constant Stress, Parallel Plate Viscometer Without Bearing for very low Shear Stresses. Journal of Physics E. 14 (1981) 745

29. H.J. Holterman. On the Rheology of Human Saliva and its Substitutes. Thesis, Twente University, the Netherlands (1989)

30. J. Krägel, S. Siegel, R. Miller, M. Born, K.-H. Schano. Measurement of Interfacial Shear Rheological Properties: An Automated Apparatues. Colloids and Surfaces A. 91 (1994) 169

31. H.O. Lee, T. Jiang, K.S. Avramidis. Measurements of Interfacial Shear Viscoelasticity with an Oscillatory Torsional Viscometer. Journal of Colloid and Interfacial Science. 146 (1991) 90

32. S.S. Feng, R.C. MacDonald, B.M. Abraham. An Exact Solution to the Viscoelastic Damping of a Torsion Pendulum by a Surface Film. Langmuir. 7 (1991) 572

33. H.A. Waterman, C. Blom, H.J. Holterman, J. Mellema. Rheological Properties of Human Saliva- A two phase Fluid. Archives Oral Biololy. 33 (1988) 589

34. J.A. de Feijter. The Propagation of Surface Shear waves. I Theory. Journal of Colloid Interface Science. 69 (1979) 375.

35. L.de Bernard. Un Nouveau Type de Viscomètre Superficiel. Méml. Serv. Chim. État (Paris). 41 (1956) 287.

36. M. Sheriff, B. Warburton. Measurement of Dynamic Rheological Properties using the principle of Externally Shifted and Restored Resonance Polymer. 15 (1974) 253.

37. D.J. Burgess, N.O. Sahin. Interfacial Rheology and Tension Properties of Protein Films. Journal of Colloid Interface Science. 189 (1997) 74

38. W. Thomson (Lord Kelvin). Philosophical. Magazine. 42 (1871) 368

39. H. Lamb. Hydrodynamics. Chapter VIII. Dover, New York, (1945)

40. V.G. Levich. Physicochemical Hydrodynamics, Chaper XI. Prentice-Hall, Englewood Cliffs, N.J., (1962)

41.     J. Lucassen. Longitudinal Capillary Waves. I Theory. Transactions of the Faraday Society. <u>64</u> (1968) 2221

42.     J. Lucassen, M. van den Tempel. Dynamic Measurements of Dilational Properties of a Liquid Interface. Chemical Engineering Science <u>27</u> (1972) 1283

43.     J.D. Ferry. Viscoelastic Properties of Liquids. Chapter 1. Wiley, New York, (1970)

44.     A.S. Lodge. Elastic Liquids. Academic Press, New York, (1964) 248

45.     J. Lucassen and M. van den Tempel, Longitudinal Waves on Visco-Elastic Surfaces. Journal of Colloid and Interface Science. <u>41</u> (1972)  491

46.     J. Lucassen and G.T. Barnes, Propagation of Surface Tension Changes over a Surface with Limited Area. Journal of the Chemical Society, Faraday Transactions. <u>68</u> (1972) 2129

47.     R. Wüstneck and H. Fruhner. Zum Scherverhalten unzerstörten Grensflächenstrukturen gespreiter n-Octadecansäuremonoschichten und adsorbierter Gelatineschichten an fluiden Phasengrenzen. Colloid & Polymer Science. <u>259</u> (1981) 1228.

48.     E. Dickinson, S.R. Euston, C.M. Woskett. Competitive Adsorption of Food Macromolecules and Surfactants at the Oil-Water Interface. Progress in Colloid & Polymer Science. <u>82</u> (1990) 65

49.     J. Chen, E. Dickinson. Surface Shear Viscosity and Protein-Surfactant Interactions in mixed Protein Films Adsorbed at the Oil-Water Interface. Food Hydrocolloids. <u>9</u> (1995) 35

50.     D.C. Clark, P.J. Wilde, D.J.M. Bergink-Martens, A.J.J. Kokelaar, A. Prins. Surface Dilational Behaviour of a Mixture of Aqueous β-Lactoglobulin and Tween 20 Solutions. Food Colloids and Polymers: Stability and Mechanical Properties. ed. E. Dickinson (1993) 354

51.     J. Castle, E. Dickinson, B. Murray, G. Stainsby. Mixed-Protein Films Adsorbed at the Oil-Water Interface. ACS Symposium Series No 343. Proteins at Interfaces: Physicochemical and Biochemical Studies. J.L. Brash and T.A. Horbett, ed. (1987).

52.     J.V. Boyd, J.R. Mitchell, L. Irons, P.R. Musselwhite, P. Sherman. The Mechanical Properties of Milk Protein Films Spread at the Air-Water Interface. Journal of Colloid and Interface Science. <u>45</u> (1973) 478.

53.     D.J. Burgess, N.O. Sahin. Interfacial Rheology of Beta-Casein Solutions; Structure and Flow of Surfactant Solutions. ACS Symposium. Series. <u>578</u> (1994) 380

54.     J. Boyd, P. Sherman. Two--Dimemsional Rheological Studies on Surfactant Film Interfaces. Journal of Colloid and Interface Science <u>34</u> (1970) 76

55.     A.A. Trapeznikov, N.N. Loznetsova. Effect of Electrolyte on the Viscoelastic Properties and Aging of Adsorption Layers of Human Serum Albumin at the Air-Water and Heptane-Water Interfaces. Kolloidnyi Zhurnal. <u>47</u> (1985) 553

56. J.B. Peng, G.T. Barnes, B.M. Abraham. The Shear Viscoelastic Properties of Poly(methylmethacrylate) and Poly(vinylstearate) monolayers on Water. Langmuir. 9 (1993) 3574

57. J. Krägel, D. Clark, P. Wilde, R. Miller. Studies of Adsorption and Surface Shear Rheology of Mixed β-lactoglobulin/Surfactant Systems. Progress in Colloid and Polymer Science. 98 (1995) 239

58. J.T. Pearson. The Application of Monolayer Techniques to a Study of Protein-Surfactant Interaction. II. Interactions in Adsorbed Films at the Air/water Interface and in Oil-in-Water Emulsions. Journal of Colloid and Interface Science. 27 (1968) 64

59. F. MacRitchie. Bonding in Protein and Polypeptide Monolayers. Journal of Macromolecular Science and Chemistry. A4 (1970) 1169

60. T. v. Vliet. private communication.

61. J. Mellema. Inleiding in de Dispersie Reologie. in " Inleiding in de Reologie". Kluwers technische boeken B.V. Deventer (1988) 99

62. E.H. Lucassen-Reynders, J. Lucassen. Surface Dilational Viscosity and Energy dissipation. Colloids and Surfaces A. 85 (1994) 211

63. B.S. Murray, E. Dickinson. Interfacial Rheology and the Dynamic Properties of Adsorbed Films of Food Proteins and Surfactants. Food Sci. Technol., Int. 2(3) (1996) 131

64. A.K. Kenzhebekov and V.N. Izmailova, Rheological Properties of Interphase Adsorption Layers of Polymethacrylic Acid on Liquid Boundaries. Influence of Time of Formation on Limiting Shearing Stress of the Interphase Adsorption Layer. Vestn. Moscow Univ. Ser.2 (Khim.) 24 (1983) 277.

65. H. Rehage, M. Veyssié. Two-Dimensional Model Networks. Angewandte Chemie. 29 (1990) 439

66. E. Dickinson, G. Iveson. Adsorbed Films of β-lactoglobulin + Lecithin at the Hydrocarbon-Water and Triglyceride-Water Interfaces. Food Hydrocolloids. 6 (1993) 533

67. A. Prins, A.M.P. Jochems, H.K.A.I. van Kalsbeek, M.E. Wijnen, A. Williams. Skin Formation on Liquid Surfaces under Non-equilibrium Conditions. Progress in Colloid Polymer Science. 100 (1996) 321

68. G.A. van Aken, M.T.E. Merks. Adsorption of Soluble Proteins to Dilating Surfaces. Colloids and Surfaces A. 114 (1996) 221

69. M. Reiner. Deformation and Flow, H.K. Lewis, London, (1949) 170

70. J. Benjamins, E. H. Lucassen Reynders. Surface Dilational Rheology of Proteins Adsorbed at Air/Water and Oil/Water Interfaces. in "Proteins at Liquid Interfaces". D. Möbius and R. Miller, Editors, Elsevier Science, Amsterdam, the Netherlands (1998)

341

71.    E. Dickinson, Y. Matsumura. Time-dependent Polymerization of β-lactoglobulin through Disulphide Bonds at the Oil-Water Interface in Emulsions. International Journal of Biological Macromolecules. $\underline{13}$ (1991) 26

# 6. MODELS FOR THE SURFACE EQUATION OF STATE OF ADSORBED PROTEIN LAYERS AND THE RELATION WITH SURFACE DILATIONAL MODULUS.

## 6.1 Introduction.

Proteins are surface active macromolecules which strongly adsorb at a great variety of interfaces. In the previous chapters it was shown that, at fluid-fluid interfaces, protein adsorption drastically changes the mechanical properties of the interface (interfacial tension, dilational and shear properties), which are thought to strongly affect the formation and stability of emulsions and foams (1).

The present chapter will discuss the 2-D surface equation of state of adsorbed protein layers, i.e the relationship between the surface pressure ($\Pi$) and the surface area per adsorbed molecule ($=1/\Gamma$)) and the temperature. For simple surfactants of low molecular weight, mathematical expressions have been derived, based on the analogy of an adsorbed layer either with a gas of molecules floating on the surface or with a two-dimensional solution of surfactant and solvent. Using the former analogy, equations derived include, e.g., (i) the Henry law for very dilute layers, (ii) the Volmer equation in which the area occupied by the adsorbed molecules is taken into account and (iii) the 2-D-van der Waals equation, which is an extension of the Volmer equation by also accounting for lateral interaction. In contrast, the 2-D solution approach emphasises the analogy between surface pressure and osmotic pressure (2,3). This approach also results in Henry's law at great dilution but, at higher values of $\Pi$, it differs from the gas-type approach: its equation of state corresponds to Langmuir adsorption if the 2-D solution is ideal, and to Frumkin adsorption if there are lateral interactions. All these equations have been derived for equilibrium. Analytical equations of state specifically derived for small surfactant molecules are not applicable to macromolecules (4).

Theoretical models specific for macromolecules are needed in the interpretation of $\Pi(\Gamma)$ curves for adsorbed proteins (see Chapter 2). In a great number of studies (3, 5-9), expressions have been developed which are based on polymer statistics using a quasi-crystalline lattice model and/or a molecular model, usually a flexible linear chain. In most cases, expressions were obtained for the free energy change, $\Delta F$, of the system, caused by the formation of the surface layer (3, 5-9). If $\Delta F$ is known as a function of $\Pi$, A and T, the 2-D equation of state can be immediately obtained. Differences between the various expressions mainly arise from different assumptions about the conformation of the polymer molecules in the surface layer and/or details of the polymer solution theories used.

The applicability of such expressions for adsorbed protein layers is limited, because these models assume flexible chain polymers with a simple structure, the conformation of which is mainly determined by the configurational chain entropy and pair interactions between

176

segments. For more complicated molecules, such as proteins, the conformation is largely determined by a large number of specific (short range) interactions between the various amino acid residues. As a consequence, proteins often have a very compact structure. In principle it is possible account for the forces between the residues, but quantitative elaboration is quite complicated. It also requires detailed information about the composition of the proteins and the nature of the forces. Such information is often not available.

A more phenomenological approach, based on Gibbs surface thermodynamics, is the 2-dimensional solution model. As in the small-molecule case, the surface is considered to be a 2-dimensional mixture of solvent and solute, but now the solute occupies a much larger molecular area than the solvent. Such treatments account to first order for non-ideal entropy of mixing (10,11) or non-zero enthalpy (12) or both (13,14).

Other theories, suitable for compact proteins, assume that the adsorbed molecules behave as a two dimensional fluid of colloidal particles, with the interfacial pressure equal to the pressure of the two-dimensional fluid (15,16,17). By assuming the adsorbed molecules to be deformable, the so-called scaled particle theory was modified into the, rather qualitative, "soft particle model" (18).

In this chapter emphasis will be put on the two-dimensional fluid (soft particle) and the two-dimensional solution approach, because they are phenemenological, i.e. they do not include detailed information of the very complicated molecular conformation and structure. In addition it will be investigated to what extent these models can be used to understand dynamic behaviour of adsorbed protein layers in terms of dilational modulus, $\varepsilon$, vs. interfacial pressure or surface concentration.

6.2 Characteristic features of adsorbed protein layers

The surface behaviour of proteins shows some characteristic features in which they differ from low molecular weight surfactants and more closely resemble synthetic macromolecules.

- Protein adsorption often has a high affinity character, implying that the surface concentration $\Gamma$ is always relatively high, even at very low bulk concentrations (19, Chapter 2). Usually, the adsorption is irreversible or semi-reversible (20,21, Chapter 2 and 3).
- Both for spread and adsorbed monolayers, the $\Pi(\Gamma)$ curve is S-shaped (Chapter 2). For adsorbed layers it was found that $\Pi$ is a unique function of the surface concentration. The $\Pi(\Gamma)$ curve of a protein reflects the flexibility/rigidity of the protein molecule. Main features to classify the proteins on this curve are (i) the minimum surface concentration ($\Gamma_{min}$) where $\Pi$ starts to deviate measurably from zero (ii) the steepness of the increase of the surface pressure upon further increasing the surface concentration. For flexible molecules like $\beta$-casein and PVA, $\Gamma_{min}$ is low and from this point onward the surface

pressure increases gradually with increasing surface concentration. For rigid globular proteins (BSA, ovalbumin and lysozyme), $\Gamma_{min}$ is higher and with a further increase of the surface concentration the surface pressure increases steeply.

- In the low $\Pi$-range, the dilational modulus, $\varepsilon$, is, within experimental error, equal to the limiting modulus $\varepsilon_0$ derived from the $\Pi(\Gamma)$ curve. At higher pressures the measured modulus is often found to be higher than the limiting value, $\varepsilon_0$.
- The initial slope of the $\varepsilon(\Pi)$ curve varies between 5 and 9, depending on protein type. This indicates considerable lateral interaction between adsorbed molecules (Chapter 3).
- At high $\Gamma$, proteins, especially the globular ones, form a strong coherent layer, giving rise to a high surface shear resistance. This is an extra indication for strong lateral interactions (Chapter 5).

6.3 Surface equation of state models derived, for flexible chain polymers, applied to adsorbed layers of PVA and proteins

6.3.1 The Singer equation

Theories on polymer adsorption mainly deal with the conformation of the adsorbed molecules. Less attention has been paid to the effect of macromolecular adsorption on the mechanical properties of fluid surfaces. Using Huggins's method, Singer (6) and Motomura et al. (9) derived an expression for the surface pressure of polymer solutions, assuming that the polymer molecules are adsorbed with all segments in direct contact with the surface. According to these theories, the surface pressure is completely determined by the segments directly adsorbed to the surface. When the number of monomer units per molecule is large, the surface pressure according to Singer is given by :

$$\Pi = \frac{kT}{a_0}\left[\frac{z'}{2}\ln\left(1 - \frac{2\Theta}{z'}\right) - \ln(1 - \Theta)\right] \qquad (1)$$

where $a_0$ is the surface area per surface cell of the two dimensional lattice (i.e. the area per statistical unit of the polymer chain), $z'$ is a number close to the co-ordination number of the lattice and $\Theta$ is the degree of surface coverage (i.e. the ratio of the surface covered by adsorbed segments to the total surface area). This equation also ignores lateral interaction between the segments. Eqn.1 predicts that the surface pressure $\Pi$ increases with $\Theta$ and becomes infinite when $\Theta \to 1$. It is to be expected, therefore, that this equation can only explain the low pressure region of the $\Pi(\Gamma)$ curve, especially because at low $\Gamma$ flexible linear chain molecules are expected to lie flat in the surface. The surface pressure equations derived by Frisch and Simha (7) and Silberberg (8) for the case when loops are formed, are identical with Eqn.1, if $\Theta$ is re-defined as the fraction of the surface occupied by the segments in direct contact with the surface. This is so because they neglect loop-loop interactions.

178

In the low pressure region the dynamic modulus, $|\varepsilon|$ is, for all proteins examined, equal to the limiting modulus, $\varepsilon_0$, derived from the $\Pi(\Gamma)$ curve. When the above-mentioned theories can be applied to proteins, this means that during compression and expansion of the surface, the segments in direct contact with the surface remain adsorbed. This is consistent with purely elastic surface behaviour (phase angle $\phi = 0$), with $|\varepsilon|$ independent of the frequency.

Since $\varepsilon = -d\Pi/d \ln A = d\Pi/d \ln\Theta$ we find from Eqn.1:

$$\varepsilon = \frac{kT}{a_0}\left[\frac{\Theta}{1-\Theta} - \frac{\Theta}{1-2\Theta/z'}\right] \tag{2}$$

With the use of Eqns. 1 and 2 theoretical $\varepsilon(\Pi)$ curves can be determined for different values of $z'$ and $a_0$. In Figure 1 curves are plotted for $z' = 4$ (random chain, cubic lattice) and $a_0$ values ranging from 0.2 to 0.9 nm$^2$. These curves are compared with experimental ones for different proteins and PVA. This comparison indicates good agreement for $\beta$-casein for $z' = 4$ and $a_0 = 0.6$ nm$^2$ per segment. Using these values and $\Gamma_{\Theta=1} = 1.2$ mg/m$^2$ (assumed for full monolayer coverage) the calculated $\Pi(\Gamma)$ curve fits well the experimental one up to $\Pi = 5$mN/m as is illustrated in Figure 2.

Figure 1.
$\varepsilon(\Pi)$ curves (dotted lines) as predicted by the Singer theory (Eqn. 2), compared to $\varepsilon_0(\Pi)$ curves for PVA, $\beta$-casein and BSA ($z' = 4$).
Chosen values of $a_0$ in nm$^2$/segment.
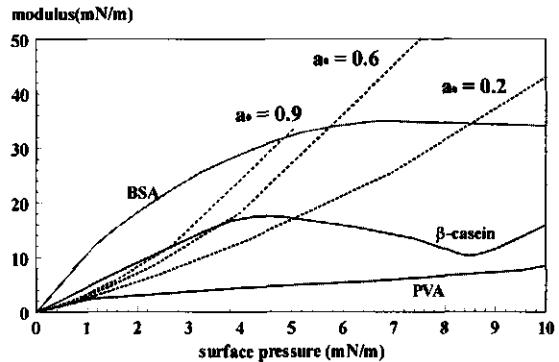


Figure 2.
$\Pi(\Gamma)$ curve of $\beta$-casein (drawn line) compared to calculated curves according to Eqn. 1 (dotted lines).
$z' = 4$



179
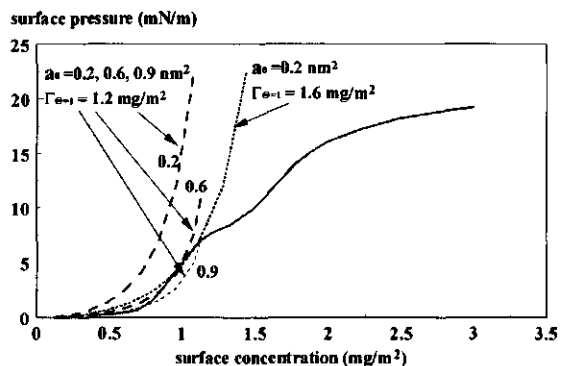
Only in the low pressure range ($\Pi \leq 5$ mN/m) can the Singer equation describe the experimental curve for $\beta$-casein satisfactory for physically realistic values of $z'$, $a_0$ and $\Gamma_{\Theta=1}$. Deviations at higher surface pressures can be ascribed to failure of the theoretical assumptions. From Fig. 1 we must conclude that for PVA, the $\epsilon(\Pi)$ curve according to Singer and the experimental one coincide only up to $\Pi = 1$mN/m. This indicates that the all-train adsorption concept is not realistic. Compared to $\beta$-casein it seems that with this flexible polymer loop formation starts at much lower $\Gamma$. In the case of BSA and ovalbumin it was also not possible to find physically realistic values for the parameters to fit calculated curves according to the Singer equation to the experimental results. This is not unexpected as these rigid globular proteins cannot be treated as flexible polymers, because it is very unlikely for these molecules to adsorb with all segments in direct contact with the surface.

6.3.2. 2-D polymer model with segment-segment interaction

Lateral interactions between segments were accounted for by Saraga and Prigogine (3), Frisch and Simha (7) and de Feijter (5). In the derivation of Saraga it was assumed that the molecules adsorb with all segments in direct contact with the surface. In the derivation of de Feijter loop-loop interaction is neglected and N is defined as the number of segments in an adsorbed train. All authors introduced a Frumkin-type correction into $\Pi$:

$$\Pi = -\frac{kT}{a_0}\left\{\ln(1-\Theta) + (1-\frac{1}{N})\Theta + (1-2m)\chi\,\Theta^2\right\} \qquad (3)$$

where $a_0$ is the area per lattice cell. The last term on the r.h.s. accounts for the lateral interaction between the adsorbed segments, hence the $\chi$ parameter. In this term m is the fraction of nearest neighbour contacts of the lattice cell in the layer. For a close-packed hexagonal lattice m=0.25.

Based on the mean field lattice theory of Scheutjens and Fleer (SF-theory) (22), Fleer derived an analytical expression for the surface equation of state of adsorbed polymers. According to this expression $\Pi$ can be calculated as the sum of the contributions of the successive lattice layers. For polymers, if the concentration profile perpendicular to the interface is known, this equation can be applied successfully. If this information is not available, as in the case of proteins, the applicability of this approach is limited. An equation almost identical to Eqn. 3 can be derived (4) by neglecting loop-loop interactions and making use of an estimation, based on segment distribution as published by Scheutjens and Fleer (22), which indicates that the train segments (first lattice layer) predominantly determine the total surface pressure.

It is interesting to note that Saraga and Prigogine applied Eqn. 3 to relatively small molecules (ethylpalmitate), while in ref. 4 a similar equation is applied to real macromolecules (M=100.000). This indicates that this equation does not require a detailed molecular model, which is an advantage in the case of proteins, where this information is not available. In section

180

6.5 a similar equation, derived for a 2-D solution model on the basis of Gibbsian surface thermodynamics, is applied. For this model no detailed molecular information is required.

Using Eqn. 3. theoretical $\Pi(\Theta)$ curves can be calculated, when an assumption is made about the values of $a_0$, N and $\chi$. For PVA at 23 °C the Flory-Huggins interaction parameter in the bulk solution is $\chi = 0.485$ (23). The high affinity of the PVA implies that the surface is a better (two dimensional) solvent than the aqueous bulk solution. It is therefore to be expected that $\chi < 0.485$. For PVA 205 a comparison is given in Figure 3 between the experimental $\Pi(\Gamma)$ curves and theoretical ones according to Eqn. 3. Only in the low $\Pi$ region (< 5mN/m) and for $\chi = 0$ is a fairly good fit obtained, assuming $\Gamma_{\Theta=1} = 1.5mg/m^2$. As in the case of the Singer equation, deviations at higher surface pressures must be attributed to loop formation, which is in accordance with the generally accepted view on flexible polymer adsorption. For $N \geq 50$, the shape of the theoretical curves becomes insensitive to the value of N. N was equated to 5.7 because this is the mean block length of the acetate groups in PVA 205.

Figure 3.
Comparison between measured and calculated surface equation of statefor PVA. Eqn. 3 with $\chi = 0$ ; $\Gamma_{\Theta=1} = 1.5$ mg/m$^2$; $a_0 = 0.2$nm$^2$/segment or residue
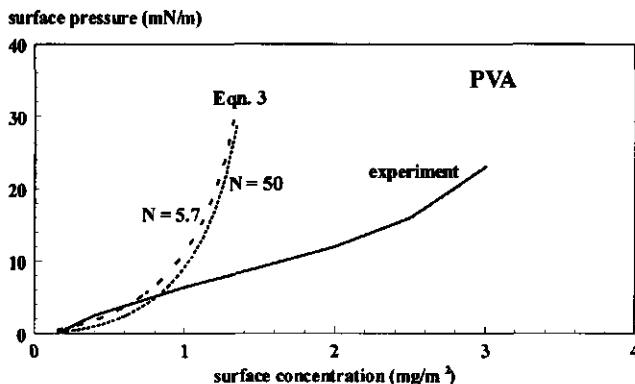


Figure 4.
Comparison between measured and calculated surface equation of state for β-casein. Eqn. 3 with $(1-2m)\chi = 0.55$; $\Gamma_{\Theta=1} = 1.5$ mg/m$^2$; $a_0 = 0.2$nm$^2$/segment or residue
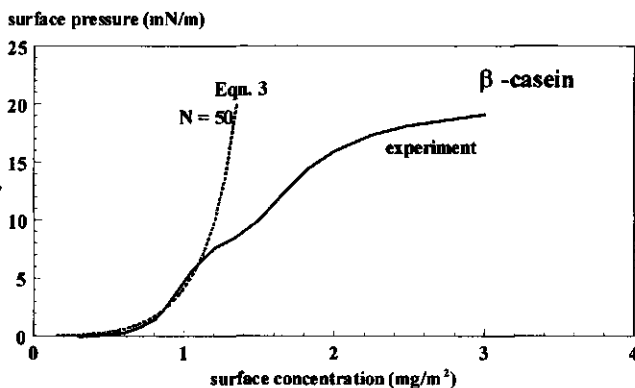


For β-casein Eq.3 fits the experimental $\Pi(\Gamma)$ curve well up to $\Pi = 7$ mN/m. In this case the interaction parameter $\chi$ must be considerably higher, $(1-2m)\chi = 0.55$, which indicates that,

compared to PVA, for β-casein the interfacial layer is a less good solvent. Especially in the case of β-casein the fit is better than in the case of the Singer equation. The rather good fit in the case of β-casein indicates that, at $\Pi< 7$ mN/m, this molecule adsorbs with a constant number of segments in contact with the surface. Within a narrow pressure range ($7<\Pi<10$ mN/m) a conformational change occurs which includes a specific loop formation (24,25). Up to $\Gamma \approx 2$ mg/m$^2$ all extra molecules adsorb in a similar configuration, with a number of aminoacids in loops that increases with increasing $\Gamma$. The decrease of the slope of the $\Pi(\Gamma)$ curve at higher surface concentrations points to more or larger loops or multilayer formation (Chapter 2).

The results of the dilational modulus measurements indicate that this adaptation of the fraction of segments in loops and train is a fast process: in the range where this loop formation is expected to occur, the measured dilational modulus is equal to $\varepsilon_0$, its limiting value. Consequently, loop adaptation occurs well within the time-scale of one compression/expansion cycle.

6.4. Models for Compact Proteins (Hard and Soft Particles )

6.4.1. A two-dimensional liquid theory applied to adsorbed protein layers

In section 6.3.1 and 6.3.2 it was attempted to apply the surface equation of state models, which were developed for flexible molecules, to protein molecules. In such models the molecules are treated as flexible chains, which can interpenetrate. This is unlikely to be true, especially for the rigid globular protein molecules which are more likely to behave as impenetrable particles. Based on this view Bull (16) proposed a surface equation of state for proteins,

$$\Pi\left(a - a_c\right) = kT \qquad (4)$$

where a is the surface area available per molecule, $a_c$ is the co-area of the protein molecules at the interface. This equation is essentially identical to the surface equation of state of dilute, nonideal, "gaseous" monolayers of low molecular weight surfactants, as proposed by Volmer (26). According to Bull, $a_c$ should be equal to the surface area $a_m$ covered by a protein molecule. However, from a more rigorous derivation of the surface pressure of "gaseous" monolayers, as given by Fowler et al. (27) it follows that $a_c = 2\, a_m$. An assumption underlying Eqn.4 is that the macromolecules behave as circular (spherical or disc-like) non-interacting hard-core particles, where $a_m$ is independent of the surface concentration. Then, Eqn.4 predicts that $\Pi a$ should be a linear function of $\Pi$. The validity of the equation is again restricted to low surface concentrations, where $a >> a_c$ (26) and $\Pi \leq 1$ mN/m (16)

For higher surface pressures ($\Pi \geq 1$ mN/m), Eqn. 4 completely breaks down. Instead of an even steeper increase of $\Pi$ with increasing $\Gamma$, the experimental curve shows an S-shape (see Chapter 2). To find an explanation for this S-shaped curve and especially for the inflection point in the $\Pi(\Gamma)$ plots at surface concentration values well below saturated monolayer coverage, de Feijter

and Benjamins (18) introduced the soft particle model. The main modification compared to the particle model of Bull is that the co-area depends on $\Gamma$. It is generally assumed that, both upon adsorption and in spreading, flexible polymer molecules undergo an expansion in the plane of the surface. This effect is most pronounced at low surface concentrations. Qualitatively, the same behaviour is expected for more compact, rigid protein molecules, although to a lesser extent. Hence, adsorbed protein molecules are expected to behave as deformable (or intrinsically "soft") particles, rather than as "hard" particles. The deformability of the particles depends on the number and strength of the intramolecular bonds between the various amino acid residues.

The Soft Particle Model (18) is an attempt to incorporate the deformability of adsorbed protein molecules in a surface equation of state. It is a modification of the scaled particle theory of fluids as put forward by Helfand et al. (17) for non-interacting particles:

$$\Pi = \frac{kT\Gamma}{(1-\Theta)^2} \tag{5}$$

where $\Theta = a_m/a = \pi R^2\Gamma$, with R being the particle radius in the plane of the surface. In this concept the two-dimensional fluid consists of (disk-shaped or spherical) "hard" particles. Like Eqn. 4, this equation predicts a steadily increasing slope of the $\Pi(\Gamma)$ isotherm with increasing surface coverage as illustrated in Figure 5 . In this figure the measured $\Pi(\Gamma)$ curve for BSA is compared with the theoretical curves according to Eqn. 5, using two (constant) radii: R=4.1 nm, calculated from the saturation adsorption value (assumed at 2mg/m$^2$) and R=5.6 nm, the plateau value for BSA given in Figure 6.

Figure 5
The surface equation of state for adsorbed
BSA at the air/water interface
Solid line: experimental curve.
Dotted lines: curve according to Eqn.5



surface pressure (mN/m)

Adsorption (mg/m $^2$)
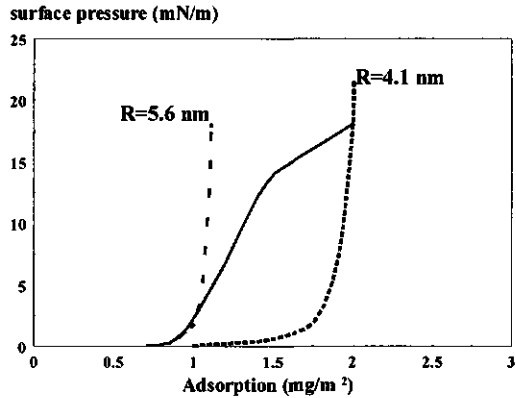
By dropping the condition that R is constant, which is of course not consistent with the assumptions underlying Eqn.5, this equation "predicts" that the $\Pi(\Gamma)$ isotherm may become S-shaped when R decreases with increasing surface concentration. This is not unrealistic, because macromolecules are likely to expand upon adsorption at low $\Pi$. The procedure for the calculation of R as a function of $\Gamma$, assuming Eqn. 5 to be valid, is as follows: first, the experimental values of $\Pi$ and $\Gamma$ are inserted into Eqn. 5 to calculate the concomitant surface

183

coverage $\Theta$. The particle radius R is then obtained from the surface coverage using $\Theta = \pi R^2 \Gamma$. In Fig.6 for BSA and β-casein the calculated R and $\Theta$ are plotted vs. the surface concentration. These curves illustrate that, to obtain complete agreement with Eqn. 5, the particle size must considerably increase with decreasing $\Pi$ and $\Gamma$. For BSA, R does not seem to further increase with decreasing $\Gamma$ for $\Gamma < 1.1$ mg/m$^2$. A constant R below a certain $\Gamma$ was also observed for ovalbumin and lysozyme, which are also rigid globular molecules. This is in agreement with Bull's finding that, for globular proteins at low surface pressure, the $\Pi$(A) isotherm is often well described by Eq. 4, as based on the assumption that R is constant (see above). For β-casein (Fig.6) it seems that up to the lowest $\Gamma$ value considered ($\Gamma \approx 0.25$ mg/m$^2$), R continuously decreases with increasing surface concentration.
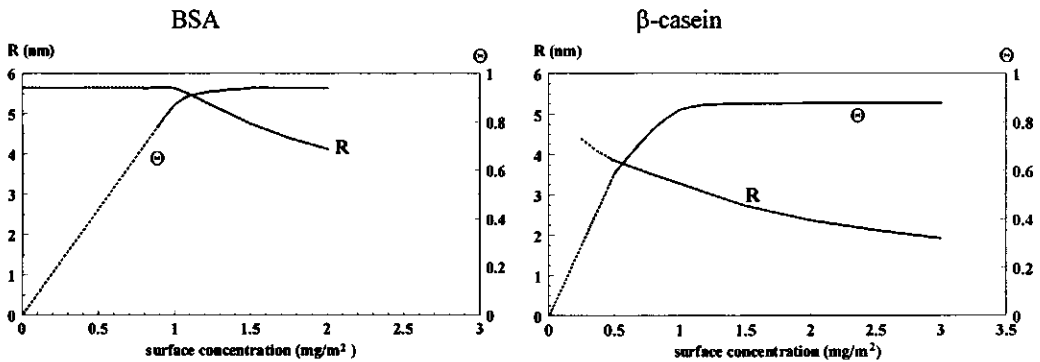


Figure 6
Particle radius, R, and surface coverage, $\Theta$, as a function of the surface concentration, $\Gamma$.

In Table 1 the calculated changes of R with increasing $\Gamma$ are collected for the different proteins. In this table $R_{max}$ is chosen at $\Gamma \approx 1$ mg/m$^2$, for lower $\Gamma$ values the $\Pi$ values are not sufficiently accurate. For $\Gamma$ values above monolayer coverage, the calculated value for R has no well-defined physical meaning. Therefore $R_{min}$ is calculated for $\Gamma$ values which are the best estimates (based on adsorbed amount and layer thickness) for monolayer coverage.

As expected, the ratio $R_{max}/R_{min}$ (see table 1) decreases with increasing rigidity of the protein molecule. An interesting point is that, according the calculated curves in Fig.6, the surface layer is practically fully occupied ($\Theta \geq 0.90$) for $\Pi \geq 5$ mN/m, with $\Theta$ being virtually independent of $\Gamma$. This would mean that, at higher surface pressures, an increase of the surface concentration $\Gamma$ would not give rise to a higher surface coverage, as expected for "hard" particles, but results in a contraction of the adsorbed protein molecule. It seems realistic that a flexible protein molecule such as β-casein may change its shape more drastically than a globular protein, such as ovalbumin.

184

Table 1. The changes of R, the radius of the adsorbed protein molecule, with increasing surface concentration.

| Protein type | $R_{max}$ nm ($\Gamma$,mg/m$^2$) | | $R_{min}$ nm ($\Gamma$,mg/m$^2$) | | $R_{max}/R_{min}$ |
|---|---|---|---|---|---|
| β-casein | 3.3 | (1.0) | 1.9 | (3.0) | 1.7 |
| BSA | 5.6 | (1.0) | 4.1 | (2.0) | 1.4 |
| ovalbumin | 4.2 | (1.0) | 3.2 | (2.1) | 1.3 |
| lysozyme | 2.1 | (1.3) | 1.9 | (1.8) | 1.1 |
| PVA 205 | 4.5 | (1.0) | 2.6 | (3.0) | 1.7 |

Even quantitatively, the calculated decrease of R with increasing $\Gamma$, for the different protein molecules seems to be realistic. Especially the finding that, over the surface concentration range, the change of R decreases with increasing rigidity of the molecule supports the conclusion that the "Soft Particle" approach is very promising. However, it must be realised that these promising results were obtained according to a method that is not completely consistent. The main inconsistency is that Eqn. 5, which is derived for "hard" particles, is applied to particles that are intrinsically "soft". Another point of concern is that at high surface concentration Eqn. 5 overestimates $\Theta$: it predicts that $\Pi\rightarrow\infty$ for $\Theta\rightarrow1$, whereas for a (hexagonally packed) monolayer of (monodisperse, circular) particles, the maximum value of $\Theta = 0.907$. Therefore, the particle radii, as calculated with Eqn.5, represent the "equivalent hard-core radii" of the protein molecules: they are not necessarily equal to the actual particle radii. Moreover, Eqn. 5 completely neglects any effect of molecular interactions on the surface pressure and, hence, on the calculated radius.

It must be noted that the decrease of the effective particle radii with increasing surface concentration cannot be ascribed to a compression of the electrical double layer of the protein molecules: for ovalbumin, $\Pi(\Gamma)$ curves at pH = 6.7 and pH = 4.6 (isoelectric point) were found to coincide.

Despite the inconsistency the soft particle concept provides a useful basis for the understanding of the surface behaviour of complicated macromolecules, such as proteins. This concept for compact macromolecules complements the "flexible chain" concept for flexible polymers.

6.4.2. The soft particle model applied to surface dilational properties

It this section it will be shown what the soft particle model predicts about the surface dilational properties. We consider the situation where a periodical dilational deformation is imposed on a surface at equilibrium, where $\Pi$ is completely determined by $\Gamma$. For not extremely low frequencies, no adsorption or desorption occurs during a compression/expansion cycle (Chapter 3). Then we have for the surface dilational modulus, $\varepsilon$, (= Eqn. 2, Chapter 3):

$$\varepsilon = d\Pi / d\ln\Gamma \qquad (6)$$

In the absence of information about the mechanical properties of the protein molecules, and consequently about the rate of reconformation, we consider two extreme cases: a) the rate of reconformation is much faster, and b) the rate of reconformation is much slower than the rate of surface deformation.

The first case a) is the more simple: it can be expected to applie at sufficiently low frequencies of the surface deformation, where the conformation is always in complete equilibrium with the surface concentration. The surface dilational modulus can then simply be calculated from the equilibrium $\Pi(\Gamma)$ curve using Eqn.6. The modulus obtained in this way is called the limiting modulus $\varepsilon_0$, which represents the minimum value of $\varepsilon$ that can be obtained in a dynamic experiment, provided no adsorption or desorption takes place. Because $\varepsilon_0$ can directly be obtained from equilibrium $\Pi(\Gamma)$ curve, it is independent of the frequency and is also model independent.

The second case b) is expected to be valid at very high frequencies of the surface deformation, where the cycle time is much shorter than the relaxation time of the reconformation process. In that case, reconformation does not occur at all. Or, in terms of the present theory; the particle radius R remains constant. Combination Eqns.5 and 6, using $\Theta = \Gamma a_m$ ,gives:

$$\varepsilon = \Pi\left[1 + \frac{2\Gamma}{(1-\Theta)}\left(a_m + \Gamma\frac{da_m}{d\Gamma}\right)\right] \tag{7}$$

For $a_m$ = constant (R= constant) this reduces to:

$$\varepsilon_{max} = \Pi\left[1 + \frac{2\Theta}{1-\Theta}\right] \tag{8}$$

$\varepsilon_{max}$ is the maximum value of the dynamic dilational modulus that can be attained. According to Eq.8 it is a function of $\Pi$ and $\theta$ only, where $\Pi$ and $\theta$ are the equilibrium values of the surface pressure and the surface coverage, respectively. This implies that, by analogy to the limiting modulus, $\varepsilon_{max}$ is independent of the frequency of the deformation cycle. Hence, both at very high and very low frequencies, the surface of the protein solution should be purely elastic, with $\varepsilon = |\varepsilon| = \varepsilon'$ and $\varepsilon'' = 0$ and $\phi = 0$. Because for the derivation of Eqn.8 we made use of Eqn.5, which is model dependent, also $\varepsilon_{max}$ is model dependent.

Fig.7 shows $\varepsilon_{max}$ and $\varepsilon_0$ as a function of $\Gamma$ for BSA. The $\varepsilon_0(\Gamma)$ curve has a maximum of ~ 35 mN/m at $\Gamma = 1.3$ mg/m$^2$ (Chapter 3); it is caused by the S-shape of the $\Pi(\Gamma)$ curve. The low pressure part of the $\varepsilon_{max}(\Gamma)$ curve almost coincides with the $\varepsilon_0$ curve. At $\Gamma \approx 1$ mg/m$^2$ $\varepsilon_{max}$ steeply increases until at 2 mg/m$^2$ the maximum calculated value of about 550 mN/m is reached (not shown). Figure 7 also shows the experimental values of the dilational modulus $|\varepsilon|$ as a function of $\Gamma$, for two angular frequencies $\omega$ (for details see Chapter 3). It is seen that over the entire $\Gamma$-range considered, $\varepsilon_0 \leq |\varepsilon| \leq \varepsilon_{max}$ as required by theory. An interesting point is that up to $\Gamma \approx 1$ mg/m$^2$ we have: $\varepsilon_0 = |\varepsilon| = \varepsilon_{max}$ and also $\phi = 0$ (elastic behaviour). This is also in complete agreement with theory. The physical reason is that, according to the present theory,

186

the conformation of the BSA molecules (i.e. the particle radius R) is independent of the surface concentration for $\Gamma \le 1$ mg/m$^2$ (see Fig.6). Hence, in this $\Gamma$-range, the dynamic dilational modulus of BSA must be independent of the frequency. For higher surface concentrations, the surface behaves visco-elastically (Chapter 3), with $|\varepsilon|$ increasing and $\phi$ decreasing with increasing angular frequency. This means that in this $\Gamma$-range, the relaxation time of the reconformation process is of the same order of magnitude as the period of the surface deformation, which for the frequencies used ranges from 7 to 70 s.

Figure 7.
Calculated, $\varepsilon_{max}$ and $\varepsilon_0$, and measured dilational moduli as a function of the surface concentration.
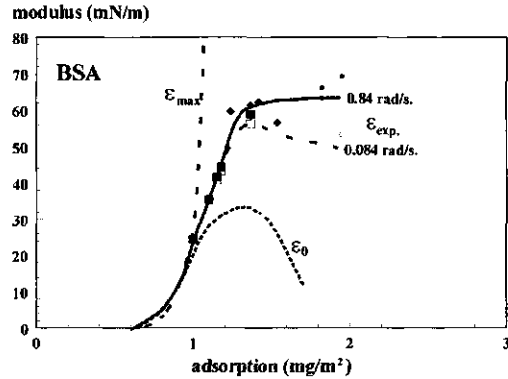


From Table 2 it can be seen that the inequality $\varepsilon_0 \le |\varepsilon| \le \varepsilon_{max}$ holds for all proteins. However, we do not find the equality of $\varepsilon_{exp}$ and $\varepsilon_{max}$ required by the zero phase angle measured (13). The reason for this may be that intermolecular interactions were ignored in Eqns. 5 and 8.

Table 2. Comparison between $\varepsilon_{max}$, $\varepsilon_0$ and $\varepsilon_{exp}$ for $\Gamma = 1.2$ mg/m$^2$

| Protein type | $\varepsilon_0$ (mN/m) | $\varepsilon_{exp}$ (mN/m) | $\varepsilon_{max}$ (mN/m) |
|---|---|---|---|
| β-casein | 12 | 18 | 112 |
| BSA | 32 | 48 | 168 |
| ovalbumin | 38 | 40 | 123 |
| PVA 205 | 7 | 7 | 147 |

Summarising, the characteristic features of the surface equation of state and the surface dilational properties of compact proteins are qualitatively but not quantitatively explained by the "soft particle" concept. However, there is reason for a more systematic incorporation of this idea in phenomenological models, since the S-shape of the $\Pi(\Gamma)$ curve is not explained by any current model.

187

6.5. Thermodynamic model for a two-dimensional solution.


Surface non-ideality of macromolecular systems is caused by a combination of non-ideal entropy and by non-zero enthalpy resulting from molecular interactions. Several theories deal with the entropy aspect, either in statistical-mechanical treatments (6,7,22,28) or in a thermodynamic theory for a two-dimensional solution (10,11), but less attention has been paid to the enthalpy. The 2-D solution model is a phenomenological approach to the surface equation of state, which is formulated regardless of molecular structure in the surface or interfacial region (For a recent review see 29). The equation of state proposed by Fainerman et al. (12), in which a protein can occupy a number of configurations with different molecular areas, does account for enthalpy of mixing of the average configuration with the solvent by a Frumkin-type expression, but considers the non-ideal entropy to be negligible.

The surface equation of state of which the applicability to adsorbed protein layers is discussed below, was derived on the basis of a 2-D-solution treatment applied to a Gibbs dividing surface defined so as to account for the presence of solvent (13,14). This model, in which Butler's expression (30) is used for the surface force field term, accounts for both entropy and enthalpy to first order. A protein molecule is assumed to be present with only one molecular area, $\omega_2$. In such a simple version, the surface pressure $\Pi$ depends on the degree of surface coverage $\Theta(=\omega_2\Gamma_2)$ according to

$$\frac{\Pi\omega_1}{RT} = -\ln(1-\Theta)-(1-1/S)\Theta - \frac{H}{RT}\Theta^2 \qquad (9)$$

where $\omega_1$ is the molar area of the solvent, S $(=\omega_2/\omega_1)$ is the factor by which the protein's molar area exceeds that of the solvent, and $H\Theta^2$ is the partial molar heat of mixing in the Frumkin model. Positive values of H represent a lack of attraction between unlike molecules in comparison to the attraction between the like molecules. The first term in Eqn. 9 is the ideal contribution to $\Pi$, the second term is related to the non-ideal entropy of a mixture of small and large molecules and the third term is the lateral interaction contribution. At this stage it is interesting to point to the similarity between Eqn. 9 and the equation derived by Fleer (4) which has the same form as Eqn. 4 (see 6.3.2). Although these equations are derived according to very different routes (thermodynamic vs statistical) there is a striking resemblance, only some of the parameters have a different meaning.

Figure 8 illustrates the pressure vs. adsorption isotherms for three cases representative of (i) ideal mixing, (ii) non-ideal entropy and (iii) non-ideal entropy combined with heat of mixing. Both the non-ideal entropy and the non-zero enthalpy are seen to depress the surface pressure at all surface coverages. The combination of the two effects, in particular, results in very low pressures at low surface coverage: for a value of 30 mN/m for $RT/\omega_1$ (S=10, H=0.8RT), the surface pressure is only 0.3 mN/m at a relatively high surface coverage of 25%. According to this model, the limiting modulus $\varepsilon_0$ is given by

$$\frac{\varepsilon_0 \omega_1}{RT} = -\frac{\Theta}{1-\Theta} - (1-1/S)\Theta - \frac{2H}{RT}\Theta^2 \qquad (10)$$

The effect of the entropic and enthalpic contributions on the modulus vs. pressure relationship is shown in Figure 10. Interestingly, it is only the combination of entropy and enthalpy that produces a steep linear ascent of the modulus at moderately high surface coverage. The slope here is very nearly equal to the slope at 50% coverage:

$$\frac{d\varepsilon_0}{d\Pi} = \frac{3+1/S-2H/RT}{1+1/S-H/RT} \qquad \text{at } \Theta = 0.5 \qquad (11)$$

So, at half coverage, the ideal mixture, with S=1 and H=0, is unable to produce a slope higher than +2, non-ideal entropy on its own can increase the slope to at most +3, but the combination of entropy and enthalpy can produce much higher slopes, e.g., +5 in the example of Figure 10 and even higher values for higher H.

Figure 9.
Effects of non-ideal entropy and enthalpy on surface pressure vs. surface coverage according to Eqn.9
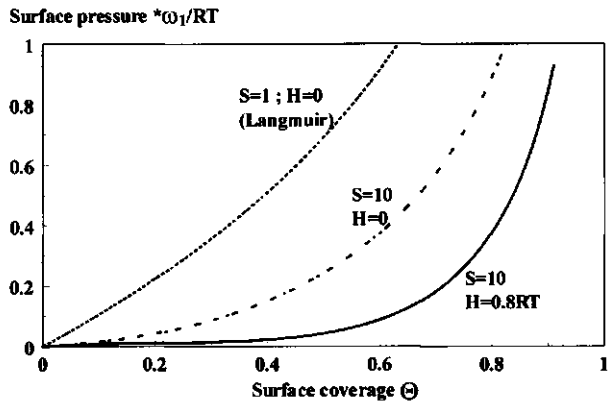


Figure 10.
Effects of non-ideal entropy and enthalpy on limiting modulus vs. surface pressure according to Eqn.10
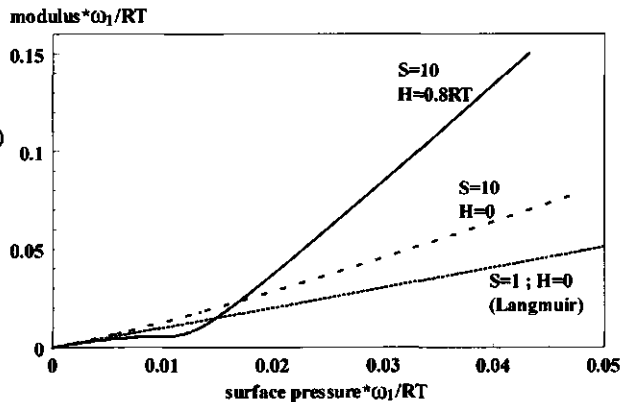


Such high values come close to the experimental results as shown in Chapter 3 (Fig. 9) and 4 (Figs. 8-10) and we propose that values of this level are indicative of enthalpy of mixing caused by intermolecular interactions in the surface (13,14). In these chapters, the initial slope of the

189

$\varepsilon_0(\Pi)$ curve for adsorbed protein layers was found to range between 2 and 9, depending on protein type and type of interface. This is significantly higher than +1, the predicted value if the surface equation of state of the adsorbed layer can be described according to the two-dimensional analogue of the ideal-gas law. In fact, most analytical equations of state reduce, at very low surface concentrations, to this two-dimensional ideal-gas law. The high values of the initial slope indicate considerable non-ideality at very low surface pressures, which reduces the range where $d\varepsilon/d\Pi=1$ to the point of invisibility. Such non-ideality, of course, is also apparent from the quite high surface concentrations needed to produce any measurable surface pressure.

In the purely-elastic range, i.e. at not too high surface pressures, $\varepsilon$ equals the limiting value $\varepsilon_0$ defined in Eqn. 6. This identity is found to persist reasonably well up to $\Pi$ values of 15 mN/m for the caseins, and over a smaller range of $\Pi$ for the globular molecules. (Fig.9, Chapter 3). Consequently, in this range, the dynamic behaviour is dominated by the surface equation of state. This observation is supported by the finding that, as illustrated in Figure 12 in Chapter 4, Eqns. 9 and 10 quite well describe a large range of the experimental data for ovalbumin at the three interfaces. The required value of the enthalpy H to describe the experimental curve depends on the interface and is 0.84RT for air/water, 0.45RT for tetradecane/water and 0 for triacylglycerol/water. The value for S used in the theoretical curves is 245 for all interfaces. If we assume that $\omega_1$ is 0.2 nm$^2$, this value agrees rather well with estimates based on independent information about molecular dimensions: from $\Gamma^\infty$ (close-packed layer of spherical molecules), $\omega_2=37$ nm$^2$ and S=185; from the hydrodynamic radius, $\omega_2=27$ nm$^2$ and S=135; from the radius that is derived with the use of the soft particle model (section 6.4), $\omega_2=55$ nm$^2$ and S=270. Especially this latter agrees surprisingly well with the fitted value of 245.



Figure 11.
Experimental results of $\Pi(\Gamma)$ for ovalbumin.
Theoretical curve for $\omega_1=0.2$ nm$^2$ and $\omega_2=49$ nm$^2$; H=0.84RT.
Different symbols indicate different concentrations in the bulk solution.
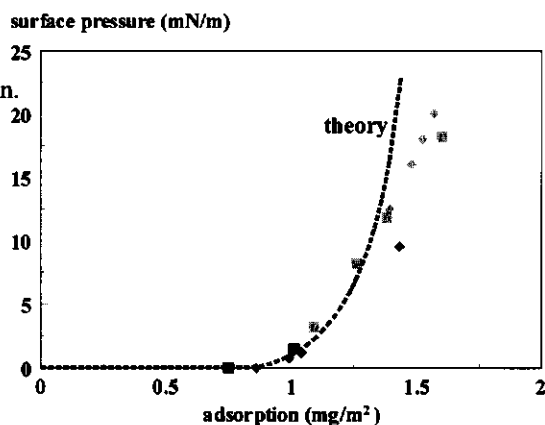
At the air/water interface, using the mentioned values for S and H , Eqn. 9 describes the experimental data ($\Pi(\Gamma)$) up to surface concentrations of 1.3 mg/m$^2$ fairly good (see Fig.11). These values of S and H are found to produce phase separation in the surface and a very steep increase of $\varepsilon_0$ at near-zero $\Pi$ (31). Finally, at high adsorptions all reasonably simple current

190

models predict that, in the absence of phase separation in the surface, both $\Pi$ and the slope $d\Pi/d\Gamma$ and also $\varepsilon$ should steadily increase with increasing surface coverage (Fig's 2,3,4,5,9,10). In this respect, all theories seriously overestimate the surface pressure since nearly all measured $\Pi(\Gamma)$ curves (see Fig. 10, Chapter 3) show a decreasing slope at high $\Gamma$. Such flattening off has been attributed qualitatively to the onset of collapse (or multilayer formation), which is a phase separation phenomenon. Since there are no abrupt changes, this should probably have to be a second-order phase transition rather than the first-order transition known for collapsed monolayers of smaller molecules, e.g., long-chain fatty acids. The explanation according to the "Soft Particle" model (see 6.4 and ref. 32) is that, in fairly close-packed layers, protein molecules undergo a reconformation into a modification with a smaller molecular area. This would imply that, at increasing $\Gamma$, the area fraction covered by the protein can remain almost constant as the molecules become increasingly more compressed and, as a result, $\Pi$ can also become almost constant.

The basic idea of the soft particle concept can be incorporated into the two-dimensional solution model. By introducing a so-called molecular compressibility (31), it seems possible to extend the validity range of the two dimensional solution approach to higher $\Pi$ and $\Gamma$ values. This modification means that from a certain $\Pi$ (=$\Pi$crit.) the area per protein molecule ($\omega_2$) decreases with increasing $\Pi$. As can be seen from Eqns. 9 and 10 this will cause a flattening off of both the $\Pi(\Gamma)$ and the $\varepsilon(\Pi)$ curve.

The two dimensional solution approach does not require detailed structural and conformational information about adsorbed molecules. Compared to the statistical mechanical treatments, this is an advantage in the case of proteins, because for these molecules such information is not available. In principle the S and H values can be obtained by finding the optimal fit of the experimental $\Pi(\Gamma)$ and $\varepsilon(\Pi)$ curves. However, independent information about the value of S can also be obtained from molecular packing at saturated monolayer adsorption or hydrodynamic radius (see above). The value of S does not need to be known very accurately, because, as can be seen from (31) the effect of S on the results is small for S>100.

6.6 Concluding remarks

It is obvious that even in the case of the polymer PVA and the random chain molecule $\beta$-casein the over-simplified statistical models only explain the very low pressure part of the experimental curves. To explain the higher pressure part progressive loop formation, and consequently decrease of molecular area, must be accounted for. The decrease of the slope of the $\Pi(\Gamma)$ curve at higher surface concentrations points to more or larger loops to increase the interaction or multilayer formation (Chapter 2).

The simplified statistical models are unable to fit any part of the experimental curves for the rigid globular molecules. This is not surprising as these molecules do not behave as random chain molecules. Upon adsorption they only slightly change their conformation as can be deduced from the thickness of the adsorbed layer (Chapter 2).

Starting with the basic assumptions that the molecular cross-sectional area decreases with increasing surface concentration and that the surface pressure can be described by the surface equation of state of a 2-D hard sphere fluid of non-interacting particles, the Soft Particle concept suggests that (i) the surface is practically fully occupied ($\Theta \geq 0.90$) as soon as the surface pressure exceeds a few mN/m, and (ii) flexible molecules like $\beta$-casein and PVA may change their shapes more drastically than the globular proteins BSA, ovalbumin and lysozyme. For $\beta$-casein and PVA this is in line with the predicted progressive loop formation predicted by the statistical models.

The experimental curves of the $\varepsilon(\Gamma)$ curves coincide with the two calculated curves for $\Gamma \leq 1$ mg/m$^2$. For higher surface concentrations, in the viscoelastic range, the measured curves are in between the two extremes: $\varepsilon_{max}$ (high frequency, no area relaxation of the molecule) and $\varepsilon_0$ (complete relaxation).

A 2-D solution model was proposed, which is able to account for the non ideal behaviour of adsorbed protein layers, deduced from (i) the high $\Gamma$ needed to produce a measurable surface pressure and (ii) the steep initial slopes of the $\varepsilon$ vs. $\Pi$ curves. The parameters in Eqn 9 to fit the experimental curves at different interfaces (air/water vs. oil/water), especially H, seem, with respect to the ranking order, to be realistic.

The two dimensional solution approach does not require detailed conformational information. This is an advantage in the case of proteins for which this information is not available.

The main deviation between the experimental $\Pi(\Gamma)$ curve and the curves according to the mathematical models described in this chapter is at higher $\Pi/\Gamma$ values. In this $\Gamma$-range the increase of $\Pi$ with increasing $\Gamma$ flattens off (S-shape), while in principle all models predict an even steeper increase. Even in case of the Soft Particle model the S-shape is not predicted but only explained as a result of a decrease of molecular area with increasing $\Pi$. Introduction of a molecular compressibility into for instance the 2-D solution model is also an option to further extend its validity range.

6.7 References.

1. E.H. Lucassen-Reynders. Dynamic Interfacial Properties and Emulsification. The Encyclopedia of Emulsion Technology, Volume 4, P. Becher, ed. (1996)
2. E.H. Lucassen-Reynders, M. van den Tempel, "Surface Equation of State for Adsorbed Surfactants", Proceedings IVth International Congress on Surface Active Substances, II, Brussels, (1964) 779
3. L.T.M. Saraga, I. Prigogine. Surface solutions of long chain molecules. Mem. Services Chim. Etat. 38 (1953) 109
4. J. Lyklema. Fundamentals of Interface and Colloid Science III.3. Academic Press, London (2000)
5. J.A. de Feijter. Unpublished results (1984)
6. S.J. Singer. Note on an Equation of State for Linear Macromolecules in Monolayers. Journal of Chemical Physics. 16 (1948) 872
7. H.L. Frisch, R. Simha. Monolayers of Linear Macromolecules. Journal of Chemical Physics. 24 (1956) 652
8. A. Silberberg. Theoretical Aspects of the Adsorption of Macromelecules. Journal of Polymer Science. 30 (1970) 393
9. K. Motomura, R. Matuura. An Equation of State for Linear Polymer Monolayers. Journal of Colloid and Interface Science. 18 (1963) 52
10. P. Joos. Approach for an Equation of State for Adsorbed Protein Surfaces. Biochemica et Biophysica Acta. 375 (1975) 1
11. E.H. Lucassen-Reynders. Competitive adsorption of emulsifiers. Colloids and Surfaces. 91 (1994) 79
12. V.B. Fainerman, R. Miller and R. Wustneck, Adsorption of Proteins at Liquid/Fluid Interfaces. Journal of Colloid and Interface Science. 183 (1996) 26
13. J. Benjamins, E.H. Lucassen-Reynders. in "Proteins at Liquid Interfaces", D. Mobius and R. Miller, Editors, Elsevier Science, Amsterdam, the Netherlands (1998) 341
14. E.H. Lucassen-Reynders and J. Benjamins. Dilational Rheology of Proteins Adsorbed at Fluid Interfaces. in E. Dickinson and J. Rodríguez Patino (Editors), Food Emulsions and Foams: Interfaces, Interactions & Stability, Special Publication No. 227, p 195-206 (Royal Society of Chemistry, London, 1999)
15. A. Doroskowski, R. Lambourne. Journal of Colloid and Interface Science. 43 (1973) 97
16. H.B. Bull. Determination of molecular weights of proteins in spread monolayers. Journal of Biological Chemistry. 185 (1950) 27
17. E. Helfand, H.L. Frisch, J.L. Lebowitz. Theory of Two- and One-Dimensional Rigid Sphere Fluids. Journal of Chemical Physics. 34 (1961) 1037

18. J.A. de Feijter, J. Benjamins. Soft-Particle Model of Compact Macromolecules at Interfaces. Journal of Colloid and Interface Science. 90 (1982) 289

19. W. Norde. Adsorption of Protein from Solution at the Solid-Liquid Interface. Advances in Colloid and Interface Science. 25 (1986) 267

20. J.C. Dijt, M.A. Cohen Stuart, G.J. Fleer. Kinetics of Polymer Adsorption and Desorption in Capillary-flow. Macromolecules. 25 (1993) 5416

21. C.A. Haynes, W. Norde. Structures and Stabilities of Adsorbed Proteins. Journal of Colloid and Interface Science. 169 (1995) 313

22. J.M.H.M. Scheutjens, G.J. Fleer. Statistical Theory of the Adsorption of Interacting Chain Molecules.1. Partition Function, Segment Density Distribution, and Adsorption Isotherms. Journal of Physical Chemistry. 83 (1979) 1619

23. G.J. Fleer. Thesis, Wageningen, the Netherlands (1971)

24. D.E. Graham, M.C. Phillips. Proteins at Liquid Interfaces; IV. Dilational Properties. Journal of Colloid Interface Science. 76 (1980) 227

25. J. Leaver, D.G. Dalgleish. Variations in the Binding of β-casein to Oil-Water Interfaces Detected by Trypsin-Catalysed Hydrolysis. Journal of Colloid Interface Science. 149 (1992) 49

26. M. Volmer. Thermodynamische Folgerungen aus der Zustandsgleichung für adsorbierte Stoffe. Zeitschrift.-Physikal Chemie. 115 (1925) 253

27. R.H. Fowler. E.A. Guggenheim. Statistical Thermodynamics. Chapter 10, University Press, Cambridge (1939)

28. M.A. Cohen Stuart, G.J. Fleer and J.M.H.M. Scheutjens, Displacement of Polymers 1, Theory. Segmental Adsorption Energy from Polymer Desorption in Binary Solvents. Journal of Colloid Interface Science. 97 (1984) 515

29. V.B. Fainerman, E.H. Lucassen-Reynders, R. Miller, Colloids and Surfaces A. 143 (1998) 141

30. J.A.V. Butler, Proceedings of the Royal Society, Series A. 138 (1932) 348

31. E.H. Lucassen-Reynders and J. Benjamins. To be published

32. G.A. van Aken, A Phenomenological Model for the Dynamic Interfacial Behaviour of Adsorbed Protein Layers. Special Publication of the Royal Society of Chemistry (E. Dickinson, D. Lorient, Eds.). 156(1995) 43

# 7. EFFECTS OF INTERFACIAL PROPERTIES ON FORMATION AND STABILITY OF EMULSIONS AND FOAMS CONTAINING PROTEINS

## 7.1 Introduction

The previous chapters described the results of a detailed investigation into the static and dynamic interfacial properties of protein layers. These properties include adsorption, adsorption rate, interfacial tension, dilational and shear modulus. Interfacial tension and dilational modulus were not only measured at air/water, but also at triacylglycerol-oil/water and tetradecane/water interfaces. The present chapter will indicate, first, how surfaces containing proteins differ from those with low molecular weight surfactants and, second, how these differences work out in foaming and emulsification. In the previous chapters it was also found that each protein has specific interfacial properties. This specificity is reflected in the formation and stability of emulsions and foams.

## 7.2 Functions of surfactants in emulsions and foams.

The basic functions of surface active materials used as emulsifiers or foaming agents are (i) to help to make drops or bubbles small and (ii) to keep them small. The latter function requires short-term stabilisation of the emulsion/foam during emulsification/foaming and long-term stabilisation afterwards.

Emulsification can be defined as a process leading to the break-up of large drops of one liquid in another, with which it is immiscible, leading to an average drop size in the 0.2 to (roughly) 100 μm range. (For foaming, the definition is similar but bubble sizes are generally larger). Deformation and break-up of a drop occur when the stress exerted on the drop by the flow is high enough to overcome the Laplace pressure. The ratio of these opposing stresses is known as the capillary number (Ca), defined by Eqn. 1 if the flow is laminar (1,2):

$$Ca = \frac{\eta_c S_r R}{\gamma} \qquad (1)$$

where $\eta_c$ is the viscosity of the continuous phase, $S_r$ is the rate of shear , R is the drop radius and γ is the interfacial tension. If the capillary number exceeds a critical value, $Ca_{cr}$, the drop will break up into two or more droplets. Numerical values of $Ca_{cr}$ cannot be predicted by simple hydrodynamic theory. Experimentally, e.g. by flow visualization, $Ca_{cr}$ is found to depend on the type of flow and on the viscosity ratio of the two liquids. The latter dependence can be fairly complex; e.g. in simple shear break-up is easiest if the viscosity ratio is roughly 1, but impossible if it exceeds a value of 4 (1,2).

From Eqn. 1 it can be seen that, at a given shear force, emulsifiers promote break-up because they adsorb at the liquid-liquid interface and, consequently, lower the interfacial tension. However, an even more essential role of emulsifiers is their stabilizing function through which recoalescence of the newly formed droplets is retarded. The reason is that during emulsification the flow of liquid along the interface can produce gradients in the surface concentration of emulsifiers, and hence gradients in interfacial tension (3,4). These gradients, in turn, make the interface resist tangential stresses from the adjoining flowing liquids, e.g. exerted by the liquid flow out of the film between two approaching droplets (5). The result is that this liquid flow will be retarded significantly, which gives more time for extra adsorption to build a more permanent stabilizing interface. Gradients in interfacial tension can be expressed in terms of the dilational modulus, $\varepsilon$, which in general has an elastic and a viscous component (see Chapters 3 and 4). Thus, the visco-elastic properties of the adsorbed interfacial layer are related to the stability of the liquid film between newly formed droplets.

These visco-elastic properties will also affect the long term stability of emulsions and foams. At this stage additional effects come into play, e.g. electrostatic and steric repulsion between adsorbed layers.

An important long-term destabilising mechanism is Ostwald ripening or disproportionation, according to which smaller bubbles or drops gradually disappear into bigger ones, without any liquid film breaking. The driving force for this process, which is particularly important in foams, is the higher Laplace pressure in smaller bubbles/drops, leading to a higher solubility of the disperse phase in the continuous phase near the smaller bubbles/drops. The resulting concentration gradient gives rise to diffusional transport of disperse-phase molecules from small to large bubbles/drops. Ostwald ripening is inevitable in surfactant-free systems, where the surface tension is constant, but it can be stopped or significantly retarded by surfactant, if the change in surface tension can compensate for the change in the bubble/drop radius. As the smaller bubbles shrink, their surface area decreases, the surface concentration ($\Gamma$) increases and hence the surface tension ($\gamma$) decreases, at least temporarily. This can be expressed in terms of the surface dilational modulus. In principle, the process stops if the following condition (4, 6) is met:

$$\varepsilon \equiv \frac{d\gamma}{d\ln A} \geq \frac{\gamma}{2} \qquad (2)$$

where $\varepsilon$ is the surface dilational modulus and A is the area.

In emulsions, the role of Ostwald ripening is generally less pronounced because of the low solubilities of oil in water and water in oil: the resulting concentration gradients are much smaller and, therefore, diffusional transport is much slower in emulsions than in foams.

Important properties of interfaces induced by emulsifiers, including proteins, are (i) the rate of decrease of interfacial tensions as determined by the rate of adsorption and the relationship between adsorbed amount and interfacial tension (or pressure), (ii) the surface dilational modulus, which is a measure for the tendency to build up tension gradients upon disturbances in the adsorbed layer. The rates of these processes have to be related to the available time scale, which is short in the production stage and much longer during storage afterwards.

7.3 Differences between interfacial properties of proteins and low molecular weight (LMW) surfactants.

An obvious difference between proteins and LMW surfactants is the difference in molecular size. This will cause a significantly lower adsorption rate for proteins. A second difference is the difference in surface activity. Compared to proteins, LMW surfactants generally give rise to lower minimum surface or interfacial tensions; however, for proteins the bulk concentration to obtain a measurable adsorption and surface tension decrease is orders of magnitudes lower (7). A third difference is the different shape of the $\Pi(\Gamma)$ curve (see Fig. 1). With LMW surfactant, a much lower $\Gamma$ will already cause a significant $\Pi$.

surface pressure (mN/m)
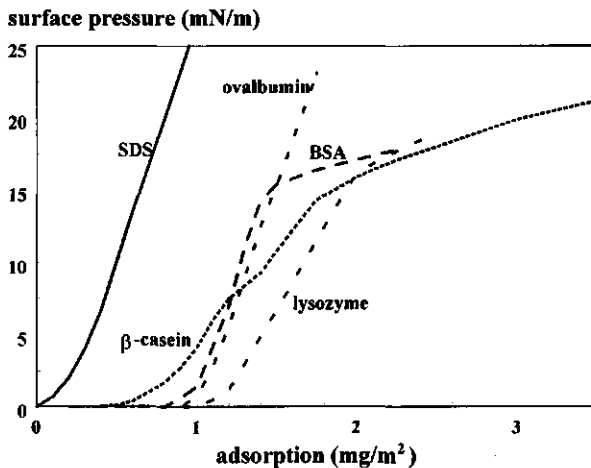


Figure 1 Surface pressure, $\Pi$, vs. surface concentration, $\Gamma$, for SDS (7), compared to some proteins (see chapter 2).

The lower interfacial tension that can be reached with LMW-surfactants and the faster adsorption, and consequently faster decrease of this tension, will in general cause break-up into smaller droplets during emulsification. The newly-formed droplets will also be stabilized against recoalescence at a shorter time scale because surface tension gradients (due to adsorption and tension lowering) can become effective at a shorter time scale, too. These differences between proteins and LMW surfactants

197

form the reason why in the preparation of many food emulsions a combination of the two emulsifier types is used.

During the emulsion production stage, initially the LMW surfactants cover the surface and promote the formation of a transiently-stable emulsion as described above. However, with time and sufficient protein present, the LMW surfactant will be displaced by the protein, at least partially (8). Under such conditions it is the adsorbed protein layer which provides the long term stability, due to its high shear and dilational modulus, steric effects and electrostatic repulsion. A combination of the two types of emulsifier is only effective if the ratio is chosen properly. A too high level of LMW surfactant will obstruct protein adsorption (9), and consequently will significantly reduce the long term stability.

## 7.4 Effect of protein type

In Chapter 2 the adsorption behaviour of proteins has been described. It was concluded that the initial stage of adsorption of all proteins is diffusion controlled. The results indicate that the adsorption rate decreases in the sequence β-casein>BSA>ovalbumin>lysozyme. In the same sequence $\Gamma_{min}$ (i.e. the minimum adsorption where the surface pressure starts to deviate measurably from zero) increases (see Fig.1). Although for oil/water interfaces no measured $\Pi(\Gamma)$ curves are available, the results described in Chapter 4 indicate a similar ranking as at the air/water surface. So, it may be justified to extrapolate predictions based on results at the air/water interface to emulsions.

Based upon these results and present views on the role of emulsifiers during emulsification and foaming, it is to be expected that initially, i.e. just after production of a foam or an emulsion, the combination of faster adsorption and lower $\Gamma_{min}$, will lead to smaller bubbles or droplets for β-casein compared to BSA, ovalbumin and lysozyme. This has two reasons: (i) the faster lowering of the interfacial tension and (ii) the faster build-up of the transient stability mechanism against recoalescence. Whether or not this ranking is found in practice depends on experimental conditions, such as protein concentration and production method. No really systematic studies, - with a variety of proteins, concentrations and methods for emulsification and foaming -, are available. Consequently, we can only consider some less comprehensive studies to check the validity of these predictions.

Graham and Phillips (10) found that the rate of foam formation by shaking protein solutions, decreases in the sequence β-casein>BSA>lysozyme, which is in line with our prediction. The long term stability of the foam (10), however, increases in that sequence. This tendency was found to be in line with drainage measurements of single films. The slower drainage in the case of BSA compared to β-casein, correlates with the difference in dilational modulus. The explanation for this correlation is that, as in

198

the case of liquid flowing out of a film between two approaching droplets, drainage out of a foam film is also hampered by the tension gradients that are formed by this drainage. According to the same authors no stable film could be formed with lysozyme, which may be attributed to a too slow rate of adsorption and a too slow surface pressure rise, in comparison with the rate of film formation. At longer time scales steric interaction and the formation of thicker and more coherent layers in the case of BSA may also contribute to the increased stability.

In ref. (11) it was found that disproportionation of a foam stabilised by SDS is much faster than one stabilised by $\beta$-lactoglobulin. For both foams the condition of Eqn. 2 is met at short times, where $\varepsilon = \varepsilon_0$. However, disproportionation is a slow process and in the case of SDS at such a long time scale the modulus can be reduced to almost zero by diffusive relaxation, which is absent in the case of proteins. For the proteins examined, the minimum value of $\gamma$ ranges from 45-55 mN/m, consequently $\varepsilon > 25$ will be sufficient. The maximum values of $\varepsilon$ given in Chapter 3 range from 25 mN/m for $\beta$-casein to 70 mN/m for BSA and 80 mN/m for ovalbumin. For ovalbumin and BSA, however, the modulus remains high over the whole frequency and concentration range. This indicates that foams with BSA and ovalbumin are expected to be stable against Ostwald ripening.

In so far unpublished measurements, we used the method of Webb et al. (12) to determine the emulsifying capacity, i.e. the maximum amount of oil that can be emulsified into a certain volume of a protein solution. The results indicated a decrease in the sequence casein $> \beta$-lactoglobulin (BLG) $>$ BSA=ovalbumin $>$ lysozyme. This method also provides information related to break-up and especially the short time stability of the emulsion droplets against recoalescence. Consequently, as in the case of foaming by shaking, this ranking can be explained on the basis of differences in adsorption rate and the rate of build-up of the initial stability mechanism based upon interfacial tension gradients. However, Smulders et al. (13), by using a high-pressure homogenizer, found the ranking based on droplet size to be somewhat different: ovalbumin>lysozyme>$\beta$-casein>$\alpha$-lactalbumin>BLG. Especially the result of the last two proteins is somewhat surprising and cannot be explained at present.

Graham and Phillips (14) also determined coalescence stability of (hexadecane in water) emulsions by using the ultracentrifuge method. Their results indicate that the coalescence stability decreases in the sequence BSA $>$ lysozyme $> \beta$-casein. In this experiment the stability of thin films between emulsion droplets is tested. Amongst other parameters, a higher dilational modulus in the case of BSA ($\varepsilon_{BSA} > \varepsilon_{\beta\text{-casein}}$ ; in this study $\varepsilon_{lysozyme}$ was not measured) may have contributed to the increased stability.

In model experiments by flow visualisation (15) of protein-covered droplets in simple shear, quasi-static break-up was found to depend on protein type and concentration. For a random coil protein ($\beta$-casein) and for low concentrations of a globular protein

(BLG), droplet break-up was more difficult to achieve than would have been predicted on the basis of the equilibrium interfacial tension. This may be attributed to an increased interfacial elasticity (16) that, in terms of the break-up condition expressed in Eqn. 1, can be accounted for as an increased interfacial tension (16) or an increased effective droplet viscosity (17). At higher BLG concentrations Williams et al. (15) observed that break-up was considerably easier than expected and independent of the viscosity ratio between droplet and continuous phase. It seemed that break-up was predominantly determined by non-dilational properties of the interfacial layer. During deformation in the shear field the droplet showed solid-like properties, which suggests the formation of a strong interfacial protein network or skin, with a high shear modulus (see Chapter 5). The easier break-up in the presence of a rigid skin around the droplet is unexpected and the physical picture is not quite clear. Intuitively, the presence of a rigid skin is expected to cause break-up to be more difficult to achieve. However, rupture of the network, at a certain deformation may initiate break-up.

The formation of an adsorbed protein layer with a high shear modulus is likely to occur under the above discussed flow visualisation break-up experiments (15), because the conditions are chosen such that break-up occurs at a time scale of 100 s, which means that there is sufficient time to achieve high surface concentrations (see Chapter 5). However, this time scale is very long compared to that involved in practical emulsification processes, which is in the order of milliseconds.

During dispersion processes under practical conditions, the effect of interfacial shear rheological properties of adsorbed protein layers is expected to be negligible. Because of the short time scale of the break-up process the surface concentration is expected to be too low for a measurable shear modulus (see Chapter 5). This will be certainly true for the fast drop break-up that is achieved in High Pressure Homogenizers. The contribution of a high interfacial shear modulus to long term stability may be related to the retarding effect on the thinning rate of films between bubbles or droplets due to the presence of rigid interfacial layers. Van Voorst Vader and Groeneweg (18) found that a high shear modulus can also increase the structure of an emulsion or foam, especially if the surfaces strongly interact. In that case a structure of sintered shells is built.

Insight into the correlation between the properties of adsorbed protein layers as discussed in the previous chapters, and emulsion and foam properties is hampered by a lack of information on the history and properties of such layers during and after production. A major problem is the very short characteristic time-scale during production. At present no techniques are available to determine interfacial rheological properties at these time-scales. Extra complicating factors: are (i) multilayer formation due to collapse after coalescence and (ii) formation of insoluble protein due to the same process. Multilayers are expected to increase stability whereas insoluble

protein is no longer active in the system and consequently may cause a decrease of stability.

To circumvent the time-scale problem and to ensure similarity of interfacial layers in production processes to those examined in model experiments, the following experiments may be considered:

i.      Stirred pot experiments with relatively low protein concentrations to create interfacial conditions similar to those during high pressure homogenisation, but at a much longer time scale. Such experiments can be performed under well known break-up conditions. In the same set-up recoalescence can be studied by first preparing the emulsion at high stirring speed and then stirring it at a lower speed.

ii.     Another possibility is to study production and stability of emulsions produced by membrane emulsification. According to this method, conditions can be chosen such that emulsion droplets are formed without recoalescence. Consequently the history of the interfacial layer is better known. An extra advantage of this method is that monodisperse emulsions can be formed, which facilitates the interpretation of coalescence experiments.

7.5 Conclusions

- In the production stage of emulsions and foams, the interfacial properties which are typical for proteins predict a larger initial drop size and a lower initial stability against re-coalescence in comparison to LMW surfactants. In the presence of both types of surfactant, concentrations and conditions can be chosen such that the LMW surfactant determines the dispersion efficiency, while the protein determines the long-term stability.

- For the different types of proteins examined, a fast foam production and a high emulsifying capacity are found to correlate with a low value of $\Gamma_{min}$, i.e. the minimum adsorption where the surface pressure starts to deviate measurably from zero This results in higher dilational moduli at short times, and hence in a faster build-up of stability against re-coalescence of newly formed emulsion droplets.

- Good long term stability is found to correlate with a high dilational modulus of adsorbed protein layers. Retardation of Ostwald ripening, i.e. the growth of large bubbles or drops at the expense of small ones, is probably the major factor here. This mechanism depends on the ratio of the modulus to the surface tension, which under relevant conditions is considerably higher for proteins than for LMW surfactants.

- Interfacial shear properties may affect long term stability of emulsions and foams, but not their initial stability during production, because in this stage the surface concentration is too low for a measurable shear modulus.

- To ensure similarity of interfacial layers, such production processes and model experiments have to be chosen, that interpretation of the results is not obscured by time-scale differences and poor control of the history of the interfacial layer.

7.6 References

1. H.P. Grace. Dispersion phenomena in high viscosity immiscible fluid systems and application of static mixers as dispersion devices in such systems. Chem. Eng. Commun. 14 2257 (1982)
2. R.A. de Bruijn. Deformation and break-up of drops in simple shear flows. Chem. Eng. Sci. 48 277 (1993); PhD Thesis Technical University Eindhoven (1989)
3. C. Marangoni. On the theory of surface viscosity of Mr J Plateau. Nuovo Cimento, Ser, 5/6 239 (1872)
4. J.W. Gibbs. On the Equilibrium of Heterogeneous Substances. Trans. Connecticut Acad., III: 108 343 (1878). Reprinted in: The scientific papers of J.Willard Gibbs, Volume 1, Dover Publications Inc., New York.
5. M. van den Tempel, The Function of Stabilizers during Emulsification, Proceedings of the 3rd International Congress on Surface Active Agents, Vol. II, Cologne, Verlag der Universitätsdruckerei Mainz, Germany, (1960), 573
6. J. Lucassen. Dynamic Properties of free Liquid Films and Foams, in "Anionic Surfactants, ed. E.H. Lucassen-Reynders, Marcel Dekker, New York (1981) 217
7. P. Walstra, A.L. de Roos. Proteins at air-water and oil-water interfaces: static and dynamic aspects. Food Reviews International. 9(4) 503 (1993)
8. E.H. Lucassen-Reynders. Competetive Adsorption of Emulsifiers 1. Theory of Adsorption of Small and Large Molecules. Colloids and Surfaces. 91 (1994) 79
9. J.A de Feijter, J. Benjamins, M. Tamboer. Adsorption Displacement of Proteins by Surfactants in Oil-in-Water Emulsions. Colloids and Surfaces. 27 (1987) 243
10. D.E. Graham, M.C. Phillips. The Conformation of Proteins at the Air/Water Interface and their role in Stabilizing Foams. In "Foams", R.J. Akers ed. Academic Press, London. (1976) 237
11. A. Prins, M.A. Bos, F.J.G. Boerboom, H.K.A.I. van Kalsbeek. Relationship between Surface Rheology and Foaming behaviour of Aqueous Protein Solutions. in "Proteins at Liquid Interfaces", D. Mobius and R. Miller, Eds., Elsevier Science, Amsterdam, the Netherlands (1998) 221

12. N.B. Webb, F.J. Ivey, H.G.Graig, V.A. Jones, R.J. Monroe. Journal of Food Science. 35 (1970) 501

13. I. Smulders, P. Caessens, P. Walstra. Formation and Stabilization of Emulsions made with Proteins and Peptides. Industrial Proteins. 5 (1998) 13

14. D.E. Graham, M.C. Phillips The Conformation of Protein at Interfaces and their role in Stabilizing Emulsions. In "Theory and Practice of Emulsion Technology", ed. A.L Smith, Academic press New York. 1976

15. A.Williams, J.J.M. Janssen, A. Prins. Behaviour of Droplets in Simple Shear Flow in the presence of a Protein Emulsifier. Colloids and Surfaces A. 125 (1997) 189

16. J.J.M. Janssen, A.Boon, W.G.M. Agterof. Influence of Dynamic Interfacial Properties on Droplet Break- in Simple Shear Flow. AIChE Journal. 40 (1994) 1929

17. E.H. Lucassen-Reynders, K.A. Kuijpers. The Role of Interfacial Properties in Emulsification. Colloids and Surfaces. 65 (1992) 175

18. F. van Voorst Vader, F. Groeneweg. Influence of the Emulsifier on the Sedimentation of Water-in-Oil Emulsions. In, R.D. Bee, P. Richmond, J. Mingins (Eds.), Food Colloids, Special Publication No 75, p. 218 (Royal Society of Chemistry, London, 1989)

## 8. SUMMARY

The aim of the investigation described in this thesis was to increase the level of understanding of the role that proteins play in the preparation and subsequent stabilisation of foams and emulsions. One aspect of this role is facilitation of break-up, due to surface tension lowering. A second aspect is the formation of a viscoelastic interfacial layer, which affects both the short-term and long-term stability of the dispersion. Therefore, a systematic study of the changes in static and dynamic interfacial properties induced by proteins was carried out.

For part of this study, dealing with the interfacial rheology, several experimental techniques were used. These techniques were either properly modified existing techniques (Chapter 3, modified longitudinal wave set-up) or newly developed (Chapter 4, Dynamic Drop Tensiometer; Chapter 5, Concentric Ring Surface Shear Rheometer) to meet the requirements for measuring the rheology of adsorbed protein layers at liquid/liquid interfaces. These requirements are (i) isotropic deformation, without leakage of the interfacial layer, for the dilational modulus measurements at air/water and oil/water interfaces and (ii) shear modulus measurements at small oscillatory deformation.

The proteins chosen for this study were $\beta$-casein, $\beta$-lactoglobulin (BLG), bovine serum albumin (BSA), ovalbumin and lysozyme. This set of proteins was chosen, because they differ considerably in relevant aspects, such as molecular weight, molecular structure and iso-electric point.

In Chapter 1 the scope and context of this study are given including a brief introduction into (i) the molecular properties of these proteins, that are relevant to the adsorption, (ii) protein adsorption and interfacial rheology, and (iii) the relation between interfacial properties and the properties of emulsions and foams.

Chapter 2 deals with the adsorption of proteins at the air/water interface. The adsorption was determined by ellipsometry, a method by which not only the adsorbed amount but also the layer thickness and protein concentration in the adsorbed layer could be determined. The ellipsometric studies were combined with surface tension measurements at the same surface.

All proteins examined show high affinity adsorption, i.e. strong adsorption at low concentration in solution. The initial rate of adsorption of all proteins is well described by a simple diffusion equation. For all proteins examined, the values of the surface pressure ($\Pi$) are protein-specific, but otherwise unique, time-independent functions of the adsorption ($\Gamma$). Time independence of the $\Pi(\Gamma)$ curve was concluded from the finding that $\Pi$ and $\Gamma$ pairs measured at different bulk concentrations and at different stages of adsorption, all collapse into one single curve. In other words, each protein has a unique surface equation of state indicated by its measured $\Pi(\Gamma)$ curve. This curve reflects the relative rigidity of the protein molecule. For flexible molecules like $\beta$-casein and PVA , $\Gamma_{min}$ ($=\Gamma$ where $\Pi$ starts to deviate measurably from zero) is low and from this point onward the surface pressure increases gradually with increasing $\Gamma$. For rigid globular proteins (BSA, ovalbumin and lysozyme) $\Gamma_{min}$

is higher and with further increase of the surface concentration the surface pressure increases steeply. At high protein concentration and long adsorption times, for most proteins multilayer adsorption takes place.

For ovalbumin, in the pH range 4-8 the effect of pH on the $\Pi$-$\Gamma$ curve is small, which indicates that electrostatic intermolecular forces do not contribute much to the surface pressure.

In Chapter 3 a longitudinal wave technique, modified to ensure isotropic surface deformation, was used to determine the dilational modulus, $\varepsilon$, of adsorbed protein layers, at the air/water interface. This modification fully eliminated the complicating shear effects that became apparent in dilational modulus measurements with adsorbed layers of some proteins in a conventional set-up.

For all proteins examined at frequencies in the range from 0.01 to 1 rad/s, the initial part of the $\varepsilon(\Pi)$ plot is a straight line through the origin. The slope of this initial part ranges between +4 and +12 . No clear relationship between the slope and the rigidity of the protein molecule was found. However, the extent of this linear range is smaller for the flexible molecules ($\beta$-casein and PVA). From the fact that this slope significantly exceeds the ideal value of +1, it must be concluded that the behaviour of the adsorbed layer is far from ideal. In the linear range, the measured moduli coincide with the limiting moduli, $\varepsilon_0$, calculated from the $\Pi(\Gamma)$ curve. This indicates that the surface pressure adjusts "instantaneously" to the changing adsorption during a compression-expansion cycle in time-scales ranging from 1 to 100 s. This also means that the modulus is purely elastic, i.e. the effect of relaxation processes is negligible. In this elastic range, differences between individual proteins are related to different degrees of non-ideality, reflected in the surface equation of state.

At higher surface concentrations a relaxation mechanism becomes operative, which is most probably not caused by diffusional exchange between surface and solution. This conclusion is based on calculations of the diffusional transport rate and the theoretical frequency spectrum of the modulus. Relaxation due to conformational changes is plausible. In the visco-elastic region $\varepsilon \geq \varepsilon_0$ for all proteins examined. This is an extra argument against diffusional exchange.

The modulus increases in the order: PVA < $\beta$-casein <BSA < ovalbumin < $\kappa$-casein. For the first four molecules the flexibility of the molecule decreases in the same order. The high modulus in the case of $\kappa$-casein cannot be attributed to the rigid molecular structure.

Chapter 4 describes a new method, the Dynamic Drop Tensiometer, especially suitable for determining the dynamic properties of proteins adsorbed at oil/water interfaces. According to this method, a small drop is subjected to sinusoidal oscillations of its volume. The corresponding area changes produce interfacial tension changes, which are evaluated from measurements of the fluctuating shape of the drop, using the Young-Laplace equation. Compared to the conventional Langmuir trough set-up, this method is particularly suited for liquid/liquid interfaces, because (i) interfacial leakage is fully eliminated and (ii) uniform

deformation is ensured even if one of the liquids is a viscous oil. An additional advantage of the method is its short response time. The dynamic properties of adsorbed protein layers at three interfaces (TAG (triacylglycerol)-oil/water, tetradecane/water and air/water) were compared. At the three interfaces, at low protein concentration, the conformation change upon adsorption is fairly fast, occurring within 1 min.. However, at high protein concentration (> 1g/l), during the first minutes after adsorption a situation exists that differs from the equilibrium $\Pi(\Gamma)$ curve. At low interfacial pressures, during a modulus measurement, the adaptation of the conformation is faster (< 1 s.). Non-ideality of the adsorbed layer increases in the sequence TAG-oil < tetradecane < air, which is probably related to a decrease of solution quality for the more hydrophobic amino acids, which decreases in the same sequence. At each of the different interfaces non-ideality increases with increasing rigidity of the protein molecule ($\beta$-casein<$\beta$-lactoglobulin<BSA<ovalbumin). Collapse-type effects and conformation-related relaxation are most pronounced at TAG-oil/water, especially with BSA, but absent at all interfaces with ovalbumin.

The surface shear properties of adsorbed protein layers are described in Chapter 5. These properties were determined with a newly developed concentric ring surface shear rheometer. The technique allows measurements over a wide range of frequencies and deformations. As the magnitude of the shear deformation markedly affects the shear modulus, $\mu_s$, an extrapolation to zero deformation is required to asses the shear properties of the undisturbed surface. Because the surface dilational modulus and the surface shear modulus both increase in the sequence PVA< Na-caseinate <BSA <ovalbumin, it is plausible that essentially the same molecular properties are responsible for the magnitude of both moduli. These properties are intermolecular interactions and the intramolecular structure. The low shear modulus for casein can be ascribed to relatively strong interactions between flexible, easily deformable molecules. With BSA and ovalbumin the interacting bonds are the weaker part of the network. So, for both moduli the rigidity of the molecule is the dominating characteristic. The finding that for most systems $\varepsilon/\mu_s \geq 3$ indicates that the adsorbed protein layer can be modelled as a thin homogeneous gel layer. Such a model points to a significant ideal monolayer contribution to $\varepsilon$ at low to medium surface concentrations.

In Chapter 6 models describing the surface equation of state of adsorbed macromolecules were applied to the experimental $\Pi(\Gamma)$ curves. These models were also applied to understand the dynamic behaviour of these layers. Statistical models, in which it is assumed that the macromolecules adsorb with all segments in direct contact with the surface, e.g. Singer equation, only explain the very low pressure part of the experimental curves of PVA and $\beta$-casein. To explain the higher pressure part, progressive loop formation and molecular interaction must be accounted for. For rigid globular proteins, simple statistical models are unable to fit any part of the experimental curves, because such molecules only slightly change their conformation upon adsorption and consequently, will adsorb with only a small fraction of the segments at the surface, even at very low pressures.

A 2-D solution model, which accounts to first order for both entropy and enthalpy, is used to describe the non-ideal behaviour of adsorbed protein layers. This non-ideality was deduced from the high $\Gamma$ needed to produce a measurable $\Pi$ and the steep initial slopes of the $\varepsilon(\Pi)$ curves.

All above models need modification to describe the S-shaped part of the $\Pi(\Gamma)$ curves at high surface concentrations. This part of the curve can be described by the Soft Particle concept, which is a modification of the surface equation of state of a 2-D hard sphere fluid. The S-shape is attributed to a decrease of the molecular cross-sectional area with increasing surface concentration. This effect appears to be more pronounced for flexible molecules like PVA and $\beta$-casein than for globular rigid molecules like BSA, ovalbumin and lysozyme. Experimental $\varepsilon(\Pi)$ curves are within the limits that are predicted by this concept. A promising option is combining a molecular compressibility as used in the Soft Particle concept with the 2-D solution model.

In Chapter 7 it is shown that interfacial properties typical for proteins predict a larger drop size and a lower stability against recoalescence during production compared to low molecular weight (LMW) surfactants.

In the presence of both types of surfactant, concentrations and conditions can be chosen such that the LMW surfactant determines the dispersion efficiency, while the protein determines the long-term stability. A comparison between the different proteins reveals that, in the production stage, a higher dilational modulus at short times correlates with a faster build-up of stability against recoalescence. For a good long term stability a high dilational modulus of adsorbed protein layers at longer times is more important. In foams, retardation of Ostwald ripening, i.e. the growth of large bubbles at the expense of small ones, is probably the major factor. This mechanism depends on the ratio of the modulus to the surface tension, which ratio is considerably higher for proteins than for LMW surfactants in relevant cases.

For a measurable shear modulus a high surface concentration is required. Therefore, shear properties may only affect long term stability of emulsions and foams, but not break-up and stability against recoalescence during production.

SAMENVATTING

Het doel van het in dit proefschrift beschreven onderzoek was het beter begrijpen van de rol van eiwitten bij het maken en stabiliseren van schuim en emulsies. Een aspect van deze rol is het opbreken van druppels makkelijker te maken, omdat door adsorptie de grenvlakspanning daalt. Een tweede aspect is de vorming van een viscoelastische laag in het grensvlak, waardoor de korte en lange termijn stabiliteit van de dispersie beïnvloed wordt. Hiertoe is een systematisch onderzoek naar, door adsorptie van eiwitten veroorzaakte, veranderingen van de statische en dynamische eigenschappen van grensvlakken gedaan.

Voor het grensvlak-reologische deel van dit onderzoek zijn diverse technieken gebruikt. Deze technieken zijn deels aangepaste bestaande technieken (Hoofdstuk 3, gemodificeerde longitudinale golf methode) of geheel nieuw ontwikkelde technieken (Hoofdstuk 4, Dynamische Druppel Tensiometer, Hoofdstuk 5, Oppervlakte Afschuif Reometer met Concentrische Ringen), om te voldoen aan de specifieke eisen voor het meten van de reologie van geadsorbeerde eiwitlagen aan lucht/water en olie/water grensvlakken. Deze eisen zijn (i) isotrope vervorming zonder lekkage van de geadsorbeerde laag, voor de dilatatie modulus metingen aan het lucht/water en olie/water grensvlak en (ii) afschuif modulus metingen bij kleine oscillerende vervorming.

De gekozen eiwitten zijn β-caseine, β-lactoglobuline (BLG), runderserum albumine (BSA), ovalbumine en lysozyme. Deze eiwitten zijn gekozen omdat ze qua moleculair gewicht, moleculaire structuur en iso-electrisch punt sterk verschillen.

In Hoofdstuk 1 wordt het kader van dit onderzoek geschetst. Dit houdt in een korte inleiding over (i) de moleculaire eigenschappen die relevant zijn voor adsorptie, (ii) eiwit adsorptie en grensvlak reologie, en (iii) de relatie tussen grensvlak eigenschappen en emulsies en schuimen.

Hoofdstuk 2 behandelt de adsorptie van eiwitten aan het lucht/water grensvlak. De adsorptie werd bepaald met behulp van ellipsometrie. Met deze methode wordt niet alleen de geadsorbeerde hoeveelheid gemeten, maar ook de dikte van de geadsorbeerde laag en dus ook de eiwitconcentratie in deze laag. Naast de ellipsometrische metingen werd van hetzelfde grensvlak ook de oppervlakte spanning gemeten.

Alle eiwitten vertonen al bij lage concentratie in de oplossing een sterke adsorptie, een eigenschap die kenmerkend is voor sterk oppervlakte actieve macromoleculen. Het eerste deel van de adorptie kinetiek wordt goed beschreven door een vereenvoudigde diffusie vergelijking. Voor alle eiwitten in dit onderzoek is de oppervlakte druk (Π) een eiwit specifieke, maar verder een unieke, tijds-onafhankelijke, funktie van de geadsorbeerde hoeveelheid (Γ). Tijdsonafhankelijkheid van deze kromme werd geconcludeerd uit het feit dat Π(Γ) paren die gemeten zijn met verschillende bulk concentraties en in verschillende stadia van de adsorptie, allemaal op een enkele kromme vallen. Voor elk eiwit wordt dus een unieke toestands vergelijking (Π(Γ) kromme) gevonden. Deze kromme weerspiegelt de relatieve

stevigheid van het eiwit molecuul. Voor flexibele moleculen zoals β-caseine en PVA is $\Gamma_{min}$ (≈$\Gamma$ waar $\Pi$ merkbaar van nul begint af te wijken) laag en vanaf dit punt stijgt de oppervlakte spanning geleidelijk met toenemende $\Gamma$. Voor globulaire eiwitten met een sterke interne structuur (BSA, ovalbumine and lysozyme) is $\Gamma_{min}$ hoger; met verdere stijging van de oppervlakte concentratie stijgt $\Pi$ steil. De meeste eiwitten vertonen multilaag adsorptie bij hoge bulk concentraties en lange adsorptie tijden.

Met ovalbumine in het pH gebied van 4-8 is de invloed van de pH op de $\Pi(\Gamma)$ kromme klein. Dit geeft aan dat de bijdrage van intermoleculaire electrostatische krachten op de oppervlakte druk gering is.

In Hoofdstuk 3 werd, voor het meten van de dilatatie modulus van geadsorbeerde eiwit lagen aan het lucht/water grensvlak, een longitudinale golf techniek gebruikt waarbij isotrope vervorming van de oppervlakte laag verzekerd is. Deze methode voorkomt de complicerende afschuif effecten, die zichtbaar werden bij metingen met de conventionele trog-methode.

Voor alle onderzochte eiwitten, in het frequentie gebied van 0.01 tot 1 rad/s, is het eerste stuk van dilatatiemodulus, $\varepsilon$, vs. $\Pi$ een rechte lijn door de oorsprong. De helling van dit beginstuk varieert tussen +4 en +12. Een duidelijk verband tussen de waarde van deze helling en de structuur van het eiwitmolecuul werd niet gevonden. Echter, dit lineaire gebied is korter voor de flexibelere moleculen (β-caseine en PVA). Uit het feit dat de helling duidelijk groter is dan +1, moeten we concluderen dat de geadsorbeerde laag zich sterk niet-ideaal gedraagt. In het lineaire gebied vallen de gemeten moduli samen met de grensmodulus, $\varepsilon_0$, berekend uit de $\Pi(\Gamma)$ kromme. Dit geeft aan dat $\Pi$ zich momentaan aanpast aan de veranderende adsorptie gedurende een compressie/expansie cyclus in een tijdschaal van 1 tot 100 s. Dit betekent ook dat de modulus geheel elastisch is; dus spelen relaxatieverschijnselen geen rol. In dit elastische gebied zijn de verschillen tussen de eiwitten toe te schrijven aan verschillen in non-idealiteit zoals weerspiegeld in de toestandsvergelijking van het oppervlak. Bij hogere oppervlakteconcentraties wordt een relaxatie mechanisme merkbaar. Deze relaxatie wordt zeer waarschijnlijk niet veroorzaakt door diffusietransport tussen oppervlak en oplossing. Deze conclusie is gebaseerd op berekeningen van de snelheid van diffusie transport en het theoretische frequentie spectrum van de modulus. Relaxatie door conformatieveranderingen is het meest waarschijnlijke mechanisme. Een extra argument tegen diffusie relaxatie is het feit dat, voor alle eiwitten, in het visco-elastische gebied $\varepsilon \geq \varepsilon_0$.

De modulus neemt toe in de volgorde PVA < β-caseine <BSA < ovalbumine < κ-caseine. Voor de eerste vier moleculen daalt de flexibiliteit in dezelfde volgorde. De hoge modulus voor κ-casein kan niet toegeschreven worden aan de stevigheid van de moleculaire structuur.

Hoofdstuk 4 beschrijft een nieuwe methode, de Dynamische Druppel Tensiometer, die vooral geschikt is voor het meten van dynamische eigenschappen van geadsorbeerde eiwitlagen aan olie/water grensvlakken. Volgens deze methode wordt een kleine druppel onderworpen aan een sinusvormige oscillatie van zijn volume. De daaruit volgende oppervlakte veranderingen veroorzaken oppervlakte-spanningsveranderingen, die worden bepaald met behulp van de Young-Laplace vergelijking toegepast op de gemeten fluctuerende druppelvorm. Vergeleken

met de conventionele Langmuir-trog opstelling heeft deze methode duidelijke voordelen voor vloeistof/vloeistof grensvlakken, want (i) er is geen lekkage van het grensvlak mogelijk en (ii) de vervorming is, zelfs als een van de vloeistoffen een viskeuze olie is, uniform. Een extra voordeel van deze methode is de korte respons tijd. Een vergelijking is gemaakt tussen de dynamische eigenschappen van geadsorbeerde eiwit lagen aan drie grensvlakken (triglyceride-olie/water, tetradekaan/water en lucht/water). Voor lage eiwit concentraties, dus langzame adsorptie, is voor alle grensvlakken de conformatieverandering bij adsorptie snel (< 1 min.). Echter, bij hoge eiwit concentratie (> 1g/l), gedurende de eerste minuten na de start van de adsorptie is er een situatie die verschilt van de evenwichts $\Pi(\Gamma)$ kromme. Bij lage oppervlakte drukken, tijdens een modulus meting, is de aanpassing van de conformatie veel sneller (< 1 s.). De afwijking van ideaal gedrag neemt toe in de volgorde triglyceride-olie < tetradekaan < lucht. Dit houdt waarschijnlijk verband met een verslechtering van de oplosmiddelkwaliteit voor de meer hydrophobe aminozuren in dezelfde volgorde. De afwijking van ideaal gedrag aan alle grensvlakken, neemt toe met toenemende sterkte van de structuur van het eiwit molecuul ($\beta$-caseine<$\beta$-lactoglobuline<BSA<ovalbumine). Collaps-achtige effecten en relaxatie via conformatieverandering, zijn het duidelijkst aan triglyceride-olie/water, vooral met BSA, en afwezig aan alle grensvlakken met ovalbumine.

De oppervlakte afschuif-eigenschappen van geadsorbeerde eiwit lagen zijn beschreven in Hoofdstuk 5. Zij werden gemeten met een nieuw ontwikkelde oppervlakte afschuif-reometer (principe van concentrische ringen). Met deze techniek kunnen metingen over een breed frequentie en vervormings bereik gedaan worden. Omdat de grootte van de vervorming een duidelijk effect heeft op de afschuif-modulus, $\mu_s$, is extrapolatie naar vervorming nul nodig, om de afschuif-eigenschappen van het ongestoorde grensvlak vast te stellen. Aangezien de oppervlakte dilatatie modulus en de afschuif-modulus beide toenemen in de volgorde PVA< Na-caseinaat<BSA<ovalbumine, is het plausibel dat dezelfde moleculaire eigenschappen verantwoordelijk zijn voor de waarde van beide moduli. De relevante moleculaire eigenschappen zijn intermoleculaire wisselwerkingen en de intramoleculaire structuur. De lage afschuif-modulus van caseine kan toegeschreven worden aan relatief sterke wisselwerking tussen flexibele, gemakkelijk vervormbare moleculen. Met BSA en ovalbumine is de wisselwerking tussen de moleculen de zwakste schakel van het netwerk. Voor beide moduli is dus de stevigheid van de moleculstructuur de dominerende factor. Het resultaat, dat voor de meeste systemen $\varepsilon/\mu_s \geq 3$, geeft aan dat een geadsorbeerde eiwitlaag kan worden beschouwd als een homogene gel laag. Dit houdt wel in dat voor niet te hoge $\Gamma$ een aanzienlijke ideale monolaag bijdrage aan $\varepsilon$ toegekend moet worden.

In Hoofdstuk 6 werden modellen die de toestandsvergelijking van geadsorbeerde macromoleculen beschrijven toegepast op de experimentele $\Pi(\Gamma)$ krommen van geadsorbeerde eiwit lagen. Deze modellen zijn ook gebruikt om het dynamische gedrag van deze lagen te begrijpen. Statistische modellen waarin wordt aangenomen dat macromoleculen met alle segmenten in direct contact met het oppervlak adsorberen, zoals b.v.de Singer

vergelijking, kunnen alleen het erg lage $\Pi$ gedeelte van de experimentele krommen van PVA en $\beta$-casein beschrijven. Het hogere $\Pi$ gedeelte van de krommen kan dan verklaard worden door aan te nemen dat steeds meer lussen gevormd worden en dat moleculaire wisselwerking ook een rol speelt. Deze modellen zijn niet geschikt om experimentele krommen van stevige globulaire eiwitten te beschrijven, omdat zulke moleculen slechts een geringe conformatie verandering bij adsorptie ondergaan en dus nooit zullen adsorberen met alle segmenten in het grensvlak, zelfs niet bij erg lage $\Pi$.

Het 2-D oplossings model, waarin rekening wordt gehouden met entropy en enthalpy, is gebruikt om het niet ideale gedrag van geadsorbeerde eiwit lagen te beschrijven. Niet-idealiteit werd geconcludeerd uit de hoge $\Gamma$ die nodig voor een meetbare $\Pi$ en de steile helling van de $\varepsilon(\Pi)$ krommen.

Alle bovengenoemde modellen moeten aangepast worden, om het S-vormige gedeelte van de $\Pi(\Gamma)$ krommen bij hogere oppervlakte concentraties, te beschrijven. Dit deel van de krommen kan worden beschreven door het Zachte Deeltjes concept, wat een modificatie is van de 2-D toestandsvergelijking van een vloeistof bestaande uit harde bollen. De S-vorm wordt toegeschreven aan een afname van de moleculaire doorsnede met stijgende oppervlakte concentratie. Dit effect is groter voor flexibele moleculen zoals PVA en $\beta$-caseine in vergelijking tot de globulaire en steviger moleculen zoals BSA, ovalbumine en lysozyme. Experimentele $\varepsilon(\Pi)$ krommen vallen binnen de grenzen die door dit concept voorspeld worden.

Het kombineren van een moleculaire compressibiliteit zoals toegepast in het Zachte Deeltjes concept met het 2-D oplossings model lijkt een veelbelovende optie.

In Hoofdstuk 7 is aangetoond dat vergeleken met kleine emulgator moleculen, bij het maken van emulsies, grensvlakeigenschappen die specifiek zijn voor eiwitten een grotere druppel en een geringere stabiliteit tegen re-coalescentie voorspellen. Als beide soorten emulgator aanwezig zijn, kunnen de concentratie en condities zo gekozen worden dat de kleine moleculen de effectiviteit van het maken van de dispersie bepalen, terwijl de eiwitten de lange termijn stabiliteit bepalen. Een vergelijking tussen de verschillende eiwitten toont aan dat, tijdens de productie, een grotere dilatatie-modulus na korte tijden, correleert met een snellere opbouw van de stabiliteit tegen re-coalescentie. Voor een goede lange termijn stabiliteit is een hogere modulus na langere tijd belangrijker. Voor schuimen is vertraging van de Ostwald rijping, d.w.z. de groei van grote bellen ten koste van de kleine, de belangrijkste factor. Dit vertragingsmechanisme wordt bepaald door de verhouding tussen de modulus en de oppervlaktespanning. Deze verhouding is in relevante gevallen groter voor eiwitten dan voor kleine emulgatoren.

Voor een meetbare afschuifmodulus is een grote oppervlakteconcentratie nodig. Daarom zullen afschuifeigenschappen alleen de lange termijn stabiliteit van schuimen en emulsies beïnvloeden, niet het opbreken van druppels en bellen en ook niet de stabiliteit tegen re-coalescentie tijdens produktie.

## CURRICULUM VITAE

Jan Benjamins werd geboren op 10 oktober 1943 in Dalerpeel, gemeente Dalen. Na het behalen van het HBS-B diploma aan het Caland Lyceum te Rotterdam in 1961, trad hij in dienst van het Unilever Research Laboratorium in Vlaardingen. In 1962 werd met goed gevolg het examen voor leerling analist afgelegd. Na het vervullen zijn zijn militaire dienstplicht (1963-1964) werden bij het Koninklijk Technicum PBNA in 1966 het diploma Kandidaat Technisch Chemicus en in 1968 het diploma Technisch Chemicus (richting Fysische Chemie) behaald.

Bij Unilever was hij werkzaam in afdelingen waar fundamenteel fysisch chemisch onderzoek werd verricht. Eerst werkte hij aan kolloid-chemische aspecten van de verwijdering van vuildeeltjes van textiel en vanaf 1971 werkte hij bijna uitsluitend aan onderwerpen die betrekking hadden op voedingsmiddelen. Binnen dit kader werden de volgende onderwerpen bestudeerd: het adsorptiegedrag van eiwitten aan het lucht/water grensvlak, de rheologisch eigenschappen van geadsorbeerde eiwitlagen aan het water/lucht en het olie/water grensvlak, schuim en emulsie onderzoek en de fysisch chemische aspecten van het spatten van margarine tijdens het braadproces. Het onderzoek betreffende het gedrag van geadsorbeerde eiwitlagen, zoals dat over een periode van meer dan 25 jaar is uitgevoerd, is het onderwerp van dit proefschrift.